

Single-chain variable fragment (scFv) inhibits platelet activation and aggregation in Heparin-Induced Thrombocytopenia (HIT)

Author:

New, Jaa Yien

Publication Date:

2013

DOI:

<https://doi.org/10.26190/unsworks/16471>

License:

<https://creativecommons.org/licenses/by-nc-nd/3.0/au/>

Link to license to see what you are allowed to do with this resource.

Downloaded from <http://hdl.handle.net/1959.4/53031> in <https://unsworks.unsw.edu.au> on 2024-04-29

**Single-Chain Variable Fragment (scFv)
Inhibits Platelet Activation and Aggregation in
Heparin-Induced Thrombocytopenia (HIT)**

Jaa Yien New

A thesis submitted in fulfilment
of the requirements for the degree of
Doctor of Philosophy

Department of Medicine
St. George Clinical School
University of New South Wales



April 2013

PLEASE TYPE**THE UNIVERSITY OF NEW SOUTH WALES
Thesis/Dissertation Sheet**

Surname or Family name: New

First name: Jaa Yien

Other name/s:-

Abbreviation for degree as given in the University calendar: PhD

School: St. George Clinical School

Faculty: Medicine

Title: Single-chain variable fragment (scFv) inhibits platelet activation and aggregation in Heparin-Induced Thrombocytopenia (HIT)

Abstract 350 words maximum: (PLEASE TYPE)

Heparin-Induced Thrombocytopenia (HIT) is a life threatening disorder affecting 0.2-5% of patients receiving heparin. HIT is mediated by an autoantibody against platelet factor 4/heparin complex. This antibody/antigen complex binds to platelet FcγRIIa receptors, cross-links the receptors and activates the platelets. Currently, there is no clinically proven treatment that can prevent this platelet activation. IV.3 is a murine monoclonal antibody (MoAb) that binds to the FcγRIIa receptor and inhibits platelet activation induced by the HIT immune complexes. This thesis proposes that a single-chain variable fragment (scFv) derived from the IV.3 MoAb will retain the capacity to inhibit platelet activation caused by HIT antibodies. This will be a novel therapeutic strategy for the treatment of HIT.

The scFv was constructed by cloning the variable heavy chain (VH) and light chain (VL) of the IV.3 antigen binding domain (Fab). The scFv was formed by joining the VH and VL chains with a flexible linker. This construct was then cloned into a periplasmic expression vector, expressed in bacteria and purified by affinity gel chromatography. The purified scFv was capable of binding human platelets as observed by flow cytometry. Moreover, the protein demonstrated potent inhibitory activity against HIT antibodies in platelet aggregation and 14C-serotonin release assays. The scFv was humanized (mutating as few residues as possible) to avoid potential immune reactions when it is administered to patients, thus improving its therapeutic usefulness. Notably, the activity of the humanized scFv was indistinguishable from that of the parental molecule. To increase its antiplatelet activity and to enhance its therapeutic potential, the molecule was fused to another scFv derived from an anti-GPIIbα MoAb. This approach, however, did not progress further due to the observation of spontaneous platelet aggregation induced by the bispecific scFv.

In conclusion, this thesis shows that both the murine and the humanized scFv demonstrate binding to the FcγRIIa on human platelets, and exhibit inhibition of platelet activation induced by the HIT antibodies. Therefore, this recombinant protein could potentially improve the treatment of HIT, particularly in preventing the patients' serious clinical sequelae.

Declaration relating to disposition of project thesis/dissertation

I hereby grant to the University of New South Wales or its agents the right to archive and to make available my thesis or dissertation in whole or in part in the University libraries in all forms of media, now or here after known, subject to the provisions of the Copyright Act 1968. I retain all property rights, such as patent rights. I also retain the right to use in future works (such as articles or books) all or part of this thesis or dissertation.

I also authorise University Microfilms to use the 350 word abstract of my thesis in Dissertation Abstracts International (this is applicable to doctoral theses only).

.....
Signature.....
Witness.....
Date

The University recognises that there may be exceptional circumstances requiring restrictions on copying or conditions on use. Requests for restriction for a period of up to 2 years must be made in writing. Requests for a longer period of restriction may be considered in exceptional circumstances and require the approval of the Dean of Graduate Research.

FOR OFFICE USE ONLY

Date of completion of requirements for Award:

THIS SHEET IS TO BE GLUED TO THE INSIDE FRONT COVER OF THE THESIS

ORIGINALITY STATEMENT

'I hereby declare that this submission is my own work and to the best of my knowledge it contains no materials previously published or written by another person, or substantial proportions of material which have been accepted for the award of any other degree or diploma at UNSW or any other educational institution, except where due acknowledgement is made in the thesis. Any contribution made to the research by others, with whom I have worked at UNSW or elsewhere, is explicitly acknowledged in the thesis. I also declare that the intellectual content of this thesis is the product of my own work, except to the extent that assistance from others in the project's design and conception or in style, presentation and linguistic expression is acknowledged.'

Signed

Date

Abstract

Heparin-Induced Thrombocytopenia (HIT) is a life threatening disorder affecting 0.2-5% of patients receiving heparin. HIT is mediated by an autoantibody against platelet factor 4/heparin complex. This antibody/antigen complex binds to platelet Fc γ RIIa receptors, cross-links the receptors and activates the platelets. Currently, there is no clinically proven treatment that can prevent this platelet activation. IV.3 is a murine monoclonal antibody (MoAb) that binds to the Fc γ RIIa receptor and inhibits platelet activation induced by the HIT immune complexes. This thesis proposes that a single-chain variable fragment (scFv) derived from the IV.3 MoAb will retain the capacity to inhibit platelet activation caused by HIT antibodies. This will be a novel therapeutic strategy for the treatment of HIT.

The scFv was constructed by cloning the variable heavy chain (VH) and light chain (VL) of the IV.3 antigen binding domain (Fab). The scFv was formed by joining the VH and VL chains with a flexible linker. This construct was then cloned into a periplasmic expression vector, expressed in bacteria and purified by affinity gel chromatography. The purified scFv was capable of binding human platelets as observed by flow cytometry. Moreover, the protein demonstrated potent inhibitory activity against HIT antibodies in platelet aggregation and ¹⁴C-serotonin release assays. The scFv was humanized (mutating as few residues as possible) to avoid potential immune reactions when it is administered to patients, thus improving its therapeutic usefulness. Notably, the activity of the humanized scFv was indistinguishable from that of the parental molecule. To increase its antiplatelet activity and to enhance its therapeutic potential, the molecule was fused to another scFv derived from an anti-GPIb α MoAb. This approach, however, did not progress further due to the observation of spontaneous platelet aggregation induced by the bispecific antibody.

In conclusion, this thesis shows that both the murine and the humanized scFv demonstrate binding to the Fc γ RIIa on human platelets, and exhibit inhibition of platelet activation induced by the HIT antibodies. Therefore, this recombinant protein could potentially improve the treatment of HIT, particularly in preventing the patients' serious clinical sequelae.

Acknowledgements

First and foremost, I would like to extend my deepest gratitude to my supervisor, Prof. Beng H. Chong for accepting me into this lab, providing guidance, suggestions and encouragement throughout the project. His kind support is truly appreciated.

Secondly, to my co-supervisor, Dr. José Perdomo (a.k.a. little boss) who went beyond the call of duty, in providing enormous guidance and sharing his vast knowledge in every aspect of the project. Thank you so much for bearing with me through the highs and lows, and being so patient even in the toughest situations. None of this would have been possible without you. To my second co-supervisor, Dr. Xing-Mai Jiang, thank you for designing the humanized sequence of the anti-Fc γ RIIa scFvs, sharing your knowledge on antibody engineering and guiding me through the steps of protein purification. To Ms. Zohra Ahmadi, thank you for conducting the Serotonin Release Assay, providing needed resources and always willing to give a helping hand. To Dr. Feng Yan, thank you for guiding me in using flow cytometry and conducting animal studies, your patience in helping out with everything is truly appreciated.

My sincere gratitude also goes out to Ms. Sinead O'Reilly and Ms. Val Reid. Thank you so much in providing assistance whenever needed throughout the years, your constant encouragement has always been a huge boost for me when I am feeling down. The same also goes to Dr. Nicola Chapman, Dr. Jian Cheng Qi, Ms. Hemaxi Ghelani, Dr. Ashish Diwan and everyone from Department of Immunology and Surgery, thank you!

To my dear friends, Anahid, Chanel, Cheryl, Choo Peng, Debbie, Dr. Jim Fang, Dr. Kumiko Tanaka, Dr. Phil Choi, Eunice, Fei Tieng, Joanne, Mahmoud, Miao, Muna, Rada, Rene, Shengyi, Stephanie, Steven, Val Soo and Xue, I thank you all for your wonderful friendship and for being there during the difficult times. A big thank you also goes out to my ex-supervisor from Monash University, Dr. So Ha Ton, I would not have made it to Sydney if it wasn't for you.

To Daddy, Mummy, Ven, Ming and Yeong, I thank you for your never ending support, encouragement and unconditional love during the undertaking of this memorable journey. You all are the best, I love you all and this thesis is dedicated to all of you.

Table of Contents

ABSTRACT	I
ACKNOWLEDGEMENTS	II
TABLE OF CONTENTS	III
LIST OF FIGURES	X
LIST OF TABLES	XV
LIST OF ABBREVIATIONS	XVI
LIST OF PUBLICATIONS AND AWARDS	XXI
CHAPTER 1 INTRODUCTION	1
1.1. Heparin	2
1.1.1. <i>Clinical Usage of Heparin</i>	2
1.1.2. <i>Mode of Action of Heparin</i>	3
1.2. History of HIT	6
1.3 Two types of HIT	8
1.3.1 <i>Mild Early-Onset Thrombocytopenia (Type I)</i>	8
1.3.2. <i>Severe Delayed-Onset Thrombocytopenia (Type II)</i>	9
1.4. Clinical Features of HIT	9
1.5. Pathogenesis of HIT/T	11
1.5.1. <i>The Immune Complex</i>	12
1.6. FcγRIIa Receptor	16
1.6.1. <i>The FcγRIIa Receptor and its Polymorphism</i>	17
1.6.2. <i>Platelet Activation by HIT Ab via FcγRIIa Receptor</i>	17
1.6.3. <i>Platelet Activation and Signaling Pathway</i>	19
1.7. Animal Models of HIT	21
1.8. Incidence of HIT	22
1.8.1. <i>Formulation of Heparin</i>	22
1.8.2. <i>Groups of Patients</i>	22
1.9. Clinical Diagnosis of HIT	24
1.10. Laboratory Diagnosis of HIT	26
1.11. Iceberg Model of HIT	29
1.12. Management of HIT	31
1.12.1. <i>Limitations of Current Anticoagulants for HIT Treatment.</i>	33
1.13. Potential Treatment for HIT	33

1.14. Is there other approach to treat HIT?	37
1.15. MoAbs as a therapeutic agent for medical treatment	38
1.16. Hypothesis and Aims	46
CHAPTER 2 MATERIALS AND METHODS	48
2.1. Materials.....	49
2.1.1. <i>Bacterial Strains</i>	49
2.1.2. <i>Cell Lines</i>	49
2.1.3. <i>Human Platelets</i>	49
2.1.4. <i>HIT Sera</i>	50
2.1.5. <i>DNA Oligonucleotides (Primers)</i>	50
2.1.6. <i>Cell Culture Reagents</i>	50
2.1.7. <i>Molecular Biology Kits</i>	51
2.1.8. <i>Molecular Biology Enzymes and Reagents</i>	51
2.1.9. <i>Protein Reagents/Kits</i>	52
2.1.10. <i>Chemical Reagents/Solutions</i>	52
2.1.11. <i>Equipment</i>	55
2.1.12. <i>Antibodies for Flow Cytometry</i>	57
2.1.13. <i>Antibodies for Immunostaining</i>	57
2.1.14. <i>Vectors</i>	58
2.1.15. <i>Online Software for Primer Design and Molecular Analysis</i>	58
2.1.16. <i>Online Software and Program for Protein Modeling</i>	58
2.1.17. <i>Blood Collection</i>	59
2.1.18. <i>Materials for Platelet Aggregometry</i>	59
2.1.19. <i>Materials for Serotonin Release Assay</i>	59
2.1.20. <i>Animal Work</i>	59
2.2. Methods	60
2.2.1. <i>Standard Molecular Biology Techniques</i>	60
2.2.2. <i>Cell Culture</i>	60
2.2.3. <i>Preparation of Protein Samples for Coomassie Staining and Western Blotting</i>	60
2.2.4. <i>Coomassie Staining of Protein Gel</i>	60
2.2.5. <i>Western Blotting</i>	61
2.2.6. <i>PCR Reaction Setup for Different DNA Polymerases</i>	61
2.2.7. <i>Digestion Reactions</i>	62

2.2.8.	<i>Ligation Reaction (Promega)</i>	62
2.2.9.	<i>Sequencing Reactions (ABI)</i>	62
2.2.10.	<i>Ethanol Purification to remove excess Big Dye Terminators</i>	63
2.2.11.	<i>Cloning and Sequencing of VH and VL</i>	64
2.2.12.	<i>Constructing scFv DNA</i>	64
2.2.13.	<i>Molecular Modeling of STG1</i>	64
2.2.14.	<i>Humanization and Construction of STG2</i>	66
2.2.15.	<i>Humanization and Construction of STG3</i>	66
2.2.16.	<i>Molecular Modeling of STG2 and STG3</i>	66
2.2.17.	<i>Construction of STGK2</i>	69
2.2.18.	<i>Protein Expression</i>	70
2.2.19.	<i>Protein Purification of Soluble Fraction of scFv with ANTI-FLAG M2 Affinity Resin</i>	71
2.2.20.	<i>Protein Purification for Soluble Fraction with HiTrap HP column</i>	71
2.2.21.	<i>Preparation and Solubilization of Inclusion Bodies</i>	72
2.2.22.	<i>Purification of Inclusion Bodies</i>	72
2.2.23.	<i>In Vitro Refolding of Inclusion Bodies using Dialysis/Stepwise Dialysis System</i>	73
2.2.24.	<i>In Vitro Refolding of Inclusion Bodies using On-Column Refolding System</i>	73
2.2.25.	<i>Protein Purification and Refolding with Styrene Maleic Acid Lipid Particle (SMALP)</i>	74
2.2.26.	<i>Preparation of Platelets for Flow Cytometry Analysis</i>	75
2.2.27.	<i>Platelet Aggregation Assay</i>	76
2.2.28.	<i>Serotonin Release Assay (SRA)</i>	76
2.2.29.	<i>Purification of Platelet Factor 4 (PF4)</i>	77
2.2.30.	<i>Purification of IV.3 MoAb</i>	78
2.2.31.	<i>Purification of Total HIT IgG</i>	79
2.2.32.	<i>Establishment of HIT Animal Model using NOD/SCID Mice</i>	80
2.2.32.1.	Subcutaneous Injection of Mice	80
2.2.32.2.	Intraperitoneal Injection of Mice	80
2.2.32.3.	Tail Vein Injection of Mice	80
2.2.32.4.	Blood Collection from Mice	81

2.2.32.5.	Preparation of Human Platelets and Determination of Human Platelets Survival	81
2.2.32.6.	Flow Cytometry Analysis of Human Platelets	81
2.2.32.7.	Set up for HIT animal model	82
2.2.33.	<i>Statistical Analyses</i>	82
CHAPTER 3 ANTI-FCγRIIA SCFV INHIBITS PLATELET ACTIVATION INDUCED BY HIT IMMUNE COMPLEXES		83
3.1.	Introduction	84
3.1.1.	<i>Generation of scFv</i>	84
3.1.2.	<i>scFv as Therapeutic Molecules</i>	87
3.1.3.	<i>Limitations of Current Treatment for HIT</i>	89
3.1.4.	<i>Hypothesis and Aims</i>	90
3.2.	Results.....	91
3.2.1.	<i>Molecular Cloning and Sequencing of the VH and VL Fragments of IV.3.</i>	91
3.2.2.	<i>scFv Construct</i>	95
3.2.2.1.	Creating Extended Variable Regions of IV.3 scFv (STG1) Short and Long Linker	95
3.2.2.2.	Generation of STG1 with Short and Medium Linkers	99
3.2.2.3.	Creating the Extended Variable Region of STG1 Long Linker	103
3.2.2.4.	Creating STG1 Long Linker	103
3.2.3.	<i>Molecular Modeling of STG1</i>	110
3.2.4.	<i>Expression and Purification of STG1</i>	112
3.2.5.	<i>STG1 Recognizes the FcγRIIa on Human Platelets</i>	117
3.2.6.	<i>STG1 Inhibits Platelet Aggregation in the presence of HIT IgG and Heparin</i>	120
3.2.7.	<i>STG1 Inhibits Serotonin Release in the presence of HIT Serum and Heparin</i>	123
3.3.	Discussion	125
CHAPTER 4 HUMANIZED ANTI-FCγRIIA SCFV INHIBITS PLATELET ACTIVATION INDUCED BY HIT IMMUNE COMPLEXES		129
4.1.	Introduction	130
4.1.1.	<i>Approaches to Humanization</i>	130
4.1.2.	<i>Generation of Humanized scFv</i>	134

4.1.3.	<i>Protein Refolding from Inclusion Bodies</i>	135
4.1.3.1.	Approaches to Protein Refolding.....	135
4.1.3.2.	Protein Refolding in the form of Nanoparticles.....	138
4.1.4.	<i>Animal Models for HIT</i>	140
4.1.5.	<i>Hypothesis and Aims</i>	141
4.2.	Results	142
4.2.1.	<i>Humanization of STG1</i>	142
4.2.2.	<i>Construction of STG2</i>	144
4.2.3.	<i>Molecular Modeling of STG2</i>	147
4.2.4.	<i>Expression of STG2</i>	149
4.2.5.	<i>Purification and One-Step Dialysis Refolding of STG2</i>	153
4.2.6.	<i>STG2 Refolded with One-Step Dialysis Fails to Inhibit Platelet Aggregation</i>	156
4.2.7.	<i>Purification and Step-Wise Dialysis Refolding of STG2</i>	158
4.2.8.	<i>STG2 Refolded with Step-Wise Dialysis Exhibits Partial Activity</i>	158
4.2.9.	<i>STG2 Refolded with Step-Wise Dialysis Did Not Bind to Human Platelets</i>	161
4.2.10.	<i>Purification and On-Column Refolding of STG2</i>	163
4.2.11.	<i>STG2 Refolded On-Column Binds to FcγRIIa on Platelets</i>	163
4.2.12.	<i>Optimization of STG2 Purification</i>	168
4.2.13.	<i>Incomplete On-Column Refolding of STG2</i>	168
4.2.14.	<i>Purification and Refolding of STG2 with SMALPs</i>	172
4.2.15.	<i>STG2 Incorporated into SMALPs Binds to FcγRIIa on Platelets</i>	172
4.2.16.	<i>Purified STG2 (Incorporated into SMALPs) Leads to Spontaneous Platelet Aggregation</i>	176
4.2.17.	<i>Purification of Soluble STG2</i>	178
4.2.18.	<i>Soluble STG2 Binds to FcγRIIa on Platelets</i>	180
4.2.19.	<i>Soluble STG2 Inhibits Platelet Aggregation in the presence of HIT IgG and Heparin</i>	182
4.2.20.	<i>Soluble STG2 Inhibits Serotonin Release in the presence of HIT Serum and Heparin</i>	182
4.2.21.	<i>Refinement of the Humanized scFv</i>	184
4.2.22.	<i>Construction of STG3</i>	184
4.2.23.	<i>Molecular Modelling of STG3</i>	187

4.2.24.	<i>Expression of STG3</i>	189
4.2.25.	<i>Purification of STG3</i>	191
4.2.26.	<i>Soluble STG3 Binds to FcγRIIIa on Platelets</i>	194
4.2.27.	<i>Soluble STG3 Inhibits Platelet Aggregation in the presence of HIT IgG and Heparin</i>	195
4.2.28.	<i>Soluble STG3 Inhibits Platelet Activation in the presence of HIT Serum and Heparin</i>	195
4.2.29.	<i>Establishing HIT Animal Model in NOD/SCID Mice</i>	197
4.2.29.1.	Calculation of the Number of Circulating Human Platelets using CountBright™ Absolute Counting Beads	197
4.2.29.2.	Human Platelets Injected into NOD/SCID Mice are Detected in the Circulation.....	200
4.2.29.3.	The NOD/SCID Animal Model Did Not Recapitulate the Features of HIT	201
4.3.	Discussion	203
CHAPTER 5 GENERATION & CHARACTERIZATION OF BSAB WITH SPECIFICITY FOR GPIIb/IIIa AND FCγRIIIa.....		
5.1.	Introduction	211
5.1.1.	<i>The Different Forms of BsAbs</i>	211
5.1.2.	<i>BsAbs in Clinical Applications</i>	213
5.1.3.	<i>GPIIb-IIIa Complex</i>	215
5.1.4.	<i>Hypothesis and Aims</i>	218
5.2.	Results	219
5.2.1.	<i>Humanization of muAK2 scFv</i>	219
5.2.2.	<i>Cloning of STGK2</i>	222
5.2.3.	<i>Expression of STGK2</i>	222
5.2.4.	<i>Purification and On-Column Refolding of Solubilized STGK2</i>	227
5.2.5.	<i>STGK2 Refolded On-Column Binds to Platelets</i>	231
5.2.6.	<i>STGK2 Leads to Spontaneous Platelet Aggregation</i>	234
5.3.	Discussion	236
CHAPTER 6 FINAL SUMMARY AND FUTURE WORK		
6.1.	Final Summary	242
6.2.	Future Work	246
APPENDIX		
		249

A1. Appendix for Chapter 2	250
<i>A1.1. Ammonium Sulphate Precipitation.....</i>	<i>250</i>
A2. Appendix for Chapter 3	251
<i>A2.1. List of Primers</i>	<i>251</i>
<i>A2.2. Sequence Analysis of Variable Regions of IV.3 MoAb with Murine Germline Sequence.....</i>	<i>253</i>
<i>A2.3. Purification of IV.3 MoAb</i>	<i>254</i>
<i>A2.4. Purification of Total HIT IgG</i>	<i>256</i>
A3. Appendix for Chapter 4	259
<i>A3.1. Sequence Analysis of Variable Regions of IV.3 MoAb with Human Germline Gene Sequence</i>	<i>259</i>
<i>A3.2. Sequence Analysis of Humanized Variable Regions (STG2) with Human Germline Gene Sequence</i>	<i>260</i>
<i>A3.3. Sequence Analysis of Humanized Variable Regions (STG3) with Human Germline Gene Sequence</i>	<i>261</i>
<i>A3.4. Purification of PF4.....</i>	<i>262</i>
REFERENCES.....	266

List of Figures

Figure 1.1	Chemical structure of heparin.	4
Figure 1.2.	The mechanism of action of different forms of heparin.	5
Figure 1.3.	Sites of action by different forms of heparin on the coagulation cascade. .	7
Figure 1.4.	Cumulative frequency of thrombosis in Type-II HIT patients.....	10
Figure 1.5.	Molecular model of the human PF4 tetramer.	13
Figure 1.6.	Schematic representation of the generation of PF4-Heparin-Ab Immune Complex.	15
Figure 1.7.	Diagram of HIT Ab-mediated signaling pathway.....	18
Figure 1.8.	An overview of the signaling pathways of 4 major groups of platelet receptors.	20
Figure 1.9.	Iceberg model of HIT.....	30
Figure 1.10.	Structural location of epitopes on FcγRIIIa recognized by IgG1 and IV.3.	39
Figure 1.11.	A diagram of MoAb generation using hybridoma technology.....	41
Figure 1.12.	A list of therapeutic MoAbs approved by FDA currently available in the United States.....	42
Figure 1.13.	Schematic representation of an IgG Ab molecule.....	44
Figure 1.14.	Schematic representation of MoAb and different Ab fragments.....	45
Figure 2.1.	Schematic representation of STG1.....	65
Figure 2.2.	Schematic representation of STG2.....	67
Figure 2.3.	Schematic representation of STG3.....	68
Figure 2.4.	Schematic representation of STGK2.....	69
Figure 3.1.	PCR assembly of scFv.	86
Figure 3.2.	PCR amplification of VH and VL regions.	93
Figure 3.3.	Nucleotide and deduced amino acid sequences of VH and VL regions of IV.3.	94
Figure 3.4.	Construction of the extended variable regions of STG1.....	97
Figure 3.5.	PCR amplification of extended VH and VL regions.	98
Figure 3.6.	An illustrated diagram showing STG1 short linker generated via overlap extension PCR.....	100
Figure 3.7.	An illustrated diagram showing STG1 medium linker generated via overlap extension PCR.....	101

Figure 3.8.	Complete construct of STG1 short and medium linker after PCR amplification.	102
Figure 3.9.	Introduction of additional linkers to create STG1 long linker.	104
Figure 3.10.	PCR amplification of additional linker segment introduced into extended VH and VL regions of STG1 long linker.....	105
Figure 3.11.	Generation of STG1 long linker by overlap extension PCR.	106
Figure 3.12.	STG1 long linker after PCR amplification.....	107
Figure 3.13.	Nucleotide and deduced amino acid sequences of short, medium and long linker.....	108
Figure 3.14.	Digested pIG6 Vector with STG1 inserts.....	109
Figure 3.15.	Proposed structural model of STG1.	111
Figure 3.16.	Bacterial growth curve of <i>E. coli</i> BL21(DE3) expressing STG1 of different linkers.	113
Figure 3.17.	Coomassie Blue Staining of <i>E.coli</i> cell lysates-before and after induction.	114
Figure 3.18.	Western Blotting of <i>E.coli</i> total cell lysates-before and after induction.	114
Figure 3.19.	Coomassie Blue Staining of <i>E. coli</i> total cell lysates-soluble and insoluble fractions.	115
Figure 3.20.	Western Blotting of <i>E.coli</i> total cell lysates-soluble and insoluble fraction.....	115
Figure 3.21.	STG1 short and medium linker purified with ANTI-FLAG M2 affinity resin.	116
Figure 3.22.	STG1 long linker purified with ANTI-FLAG M2 affinity resin.....	116
Figure 3.23.	Binding of IV.3 MoAb to human platelets.....	118
Figure 3.24.	The generated STG1 interacts with human platelets.....	119
Figure 3.25.	Platelet aggregation curves.....	121
Figure 3.26.	IV.3 MoAb inhibits platelet aggregation induced by HIT IgG.	122
Figure 3.27.	STG1 inhibits platelet aggregation induced by HIT IgG.	122
Figure 3.28.	IV.3 MoAb inhibited platelet activation induced by HIT serum and heparin.	124
Figure 3.29.	STG1 blocked platelet activation induced by HIT serum and heparin.	124

Figure 4.1.	Illustration of the humanization of the VL region of a murine antibody.	131
Figure 4.2.	The structure of a variable domain of VL.	132
Figure 4.3.	Diagram of protein refolding course.	136
Figure 4.4.	Schematic illustration of both lipid and membrane protein encapsulated with SMA co-polymer.	139
Figure 4.5.	Amino acid sequence alignment between the variable regions of STG1 and STG2.	143
Figure 4.6.	Nucleotide and deduced amino acid sequences of VH and VL regions of STG2.	145
Figure 4.7.	Digested (A) pJa Vector and (B) pET11a with STG2 insert.	146
Figure 4.8.	Superimposed diagram of STG1 and STG2 in lateral view.	148
Figure 4.9.	Bacterial growth pattern of <i>E. coli</i> BL21(DE3) expressing STG2.	150
Figure 4.10.	Gel analysis of pET11a-STG2 expressed in <i>E. coli</i> BL21 (DE3).	151
Figure 4.11.	Gel analysis of soluble and insoluble fractions of pET11a-STG2.	152
Figure 4.12.	Purification profile of solubilized STG2.	154
Figure 4.13.	Gel analysis of solubilized STG2 purified with Nickel-Chelating Resin.	155
Figure 4.14.	STG2 refolded with one-step dialysis fails to inhibit platelet aggregation induced by HIT IgG and heparin.	157
Figure 4.15.	Purification profile of solubilized STG2.	159
Figure 4.16.	STG2 refolded with step-wise dialysis inhibits platelet aggregation induced by HIT IgG and heparin.	160
Figure 4.17.	STG2 refolded with step-wise dialysis did not interact with human platelets.	162
Figure 4.18.	Purification and on-column refolding profile of solubilized STG2. ...	164
Figure 4.19.	Gel analysis of the purified refolded STG2.	165
Figure 4.20.	STG2 refolded on-column interacts with human platelets.	167
Figure 4.21.	Elution profile of STG2 after on-column refolding.	170
Figure 4.22.	Binding activity of on-column refolded STG2.	171
Figure 4.23.	Elution profile of STG2 after incorporation into SMALPs.	173
Figure 4.24.	Gel analysis of purified STG2 incorporated into SMALPs.	174
Figure 4.25.	STG2 (incorporated into SMALPs) interacts with human platelets.	175

Figure 4.26.	Purified STG2 (incorporated into SMALPs) leads to spontaneous platelet aggregation.....	177
Figure 4.27.	Elution profile of soluble STG2.....	178
Figure 4.28.	Gel analysis of purified soluble STG2.....	179
Figure 4.29.	Soluble STG2 interacts with human platelets.....	181
Figure 4.30.	STG2 inhibits platelet aggregation induced by HIT IgG and heparin.	183
Figure 4.31.	Soluble STG2 inhibits platelet activation induced by HIT serum and heparin.....	183
Figure 4.32.	Amino acid sequence alignment between the variable regions of STG1 and STG3.....	185
Figure 4.33.	Nucleotide and deduced amino acid sequences of VH and VL regions of STG3.....	186
Figure 4.34.	Superimposed diagram of STG1 and STG3 in lateral view.....	188
Figure 4.35.	Bacterial growth pattern of <i>E. coli</i> BL21(DE3) expressing STG3.....	189
Figure 4.36.	Gel analysis of pET11a-STG3 expressed in <i>E. coli</i> BL21 (DE3).....	190
Figure 4.37.	Elution profile of soluble STG3.....	192
Figure 4.38.	Gel analysis of purified soluble STG3.....	193
Figure 4.39.	Soluble STG3 interacts with human platelets.....	194
Figure 4.40.	STG3 inhibits platelet aggregation induced by HIT IgG.....	196
Figure 4.41.	Soluble STG3 inhibits platelet activation induced by HIT Serum and heparin.....	196
Figure 4.42.	Determination of circulating human platelet numbers using counting beads.....	198
Figure 4.43.	Calculation of the concentration of human platelets circulating in mice using counting beads.....	199
Figure 4.44.	Human platelets detected in NOD/SCID mice over a period of 24 h.	200
Figure 4.45.	Survival of human platelets in NOD/SCID mice after introduction of HIT IgG, PF4 and Heparin.....	202
Figure 5.1.	Diagrammatic representation of different formats of BsAb.....	212
Figure 5.2.	Diagram of the GPIb-IX-V complex.....	216
Figure 5.3.	Functional binding sites located on GPIb α	217
Figure 5.4.	Nucleotide and deduced amino acid sequences of VH and VL regions of muAK2.....	220

Figure 5.5.	Amino acid sequence alignment between the variable regions of muAK2 and huAK2.	221
Figure 5.6.	Nucleotide and deduced amino acid sequences of VH and VL regions of humanized AK2.	223
Figure 5.7.	Cloning of STGK2 into pET11a.	224
Figure 5.8.	Bacterial growth pattern of <i>E. coli</i> BL21(DE3) producing STGK2.	225
Figure 5.9.	Gel analysis of STGK2 expressed in <i>E. coli</i> BL21 (DE3).	226
Figure 5.10.	Affinity chromatography of purification and on-column refolding of solubilized STGK2.	228
Figure 5.11.	Gel analysis of the purified refolded STGK2.	229
Figure 5.12.	Binding of AK2 MoAb to human platelets.	232
Figure 5.13.	Refolded STGK2 interacts with human platelets.	233
Figure 5.14.	STGK2 leads to platelet aggregation in the absence of HIT IgG.	235
Figure 5.15.	Diagrams illustrating the interactions between GPIIb/IIIa and FcγRIIIa in the presence of different molecules.	240

List of Tables

Table 1.1.	Clinical Scoring System for HIT: The “4 T’s”	25
Table 1.2.	HIT Expert Probability (HEP) Score	28
Table 1.3.	Non-heparin anticoagulants for the treatment of Heparin-Induced Thrombocytopenia	34
Table 1.4.	Possible new approaches for the treatment of HIT	36
Table 3.1.	PCR conditions for VH amplification	92
Table 3.2.	PCR conditions for VL amplification	92
Table 3.3.	PCR conditions for extension of VH and VL regions	98
Table 3.4.	PCR conditions for creating STG1 short and medium linker	102
Table 3.5.	PCR conditions to introduce additional segments to both extended variable regions of STG1 long linker	105
Table 3.6.	PCR conditions to create STG1 long linker	107
Table 4.1.	Summary on purification and refolding of STG2	166
Table 5.1.	BsAbs developed for clinical usage	214
Table 5.2.	Summary on purification and refolding of STGK2	230

List of Abbreviations

¹⁴ C-5HT	Hydroxytryptamine Binoxalate, 5-[2- ¹⁴ C]-(Serotonin)
aa	Amino Acid
ABI	Applied Biosystems
Ab	Antibody
ACD	Acid Citrate Dextrose
ACT	Activated Coagulation Time
ADP	Adenosine Diphosphate
AF488	Alexa Fluorophore [®] 488
AF594	Alexa Fluorophore [®] 594
AF647	Alexa Fluorophore [®] 647
AK1	Anti-GPIX Monoclonal Antibody
AK2	Anti-GPIb α Monoclonal Antibody
aPTT	activated Partial Thromboplastin Time
ATCC	American Type Collection Culture
ATIII	Antithrombin III
β -OG	n-octyl- β -D-glucoside
β -ME	2-mercaptoethanol
BLAST	Basic Local Alignment Search Tool
bp	base pair
BsAb	Bispecific Antibody
BSA	Bovine Serum Albumin
BSS	Bernard-Soulier Syndrome
cDNA	complementary Deoxyribonucleic Acid
CDR	Complementarity Determining Region
CO ₂	Carbon Dioxide
CV	Column Volume
DAG	Diacylglycerol
DMEM	Dulbecco's Modified Eagle's Medium
DMPC	Dimyristoylphosphatidylcholine
DMSO	Dimethyl Sulfoxide
DNA	Deoxyribonucleic Acid
dNTP	Deoxyribonucleotide Triphosphate

DPBS	Dulbecco's Phosphate Buffered Saline
DTI	Direct Thrombin Inhibitor
DTT	DL-Dithiothreitol
DVT	Deep Vein Thrombosis
EBI	European Bioinformatics Institute
EC	Endothelial Cell
<i>E. coli</i>	<i>Escherichia Coli</i>
EDTA	Ethylenediaminetetraacetic Acid
EIA	Enzyme-linked Immunosorbent Assay
Fab	Monovalent Antigen-binding Fragment of IgG
F(ab') ₂	Bivalent Antigen-binding Fragment of IgG
Factor IIa	Thrombin
FBS	Fetal Bovine Serum
Fc	Crystallisable Fragment of IgG
FcγRIIa	Low affinity immunoglobulin gamma platelet Fc receptor. Also known as CD32a.
FDA	Food and Drug Administration
FITC	Fluorescein Isothiocyanate
FR	Framework Region
Fv	Variable Fragment of IgG
g	gram
g	gravitational force
GAG	Glycosaminoglycan
Gly	Glycine
GP	Glycoprotein
GSH	L-Glutathione reduced
GSSG	-(-)Glutathione, oxidized
H	Histidine
h	Hour
H ₂ O	Water
HAMA	Human Anti-Murine Antibody
HCl	Hydrochloride
HEP	Heparin-Induced Thrombocytopenia Expert Probability Score

HF	High-Fidelity
HIPA	Heparin-Induced Platelet Activation
His	Histidine
HIT	Heparin-Induced Thrombocytopenia
HR	High Responder
HRP	Horseradish Peroxidase
hu	human
IEC	Ion-Exchange Chromatography
IgA	Immunoglobulin A
IgG	Immunoglobulin G
IgM	Immunoglobulin M
IMAC	Immobilized Metal Ion Affinity Chromatography
IMGT®	The international ImMunoGeneTics information system®
IP ₃	Inositol 1,4,5-triphosphate
IPTG	Isopropyl-β-galactopyranoside
ITAM	Immunoreceptor Tyrosine-based Activation Motif
ITP	Immune Thrombocytopenia
IU	International Unit
IV	Intravenous
IV.3	Anti-FcγRIIa Monoclonal Antibody
kb	kilo base pair
kDa	kiloDalton
kg	kilogram
KKO	Murine monoclonal anti-human PF4/heparin antibody
L	litre
LMWH	Low Molecular Weight Heparin
LR	Low Responder
M	Molarity
MAPK	Mitogen-Activated Protein Kinase
MgCl ₂	Magnesium Chloride
μg	microgram
mg	milligram
min	minute

μl	microlitre
ml	milliliter
μm	micrometer
μmol	micromole
μM	microMolarity
mM	milliMolarity
MoAb	Monoclonal Antibody
mRNA	messenger Ribonucleic Acid
mu	murine
NCBI	National Centre for Biotechnology Information
NEB	New England Biolabs
ng	nanogram
nm	nanometer
nM	nanoMolarity
NOD/SCID	Non-obese Diabetic /Severe Combined Immunodeficiency Mice
OD	Optical Density
ODSH	2-O, 3-O Desulfated Heparin
PaGIA [®]	Particle Gel Immunoassay ID-heparin (H)/PF4
PARs	Protease-Activated Receptors
PBS	Phosphate Buffered Saline
PCR	Polymerase Chain Reaction
PDB	Protein Data Bank
PelB-ss	PelB secretion signal
PE	Phycoerythrin
PF4	Platelet Factor 4
PI3K	Phosphatidylinositol 3-Kinase
PIP ₂	Phosphatidylinositol 4,5-biphosphate
PIP ₃	Phosphatidylinositol 3,4,5-triphosphate
PKC	Protein Kinase C
PLC	Phospholipase C
pmol	picomole
PMSF	Phenylmethylsulfonide Fluoride
PPP	Platelet Poor Plasma

PRP	Platelet Rich Plasma
qRT-PCR	quantitative Reverse-Transcription polymerase chain reaction
R	Arginine
RA	Rheumatoid Arthritis
RNA	Ribonucleic Acid
rpm	round per minute
scFv	single-chain Variable Fragment
SD	Standard Deviation
SDR	Specificity-Determining Residue
SDS-PAGE	Sodium Dodecyl Sulfate-Polyacrylamide Gel Electrophoresis
sec	second
Ser	Serine
SFK	Src Family Kinases
SIB	Swiss Institute of Bioinformatics
SMALP	Styrene Maleic Acid Lipid Particle
SRA	Serotonin Release Assay
STG1	IV.3 derived scFv
STG2	Humanized STG1 (1 st Version)
STG3	Humanized STG1 (2 nd Version)
STGK2	Bispecific Antibody Humanized AK2 scFv linked to STG2
Syk	Spleen tyrosine kinase
TAE	Tris base, Acetic Acid, EDTA
TBST	Tris base, NaCl, Tween-20
TE	Tris-EDTA buffer
TP	Thromboxane A ₂ /Prostaglandin H ₂ receptor
UFH	Unfractionated Heparin
ULC	Ultra-large Complex
vWF	von Willebrand factor
VH	Variable Heavy Chain
VL	Variable Light Chain
vWF	von Willebrand factor

List of Publications and Awards

Conference Proceedings

Jaa Yien New, Jose Perdomo, Xing-Mai Jiang, and Beng Chong. (2012). *Heparin-Induced Thrombocytopenia and Thrombosis: Therapeutic Strategy Using a Single-Chain Variable Fragment (scFv) Antibody*. Blood (ASH Annual Meeting Abstracts), Nov 2012; 120: 3346.

Jaa Yien New, Jose Perdomo, Xing-Mai Jiang, and Beng Hock Chong. (2011). *Heparin-induced thrombocytopenia and thrombosis – a new emerging therapeutic strategy*. Journal of Thrombosis and Haemostasis, July 2011; 9(s2): 530.

Conference Presentations

XXIII Congress of the International Society on Thrombosis and Haemostasis (ISTH), 2011 – Kyoto International Conference Centre, Kyoto, Japan. Abstract accepted for poster presentation: *Heparin-Induced Thrombocytopenia and Thrombosis - A New Emerging Therapeutic Strategy*.

The St. George and Sutherland Medical Research Symposium, 2011 – St. George Bank Auditorium, Kogarah NSW, Australia. Abstract accepted for oral presentation: *Heparin-Induced Thrombocytopenia and Thrombosis-Therapeutic Strategy using Single-Chain Variable Fragment (scFv)*.

HAA-ISHAPD 2011 – Darling Harbour Convention Centre, Sydney NSW, Australia. Abstract accepted for poster presentation: *Heparin-Induced Thrombocytopenia and Thrombosis-A New Emerging Therapeutic Strategy*.

Australian Society for Medical Research (ASMR) New South Wales Annual Scientific Meeting, 2012 – Australian Technology Park, Redfern NSW, Australia. Abstract accepted for oral presentation: *Heparin-Induced Thrombocytopenia and Thrombosis-Therapeutic Strategy using Single-Chain Variable Fragment (scFv)*.

Asian-Pacific Society on Thrombosis and Hemostasis (APSTH)/ Japanese Society of Thrombosis and Hemostasis (JSTH) Joint Symposium at the Annual Meeting of JSTH,

2012 – Hyatt Regency Hotel, Tokyo, Japan. Abstract accepted for oral presentation: *Heparin-Induced Thrombocytopenia and Thrombosis-Therapeutic Strategy using Single-Chain Variable Fragment (scFv)*.

Australian Vascular Biology Society (AVBS) 20th Annual Scientific Meeting, 2012 – Hyatt Regency, Sanctuary Cove, Gold Coast, Queensland, Australia. Abstract accepted for poster presentation: *Heparin-Induced Thrombocytopenia -Therapeutic Strategy Using Single-Chain Variable Fragment (scFv)*.

American Society of Hematology (ASH) 54th Annual Meeting, 2012 – Georgia, Atlanta, America. Abstract accepted for poster presentation: *Heparin-Induced Thrombocytopenia and Thrombosis: Therapeutic Strategy Using a Single-Chain Variable Fragment (scFv) Antibody*.

List of Awards

University International Postgraduate Award (UIPA) from The University of New South Wales - Scholarship covers tuition fee and provides living allowance of \$20,000 PA, 2009-2013.

Postgraduate Support Research Scheme (PRSS) from The University of New South Wales (\$3,300), 2011- Travel allowance to attend the XXIII Congress of the International Society on Thrombosis and Haemostasis (ISTH) 2011 held at Kyoto, Japan.

Young Investigator Award (\$1,500) for the best basic science oral presentation at the St. George and Sutherland Medical Research Symposium, 2011.

Young Investigator Award for oral presentation at the APSTH/JSTH Joint Symposium, 2012 – Travel allowance to attend the symposium held at Tokyo, Japan. An article in relation to this award was published in the 4th Issue of APSTH Newsletter (July 2012, Volume 1).

1st Runner Up and People's Choice Award (\$500) at the St. George Clinical School Postgraduate Three Minute Thesis Competition, 2012 held at Novotel, Brighton Beach, Sydney NSW, Australia.

Chapter 1

Introduction

Heparin-Induced Thrombocytopenia

Heparin-Induced Thrombocytopenia (HIT) is a life and limb threatening disorder that occurs in patients receiving heparin therapy. The occurrence of HIT is due to the generation of a specific antibody (Ab) that recognizes the immune complex formed between a specific platelet protein and heparin. Clinical diagnosis of HIT is based on features such as a drop in platelet count (5 days after initiation of heparin therapy) and the development of thrombosis. Laboratory diagnosis relies on the detection of HIT antibodies (Abs) via EIA and platelet activation in the presence of heparin. The current treatment for HIT is limited and relies primarily on immediate cessation of heparin and prescription of alternative anticoagulants.

1.1. Heparin

Heparin is one of the oldest biological drugs in the field of thrombosis and haemostasis. It was accidentally discovered in 1916 by McLean and the term 'heparin' was coined two years later by Howell in reference to its origin from the liver (1, 2). The isolation of heparin was subsequently attempted by several groups and it was shown that crude preparations of heparin administered to human patients gave rise to toxic reactions like severe headache, high fever and nausea (3, 4). It was not until 1935 that a highly purified form of heparin deemed safe for clinical usage was obtained by Jorpes (5). Both Crafoord and Murray then went on to demonstrate that thrombosis could be prevented with heparin (6, 7). Following a string of clinical trials, heparin was then introduced as an effective anticoagulant for the prevention and treatment of venous and arterial thromboembolic diseases.

1.1.1. Clinical Usage of Heparin

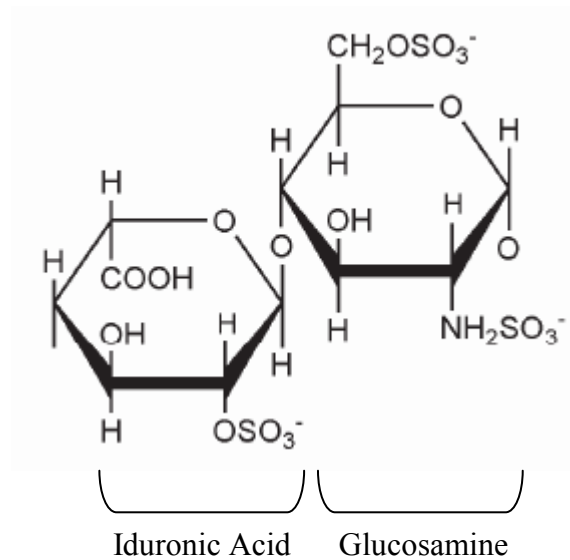
As of 2011, it was reported that therapeutic heparin records gross sales of approximately \$4 billion annually, which demonstrate its wide application in medical care (8). Several advantages such as low cost, immediate onset of action, short half-life, ability to be reversed (using protamine) and easy laboratory monitoring makes it the primary choice of anticoagulant. Besides its use in patients at risk of venous thromboembolism (i.e. pulmonary embolism), heparin also plays an important role in cardiovascular therapy. It is used in therapeutic procedures like percutaneous

transluminal coronary angioplasty and coronary artery bypass surgery (9). In addition, heparin is prescribed to patients for treatment of unstable angina and for prevention of acute myocardial infarction due to coronary thrombosis (10). Other clinical settings that involve the usage of heparin include hemodialysis (patency of extracorporeal circuit) and hip replacement therapy (11, 12). During the course of heparin treatment, the dosage is closely monitored as the anticoagulant response could vary among patients. The concentration of therapeutic plasma heparin is measured with either protamine titration, which usually falls between 0.2 to 0.4 I.U./mL or anti-factor Xa chromogenic assay that falls between 0.3 to 0.7 I.U./mL. This should be equivalent to a ratio of 1.5 to 2.5 calculated in the activated partial thromboplastin time (aPTT) test, which is the recommended therapeutic range (13).

1.1.2. Mode of Action of Heparin

Heparin consists of repeating disaccharide subunits of uronic acid (iduronic or glucuronic acid) and glucosamine. The majority of disaccharide repeats contain 80% of both iduronic acid and a disulfated glucosamine (Figure 1.1A) (14). Currently, two forms of heparin - unfractionated heparin (UFH) and low molecular weight heparin (LMWH) - are available in the market. Unfractionated heparin is a heterogeneous mixture of glycosaminoglycans (GAGs) with a mean molecular weight ranging from 12-15,000 Daltons (15). It binds antithrombin III (ATIII) through the pentasaccharide sequence found in one-third of heparin chains (Figure 1.1B) (14). This enhances the serine protease inhibitory activity of ATIII by 1,000 fold. Together, UFH and ATIII specifically inhibit activated factors IIa (thrombin) and X (Figure 1.2) while factors IXa, XIa and XIIa are less affected (16). Due to the fact that only one-third of the heparin chains are needed to exert its high affinity binding to AT-III, a shorter version of heparin was developed in the 1980s (17).

A



B

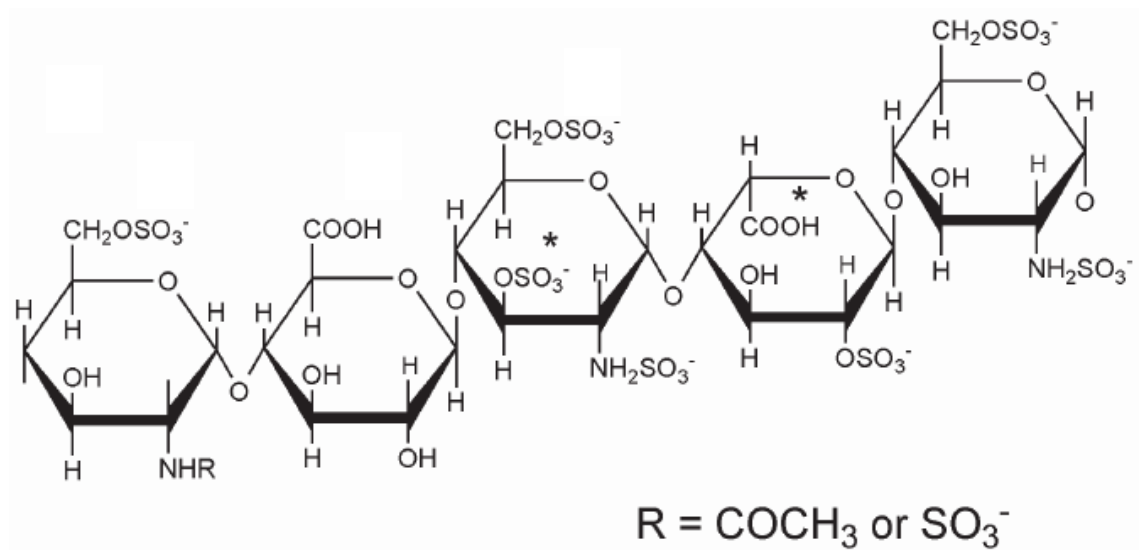


Figure 1.1 Chemical structure of heparin. A. Main repeating disaccharide unit of heparin and B. Pentasaccharide sequence in heparin that binds antithrombin III with high affinity. Reprinted with permission from Gray et al (18).

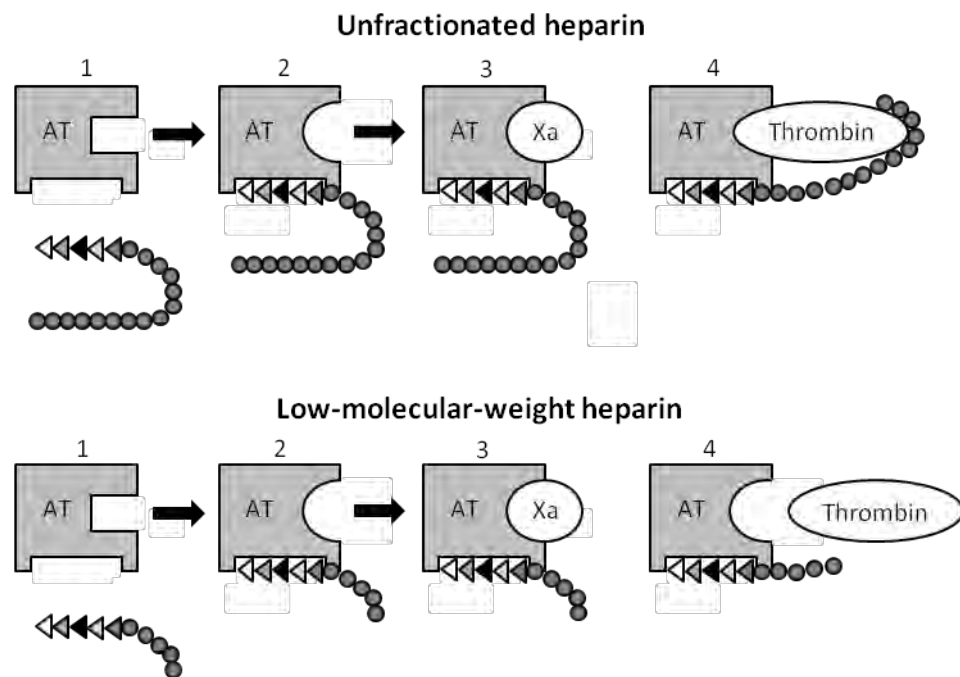


Figure 1.2. The mechanism of action of different forms of heparin. Both unfractionated and low molecular weight heparin bind to Antithrombin III which further inhibit factor Xa. Unfractionated heparin is able to simultaneously bind AT-III and thrombin (factor IIa); low molecular weight heparin inhibits thrombin to a lesser extent due to the shorter length of its saccharide units. Adapted from Nutescu and Racine (19).

LMWH is synthesized from UFH by enzymatic or chemical depolymerisation and has a mean molecular weight ranging from 5-8,000 Daltons (15). Similarly to UFH, LMWH binds and induces a conformational change in AT-III. This accelerates the activity of ATIII to interact with factors II and X (Figure 1.2). However, due to the shorter length of LMWH, it is more specific for factor Xa and have less inhibitory effect on factor IIa as compared to UFH (Figure 1.3) (19). LMWH has a longer plasma half-life (4 to 6 hours) compared to UFH (1 to 2 hours) and has higher bioavailability. This serves as an advantage, for example in the prevention of deep vein thrombosis (DVT), where a single daily subcutaneous injection is needed instead of continuous infusion, rendering laboratory monitoring unnecessary (17).

1.2. History of HIT

The side effects of heparin were first reported in 1942 when a drop in platelet count in mice and dogs was observed after heparin administration (20). However, it was only in 1969 that the term “heparin-induced thrombocytopenia” was used by Natelson where he describes a 78-year-old man suffered from pulmonary embolism developed severe thrombocytopenia after receiving heparin treatment for 10 days (21). The first initial indication that heparin may lead to thrombotic events was presented in 1958. A report was published by Weismann and Tobin demonstrating that 10 patients receiving heparin presented with femoral arterial thromboembolism. However, they suggested that this was due to the pre-existing mural aortic fibrin-platelet thrombi in these patients, which upon administration of heparin as an anticoagulant were dislodged and migrated to the lower limb arteries leading to emboli (22). A causative action of heparin inducing thrombosis was not recognized at that time. Five years later, another group of vascular surgeons reported that 11 patients receiving heparin for 10 days or more developed arterial embolism (23). The fact that these thrombotic events occurred approximately 1 week after heparin administration clearly demonstrates the delayed-onset of HIT.

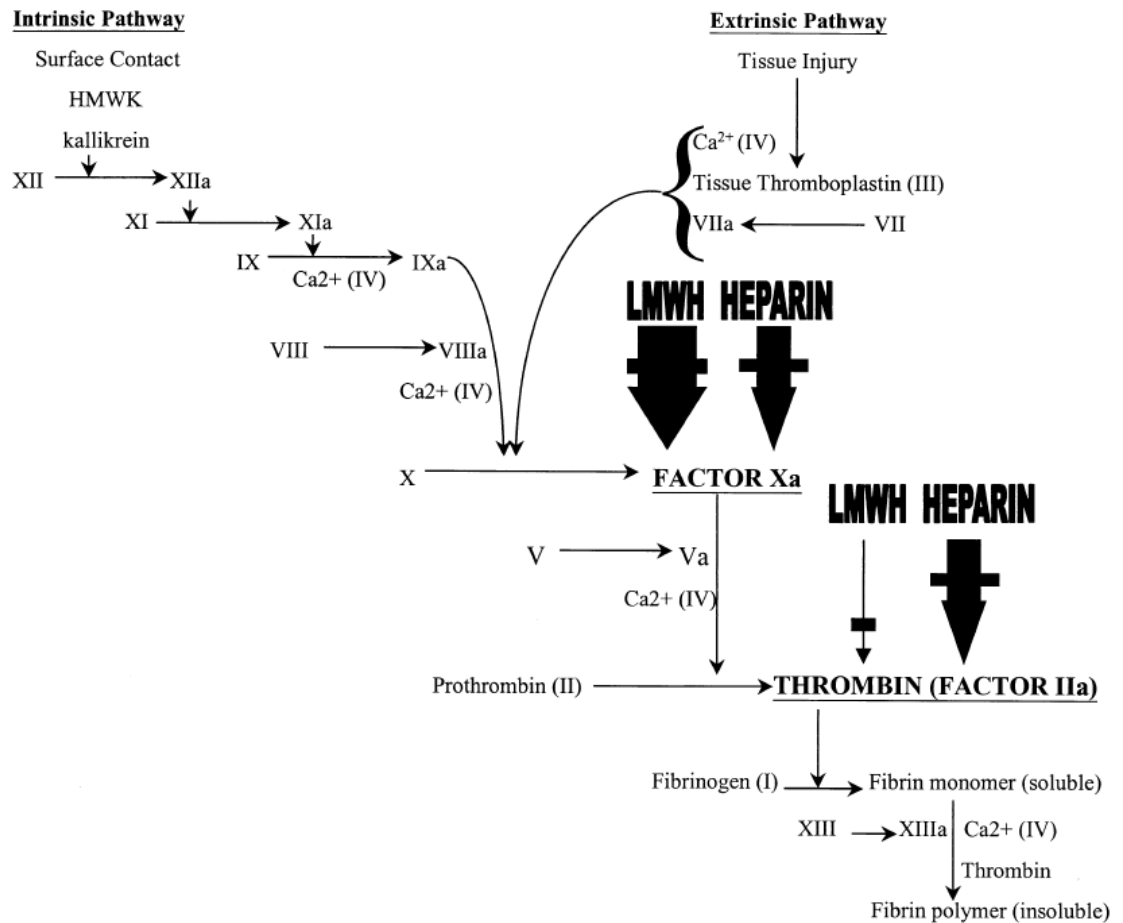


Figure 1.3. Sites of action by different forms of heparin on the coagulation cascade. Unfractionated heparin has the same inhibitory activity on both factor IIa (Thrombin) and factor Xa; low molecular weight heparin has a greater inhibitory activity on factor Xa but lesser on factor IIa. Reprinted with permission from Frangos et al (16).

In 1973, Rhodes and co-workers established the immune pathogenesis of HIT which links thrombocytopenia and thrombosis to heparin. They made a key observation of HIT where patients developed thrombocytopenia immediately after re-exposure to heparin (24). The immune basis for HIT was then suggested, based on the circulating heparin dependent, platelet aggregating substance-immunoglobulin (IgG) that was found in the patient's blood. This pathogenesis was further supported by another report by Rhodes showing that eight patients suffered from thrombocytopenia, accompanied with complications of thromboembolic and hemorrhagic events after heparin administration (25). Heparin-dependent Abs were also detected in five of the patients. More reports with patients presenting side effects of heparin emerged towards the end of 1970s together with the evidence of platelet aggregation induced by IgG purified from patient's blood (26-29). These observations suggested that HIT is primarily immune-mediated. However, as more studies were being conducted, it was soon discovered that HIT could also occur in the absence of immune responses (27, 30, 31). This eventually led to the establishment of two different groups of HIT, which were coined by Chong and Berndt in 1989 as "Type I HIT" for nonimmune/mild early-onset of HIT and "Type II HIT" for immune/delayed-onset of HIT (32).

1.3 Two types of HIT

1.3.1 Mild Early-Onset Thrombocytopenia (Type I)

Type I HIT is regarded as the benign form of heparin-induced thrombocytopenia and occurs during the first few days of the therapy. This is due to the direct interaction between heparin and circulating platelets leading to a proaggregating effect. The extent of aggregation is largely dependent on the degree of sulphation of heparin (33). The activated platelets are subsequently sequestered by the spleen resulting in thrombocytopenia (34). The platelet count rarely falls below $100 \times 10^9/L$ and usually restores even with continuation of heparin therapy (35).

1.3.2. Severe Delayed-Onset Thrombocytopenia (Type II)

Type II HIT is the more severe form with a delayed onset that develops after 5-10 days of heparin therapy. It is classically defined as a low platelet count (<150,000 per cubic millimeter) or with a decrease of 50 percent or more from the baseline (36). After cessation of heparin, the platelet count usually restores to normal levels within five to seven days (35). In rare cases, HIT could also develop in patients no longer receiving heparin. The phenomenon occurs more than 10 days after heparin exposure but rarely after 15 days (37, 38). Type II HIT patients not only risk developing thrombocytopenia, but also risk suffering from thrombotic complications which often results in morbidity and mortality. These complications include arterial thrombosis such as acute myocardial infarction, stroke; venous thrombosis such as skin necrosis and end-organ damage (39). The severity of the second form of HIT has always been an active research area and is often regarded as ‘HIT’ alone without stating the type (40).

1.4. Clinical Features of HIT

HIT is usually associated with thromboembolic events which could occur in approximately 50% of HIT patients (Figure 1.4) (41). As the platelet count continues to decrease, patients are at a higher risk of developing HIT-related thrombosis (42). The occurrence of venous thrombosis such as lower extremity deep vein thrombosis (DVT) and pulmonary embolism predominate over arterial thrombosis by an overall ratio of 2.4:1 (42). If the patient with DVT is further treated with coumarin such as warfarin, before their underlying thrombosis has been well controlled by an alternative anticoagulant, they are at risk of developing venous limb ischemia such as venous limb gangrene or *phlegmasia cerulea dolens* (43, 44). This is due to the disturbed procoagulant-anticoagulant balance where the occurrence of HIT creates a hypercoagulability state (marked increase in thrombin generation) and warfarin impairs synthesis of Protein C and Protein S (Vitamin K-dependent anticoagulant factor) (43). Approximately 5 to 15% of HIT patients who suffer from limb gangrene require amputation (45).

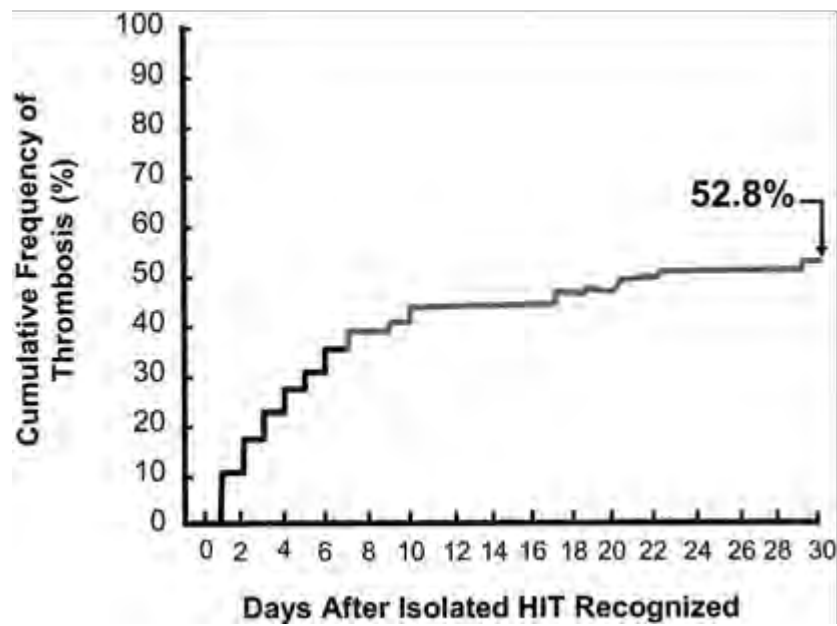


Figure 1.4. Cumulative frequency of thrombosis in Type-II HIT patients. Approximately 50% of HIT patients with isolated thrombocytopenia developed thrombosis during the subsequent 30-day period. Reprinted with permission from Warkentin and Kelton (41) .

Venous thrombosis could also occur at the upper limb. This was observed in 10% of HIT patients inserted with central venous catheter (CVC) (46). The study demonstrated that the use of such catheters or devices causes vascular injury (localizing factor) and interacts with the systemic hypercoagulability state of HIT. This risk factor could therefore influence the location of thrombosis. Other examples of HIT-associated thrombosis are cerebral sinuses thrombosis and adrenal venous occlusion leading to bilateral adrenal hemorrhage and adrenal failure (41, 47). The death of patients suffering from the consequences of HIT can be as high as 20% (45), regardless of the alternative treatment received.

The ratio of venous thrombosis preceding arterial thrombosis is altered in patients exposed to different risk factors. This was noted in patients undergoing cardiovascular surgery, with a predominance of arterial thrombosis (42). Arterial thrombosis most frequently involves distal aorta and lower extremities. This leads to ischemic gangrene of digits with absence of pulses (39). In some HIT patients, the occurrence of arterial thrombotic events might lead to stroke (death in worst case scenario), acute myocardial infarction, bowel infarction and renal infarction. This is due to the formation of thrombi either *in situ* or embolism mobilized from a more proximal location that occludes the arteries, resulting in these clinical complications (48). Some patients may present with skin lesions at the subcutaneous heparin injection sites (49, 50). These skin lesions may range from erythematous plaques to skin necrosis. Intravenous bolus heparin injection which leads to acute systemic reactions and the presentation of overt disseminated intravascular coagulation are some of the rare clinical pictures that could be potentially observed in HIT patients (39).

1.5. Pathogenesis of HIT/T

HIT is an autoimmune disease mediated by an Ab that activates platelets. This specific Ab is induced by an endogenous protein platelet factor 4 (PF4) that undergoes conformational changes in the presence of heparin thus exposing the cryptic neoepitopes that constitute the antigenic site (51, 52).

1.5.1. The Immune Complex

PF4 belongs to the CXC chemokine family and mature human PF4 is a single chain 70 amino acid molecule with a molecular weight of 7780 daltons (53, 54). The protein is stored in the alpha-granules of platelets. Through a dimer intermediate, it aggregates via a bimolecular mechanism and exists as a tetramer in solution (55). At a neutral pH, PF4 exposes the basic amino acids lysine and arginine, which form a ring of positive charges around the tetramer (Figure 1.5(1)) (56, 57).

Under normal conditions, trace levels (~3ng/ml) of circulating PF4 is associated with heparan sulfate (a form of GAGs), present on the endothelial cell surfaces (58). When heparin is administered, its higher binding affinity displaces PF4 from the endothelial cell storage pool, or from the platelets surface, increasing the circulating PF4 level 15- to 30-fold for several hours (57). The linear polysaccharide heparin molecule wraps around PF4, spanning the circumference of the symmetric PF4 molecule, resulting in the exposure of binding sites for specific HIT IgG Ab (Figure 1.5(2)) (51) These binding sites, or neoepitopes have been successfully characterised by several groups using either a monoclonal anti-human PF4/heparin Ab known as KKO or IgG from HIT patients (59-62).

The complexes that form between heparin (or other GAGs) and PF4 largely depends on the nonspecific electrostatic interactions, sulphation grade, and the length of the polysaccharide chain (63). In 2005, Rauova and colleagues demonstrated that UFH and tetrameric PF4 formed ultra-large complexes (ULCs) with a molecular weight of over 670kDa in solution. It was observed that the maximal amount of the complex formed exclusively over a narrow range of PF4-Heparin molar ratio of 2:1. At a ratio of 1:1, more ULCs were formed but were accompanied by the formation of smaller complexes. The efficiency of ULCs formation decreases when incubated with low-molecular-weight heparin and no complexes were formed when PF4 was incubated with pentasaccharide fondaparinux sodium (64). This finding is consistent with the result of another study that demonstrates that heparin fractions containing at least 12 monosaccharides subunits are needed to form antigenic complexes with PF4 that are recognized by HIT patients' Abs (65). In the subsequent year, Rauova et al showed that surface-bound PF4 is able to form ULC complexes with endogenous GAGs. These

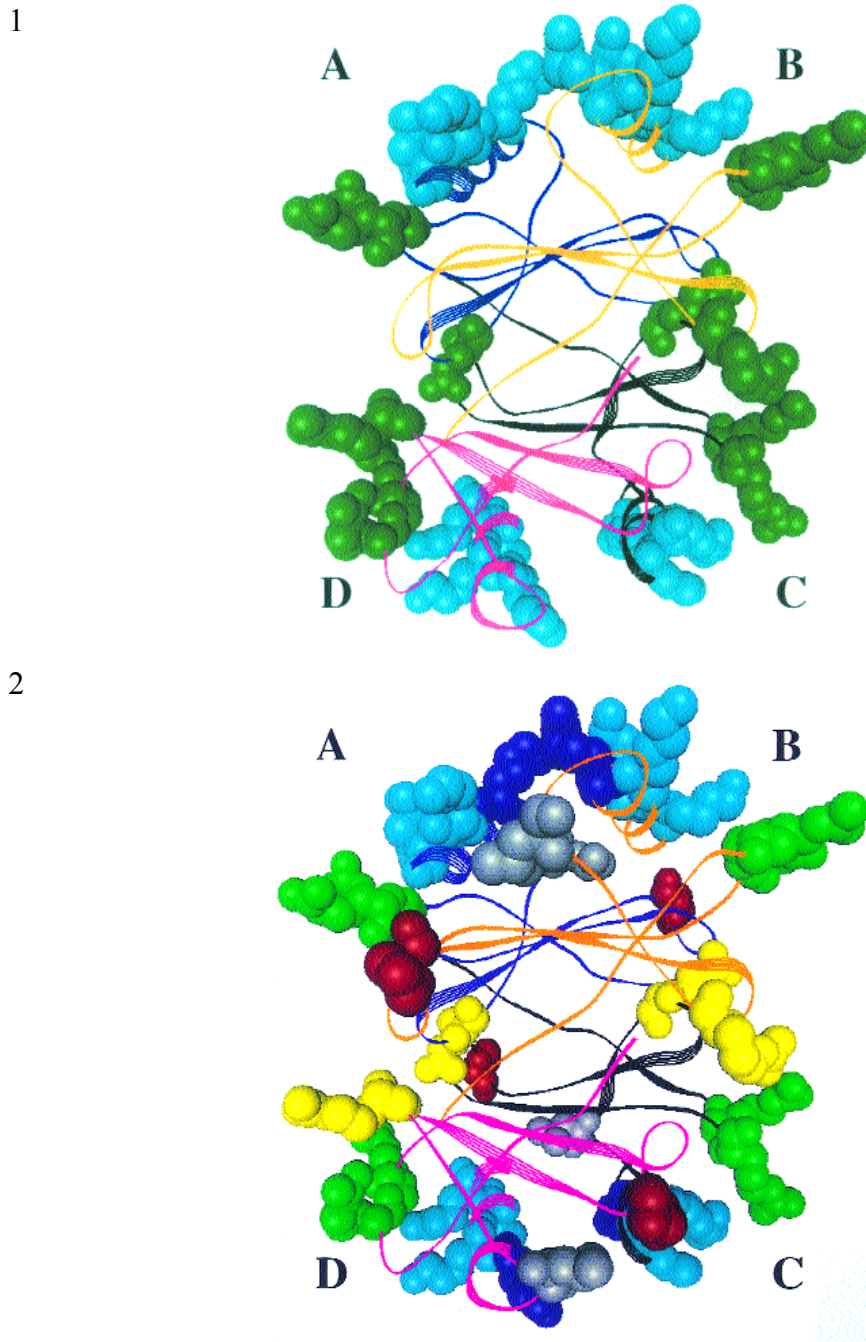


Figure 1.5. Molecular model of the human PF4 tetramer. Each monomer is represented in a ribbon diagram: A (blue), B (orange), C (black), D (pink). 1. Amino acid residues involved in heparin binding (Lysine in light blue and Arginine in green) are shown. 2. Amino acid residues involved in recognition by HIT Ab (Proline in red, Arginine in yellow, Leucine in gray, Lysine in purple) are shown. Reprinted with permission from Visentin (66)

complexes are also antigenic and individuals with high platelet PF4 levels are more susceptible to develop HIT Abs after heparinization. Thus, it was proposed that the development of thrombocytopenia could be prevented by interfering with the formation of surface PF4-GAG complexes (67).

The specific HIT IgG that is produced via the recognition of the PF4-heparin antigenic complex binds to its epitopes with high functional affinity ($K_d = 7-30\text{nM}$) (68). The Ab is of polyclonal nature with IgG1 predominating relative to the smaller amounts of IgG2 (69). Together, the PF4-heparin-Ab complex interacts with the Fc receptor on platelets (Figure 1.6) (70-72). The HIT IgG participates in the mechanism of platelet activation via both the Fab and Fc portions of the Ab. Previously, various models were proposed as to how the interaction took place. Kelton et al (1988) and Chong et al (1989) independently demonstrated that the immune complex binds to platelet Fc γ RIIa via the Fc moiety of the IgG. These investigators showed that the anti-Fc γ RIIa monoclonal Ab IV.3 neutralized the receptor and inhibited platelet activation by HIT IgG, suggesting that platelet/immune complex interaction occurred via platelet Fc receptor (70, 71).

Subsequently, other studies confirmed that the Kelton-Chong's model is true. Another finding however provided additional insights. It suggested that the HIT IgG could also interact with the platelets indirectly via the Fab portion. This was shown when the inclusion of either IV.3 or rabbit IgG (both bind to Fc γ RIIa receptors) did not prevent HIT IgG from interacting with activated platelets (73). Further evidence was provided by Newman and Chong (2000) showing that the degree of platelet activation correlates and promotes HIT IgG binding due to the release of more PF4 from the activated platelets. Similarly, blocking the Fc γ RIIa with IV.3 did not prevent HIT IgG from interacting with activated platelets. Altogether these findings suggested that the Fab portion of the HIT IgG could also associated with the platelets directly by binding to PF4-heparin complexes present on the platelet surface (Figure 1.6C). Subsequently, the Fc portion of the HIT Ab occupies the Fc γ RIIa receptor on adjacent platelets to amplify the platelet activation process (74).

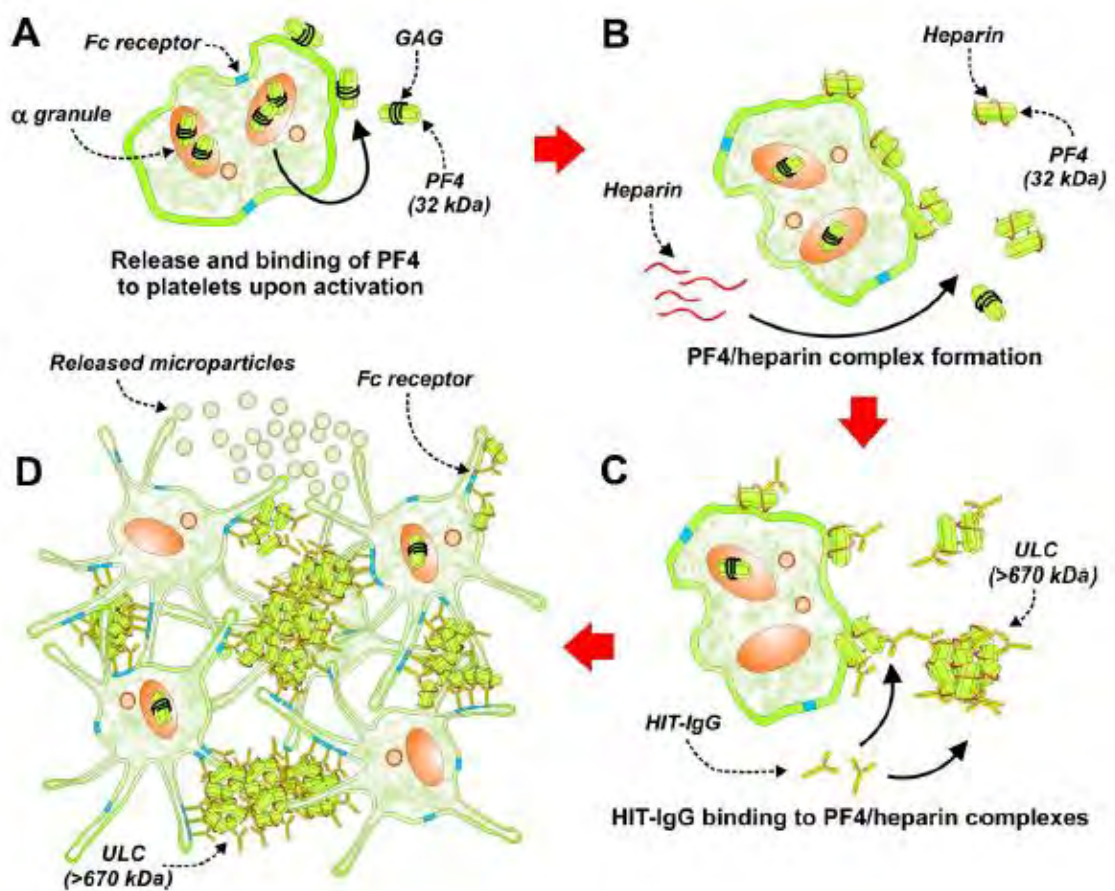


Figure 1.6. Schematic representation of the generation of PF4-Heparin-Ab Immune Complex. A. Activation of platelets leads to the release of PF4 from α -granules, some PF4 molecules enter the circulation, while other adhere to the platelet surface. B. Injected heparin displaces GAG from the surface of PF4 and binds with higher affinity. C. The exposed neoepitopes on PF4 lead to the generation of specific HIT IgG Ab. Together with PF4 and heparin, an ultra-large complex (ULC) is formed with a size of more than 670kDa. D. The ULC interacts with platelets via the Fc γ RIIa receptor on the platelet's surface, leading to the activation of platelets and the release of platelet microparticles. Reprinted with permission from Kelton and Warkentin (40).

PF4-heparin-Ab complexes binding to platelet Fc γ RIIas leads to cross-linking of the receptors, causing platelets activation and the release of platelet granular contents such as PF4, thromboxane A₂, and platelet-derived microparticles with procoagulation activity (31, 75). This causes platelet aggregation and activation of the blood coagulation pathways, thus resulting in thrombin generation and thrombosis (44, 76). The occurrence of thrombocytopenia on the other hand may be in part also due to the clearance of the PF4-heparin-Ab bound platelets by the reticuloendothelial system (77) and in part due to platelet consumption by thrombi formation.

As mentioned previously, some GAGs such as heparan sulphate, present on the endothelial cell (EC) surface, are associated with PF4 under normal conditions. However, as platelets are activated in the scenario of HIT, more PF4 is released, binds to the endothelium and forms complexes recognized by HIT Abs. Studies have demonstrated that Abs from HIT patients not only recognize EC in the presence of PF4 alone, but it can also provoke direct activation of the microvascular EC (52, 78). The injured endothelial cells could therefore lead to the initiation of the coagulation pathway. Besides EC, GAGs are also present on the surface of monocytes. Once PF4 forms complexes with these GAGs, it creates targeted binding site for HIT Abs which trigger tissue factor expression by monocytes (79, 80). Both EC and monocytes that serve as a binding site for the HIT immune complexes could therefore play a role in the pathogenesis of HIT, as proaggregating stimuli are released upon activation, resulting in thrombin generation and thrombosis.

1.6. Fc γ RIIa Receptor

The Fc γ RII (CD32) receptor is the most distributed and expressed Fc receptor on monocytes, macrophages, neutrophils, B lymphocytes and platelets (81). However, the receptor subtype-Fc γ RIIa is the only IgG Fc receptor expressed on platelets with approximately 400 to 2000 molecules per platelet (82, 83).

1.6.1. The FcγRIIa Receptor and its Polymorphism

FcγRIIa is present in two major allelic variants where a single base change from G to A causes an amino acid change in the second extracellular domain from arginine (R) to histidine (H) at position 131 (84). This change leads to a difference in the binding affinity to different subgroups of IgG. FcγRIIa-R/R131 preferentially binds to murine IgG1 and is designated as high responder (HR); FcγRIIa-H/H131 binds murine IgG1 poorly and thus is called low responder (LR) (85, 86). However, the low responder receptor on platelets is the only Fcγ receptor that interacts with human IgG2 (87).

The role of FcγRIIa polymorphisms in the pathogenesis of HIT has been debated for some time. It has been claimed that there is overrepresentation of the LR FcγRIIa gene among HIT patients as compared with control subjects (69, 88). However, contrasting observations were reported by two groups who found no statistical difference in the allele frequency of HR or LR FcγRIIa genotype between HIT patients and controls (83, 89, 90). The discrepancy of the results might be due to the low number of patients analyzed, which leaves the controversy about receptor genotype and platelet activation in HIT unresolved.

1.6.2. Platelet Activation by HIT Ab via FcγRIIa Receptor

The pathogenesis of HIT is caused by the formation of HIT immune complexes that engaged with FcγRIIa on platelets. The cross-linking of these receptors initiates a chain of signaling pathways, leading to platelet activation, producing the side effects observed in HIT patients. FcγRIIa contains an immunoreceptor tyrosine-based activation motif (ITAM). Upon receptor engagement by HIT immune complexes, the tyrosine phosphorylated FcγRIIa serves as a docking protein for tandem Src homology (SH)2 domain-containing signaling proteins, notably Lyn. This leads to the recruitment of the spleen tyrosine kinase-Syk (91, 92). The downstream effect of this Syk activation leads to recruitment of several enzymes in the signaling pathway, including phospholipase Cγ2 (PLCγ2), phosphatidylinositol 3-kinase (PI3K) and protein kinase C (PKC), ultimately resulting in the activation of platelets (Figure 1.7).

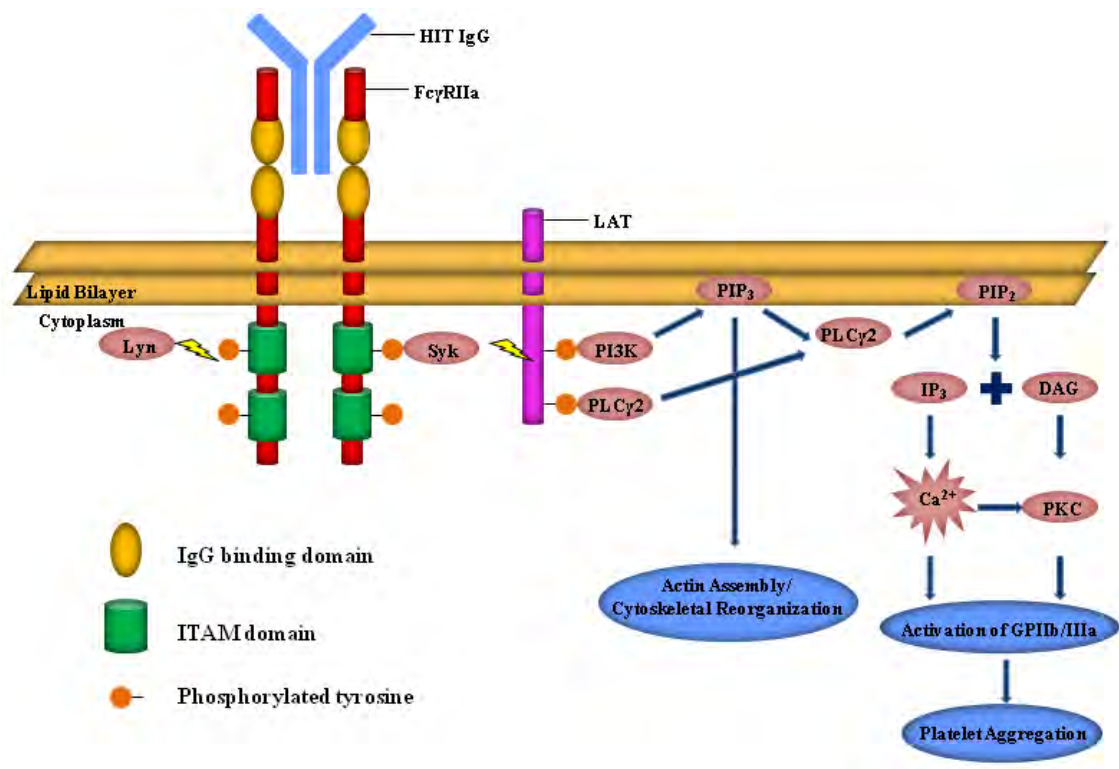


Figure 1.7. Diagram of HIT Ab-mediated signaling pathway. The tyrosine residues of the ITAM domain become phosphorylated by a Src kinase, notably Lyn when the HIT Antibody engages and initiates cross-linking of the receptor. This brings about the recruitment of Syk, which further phosphorylates the tyrosine residues in the adaptor protein LAT (Linker for Activation of T cells), resulting in the activation of phosphoinositide 3-kinase (PI3K) and phospholipase C γ 2 (PLC γ 2). The p85 α subunit of PI3K then leads to the formation of a second messenger phosphatidylinositol 3,4,5-triphosphate (PIP₃), which also recruits PLC γ 2 to the membrane. PLC γ 2 hydrolyzes phosphatidylinositol 4,5-biphosphate (PIP₂), mediating the activation of second messengers inositol 1,4,5-triphosphate (IP₃) and diacylglycerol (DAG). IP₃ causes influx of calcium while DAG activates protein kinase C (PKC), both events lead to the activation of integrin glycoprotein (GP) IIb/IIIa, promoting platelet adhesion and aggregation.

1.6.3. Platelet Activation and Signaling Pathway

Previously, the signalling pathway of Fc γ RIIIa leading to platelet activation was highlighted. While the initial platelet activation pathways of Fc γ RIIIa are different from other platelet receptors, it is interesting to note that the downstream effector signalling pathways eventually cross-link with the pathways of other platelet receptors, converging into common intracellular signalling events. The subsequent release of platelet contents such as adenosine diphosphate (ADP), thromboxane A₂, PF4, serotonin and microparticles further promote platelet activation and propagate the initiation coagulation pathways, which are crucial in the pathogenesis of HIT. This section will give a brief overview on these platelet receptors, mediators and their signalling pathways.

Platelets play important physiological roles in the events of vascular injury, thrombosis, inflammation, and atherosclerosis (93-96). However, its best known function is to maintain haemostasis by forming mechanical plugs to prevent further bleeding during injury of blood vessels. This requires several platelet functions including adhesion, aggregation, release of mediators, and further activation of platelets. All these processes are accompanied by induction of signaling events via particular receptors (Figure 1.8).

Platelet adhesion is initiated by adhesion receptors –glycoprotein (GP) Ib-IX-V and GPIIb/IIIa that interact with von Willebrand factor (vWF) and collagen. The signal transduction of both generally involves the ITAM domain present on each receptor, which is then phosphorylated by the Src family kinases (SFK) such as Lyn and Fyn (97, 98). This causes activation of PI3K, which could initiate either the Akt or the PLC γ 2 downstream signaling pathway, ultimately leading to cytoskeletal changes with changes in platelet shape, integrin activation, and granule secretion of various agonists (99-102). Different groups of platelet integrins are expressed on platelets with integrin α IIB β 3 being the most abundant. When platelet integrin α IIB β 3 is activated via inside-out signaling, it subsequently binds to vWF or fibrinogen, prompting further platelet activation, adhesion and aggregation (103).

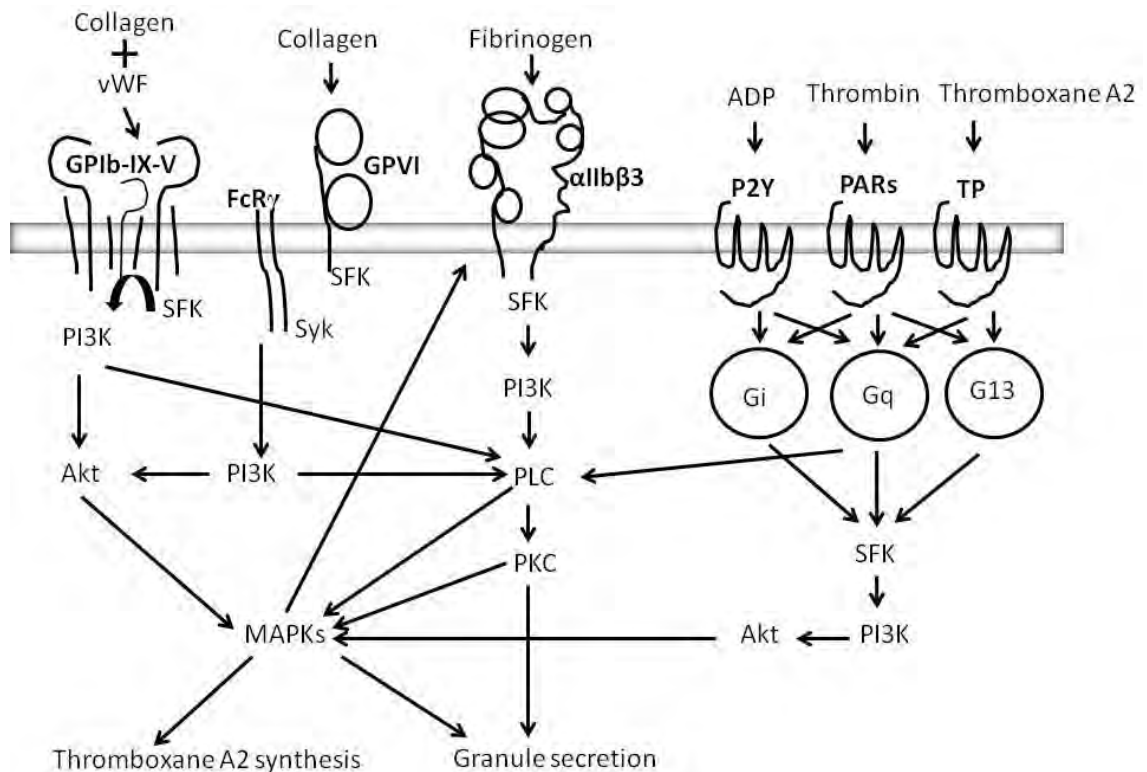


Figure 1.8. An overview of the signaling pathways of 4 major groups of platelet receptors. The binding of GPIb-IX-V and GPVI to collagen or von Willebrand factor (vWF) causes phosphorylation of Src family kinases (SFK) that activates phosphoinositide 3-kinase (PI3K). This in turn activates the Akt or phospholipase C (PLC) signaling pathway, recruiting signaling molecules that includes mitogen-activated protein kinase (MAPK). The activated MAPK subsequently initiates the inside-out signaling of integrin α IIb β 3, further activating the ligand-binding function of the integrin. In addition, thromboxane A2 is also synthesized along with secretion of granular content such as adenosine diphosphate (ADP), thrombin and thromboxane A2. These agonists mediate signal amplification via G-protein-coupled receptors (P2Y families, protease-activated receptors (PARs) and thromboxane A₂/prostaglandin H₂ receptor (TP)) involving subfamilies of G protein (Gi, Gq and G13). PI3K is then activated via phosphorylation of SFK, initiating the Akt/MAPK pathway, similarly with the signaling pathways of GPIb-IX-V and GPVI. All these signaling events ultimately lead to platelet activation, adhesion and aggregation. Adapted from Li et al (104). Abbreviations: PKC, protein kinase C.

The release of different agonists from stimulated platelets is essential for activating platelets and accelerating the coagulation cascade. Various mediators such as ADP, thrombin, serotonin or thromboxane A₂ interact with different groups of G-protein coupled receptors and activate respective signaling complexes. In addition, thrombin also serves as an agonist that activates GPIb receptor (105). All these result in the reinforcement of integrin α IIb β 3-dependent platelet aggregation, granule secretion inducing platelet activation and clot stabilization. In the scenario of HIT, the release of several agonists also contributes to its pathogenesis. The secretion of PF4 from α -granules prompts more formation of HIT immune complexes while the formation of microparticles further enhances coagulation by exposing aminophospholipids, providing binding sites for activated factor V, factor VIIIa and factor IXa, resulting in thrombin formation (106).

1.7. Animal Models of HIT

Research on animal models is important to bridge the understanding between *in vitro* and human studies. For HIT, several studies using animal models have been conducted over the past decade. However, the most notable advance was the creation of transgenic mice that express human proteins involved in HIT pathogenesis. This is due to the fact that mice do not express an analog of human Fc γ RIIa receptor on their platelets. In addition, the heparin/mouse PF4 complex is not recognized effectively by human HIT IgG (61). Transgenic mice that expressed both human Fc γ RIIa receptors and human PF4 were first created in 2001 (107). Thrombocytopenia was observed after the mice were injected with KKO (murine monoclonal Ab that recognizes human PF4/heparin complexes)(61) and heparin. A higher dosage of heparin leads to thrombosis in these mice (107). Overall, this model exhibits features consistent with those observed in HIT patients, and is therefore suitable for the study of HIT *in vivo*.

Using the same double transgenic model, further modification was made to create murine PF4 knockout mice. Studies in this animal demonstrated that hypercholesterolemia serves as a risk factor in leading to thrombocytopenia and thrombosis after KKO and heparin injection (108). A better understanding of the immunogenicity of PF4/Heparin was demonstrated using transgenic mice that expressed human FcγRIIa receptors and different levels of human PF4 (67). These studies concluded that the severity of thrombocytopenia is directly correlated to both the level of PF4 and the dosage of the Ab (KKO). It proposed that the maximal ULCs formation between PF4 with surface bound GAGs leads to greater antigenicity for KKO binding, and thus increased thrombocytopenia (67). **1.8. Incidence of HIT**

The occurrence of HIT is largely correlated with the heparin polysaccharide formulation and the clinical setting of the patients.

1.8.1. Formulation of Heparin

The formation of HIT can be attributed to the degree of sulfation of heparin with UFH demonstrating a higher possibility of causing the clinical sequelae in comparison to LMWH. Several HIT studies have been conducted in orthopedic patients (either hip or knee replacement surgery), which undergo post-surgery antithrombotic prophylaxis. Approximately 2.6%-5.2% of these patients treated with UFH developed HIT compared to 0%-0.6% of those prescribed with LMWH (36, 109, 110). Similarly, the seroconversion rate of HIT Abs detected via antigen assays was reported to be 50% in cardiac patients receiving UFH and 7.5% in orthopedic patients receiving LMWH (111). Studies conducted on cardiac patients treated with UFH detected heparin Abs in 8.7%-26.2% of patients, followed by the occurrence of HIT and complication of thrombotic events at a later stage (112, 113). Nevertheless, due to lower drug costs and certain clinical advantages e.g. drug reversibility in the prevention and treatment of deep vein thrombosis and pulmonary embolism, UFH is still widely used in clinical practice (114).

1.8.2. Groups of Patients

The incidence of HIT differs in distinct patient groups. Surgical patients are 3-fold more likely to develop HIT as compared with medical patients (115). For surgical patients that undergo major procedures, the development of HIT and seroconversion rates are found to be significantly higher relative to those with minor surgery (116). This could be due to a greater release of PF4 from activated platelets during major surgery, thus,

increasing the formation of immunogenic complexes and enhancing the immune response (117). In one study which used platelet adhesion assay for HIT Abs detection, Abs were detected in 69% of cardiac patients, 43.6% of stroke patients, and 38% of haemodialysis (HD) patients (11). Despite the frequent formation of HIT Abs in these patients, the incidence rate of developing HIT in cardiac and hemodialysis patients was reported to be less than 2% (112, 118). This was reflected in other studies where HIT occurs only in a minority of patients despite the presence of HIT Abs (111, 119-121). This phenomenon can be represented with the “Iceberg Model of HIT”, which will be reviewed later in this chapter. Two studies were also conducted on pregnant patients showing that no cases of HIT were reported even when they received heparin for up to 6 weeks post partum, however this remains to be confirmed due to the absence of a reliable study on obstetric patients treated with heparin (122, 123).

It is an intriguing fact that heparin naive patients are also at risk of developing HIT. This was particularly observed in patients suffering from bacterial infection. An explanation was then proposed whereby bacteria might be a risk factor in the development of HIT. The mechanism is such that PF4 can bind to the polyanions present on the bacterial surface, the exposed neoepitopes on PF4 thus lead to the cross-reactivity of anti-PF4/heparin Abs, forming immune complexes. This was clearly demonstrated in mice with polymicrobial sepsis where anti-PF4/heparin Abs were formed even in the absence of heparin (124). In addition, work by Greinacher et al. shows that periodontitis involving periodontal pathogens can be linked to the formation of anti-PF4/heparin Abs (125). Another interesting case study was presented by Olah et al (126). A patient was admitted with a suspected case of HIT without prior exposure to heparin. The patient, with a resolved septicemia five days earlier, succumbed to thrombocytopenia and heparin-induced necrosis 36 hours after heparin (enoxaparin) therapy. Limb gangrenes were also formed in the subsequent 24 hours. This supports the hypothesis that anti-PF4/heparin Abs can be formed in the primary response against PF4/bacteria complexes, which subsequently bind to PF4/heparin complexes, leading to rapid-onset of HIT (126).

1.9. Clinical Diagnosis of HIT

HIT should be suspected whenever thrombocytopenia occurs in patients that received heparin. For heparin naïve patients, a drop in platelet count is usually observed between 5 to 14 days after initiation of heparin. Rapid onset (within hours of re-exposure) could also occur in patients that have pre-existing HIT Abs receiving heparin in the previous 3 months (127). Thrombocytopenia of HIT is moderately severe (median platelet count nadir of $60 \times 10^9/L$) in comparison with other immune thrombocytopenic disorders such as drug-induced thrombocytopenia (median platelet count nadir of $10 \times 10^9/L$) (128). Severe thrombocytopenia (platelets less than $15 \times 10^9/L$) is not usually observed in these patients. To aid in the diagnosis of HIT, a Warkentin pretest scoring system, termed “the four T’s” (Table 1.1) was drawn up and takes into account typical features presented in HIT patients (129). These include severity of thrombocytopenia, the timing of the onset, presence of thrombosis, and the presence of other causes of thrombocytopenia (i.e. other drug-induced thrombocytopenia, autoimmune thrombocytopenia and viral or bacterial infections).

Table 1.1. Clinical Scoring System for HIT: The “4 T’s”. Reprinted with permission from Warkentin (129).

	Points (0, 1, or 2 for each of 4 categories: maximum possible score = 8)		
	2	1	0
Thrombocytopenia	> 50% fall or platelet nadir $20\text{--}100 \times 10^9/l$	30–50% fall or platelet nadir $10\text{--}19 \times 10^9/l$	fall < 30% or platelet nadir $< 10 \times 10^9/l$
Timing* of platelet count fall or other sequelae	Clear onset between d 5–10; or less than 1 d (if heparin exposure within past 100 d)	Consistent with immunization but not clear (e.g. missing platelet counts) or onset of thrombocytopenia after d 10	Platelet count fall too early (without recent heparin exposure)
Thrombosis or other sequelae (e.g. skin lesions)	New thrombosis; skin necrosis; post heparin bolus acute systemic reaction	Progressive or recurrent thrombosis; erythematous skin lesions; suspected thrombosis not yet proven	None
Other cause for thrombocytopenia not evident	No other cause for platelet count fall is evident	Possible other cause is evident	Definite other cause is present
Pretest probability score: 6–8 = High; 4–5 = Intermediate; 0–3 = Low			

*First day of immunizing heparin exposure considered d 0; the day the platelet count begins to fall is considered the day of onset of thrombocytopenia (it generally takes 1–3 d more until an arbitrary threshold that defines thrombocytopenia is passed).

1.10. Laboratory Diagnosis of HIT

Generally, two types of assays (functional and immunoassays) can be conducted to diagnose HIT. Functional assays like serotonin release assay (SRA) and heparin-induced platelet activation test (HIPA) detect platelet activation after it is induced by heparin-dependent Abs. For the former, washed platelets from 2-4 donors are incubated with patient serum and with heparin after uptake of radiolabelled serotonin into the platelets (130). For HIPA, the test monitors platelet aggregation occurring in wells of microtitre plates with constant stirring by magnetic stirrers (131). In both assays, positive results occur when therapeutic concentrations of heparin (0.1 to 0.3 IU/ml) induce release of ^{14}C -serotonin or platelet aggregation but not as high heparin concentration i.e. 100 IU/ml (77). These two functional assays were reported to have high sensitivity ranging from 88 to 100% and specificity greater than 89% (SRA) (132, 133). However, the process is laborious and technically demanding.

Compared to functional assays, immunoassays provide higher sensitivity and are available as commercial kits. Tests such as enzyme-linked immunosorbent assay (EIA) are conducted based on the detection of Abs of all major subclasses (IgG, IgA and IgM) binding to the PF4/Heparin antigenic immune complex (77). Although sensitive, this assay is also regarded as less specific/clinically significant due to the detection of IgA and IgM which do not cross-link platelet Fc γ RIIas and cause platelet activation. Debates are still ongoing on whether these Abs are pathogenic in the scenario of HIT. This leads to the possibility of over-diagnosed HIT by laboratories that rely only on EIA for diagnosis and maybe costly in terms of replacing heparin with more expensive anticoagulants like hirudin or danaparoid (134, 135). However, in 2007, a modified EIA assay that only detects IgG class Abs (termed IgG-EIA) was commercially released and it has been regarded as having similar sensitivity but greater specificity than the conventional immunoassay (136).

In 2008, a clinical-laboratory approach was demonstrated to provide a better and accurate diagnosis for HIT within 1-2h after blood sampling. The Warkentin “4T’s” scoring system are combined with particle gel immunoassay ID-heparin (H)/PF4 PaGIA[®] to confirm the diagnosis of HIT (137). Alternatively flow cytometry could also be used to detect platelet activation induced by heparin-dependent Ab using platelet

activation markers such as P-Selectin (CD62p) and Annexin V. However, in a separate evaluation by Bakchoul and coworkers, it was shown that a modified IgG-EIA provides a better diagnostic information for calculating the clinical probability of patients suspected with HIT as compared with PaGIA (138). Thus, it might be feasible to use IgG-EIA for confirmation of HIT instead of PaGIA.

Recently, a group led by Cuker proposed a pretest clinical scoring model termed HIT Expert Probability (HEP) Score (Table 1.2). The scoring system comprises clinical features of HIT which were identified via comprehensive literature review and was subsequently evaluated against the Warkentin “4T’s” scoring system. Conducted on 50 potential HIT patients, the HEP Score successfully identify HIT patients with up to 100% sensitivity and 60% specificity even before the laboratory results were known (139). However, due to the small sample size, the author stresses that a larger multicentre study is needed to prove the validity of the scoring system. Eventually, the outcome will be useful in guiding clinicians to identify patients with suspected HIT, avoiding the costs of misdiagnosis and inappropriate treatment with alternative anticoagulants.

Table 1.2. HIT Expert Probability (HEP) Score. Reprinted with permission from Cuker et. al. (139)

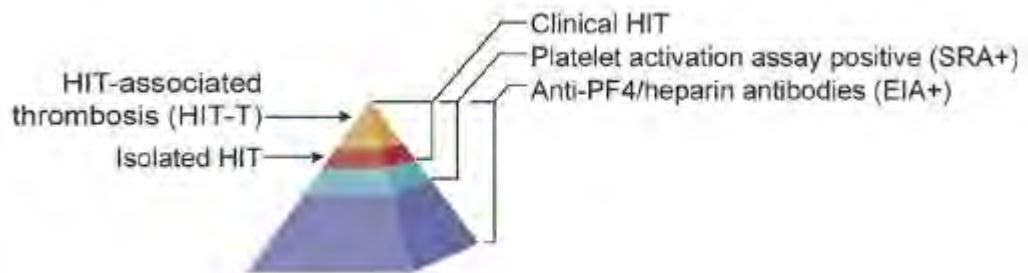
Clinical feature	Score
1. Magnitude of fall in platelet count (measured from peak platelet count to nadir platelet count since heparin exposure)	
a. < 30%	-1
b. 30% -50%	1
c. > 50%	3
2. Timing of fall in platelet count	
<i>For patients in whom typical onset HIT is suspected</i>	
a. Fall begins < 4 days after heparin exposure	-2
b. Fall begins 4 days after heparin exposure	2
c. Fall begins 5-10 days after heparin exposure	3
d. Fall begins 11-14 days after heparin exposure	2
e. Fall begins > 14 days after heparin exposure	-1
<i>For patients with previous heparin exposure in last 100 days in whom rapid onset HIT is suspected</i>	
f. Fall begins < 48 h after heparin re-exposure	2
g. Fall begins > 48 h after heparin re-exposure	-1
3. Nadir platelet count	
a. $\leq 20 \times 10^9 \text{ L}^{-1}$	-2
b. $> 20 \times 10^9 \text{ L}^{-1}$	2
4. Thrombosis (Select no more than one)	
<i>For patients in whom typical onset HIT is suspected</i>	
a. New VTE or ATE ≥ 4 days after heparin exposure	3
b. Progression of pre-existing VTE or ATE while receiving heparin	2
<i>For patients in whom rapid onset HIT is suspected</i>	
c. New VTE or ATE after heparin exposure	3
d. Progression of pre-existing VTE or ATE while receiving heparin	2
5. Skin necrosis	
a. Skin necrosis at subcutaneous heparin injection sites	3
6. Acute systemic reaction	
a. Acute systemic reaction after intravenous heparin bolus	2
7. Bleeding	
a. Presence of bleeding, petechiae or extensive bruising	-1
8. Other causes of thrombocytopenia (Select all that apply)	
a. Presence of a chronic thrombocytopenic disorder	-1
b. Newly initiated non-heparin medication known to cause thrombocytopenia	-2
c. Severe infection	-2
d. Severe DIC (defined as fibrinogen $< 100 \text{ mg dL}^{-1}$ and D-dimer $> 5.0 \mu\text{g mL}^{-1}$)	-2
e. Indwelling intra-arterial device (e.g. IABP, VAD, ECMO)	-2
f. Cardiopulmonary bypass within previous 96 h	-1
g. No other apparent cause	3

VTE, venous thromboembolism; ATE, arterial thromboembolism; DIC, disseminated intravascular coagulation; IABP, intra-aortic balloon pump; VAD, ventricular assist device; ECMO, extracorporeal membrane oxygenation.

1.11. Iceberg Model of HIT

In 1994, Warkentin and Kelton proposed that the interrelationships among clinical features of HIT and the detection of HIT Abs with different laboratory assays can be conceptualized as an “iceberg” (Figure 1.9A) (140). The mass of the iceberg represents a broad spectrum of anti-PF4/heparin Abs which can be detected by the sensitivity of immunoassays. However, only half of these Abs have platelet activating properties and could be specifically detected by functional assays. Interestingly, for some patients with strong platelet-activating Abs, clinical features of HIT weren’t observed. This might be attributed to the risk factors demonstrated by the patients such as variability of platelet FcγRIIa receptor numbers (141), availability of circulating PF4 to form immune complex (64, 67, 142), and different patient populations (111). Patients positive for HIT Abs are at risk of developing either thrombocytopenia alone, or both HIT associated with thrombocytopenia and thrombosis that forms the tip of the iceberg. The iceberg model of HIT was further utilized to represent the immunogenicity and cross-reactivity (capacity of heparin/heparin fraction to form antigens with PF4 recognized by HIT Abs) (Figure 1.9B).

A



B

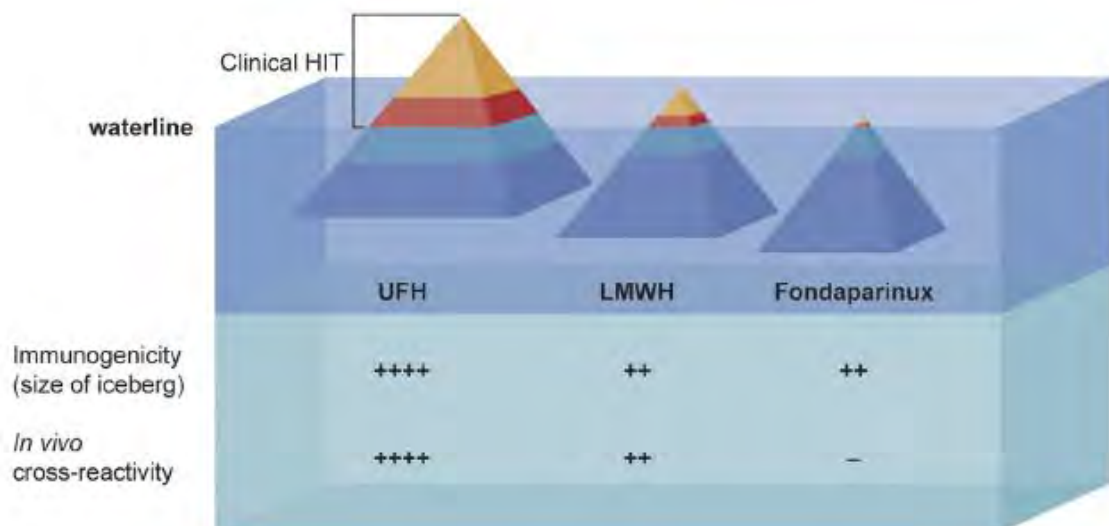


Figure 1.9. Iceberg model of HIT. A. The iceberg model of HIT illustrates the relationship among HIT-associated thrombosis, thrombocytopenia, pathogenic HIT Abs detected by serotonin release assay (SRA) and non-pathogenic HIT Abs detected by enzyme-linked immunosorbent assay (EIA). B. Different types of heparin exhibit distinct levels of immunogenicity and cross-reactivity. Visible component above the waterline represents the clinical features of HIT which sees both UFH and LMWH protrude significantly, but with UFH exhibiting much higher immunogenicity and cross-reactivity *in vivo*. In contrast, Fondaparinux forms poorly recognized antigens. Reprinted with permission from Kelton and Warkentin (40).

1.12. Management of HIT

All heparin treatments, including heparin-containing flushes and catheters should be discontinued once the patient is suspected or has been diagnosed with HIT. Though platelet count is low in HIT patients, platelet infusion should never be given since it could exacerbate the hypercoagulable state by further platelet activation by circulating HIT Ab. An alternative anticoagulant must be immediately prescribed (143). In this context, drugs that are currently available for the treatment of HIT patients will be briefly reviewed, highlighting their mode of action. For treatment of HIT, drugs that are normally available act on the coagulation cascade by inhibiting factor Xa (FXa) (directly or indirectly) or thrombin or both.

Three drugs, danaparoid, lepirudin and argatroban, have been extensively used for treatment of patients with HIT. There are large body of clinical data confirming their efficacy. Danaparoid is a low molecular weight heparinoid that is structurally distinct from unfractionated heparin. It also inhibits factor Xa indirectly via antithrombin III inhibition. In the only prospective randomized control study in the treatment of HIT, danaparoid was found to be efficacious in the management of venous and arterial thrombosis in patients with HIT and was more effective compared to dextran 70 (144). Danaparoid also has a long plasma half-life (25hour (h)) and its anticoagulant effect cannot be neutralized by protamine sulfate. Danaparoid is thus not the anticoagulant of choice for cardiopulmonary bypass surgery for patients with HIT as significant bleeding has been observed with its use for this indication. Although danaparoid generates *in vitro* cross-reactivity with the heparin-induced Ab (5-10%), but this is of no clinical significance as it does not adversely affect patient's clinical outcomes (145). *In vivo* cross-reactivity is rare.

Lepirudin is a recombinant hirudin (natural anticoagulant produced by leech) and a direct thrombin inhibitor (DTI). Lepirudin acts by forming a stoichiometric complex with one molecule of thrombin, neutralizing its thrombogenic activity (146). It is a bivalent DTI that binds to two sites of thrombin (active catalytic site and an anion-binding exosite for fibrin recognition). Unlike heparin, Lepirudin inhibits thrombin directly without the need of antithrombin III and it has a short half-life (80 minutes (min)). Thus, it is an alternative anticoagulant for patients with HIT undergoing

cardiopulmonary bypass surgery (147, 148). However, the elimination of Lepirudin is prolonged (by a factor of ten) in patients with severe renal insufficiency (creatinine clearance of 12-27min) (149). Due to the absence of antidote and slow reduction of plasma levels, it is necessary to reduce the dosage administered to renally compromised patients (48, 148). Its production has now been discontinued and is now unavailable for clinical use (150).

Argatroban is another DTI which was approved by Food and Drug Administration (FDA) in United States (US) for the treatment of HIT (52). It is a univalent thrombin inhibitor that binds to the active catalytic site of thrombin (78). With its relatively small size of 527Da, Argatroban effectively inhibits both fluid-phase and clot-bound thrombin (80). In contrast to Lepirudin, Argatroban is excreted via the hepatobiliary route. Thus, this drug which does not have an antidote should be carefully prescribed with a reduction in the initial treatment dose to HIT patients with liver dysfunction or any degree of hepatic insufficiency (151, 152). HIT treatment with Argatroban was proven to be efficacious in two historically controlled studies by Lewis and coworkers. In comparison to control patients, the Argatroban treatment group suffered much lesser events of new thrombosis (45, 153).

Bivalirudin is a synthetic DTI, a hirulog i.e. one of the drugs designed from the structure of hirudin. It undergoes partial plasma enzymatic inactivation (80%) and renal clearance (20%) (154). The anticoagulation effect of Bivalirudin is usually monitored with activated coagulation time (ACT) or activated partial or activated partial thromboplastin time (aPTT). Due to its sequence homology to Lepirudin and its short half-life (25 min), Bivalirudin was explored in the 1990s as a potential valuable alternative to heparin. It was given to patients undergoing percutaneous coronary intervention for unstable angina and as compared to heparin, lower incidence of bleeding was reported (155). Later on, favorable results were demonstrated by two studies showing that Bivalirudin is a safe and effective alternative of heparin for HIT patients that undergo cardiopulmonary bypass (156, 157). In addition, both studies also deemed Bivalirudin as safe to use in patients with moderate impaired renal function. With properties like rapid onset of action and rapid elimination, independent of specific organ involvement, Bivalirudin is potentially set to become the primary choice of DTI in the management of HIT patients that need to undergo cardiovascular surgery (156).

Recently, fondaparinux and idraparinux which inhibit factor Xa indirectly via inhibition of antithrombin (158) have been used to treat a small number of patients with HIT. In one study, fondaparinux was successful in treating HIT patients complicated with thrombosis by normalizing the platelet count between 2 and 9 days (146). However, their long half life (17 h for Fondaparinux and up to 130 h for Idraparinux) and the absence of effective antidotes must be taken into consideration when prescribing these anticoagulants (158).

1.12.1. Limitations of Current Anticoagulants for HIT Treatment.

Although the current anticoagulants have been shown to be efficacious in treating HIT, these treatments do come with several drawbacks. The administration of these drugs is via continuous intravenous infusion that requires frequent laboratory monitoring (by aPTT) and frequent dose adjustments. This is further hindered by the absence of effective antidotes and long plasma half life (i.e. Fondaparinux and Danaparoid).

1.13. Potential Treatment for HIT

Dabigatran and rivaroxaban were originally developed for the treatment of venous thromboembolism and stroke prevention in patients with atrial fibrillation (159).

Dabigatran is a specific, reversible thrombin inhibitor while rivaroxaban is a reversible factor Xa inhibitor (159). Neither drug cross-react with anti- PF4/heparin Abs (160).

Most importantly, these drugs don't induce platelet activation in the presence of anti-PF4/heparin Ab. However, further clinical data are needed to complement these *in vitro* observations to support their therapeutic use. Recently, a new compound with a potential use in HIT treatment was described.

Table 1.3. Non-heparin anticoagulants for the treatment of Heparin-Induced Thrombocytopenia.

Agent	Direct Thrombin Inhibitors			Indirect Factor Xa Inhibitors	
	Lepirudin	Argatroban	Bivalirudin	Danaparoid	Fondaparinux
Clearance	Renal	Hepatobiliary	Enzymatic (80%) and Renal (20%)	Renal	Renal
Half-life	80 min	39 to 51 min	25 min	25 h	17 to 20 h
Monitoring	aPTT	aPTT	ACT	Anti-factor Xa activity	None
Therapeutic Dosing	Bolus at 0.2mg/kg, IV	Continuous infusion at 2µg/kg/min, IV	Continuous infusion at 0.15 to 0.20 mg/kg/h, IV	Bolus at 2250U, IV; Accelerated initial infusion at 400U/h x 4 h, then 300U/h x 4h; Maintenance infusion at 200U/h.	Not established for HIT
Adverse Effects	Bleeding with therapeutic dose; Formation of Antilepirudin Abs	Bleeding with therapeutic dose	Bleeding with therapeutic dose	Bleeding with therapeutic dose; cross-reactivity with PF4-heparin Abs	Minimal data available.

aPTT, activated partial thromboplastin time; ACT, activated coagulation time; IV, intravenous.

Data compiled from (150, 161, 162).

2-O, 3-O desulfated heparin (ODSH), a minimal anticoagulant derived from UFH was initially used as an anti-inflammatory agent in treating various lung disorders and ischemic myocardial reperfusion injury (163, 164). The reduced anticoagulant property denotes that it has low affinity for anti-thrombin III, anti-Xa, anti-IIa and does not activate factor XII (165). ODSH first demonstrated its potential as a treatment for HIT when the compound was able to prevent platelet activation in the presence of HIT Abs and heparin itself(165). Further analysis revealed that ODSH at high concentrations exerted its action by disrupting the PF4/heparin complexes, thus preventing platelet activation by anti-PF4/heparin Abs (160). Thus, it was proposed that ODSH could be administered together with heparin to prevent the adverse effect of HIT.

In recent years, the focus on the treatment of HIT has shifted towards targeting the FcγRIIa signaling pathways. FcγRIIa contains an immunoreceptor tyrosine-based activation motif (ITAM). Upon receptor engagement, ITAM gets phosphorylated and serves as a docking protein for tandem Src homology (SH)₂ domain-containing signaling proteins, such as the spleen tyrosine kinase-Syk (91, 166). Up to date, two inhibitors of Syk have been tested for the treatment of HIT. PRT-318 was tested in transgenic HIT mice and was found to prevent the drop in platelet count and thrombosis in the presence of KKO (167). R406 on the contrary was studied *in vitro* and also yielded promising results and was able to prevent platelet aggregation in the presence of HIT Abs (118).

Besides platelets, Syk is also expressed in B cells, macrophages, mast cells, erythrocytes, hepatocytes, and other cell types (168). This demonstrates the important role of Syk in the pathogenesis of multiple diseases such as rheumatoid arthritis (RA)(169), immune thrombocytopenia (ITP)(170) and systemic lupus erythematosus (171). The development of Syk inhibitors to target these diseases is therefore of huge interest, with some drugs, such as fastamatinib (R788) are already at the stage of clinical trials (172). R788, a prodrug of Syk inhibitor R406, demonstrated promising results in reducing inflammatory mediators which often leads to joint destruction, thus ameliorating clinical symptoms suffered by RA patients (172).

Table 1.4. Possible new approaches for the treatment of HIT.

	Mode of Action	Test conducted	References
Dabigatran	Reversible thrombin inhibitor	Prevents platelet activation in the presence of PF4-heparin Ab.	(159, 160)
Rivaroxaban	Reversible Factor-Xa inhibitor		
2-O, 3-O desulfated heparin (ODSH)	Thrombin, Factor-Xa and Factor-IIa inhibitor (low binding affinity)	Prevents platelet activation in the presence of PF4-heparin Ab	(160, 165)
PRT-318	Syk inhibitor	Prevents thrombocytopenia and thrombosis in the presence of KKO in HIT transgenic mice	(167)
R406	Syk inhibitor	Prevents platelet aggregation in the presence of PF4-Heparin Ab <i>in vitro</i>	(118)

Nevertheless, several side effects associated with R788 have been reported such as gastrointestinal intolerance, neutropenia and elevated level of liver enzyme alanine aminotransferase. Though these side-effects have been regarded as not significant, the implications that it might have on patients with existing liver or digestive problems remains to be critically evaluated. In addition, R788 also blocks the activation of macrophages, neutrophils, B cells and the release of inflammatory mediators (i.e. cytokines) (172). Thus, the use of Syk inhibitors might be effective but may lack specificity due to the wide expression of Syk enzyme in many cell types.

1.14. Is there other approach to treat HIT?

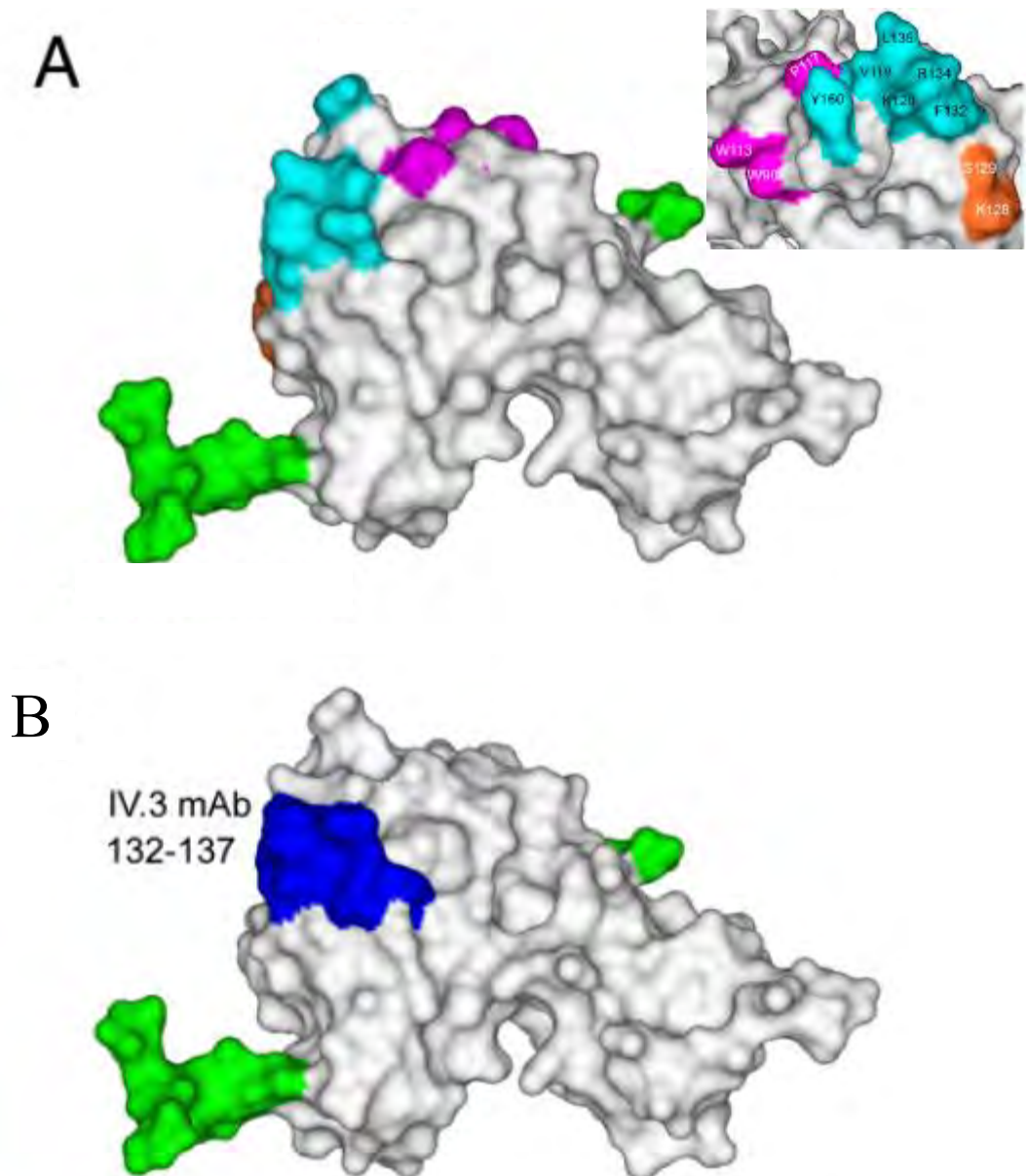
The pathogenesis of HIT involves several stages. First, the administered heparin binds to PF4 and leads to the expression of neoepitopes. In recognition of the newly formed antigenic surface, specific Ab-IgG is produced which then binds to the PF4/Heparin complex. Together, these immune complexes interact with the Fc γ RIIa receptors via the Fc portion of the IgG. The cross-linking of the Fc γ RIIa receptor causes platelet activation, which release more PF4 and platelet microparticles with proaggregating stimuli. This initiates the activation of the coagulation pathway, leading to thrombocytopenia and thrombosis.

The conventional approach in treating HIT has always been targeted at the downstream coagulation pathway, e.g. by inhibiting thrombin or Factor Xa. However, these treatments do not inhibit the key factor that initiates the prothrombotic events of HIT, in this case, platelet activation by the HIT immune complexes. Emerging treatments, which are still at the experimental stage, such as ODSH and Syk enzyme inhibitor, aim to block this initial event, which are often the cause of disastrous outcome in patients with HIT. Thus, these newly develop drugs may be a more effective approach for HIT management. ODSH disrupts the formation of PF4/heparin complexes whereas Syk inhibitors block the signaling pathway of Fc γ RIIa. Both prevent the activation of platelets. Although these new possible treatments warrant further evaluation and more supporting clinical data, they prove to be more efficacious than the conventional treatments i.e. anticoagulant therapies.

To date, no strategies that target the Fc γ RIIa receptor itself have been proposed. The platelet receptor which engages the HIT immune complexes and subsequently initiates platelet activation, plays a central role in the pathogenesis of HIT. Thus, by blocking this receptor, the events leading to HIT could be effectively abolished at an early stage, preventing activation of both platelets and coagulation pathways.

1.15. MoAbs as a therapeutic agent for medical treatment

IV.3 is a mouse MoAb specific for the Fc γ RIIa receptor and has been available for close to two decades. IV.3 belongs to the IgG2b subgroup and was initially raised against Fc γ RIIa to differentiate the subclass of Fc γ receptors present on human monocytes and a related U937 cell line (173). Since then, it has been widely used in studies to block Fc γ RIIa (74, 174, 175) and for confirmation of HIT (77). Recently, the epitopes of the IV.3 MoAb on Fc γ RIIa was mapped and found to be localized to residues Phenylalanine 132 to Proline 137 (176). Both HR/LR polymorphism of Fc γ RIIa bind to IV.3 suggesting that neither arginine nor histidine at position 134 affects IV.3 binding. When the residue L135 was mutated, the IV.3 epitope was completely abolished, indicating that L135 is a key determinant of IV.3 specificity. Importantly, the same region of the Fc γ RIIa is required for recognition of IgG1 (Figure 1.10) (176). Thus, it is clearly established that IV.3 is a blocking MoAb that competitively inhibits interaction of IgG1 with its receptor, which could therefore be advantageous for the treatment of HIT.



Copyright 2011. The American Association of Immunologists, Inc.

Figure 1.10. Structural location of epitopes on Fc γ RIIa recognized by IgG1 and IV.3. A. The Fc ligand of IgG1 interacts with Fc γ RIIa on three separate regions represented in orange, magenta, and cyan. Inset shows the amino acid residues involved in the interaction. B. The epitope region that binds to IV.3 localized to residues 132-137. Both molecules recognize the same region on the Fc receptor, which shows that IV.3 is a direct inhibitor of IgG1. Green area represents N-linked oligosaccharides. Reprinted with permission from Ramsland et al (176).

The hybridoma technology to produce MoAbs (Figure 1.11) was first introduced in 1975 by Kohler and Milstein (177). Soon after, it was applied to produce reagents, diagnostics and even extended to therapeutic purposes for various diseases. The first successful treatment using a murine MoAb was reported by Miller and coworkers in 1982. The murine anti-idiotypic MoAb was used to treat a B-cell lymphocytic lymphoma patient, resulting in complete remission of the disease (178). Subsequently in 1986, FDA approved the first murine MoAb which targets CD3. The drug named Muromonab (OKT3) was used in the treatment of allograft rejection (179). The hybridoma technology confers scientists the advantage to generate large quantities of pure, specific Abs directed against any antigen. However, it was soon realized that these murine MoAbs are highly immunogenic in humans through repeated administrations, inducing a potent human anti-murine antibody (HAMA) response. The administered murine Ab leads to the formation of immunocomplexes, resulting in rapid clearance from the serum and reduced therapeutic efficacy (180). Patients have also been reported suffering from occasional anaphylactic reactions and mild allergic phenomena (rash, hives, flushing, etc) (181).

These issues led to efforts to reduce or eliminate the inherent immunogenicity of murine MoAbs. This gave rise to the establishment of Ab engineering. The approach involves either chimerization, where the murine variable domains is grafted onto human constant domains (182-184), or humanization where the murine complementarity determining regions (CDRs) are grafted onto human framework regions (185) (Further details about humanization will be discussed in Chapter 4). With these improvements, MoAbs have been widely applicable to treat different clinical conditions such as organ transplantation (186), inflammation (187), cancer (188) and infectious diseases (189). Up to date, nearly 30 Ab drugs approved by the FDA are available in the US market (Figure 1.12) (190).

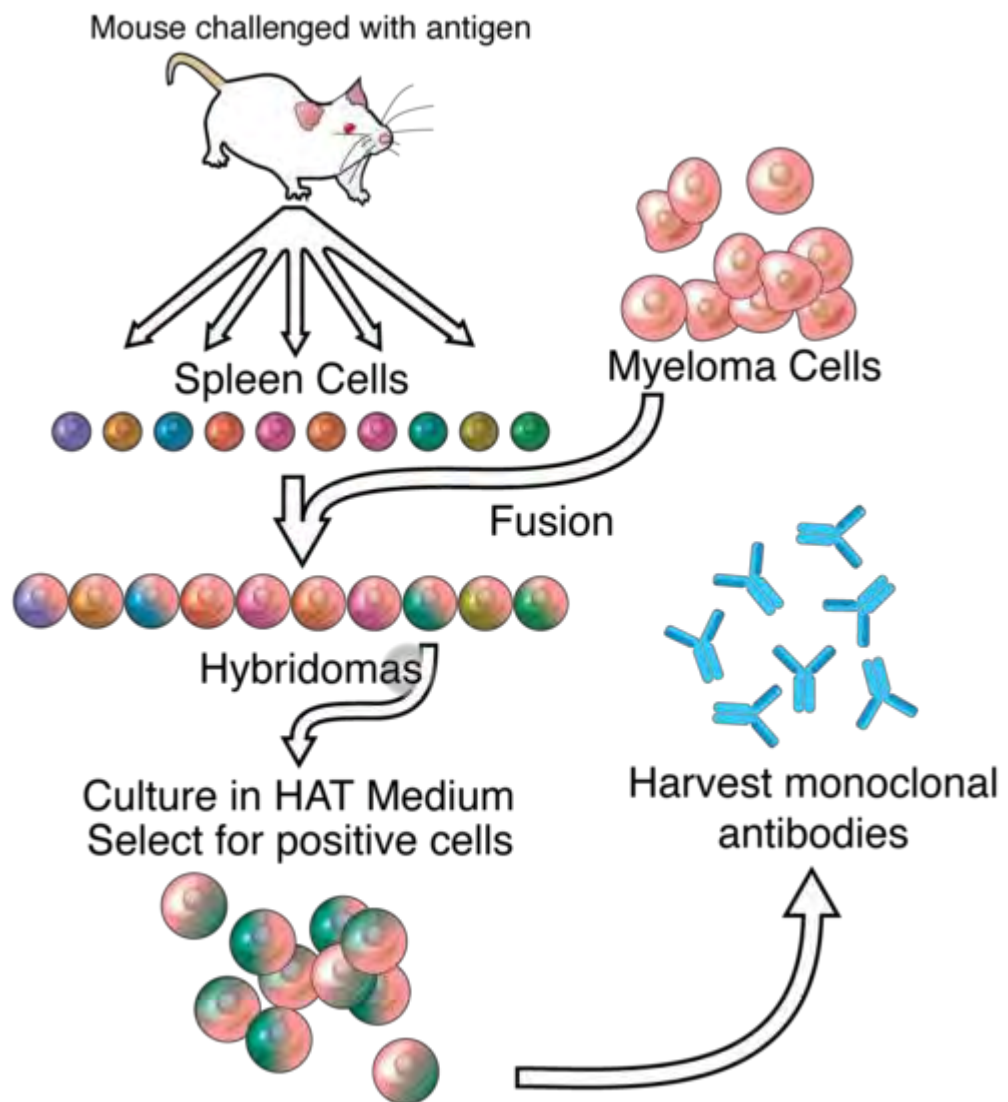


Figure 1.11. A diagram of MoAb generation using hybridoma technology. Spleen cells are obtained from mouse immunized with desired antigen and fused with immortal myeloma cells to generate Ab-producing hybridomas. The mixtures of cells which consist of nonproducing hybridomas, Ab-producing hybridomas and unfused cells are then further selected in HAT medium. Only the hybridomas from the fusion between splenocytes and myeloma cells will survive, allowing the production of a highly specific MoAb (Source of diagram: Wikimedia Commons).

Hybridoma Origin (26 mAbs)	Murine mAb (-omab) 3	ORTHOCLONE OKT3® <i>muromonab-CD3</i> (1986)	ZEVALIN® <i>ibrutinomab</i> <i>tiuxetan</i> (2002)	BEXXAR® <i>tositumomab</i> (2003)						
	Chimeric mAb (-ximab) 5	REOPRO® <i>abciximab</i> (1994)	RITUXAN®/ MABTHERA® <i>rituximab</i> (1997)	SIMULECT® <i>basiliximab</i> (1998)	REMICADE® <i>infliximab</i> (1998)	ERBITUX® <i>cetuximab</i> (2004)				
	Humanized mAb (-zumab) 11	ZENAPAX® <i>dacizumab</i> (1997)	SYNAGIS® <i>palivizumab</i> (1998)	HERCEPTIN® <i>trastuzumab</i> (1998)	CAMPATH® MABCAMPAT® <i>alemtuzumab</i> (2001)	XOLAIR® <i>omalizumab</i> (2003)				
		AVASTIN® <i>bevacizumab</i> (2004)	TYSABRI®/ ANTEGREN® <i>natalizumab</i> (2004)	LUCENTIS® <i>ranibizumab</i> (2006)	SOLIRIS® <i>eculizumab</i> (2007)	CIMZIA® <i>certolizumab pegol</i> (2008)				
		Actemra® <i>Tocilizumab</i> (2010)								
	Human mAb (-umab) 7	VECTIBIX® <i>panitumumab</i> (2006)	SIMPONI® <i>golimumab</i> (2009)	STELARA® <i>ustekinumab</i> (2009)	ARZERRA® <i>ofatumumab</i> (2009)	ILARIS® <i>canakinumab</i> (2009)				
		PROLIA®/ XGEVA® <i>Denosumab</i> (2010)	YERVOY® <i>ipilimumab</i> (2011)							
	Other Approach (2 mAbs)	Human mAb (-umab) 2	HUMIRA®/ TRUDEXA® <i>adalimumab</i> (2002)	BENLYSTA® <i>belimumab</i> (2011)						

Figure 1.12. A list of therapeutic MoAbs approved by FDA currently available in the United States. Most of these Abs are present in the format of full-length molecular Ab which includes the murine, chimeric, humanized and human Ab category. The trade name, generic monoclonal Ab name and the year of approval by the FDA for each Ab drug are indicated in the figure. Reprinted with permission from Zhang (191).

Besides immunogenicity, the use of whole Abs also presents other therapeutic challenges. Intact IgG (Figure 1.13) with a molecular weight of 150kDa has poor penetration properties (e.g. into a solid tumor mass) and slow clearance rates (192). This is further hindered by the presence of the Fc portion of the antibody where Fc-mediated effects may be undesirable under certain situations. These include inappropriate cytokine release from Fc receptor expressing cells leading to various adverse effects (193). The antigen binding specificity occurs at the variable fragment-Fv of the IgG, which consists of variable heavy (VH) and variable light (VL) domains (194). These two variable domains can be easily cloned from the Ab expressing hybridoma cells to form antibody fragments including antigen-binding fragment (Fab) or single-chain Fv (scFv) Ab fragment (Figure 1.14). Smaller antibody fragments retain target specificity and exhibit high-affinity binding of antigen. scFvs as an example, are capable of binding their target antigens with a similar affinity to that of the parent MoAb (195) (Further details about scFv will be discussed in Chapter 3). In addition, these fragments are ideal to use in areas like radio-imaging and radio-therapy due to characteristics such as better clearance rate from the blood and better penetration into tumour or tissue.

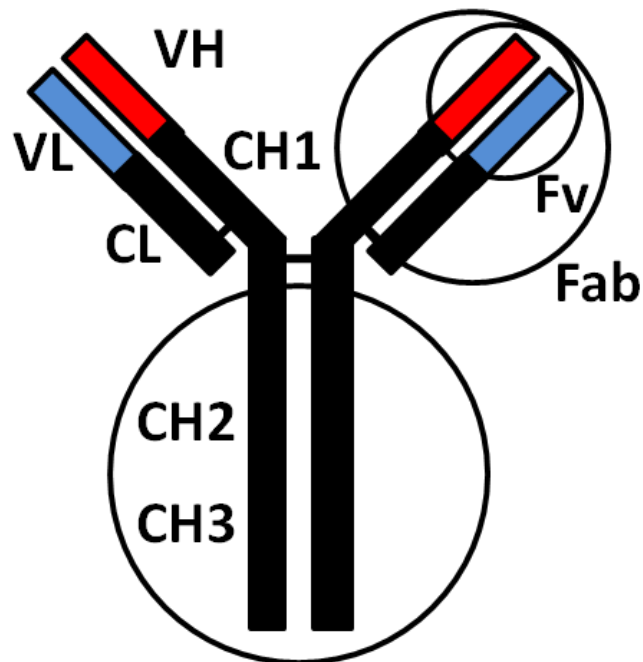


Figure 1.13. Schematic representation of an IgG Ab molecule. IgG Abs are heterotetramers of two identical heavy chains and two identical light chains that are joined with a series of disulfide bonds. Each light chain contains one variable domain (VL) and one constant domain (CL); each heavy chain contains one variable domain (VH) and three constant domains (i.e. CH1, CH2 and CH3). The variable fragment (Fv), present at the N-terminal of the antigen-binding fragment (Fab) consists of the non-covalent complex of the VH and VL domains that holds antigenic binding specificity. The two constant domains, CH2 and CH3 of the heavy chain form the crystallisable fragment (Fc) that mediates biological effector functions. Adapted from Chowdhury and Wu (192).

Fragments of Monoclonal Antibodies

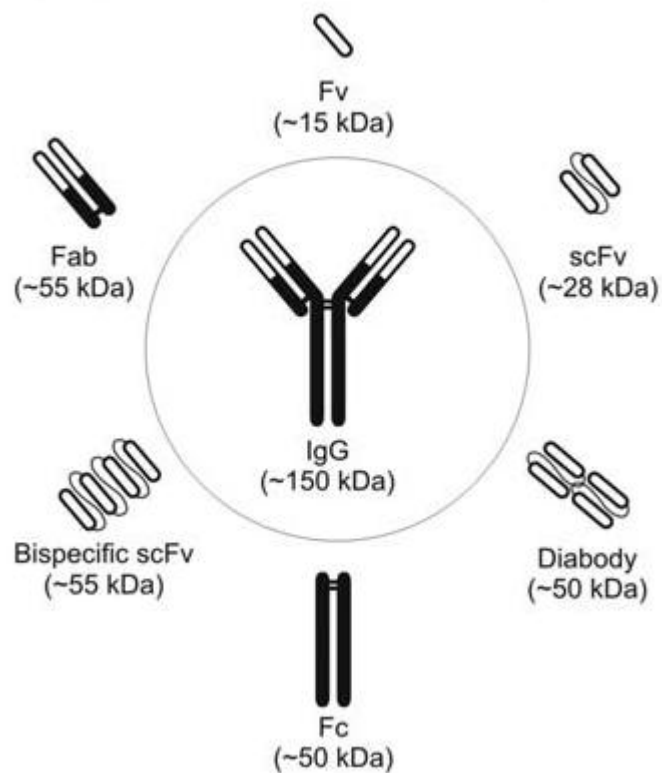


Figure 1.14. Schematic representation of MoAb and different Ab fragments.
Reprinted with permission from Pucca et al. (196).

1.16. Hypothesis and Aims

As mentioned previously, it is well known that the IV.3 murine MoAb recognizes and binds strongly and specifically to Fc γ RIIa on the cell surface. This is a typical antigen-antibody interaction and takes place via the Fab domain of the Ab. The Ab not only blocks HIT immune complexes binding to the platelets but also inhibits platelet aggregation induced by the HIT IgG. Since it has been shown that antibody fragments (i.e. scFv) are able to retain the binding characteristics of the parent antibody (195), we will investigate the properties of a scFv derived from the IV.3 MoAb. A functional scFv should block the interaction of HIT immune complexes with Fc γ RIIa and should prevent HIT Ab-mediated platelet activation.

We hypothesize that:

- An Ab fragment, such as a scFv derived from the IV.3 antibody will retain and recapitulate the functional properties of the parent antibody.
- This scFv should be able to bind Fc γ RIIa, prevent binding of the HIT immune complexes to the receptor and thus inhibits HIT Ab-induced platelet activation.
- The humanized scFv should retain functional properties similar to the murine scFv and the parental antibody.

To examine these hypotheses, our aim would therefore be:

- To clone the gene sequence of the variable regions of the IV.3 MoAb.
- To create a scFv construct. The derived variable sequence of VH and VL will be connected with a flexible peptide linker.
- To express the scFv. The protein will be expressed using *Escherichia coli* (*E.coli*) cells and purified by affinity chromatography.

- To characterize the properties of the scFv. The binding and functional activities of the protein will be evaluated using flow cytometry, serotonin release and platelet aggregation assays.
- To humanize the scFv. The antibody fragment will be humanized using the CDR grafting approach and expressed in *E.coli*. After purification, the binding and functional properties will be characterized as mentioned above.

Chapter 2

Materials and Methods

2.1. Materials

2.1.1. Bacterial Strains

Competent bacterial cells were either obtained commercially from Invitrogen (Carlsbad, CA, USA) or prepared in the laboratory from existing stock.

E. coli DH5 α : F- Φ 80dLacZ Δ M15 Δ (LacZYA-argF)U169 deoR recA1 endA1 hsdR17 (r_k^- , m_k^+) phoA supE44 thi-1 gyrA96 relA1, λ^- .

E. coli TOP10: F- mcrA Δ (mrr-hsdRMS-mcrBC) Φ 80lacZM15 Δ lacX74 recA1 araD139 Δ (ara-leu)7697 galU galK rpsL (StrR) endA1 nupG.

E. coli BL21(DE3): F- *ompT hsdSB* (rB-mB-) *gal dcm* (DE3).

2.1.2. Cell Lines

IV.3 Monoclonal Antibody (MoAb) (IgG_{2b}) producing hybridoma cells (American Type Collection Culture (ATCC) (Manassas, VA, USA) clone number HB-217TM).

2.1.3. Human Platelets

For *in vitro* studies:

Human platelets were prepared from blood collected from patients at Ambulatory Care Unit (ACU), St. George Public Hospital, Kogarah NSW. These patients had haemachromatosis and were normal except for elevated serum ferritin.

Human platelets were collected from healthy individuals with no recent exposure to aspirin or heparin.

For *in vivo* studies:

Human platelets were collected from healthy individuals with no recent exposure to aspirin or heparin.

For Platelet Factor 4 (PF4) purification:

Expired Human Platelets were kindly provided by the Blood Bank, St. George Public Hospital, Kogarah, NSW.

2.1.4. *HIT Sera*

HIT Sera were collected with informed consent from patients with HIT.

2.1.5. *DNA Oligonucleotides (Primers)*

All primers used throughout this PhD project were ordered from Sigma-Aldrich® (Castle Hill, NSW, AU), prepared via desalted purification, suspended at a concentration of 100µM in water. The primers were then diluted in TE Buffer to a concentration of 10pmol/µl as a stock for all PCR experiments. The sequences for all the primers are shown in the Appendix.

2.1.6. *Cell Culture Reagents*

2-Mercaptoethanol (β-ME)	Gibco (Invitrogen Co, Penrose, Auckland, NZ)
5% Trypsin/EDTA Solution (10X)	Gibco
Australian Fetal Bovine Serum (FBS)	Lonza (Walkersville, MD, USA)
Dimethyl Sulfoxide (DMSO)	Sigma (St Louise, MO, USA)
Dulbecco's Modified Eagle's Medium (DMEM)	Gibco
Dulbecco's Phosphate Buffered Saline (DPBS) (1X)	Gibco
L-glutamine	Invitrogen (Invitrogen Co, Penrose, Auckland, NZ)
Penicillin/Streptomycin	Gibco
Trypan Blue Solutions (0.4%)	Sigma
Bright-Line™ Hemacytometer	Hausser Scientific (Horsham, PA, USA)
Bright-Line™ Hemacytometer cover slip	Hausser Scientific

2.1.7. Molecular Biology Kits

PureLink® HiPure Plasmid Maxiprep Kit	Invitrogen (Carlsbad, CA, USA)
QIAquick Gel Extraction Kit	Qiagen (Hilden, Germany)
RNeasy Mini Kit	Qiagen
SuperScript™ III First-Strand Synthesis SuperMix for qRT-PCR	Invitrogen
Wizard® <i>Plus</i> SV Minipreps DNA Purification System	Promega (Madison, WI, USA)
Zero Blunt ® PCR Cloning Kit	Invitrogen

2.1.8. Molecular Biology Enzymes and Reagents

1kb Plus DNA Ladder	Invitrogen
5X Sequencing Buffer	Applied Biosystems (ABI) (Warrington, Cheshire, UK)
<i>Bam</i> HI Restriction Enzyme	New England Biolabs (NEB) (Ipswich, MA, USA)
BigDye Terminator v3.1	ABI
Bovine Serum Albumin (BSA) (100X)	NEB
Buffers for Restriction Enzymes	NEB
<i>Eco</i> RV Restriction Enzyme	NEB
<i>Eco</i> RI Restriction Enzyme	NEB
GeneRuler™ 1kb DNA Ladder	Fermentas (ThermoFischer Scientific, Waltham, MA, USA)
<i>Hind</i> III Restriction Enzyme	NEB
KOD DNA Polymerase	Novagen, Merck (Darmstadt, Germany)
<i>Nde</i> I Restriction Enzyme	NEB
<i>PfuUltra</i> ™ High-Fidelity DNA Polymerase	Stratagene (La Jolla, CA, USA)
Platinum® <i>Taq</i> DNA Polymerase	Invitrogen
SYBR® Safe DNA Gel Stain	Invitrogen
T4 DNA Ligase	Promega

2.1.9. Protein Reagents/Kits

Bio-Rad Protein Assay	Bio-Rad (Hercules, CA, USA)
Brilliant Blue R	Sigma
Bromophenol Blue	Progen Industries Ltd. (Brisbane, QLD, AU)
Precision Plus Protein™ Standards Dual Colour	Bio-Rad
PageRuler™ Prestained Protein Ladder	Fermentas
NuSep Longlife Gels	NuSep Ltd (Frenchs Forest, NSW, AU)
Mini-PROTEAN® TGX™ Precast Gels	Bio-Rad
Western Lightning® Plus-ECL, Enhanced Chemiluminescence Substrate	PerkinElmer (Waltham, MA, USA)
ECL Plus Western Blotting Detection Reagents	Amersham Biosciences (GE Healthcare, Uppsala, Sweden)
Immobilon-P Transfer Membrane	Millipore (Millipore Co, Billerica, MA, USA)
3MM Chr Blotting Papers	Whatman™ (GE Healthcare, Buckinghamshire, UK)
Poly-Prep® Chromatography Columns	Bio-Rad
Econo-Column Chromatography Columns	Bio-Rad

2.1.10. Chemical Reagents/Solutions

-(-)Glutathione, oxidized (GSSG)	Sigma
2-propanol	Sigma
Absolute Ethanol	Sigma
Albumin, from Bovine Serum	Sigma
Ammonium Sulfate	Scharlau (Sentmenat, Barcelona, Spain)
Ampicillin sodium salt	Sigma
ANTI-FLAG® M2 Affinity Gel	Sigma
Anti-c-Myc Agarose Conjugates	Sigma
Apyrase	Sigma
Bio-Beads SM Adsorbents	Bio-Rad

Calcium Chloride	Sigma
Complete Protease Inhibitor Cocktail Tablets, EDTA-free	Roche (Mannheim, Germany)
DL-Dithiothreitol (DTT)	Sigma
Dimyristoylphosphatidylcholine (DMPC)	Sigma
Ethylenediaminetetraacetic Acid (EDTA), Free Acid	Amresco (Solon, Ohio, USA)
Ficoll Molecular Biology Reagent	Sigma
Formaldehyde	Sigma
Gelatin Glycerol	Sigma
Glacial Acetic Acid	Sigma
Glucose	Amresco
Glycerol, for molecular biology $\geq 99\%$	Sigma
Glycine	Amresco
Guanidine Hydrochloride (HCl)	Sigma
Heparin Sepharose TM 6 Fast Flow	GE Healthcare (Uppsala, Sweden)
HiTrap HP Column	GE Healthcare
Hydrochloric Acid	Sigma
Hydroxytryptamine Binoxalate, 5-[2- ¹⁴ C]- (Serotonin)(¹⁴ C-5HT)	Perkin-Elmer
Imidazole	Sigma
Isopropyl- β -galactopyranoside (IPTG)	Sigma
Kanamycin Sulfate	CalBioChem (EMD Biosciences, San Diego, CA, USA)
L-Arginine	Sigma
L-Glutathione reduced (GSH)	Sigma
Luria-Bertani (LB) Medium	MP Biomedicals (Solon, Ohio, USA)
Magnesium Chloride	Sigma
Methanol	ThermoFisher Scientific (Waltham, MA, USA)
n-octyl- β -D-glucoside (β -OG)	Affimetrix (Maumee, Ohio,

	USA)
Phenylmethylsulfonide Fluoride (PMSF)	Sigma
Phosphate Buffered Saline (PBS) (Tablets)	Amresco
Potassium Chloride	Sigma
ProBond™ Nickel-Chelating Resin	Invitrogen
Prostaglandin E1	Sigma
Protein G Agarose	Roche
SMA copolymer	Malvern Cosmeceutics Ltd (Gloucestershire, UK)
Sodium Azide	Sigma
Sodium Chloride	Sigma
Sodium Bicarbonate	Sigma
Sodium Dodecyl Sulfate (SDS)	Bio-Rad
Sodium Hydroxide	Sigma
Sodium Phosphate	Sigma
Sucrose	Sigma
Superdex 75	GE Healthcare
Tris	Amresco
Triton X-100	Bio-Rad
Tween® 20	Sigma
Urea	Sigma
Ultra-Pure Agarose	Invitrogen
Xylene Cyanol FF	Sigma

2.1.11. Equipment

4 Degree Fridge	Kelvinator Opal/Westinghouse (NSW, AU)
Autoclave	Mercer Medical (S.B. Autoclaves, Kirrawee, NSW, AU)
Aggregometer	Chrono-log Aggro/Link™ (Chrono-log Co., Havertown, PA,USA)
AKTA purifier chromatography system	GE Healthcare
Benchtop Centrifuge Z513K	Hermle (Wehingen, Germany)
Biological Safety Cabinet Class I	Gelman (NSW, AU)
Sciences Biological Safety Cabinet Class II	Email Westinghouse Pty Ltd (NSW, AU)
Centrifuge 5702 R	Eppendorf (North Ryde, NSW, AU)
Centrifuge 5810 R	Eppendorf
CERTOMAT®HK Shaking Incubator	B.Braun (B. Braun Biotech International, Sartorius Group, Goettingen, Germany)
Cyto-Tek® Cytocentrifuge	Sakura (Sakura Finetechnical Co., Ltd., Tokyo, Japan)
DMIRB Inverted Microscope	Leica (Wetzlar, Germany)
Dry Block Heater	Thermoline Scientific (NSW, AU)
F-120C Ice Maker	Rinnai (Hoshizaki Electric Co., Ltd, Shimane, Japan)
FACSCalibur™ flow cytometer	Becton-Dickinson (San Jose, CA, USA)
GelDoc 2000	Bio-Rad
GeneAmp PCR System 2400	ABI
GW3050 Glassware Washer	Gallay Medical & Scientific Pty. Ltd. (Auburn, NSW, AU)
ImageQuant LAS4000	GE Healthcare
Incubator	Memmert (Schwabach, Germany)

Laboratory Counter	ClayAdams (Parsippany, NJ, USA)
Microfuge® 18 Centrifuge	Beckman Coulter™ (Lane Cove, NSW, AU)
Microson™ XL2000 Ultrasonic Cell Disruptor	Misonix (Farmingdale, NY, USA)
Microscope CK2	Olympus (Tokyo, Japan)
Microwave	Samsung (Korea)
Mini-PROTEAN Tetra Cell (Protein Gel Electrophoresis)	Bio-Rad
Mini-Sub Cell GT Cell Tanks (Agarose Gel Electrophoresis)	Bio-Rad
MiniSpin ® Plus Benchtop Centrifuge	Eppendorf
Minus 20 Freezer	Haier (Lidcombe, NSW, AU)/Kelvinator
Minus 80 Freezer	Thermo Forma (Marrietta, OH, USA)
Monair 30 Recirculating Fumehood	Astec (Bioquell PLC, Hampshire, UK)
MR3001 Stirrer/Heater	Heidolph (Germany)
NanoDrop 2000c Spectrophotometer	Thermo Scientific (NSW, AU)
Optima™ L-100 XP Ultracentrifuge	Beckman Coulter™
pH Meter	TPS (Springwood, QLD, AU)
Power Pac	Bio-Rad
PowerWaveX Select Microplate Spectrophotometer	Bio-Tek Instrument, Inc. (Millennium Science, Mulgrave, VIC, AU)
Reverse Osmosis and MilliQ Water Dispenser	Millipore
Series II Water Jacketed CO ₂ Incubator Hepa Filter	Thermo Forma
Shaker Unimax1010	Heidolph
SmartSpec™3000	Bio-Rad
Sonifier® Cell Disruptor B15	Branson (Germany)
Tri-Carb® 2100TR Liquid Scintillation Counter	Packard (Canberra, AU)

Veriti® 96-well Thermal Cycler	ABI
Vortex Reax 2000	Heidolph
Waterbath	Memmert

2.1.12. Antibodies for Flow Cytometry

(dilutions used are in brackets)

Alexa Fluor® 488 (AF488)-conjugated anti-c-Myc (1:50); sc-40	Santa Cruz (Dallas, Texas, USA)
AF488-conjugated anti-mouse IgG (1:200); A11001	Invitrogen
Alexa Fluor® 594 (AF594)-conjugated F(ab') ₂ fragment of anti-mouse IgG (H+L)(1:500); A11020	Invitrogen
Alexa Fluor® 647 (AF647)-conjugated anti-mouse IgG _{2b} (γ2b)(1:200); A21242	Invitrogen
AF647-conjugated anti-human CD41(1:10); MCA467A647	AbD Serotec (Bio-Rad, Hercules, CA, USA)
CaliBrite Beads; 340486	BD Biosciences (San Jose, CA, USA)
CountBright™ Absolute Counting Beads; C36950	Invitrogen
Fluorescein isothiocyanate (FITC)-conjugated anti-human CD42a (1:5); 348083	BD Biosciences
Mouse IgG1 Negative Control AF647 (1:10); MCA1209A647	AbD Serotec
Phycoerythrin (PE) Rat IgG1, κ isotype control (1:100); 553925	BD Biosciences
PE Rat anti-mouse CD41 (1:100); 558040	BD Pharmingen™ (San Diego, CA, USA)
PE-conjugated anti-human CD41a (1:5); 555467	BD Pharmingen™
Simultest control γ ₁ /γ ₁ (1:5); 349526	BD Biosciences

2.1.13. Antibodies for Immunostaining

(dilutions used are in brackets)

AF488-conjugated mouse anti-c-Myc (1:500); sc-70463	Santa Cruz
---	------------

Monoclonal ANTI-FLAG [®] M2, Clone M2 (1:1000); F3165	Sigma
Penta-His Antibody, BSA-free (1:2000); 34660	Qiagen
Polyclonal Rabbit Anti-Mouse Immunoglobulins/ Horseradish Peroxidase (HRP) (1:3000); P0260	Dakocytomation (Glostrup, Denmark)

2.1.14. Vectors

pCR-Blunt Vector

pET-11a Vector

pIG6 Vector

2.1.15. Online Software for Primer Design and Molecular Analysis

Basic Local Alignment Search Tool (BLAST) from National Centre for Biotechnology Information (NCBI) homepage. <http://blast.ncbi.nlm.nih.gov/Blast.cgi>

BiSearch: Primer Design and Search Tool. <http://bisearch.enzim.hu/>

Clustal Omega from European Bioinformatics Institute (EBI) homepage.

<http://www.ebi.ac.uk/Tools/msa/clustalo/>

ExpASy Translate Tool from Swiss Institute of Bioinformatics (SIB) Bioinformatics Resource Portal. <http://web.expasy.org/translate/>

Molarity Calculator from GraphPad Software.

<http://www.graphpad.com/quickcalcs/Molarityform.cfm>

NEBcutter V2.0 (Online DNA restriction mapping tool) from NEB

<http://tools.neb.com/NEBcutter2/>

OligoCalc: Oligonucleotide Properties Calculator.

<http://www.basic.northwestern.edu/biotools/oligocalc.html>

2.1.16. Online Software and Program for Protein Modeling

Swiss-Model Workspace (Structure homology modeling) from SIB Bioinformatics Resource Portal. <http://swissmodel.expasy.org/workspace/>

Phyre² (3D structure prediction) by Structural Bioinformatics Group, Imperial College, London. <http://www.sbg.bio.ic.ac.uk/phyre2/html/page.cgi?id=index>

Pymol (Molecular graphics visualization) by Schrödinger, LLC. <http://www.pymol.org/>

2.1.17. Blood Collection

23 G x 0.75 in needle x 12 in tubing BD Safety-Lok™	BD Diagnostics (San Jose, CA, USA)
blood collection and infusion set with luer adapter	BD Diagnostics
BD Vacutainer® one-use, non-stackable holder	BD Diagnostics
Whole Blood Tube w/ Anticoagulant, Acid Citrate Dextrose (ACD) Sol A	BD Diagnostics

2.1.18. Materials for Platelet Aggregometry

Glass Cuvettes	Chrono-log Corporation
Stir bar, disposable siliconized for P/N 312 cuvettes	Chrono-log Corporation

2.1.19. Materials for Serotonin Release Assay

Magnetic Stir Bars	Paton Scientific (Victor Harbor, SA, AU)
Scintillation tubes and lids	Packard (Canberra)

2.1.20. Animal Work

Non-obese Diabetic/Severe Combined Immunodeficiency (NOD/SCID) Mice	Animal Resources Centre (ARC) (Perth, WA, AU)
27G x 0.5" needle	BD Diagnostics
1ml insulin syringes with 27g x 0.5" needles	Terumo (Macquarie Park, NSW, AU)
Microvette® CB 300 Kalium-EDTA	Sarstedt (Adelaide, SA, AU)
Petroleum Jelly	Vaseline (Unilever, Rotterdam, Netherlands)
Shaver	

2.2. Methods

2.2.1. Standard Molecular Biology Techniques

Molecular techniques involving kits or certain reagents were conducted according to standard protocols provided by the manufacturers. These include cDNA synthesis, isolation and purification of DNA and RNA. Other techniques such as Agarose Gel Electrophoresis, Polymerase Chain Reaction (PCR) and Vector Transformation were performed based on the protocols described by Sambrook et al (197).

2.2.2. Cell Culture

IV.3 MoAb-producing hybridoma cells were cultured in DMEM medium containing 10% FBS, supplemented with 1% of penicillin and streptomycin, 1% of L-glutamine, and 0.05mM of β -ME. The culture was maintained in the humidified incubator at the aeration of 5% CO₂ at 37°C.

2.2.3. Preparation of Protein Samples for Coomassie Staining and Western Blotting

Protein samples were firstly prepared in a 2 (sample):1 (loading dye) ratio with 2X Sample loading buffer (100mM of Tris, pH 6.8, 4% SDS, 0.2% bromophenol blue, and 20% glycerol and 10% of 1M DTT) and boiled for 5 min at 90°C on a dry block heater. The protein samples were run on either 10% or 4-20% Tris-Glycine Polyacrylamide gels for about 50 min at 150Volts.

2.2.4. Coomassie Staining of Protein Gel

Gels were stained with Protein Staining Solution (45% methanol, 10% glacial acetic acid, 45% water and 3g/L Brilliant Blue R) for 30 min. Gels were destained with Destaining Solution (50% water, 40% methanol, 10% glacial acetic acid) and incubated for another 30 min. The destaining solution was then exchanged with distilled water and the gels destained until a clear background was observed.

2.2.5. Western Blotting

Proteins were transferred from the gel to the Immobilon-P Transfer Membrane for 1 h at 110 Volts or overnight at 30 Volts at 4°C. The membrane was blocked with 5% skim milk dissolved in TBST (0.05M of Tris, pH 7.4, 0.15M NaCl, 0.05% Tween-20) for at least 15 min (2X). The primary antibody (in TBST) was added and incubated with the membrane for 1 h. The membrane was then washed with TBST for 5 min (3X). This was followed by the addition of secondary antibody (in TBST) and incubated for 1 h. The membrane was then washed for 5 min (3X), developed by chemiluminescence and imaged using the Image Analysis System on ImageQuant LAS4000 (GE Healthcare).

2.2.6. PCR Reaction Setup for Different DNA Polymerases

*PfuUltra*TM High-Fidelity (HF) DNA Polymerase (Stratagene)

Component	Volume (μl)
10x <i>PfuUltra</i> TM HF reaction buffer	5
dNTP (10mM)	1
cDNA template	1
Forward Primer (10pmol/μl)	2.5
Reverse Primer (10pmol/μl)	2.5
<i>PfuUltra</i> TM HF DNA polymerase (2.5 IU/μl)	0.5
DMSO	5
Distilled H ₂ O to a final volume of	50

Platinum® *Taq* DNA Polymerase (Invitrogen)

Component	Volume (μl)
10x PCR Buffer (no MgCl ₂)	5
dNTP (10mM)	1
MgCl ₂ (50mM)	1.5
Forward Primer (10pmol/μl)	2.5
Reverse Primer (10pmol/μl)	2.5
cDNA template	1
Platinum® <i>Taq</i> DNA Polymerase	0.5
Distilled H ₂ O to a final volume of	50

KOD DNA Polymerase (Novagen)

Component	Volume (μ l)
10x Buffer for KOD DNA Polymerase	5
MgCl ₂ (1mM)	2
dNTPs (0.2mM)	5
Forward Primer (10 pmol/ μ l)	2
Reverse Primer (10 pmol/ μ l)	2
DNA Template	Up to 50ng
KOD DNA Polymerase (2.5 IU/ μ l)	0.4
Distilled H ₂ O to a final volume of	50

2.2.7. Digestion Reactions

Digestion Reaction Setup for either 20 μ l or 50 μ l reaction volume. Appropriate digestive enzymes and buffers were used according to the respective restriction sites. Digestions were conducted according to the manufacturer's instructions.

2.2.8. Ligation Reaction (Promega)

Component	Volume (μ l)
Vector	Calculated based on formula
Insert	Calculated based on formula
10x Ligation Buffer	1
T4 DNA Ligase (4 IU/ μ l)	1
Distilled H ₂ O to a final volume of	10

The ligation reactions were incubated at 16°C for 1 h or at 4°C overnight.

2.2.9. Sequencing Reactions (ABI)

Component	Volume (μ l)
Big Dye Terminator	1
Template (Plasmid DNA)	1
Primer (1pmol/ μ l)	3.2
Sequencing Buffer (5x)	1.5
Distilled H ₂ O to a final volume of	20

PCR Condition for sequencing samples

Denature	96°C	5 min	
Denaturation	96°C	10 sec	} 25 cycles
Annealing	50°C	5 sec	
Extension	60°C	4 min	
Final Temp.	4°C	30 min	

2.2.10. Ethanol Purification to remove excess Big Dye Terminators

The PCR product (20µl) was mixed with sterile MilliQ water (16µl) and 95% Ethanol (64µl) in a 1.5ml eppendorf tube. The tube was vortexed briefly and incubated for 1 h at room temperature. After the incubation, the tube was centrifuged at maximum speed for 20 min, and the supernatant was aspirated. 250µl of 70% ethanol (freshly prepared) was added and the tube was vortexed briefly, centrifuged for 10 min at maximum speed and the supernatant aspirated. The sample was dried on a dry block heater at 90°C for 1 min and then sent to the sequencing facilities at The Ramaciotti Centre, University of New South Wales.

2.2.11. Cloning and Sequencing of VH and VL.

Total RNA was isolated from antibody-producing hybridoma cells using the RNeasy Mini Kit (Qiagen) according to the manufacturer's instructions. The first-strand cDNA was synthesized with the SuperScriptTM III First-Strand Synthesis SuperMix for qRT-PCR (Invitrogen). DNA fragments encoding the heavy or the light chain (VH and VL) region of the monoclonal antibody were amplified separately with the respective primers at the concentration of 25pmol and cloned into pCR[®]-Blunt vector. The nucleotide sequences of the VH and VL region were determined by using the BigDye Terminator v3.1 Cycle Sequencing Kit (ABI).

2.2.12. Constructing scFv DNA.

Both variable regions of IV.3 MoAb were extended separately to yield VH fragment with PelB secretion signal at the N-terminal; VL fragment with FLAG and c-Myc tag at the C-terminal. The scFvs with three different linker sizes were constructed by assembling VH -15amino acids(aa) Gly₁₂-Ser₃ linker- VL, 21aa Gly₁₆-Ser₅ and 30aa Gly₂₃-Ser₇ variant using overlap extension PCR. Finally, 5'-*EcoRV* and 3'-*EcoRI* flanking restriction sites are included in all these constructs (Figure 2.1). The final amplified PCR product was run on 1.5% Tris base, acetic acid and EDTA (TAE) Agarose Gel (Invitrogen) and extracted with the QIAquick Gel Extraction Kit (Qiagen). The scFv fragment was digested with *EcoRV* and *EcoRI* for ligation into the periplasmic expression vector pIG6 at the corresponding restriction sites. The resulting plasmid pIG6-scFv was chemically transformed into the competent *E. coli* BL21 (DE3) cells and plated on LB plate containing 50µg/ml Ampicillin.

2.2.13. Molecular Modeling of STG1

The variable domains of IV.3 scFv (termed STG1) were individually modeled from their sequences by the Swiss-Model Workspace program (198); the whole structure of the scFv was modeled by the Pyre² program (199). The modeled structures were viewed with Pymol program (200).

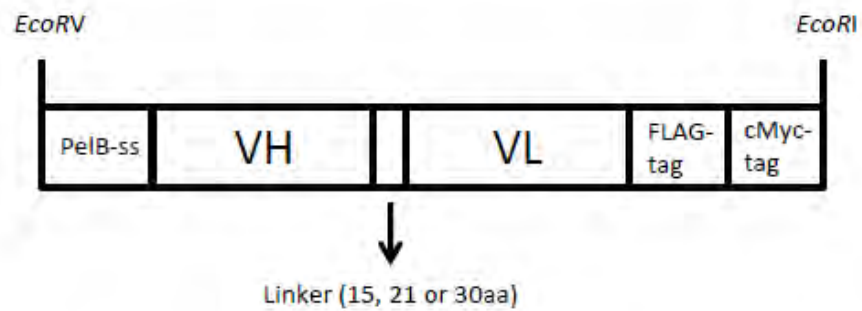


Figure 2.1. Schematic representation of STG1. The construct contains PelB secretion signal (PelB-ss) at the 5' end, heavy chain (VH), linker, light chain (VL), FLAG and cMyc tag at 3' end. *EcoRV* and *EcoRI* restriction sites were added to the complete construct for ligation into the periplasmic expression vector pIG6, for expression in *E. coli* BL21 (DE3) cells.

2.2.14. Humanization and Construction of STG2

STG1 was humanized by using the Complementarity Determining Region (CDR)-grafting and point mutation approach (201-203). The sequences of the six CDRs were preserved and selected amino acid residues were changed in the framework regions (FRs) regions to reflect the subgroups of human VH and VL domain. This was conducted with reference to the IMGT database available on the website (<http://www.biochem.unizh.ch/antibody>) (204). The DNA for the newly humanized IV.3 scFv (termed STG2), including codon optimization for protein production in *E. coli*, was synthesized by DNA2.0 (Menlo Park, CA). It is of the format of VH-Gly₂₃-Ser₇-VL, which include cMyc and His₆-tag at the C-terminus (Figure 2.2). The complete construct, which is flanked by *Nde*I and *Bam*HI restriction sites, was then digested from the commercial standard pJa vector and subcloned into the expression vector pET11a, which carries a T7 promoter. This new vector, pET11a-STG2 was chemically transformed into the competent *E. coli* BL21 (DE3) cells and plated on LB plates containing 50µg/ml Ampicillin.

2.2.15. Humanization and Construction of STG3

A further refinement for a humanized STG1 was conducted, and this construct was termed STG3. The humanization approach was carried out similarly as with STG2 (Section 2.2.14), but with fewer residue changes in the FRs. The DNA was synthesized by Genscript (New Jersey, US) in the format of VH-Gly₁₂-Ser₃-VL, which includes a PelB secretion signal at the N-terminus, and cMyc and His₆-tag at the C-terminus (Figure 2.3). The complete construct with *Nde*I and *Bam*HI restriction sites was cloned into the expression vector pET11a. The vector was chemically transformed into the competent *E. coli* BL21 (DE3) cells and plated on LB plates containing 50µg/ml Ampicillin.

2.2.16. Molecular Modeling of STG2 and STG3

The variable domains STG2 and STG3 were individually modeled from their sequences by the Swiss-Model Workspace program (198); the modeled structures were viewed and alignment was conducted with Pymol program (200).

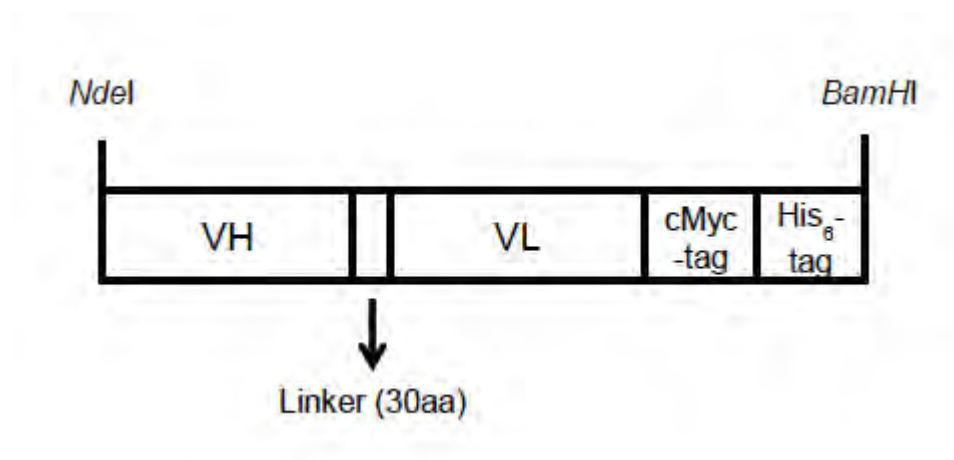


Figure 2.2. Schematic representation of STG2. The scFv contains VH, linker, VL with cMyc and His₆-tags at the 3' end. *NdeI* and *BamHI* restriction sites were added to the complete construct for ligation into the expression vector pET11a, for expression in *E. coli* BL21(DE3) cells.

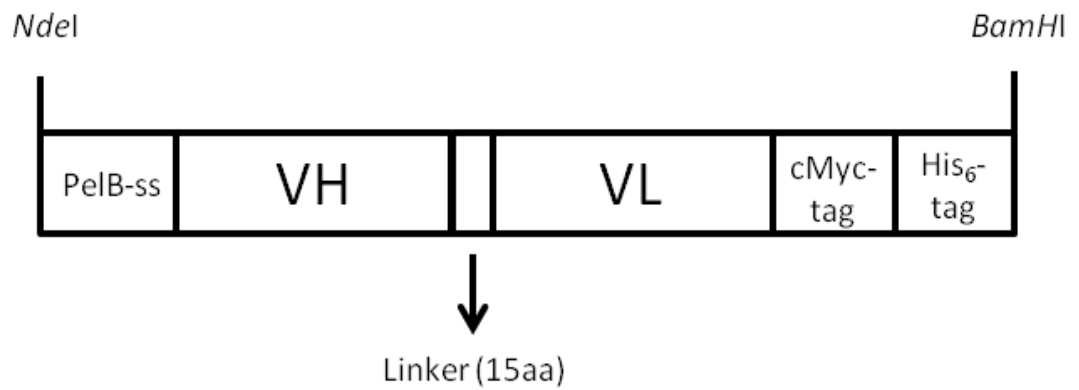


Figure 2.3. Schematic representation of STG3. The scFv contains PelB secretion signal (PelB-ss) at the 5' end, VH, linker, VL, cMyc and His₆-tag at 3' end. *NdeI* and *BamHI* restriction sites were added to the complete construct for ligation into the expression vector pET11a, for expression in *E. coli* BL21 (DE3) cells.

2.2.17. Construction of STGK2

A bispecific antibody (BsAb) in the form of Tandem scFv that targets both GP1b α and Fc γ RIIa was constructed. Here, a humanized scFv derived from parental antibody AK2 (anti-GP1b α) was linked with STG2 (short linker Gly₁₂Ser₃). The scFv derived from AK2 was humanized adopting the CDR-grafting and point mutation approach (201-203). The construct termed STGK2, was synthesized by DNA2.0 which includes codon optimization for protein production in *E. coli*. It was arranged in the format of humanized AK2 scFv (VH-Gly₁₂Ser₃-VL) attached to STG2 (VH-Gly₁₂Ser₃-VL) through a long linker Gly₂₃-Ser₇ (Figure 2.4). Two tags, cMyc and His₆ were included at the C-terminal end. Lastly, the final construct was flanked by *Nde*I and *Bam*HI restriction sites. The insert was digested from the commercial standard pJa vector and subcloned into the expression vector pET11a.

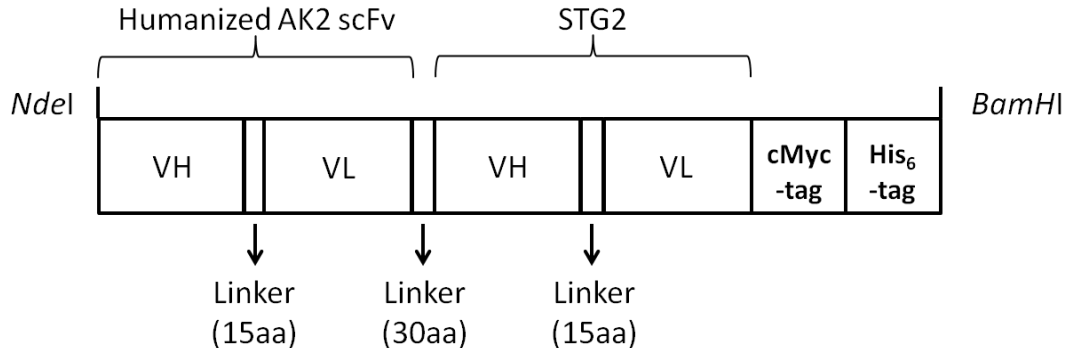


Figure 2.4. Schematic representation of STGK2. The construct contains two scFvs (derived from AK2 and IV.3) that target GP1b α and Fc γ RIIa respectively. Each scFv contains heavy chain (VH), short linker, light chain (VL). Both scFvs were then linked with a long linker, and two tags (cMyc and His₆) were included at the 3' end. *Nde*I and *Bam*HI restriction sites were included for ligation into the expression vector pET11a, for expression in *E. coli* BL21 (DE3) cells.

2.2.18. Protein Expression

Single colonies from a fresh LB plate were inoculated in 10ml of LB media containing 50µg/ml of Ampicillin and grown overnight at 37°C with shaking at 225rpm. The overnight preculture was used to inoculate 200ml of LB medium containing 50µg/ml of Ampicillin and incubated at 37°C. Protein expression was induced with 1mM of isopropyl-β-galactopyranoside (IPTG) when the culture reached an OD600 of 0.5-0.6. The culture was incubated for another 4h at 25°C. Samples containing 1ml of culture were collected right before induction and 4h post-induction. Bacterial pellets were obtained from these samples by centrifugation at 5000rpm for 10 min. The expression of the target scFv was analyzed by sodium dodecyl sulfate polyacrylamide gel electrophoresis (SDS-PAGE) under reducing conditions; detected by Western blotting with ANTI-FLAG antibody (Sigma-Aldrich; F3165) or c-Myc antibody (Santa Cruz; sc-70463) and visualized with ECL Plus Western Blotting Detection Reagents (Amersham Biosciences).

At the end of the expression period, bacterial pellets were collected and subjected to osmotic shock protocol for soluble (periplasmic) and insoluble fraction preparation. The cells were first suspended in 1ml of 0.033M Tris-HCl buffer followed by 1ml of TES buffer (0.033M Tris-HCl, 1.5mM EDTA and 20% sucrose) and incubated at room temperature for 15 min. After centrifugation at 5000rpm for 10min, the supernatant was discarded. 1ml of ice-cold 1mM MgCl₂ was added immediately and incubated on ice for 10 min. The insoluble fraction was collected by centrifugation at 5000rpm for 10 min at 4 °C, and separated from the periplasmic fraction. Both fractions were subjected to SDS-PAGE and Western Blot analysis. The insoluble fraction was kept for the subsequent inclusion bodies solubilization protocol prepared using urea.

For larger culture volumes (i.e. 1 L), the collected pellet after expression period was suspended first in 5ml of PBS and 10ml of TES buffer. The mixture was inverted gently a few times. After incubation at room temperature for 15 min, the partially lysed cells were subjected to sonication on ice (6X 15 sec bursts with 1min intervals to avoid overheating and prevent protein denaturation). The whole cell lysate was centrifuged for 10 min at 12,000rpm or even longer to obtain a clear supernatant solution. The supernatant was transferred to a clean 50ml tube and filtered through a 0.45µm filter unit to remove any insoluble particles.

2.2.19. Protein Purification of Soluble Fraction of scFv with ANTI-FLAG M2 Affinity Resin

Purification of FLAG-c-Myc-tagged scFv was carried out with ANTI-FLAG M2 affinity resin (Sigma-Aldrich; A2220). An empty chromatography column (Bio-Rad) was placed on column rack. The empty column was rinsed twice with PBS. Then a 400 μ l aliquot affinity resin was transferred to the column. The gel bed was drained and the gel was washed with three sequential column volumes (CVs) of 0.1M glycine HCl, pH 3.5, the solution was allowed to drain completely before subsequent addition. The resin was equilibrated with five CVs of PBS. An end cap was enclosed at the column outlet and the filtered bacterial supernatant was dispensed onto the column. It was then capped and the resin was loosened by gentle tapping. The column was then placed on a rotor and spun at 10rpm, overnight at 4°C.

The next day, the column was placed on the column rack to allow the resin to settle for approximately 30 min. The supernatant was then allowed to flow through and collected. This is the unbound fraction. The column packed with resin was washed with 10-20 CVs of PBS to remove any unbound proteins (the column was drained completely between CVs). The FLAG-tagged scFv was eluted with six 1ml aliquots of 0.1M glycine HCl, pH 3.5 into 1.5ml of eppendorf tubes containing 20 μ l of 1M Tris, pH 8.0. This was followed by re-equilibration to neutral pH with PBS. The column was regenerated by washing with three CVs of 0.1M glycine HCl, pH 3.5 and again re-equilibrated with PBS until the effluent returned to neutral pH. The column was stored by washing with ten CVs of 50% glycerol suspended in PBS buffer with 0.02% sodium azide and stored in 5ml of the same buffer at 4 °C without draining. The purified proteins were visualized by SDS-PAGE and Western Blot.

2.2.20. Protein Purification for Soluble Fraction with HiTrap HP column

5ml of lysis buffer (50mM Tris.HCl, 300mM NaCl, 1mM PMSF, 1% Triton X-100, and Protease Inhibitor (1X), pH 8.0) was added to the bacterial pellet collected from a 200ml culture. The pellet was then sonicated on ice (6X 15 sec bursts with 1min intervals to avoid overheating and prevent protein denaturation) and centrifuged at 10,000xg for 20min. The supernatant, which contains the soluble protein fraction was collected and filtered through a 0.45 μ m Millipore filter. 1ml of HiTrap HP column was positioned at the AKTA chromatography system (GE Healthcare) and equilibrated with

five CVs of the equilibration/binding buffer (50mM Tris.HCl, 300mM NaCl, 10mM imidazole, pH 8.0). This was followed by manual loading of the filtered soluble protein fraction via a luer connector. The fraction was passed through twice to maximize protein binding to the column. The bound protein was then eluted with 350mM imidazole in binding buffer at a flow rate of 1ml/min. The total gradient volume was 30 ml. The eluted peak was collected and dialyzed against 2 L of 50mM Tris.HCl, 300mM NaCl, pH 8.0 at 4°C, overnight. The sample was then concentrated using ultracentrifugal unit (10kDa) (Millipore) down to ~300µl and detected with SDS-PAGE and Western Blot.

2.2.21. Preparation and Solubilization of Inclusion Bodies

The inclusion bodies of the insoluble fraction of the bacterial pellet were washed twice (2x20ml) with inclusion bodies washing buffer containing 2M urea, 10mM EDTA, 2% Triton X-100, 50mM Tris, 500mM NaCl and 5mM DTT, pH 7.5 (205). The inclusion bodies were further washed twice (2x20ml) to remove the residual detergent with buffer containing 50mM Tris, 10mM EDTA, pH 7.5. All the above centrifugations were conducted at 5,000xg for 20min at 4°C. The collected inclusion bodies were solubilized overnight at 4°C in 5-10ml of 8M urea with 50mM Tris and 0.5mM β-ME (pH 8.0). The solubilized fraction was collected by centrifugation at 12,000xg, for 30 min at 4°C and used for protein purification.

2.2.22. Purification of Inclusion Bodies

Protein purification of His₆-c-Myc-tagged STG2 was carried out with the AKTA purifier chromatography system (GE Healthcare). The ProBondTM Nickel-Chelating Resin (Invitrogen) which is stored as 50% slurry in 20% ethanol was gently resuspended. And 5ml was then pipetted into an empty chromatography column (1.5 x 5cm; Bio-Rad). The resin was allowed to settle completely by gravity (~20 min). 8ml of sterile, distilled water was added, the resin was resuspended and then allowed to settle and the supernatant was aspirated. The prepared column was then equipped to the AKTA purifier chromatography system. The purification of the inclusion bodies was performed under denaturing condition. The inclusion bodies previously solubilized in 8M urea were loaded onto the column equilibrated with 10mM imidazole in binding buffer (8M urea, 50mM Tris, and 0.5M NaCl, pH 8.0) (206). After sample loading, the column was washed with 4 CVs of 20mM imidazole in binding buffer. The bound protein was then

eluted with a linear gradient of 500mM imidazole in binding buffer. The peaks of the elution were collected and visualized with SDS-PAGE and Western Blot.

2.2.23. In Vitro Refolding of Inclusion Bodies using Dialysis/Stepwise Dialysis System (205, 207, 208)

The *in vitro* refolding of inclusion bodies was tested with two approaches. The first approach involves a one step dialysis of the purified solubilized sample from 8M urea against 1M urea, 0.8M L-Arginine and 2mM GSH: 0.2mM GSSG. This was continued with another round of dialysis against 1 L of PBS. For the second approach, the eluted sample in 8M urea binding buffer with various concentrations of imidazole was refolded by gradual removal of urea. The stepwise dialysis started from 3M to 2M urea in buffer containing 50mM Tris, and 1M urea with 0.5M L-Arginine, and 0.5mM GSSG. The dialysis buffer was then diluted 1:2. In the end, the sample was dialyzed against PBS to remove the remaining denaturant. Each dialysis step was carried out overnight at 4 °C.

2.2.24. In Vitro Refolding of Inclusion Bodies using On-Column Refolding System (209)

1ml of the ProBond™ Nickel-Chelating Resin (Invitrogen) was manually packed into an empty chromatography column and equipped to the AKTA purifier chromatography system. The column was equilibrated with 5ml of binding buffer (50mM Tris, 500mM NaCl, 8M urea, 1mM β-ME and 10mM imidazole, pH 8.0). Three mg of the solubilized inclusion bodies were loaded onto the column at a flow rate of 0.5ml/min. After loading, the column was washed with five CVs of 20mM imidazole in binding buffer. The bound protein was then refolded on-column by a linear urea gradient of 8.0 to 0M, starting with the washing buffer and gradually replaced with a refolding buffer (50mM Tris, 500mM NaCl, 1mM β-ME, 1mM GSSG, 1mM GSH and 20mM imidazole, pH 8.0). The total gradient volume was 50ml and the refolding was conducted at a flow rate of 0.5ml/min. The refolded protein was then eluted with elution buffer (50mM Tris, 500mM NaCl, 1mM β-ME, 350mM imidazole, pH 8.0). The eluate was pooled and dialyzed against PBS overnight at 4°C to remove imidazole. The eluate was collected and concentrated using ultracentrifugal unit (10kDa) (Millipore). The protein was then analyzed by SDS-PAGE and Western Blot.

2.2.25. Protein Purification and Refolding with Styrene Maleic Acid Lipid Particle (SMALP) (210, 211)

The bacterial pellet from a 200ml culture was collected and suspended in 20ml of chilled 50mM Tris.HCl (pH 8.0) 5.0mM EDTA. The pellet was then disrupted by sonication. The cell lysate was spun down at 35,000xg and resuspended in 20ml of 50mM Tris.HCl (pH 8.0) with 2% Triton X-100 by vigorous stirring at room temperature for 1h. This was followed by washing twice with the same buffer without Triton X-100, the centrifugation was carried out at 5,000rpm, 20 min at 4°C. The pellet was dissolved in 5% SDS and dialyzed for five days with two buffer changes against 50mM Tris pH 8.0 to remove excess SDS. The concentration of the protein sample was then adjusted to 0.5mM.

Solid n-octyl- β -D-glucoside (β -OG) (Affimatrix) was dissolved in water to a concentration of 100mM. Ethanol was added to a final concentration of 1% (v/v). Dimyristoylphosphatidylcholine (DMPC) (Sigma-Aldrich) was added to a concentration of 2% (w/v) and stirred until completely solubilized. Bio-Beads SM Adsorbents (Bio-Rad) were then added at twice the manufacturer's specifications to remove β -OG detergent. The sample was mixed by rotation at 4°C, overnight. Then, 5% of SMA copolymer (Malvern Cosmeceutics Ltd UK) solution in 50mM Tris pH8.0 was added to 1:1 (v/v) and left stirring until a clear solution was obtained. The excess copolymer/lipid was then removed and the protein purified with 1ml HisTrap HP column (GE Healthcare). The column was first equipped to the AKTA purifier chromatography system, and equilibrated with five CVs of binding buffer (50mM Tris, 300mM NaCl and 10mM imidazole, pH 8.0). The protein sample was then loaded manually onto the column, followed by elution with elution buffer (50mM Tris, 300mM NaCl and 350mM imidazole, pH 8.0) at a flow rate of 0.5ml/min. The total gradient volume was 15ml. The eluted protein fraction was detected on SDS-PAGE and Western Blot analysis.

2.2.26. Preparation of Platelets for Flow Cytometry Analysis

The binding of the protein of interest to human platelets was assessed by flow cytometry. Platelet-rich plasma (PRP) was first obtained from whole blood after centrifugation at 200xg for 10 min. Washing/Suspension buffer (PBS, 0.5% BSA, 25mM EDTA, pH 6.8) was used for platelet preparation throughout the experiment. Platelets (5×10^5 to 25×10^6 cells were used) were first washed with 500 μ l of buffer and centrifuged at 4000rpm for 5 min. After discarding the supernatant, the pellet was suspended in 25 μ l of buffer and incubated with the primary antibody for 30 min at 4°C. Cells were washed once with 500 μ l of buffer and incubated with the secondary antibody. After washing, platelets were suspended in 150-200 μ l of PBS and analyzed using a FACSCalibur™ flow cytometer (Becton-Dickinson). Controls were prepared by incubating platelets with secondary antibody alone for nonspecific binding and/or with isotype controls. A single platelet gate was created based on the forward- and side-scatter profiles of human platelets, eliminating small debris, platelet doublets and clumps. At least 10,000 events were collected for each sample.

Platelets were incubated with primary antibody of either

- a) IV.3 MoAb against Fc γ RIIa,
- b) AK2 MoAb against GPIb α ,
- c) Phycoerythrin (PE)-conjugated anti-human CD41a (1/5; BD Pharmingen™),
- d) Fluorescein isothiocyanate (FITC)-conjugated anti-human CD42a (1/5; BD Biosciences),
- e) Simultest control γ_1/γ_1 (1/5; BD Biosciences),
- f) Protein of interest.

Secondary antibodies

- a) Alexa Flour® 488 (AF488)-conjugated anti-mouse IgG (1:200; Invitrogen),
- b) AF488-conjugated anti-c-Myc (1:50; Santa Cruz; sc-40).

2.2.27. Platelet Aggregation Assay (212)

Platelet aggregation assay was performed by mixing samples at 1200rpm, 37°C for 15 min in an aggregometer (Chrono-log Aggro/Link™). The reaction mixture (Final volume of 500 µl) consisted of 300µl of healthy donor PRP, with 20µl of HIT patient serum or purified Total HIT IgG (0.8 to 3.5mM, adjusted according to different donor platelets) and 10µl heparin (0.5IU/ml). As a positive control, IV.3 MoAb was added to a final concentration of 10 to 20nM. Test assays contained different amounts of the protein of interest as described in the appropriate Results section. The degree of aggregation was determined by the increase in light transmittance. Platelet aggregation levels over 20% were considered positive.

2.2.28. Serotonin Release Assay (SRA) (130)

SRA is the gold standard to confirm the presence of platelet-activating HIT antibodies (130). HIT patient serum were first heat inactivated at 56°C for 60 min followed by centrifugation at 12,000rpm for 2 min to remove precipitated fibrinogen. PRP from a healthy donor was then incubated with Hydroxytryptamine Binoxalate, 5-[2-¹⁴C]- (Serotonin) (¹⁴C-5HT) (1.5µl/ml), at 37°C for 45 min. At the end of the incubation, PRP was centrifuged at 2300 rpm for 10 min and the platelet poor plasma (PPP) was discarded. The ¹⁴C-serotonin-labeled platelets were then washed once with calcium/albumin free Tyrode's buffer pH 6.2 (130mM NaCl, 2.7mM KCl, 12 mM NaHCO₃, 0.4 mM NaH₂PO₄, 2 mM MgCl₂, 5.6 mM Glucose and 2 IU/ml of apyrase) and incubated at 37°C for 15 min. After centrifugation at 2300 rpm for 10 min, the supernatant was discarded. The platelets were then resuspended in the same buffer, without apyrase, but with 2mM CaCl₂, and pH was adjusted to 7.4. The platelets were incubated at 37°C for 15 min and the final concentration was set to around 600,000 platelets/µl.

20µl of HIT serum was mixed with 5µl of heparin (0.1 (low dose) or 100 IU/ml (high dose)) and 37.5µl of ¹⁴C-serotonin-labeled platelets. The protein of interest was then added and the volume adjusted to 100µl. The platelet mixture was incubated in microtitre wells that contained a magnetic stir bar. The plate was covered with parafilm and incubated at room temperature for 1 h on a magnetic stirrer set at low speed. 100µl of 1% EDTA was then added into each well to terminate the reaction. The platelets were centrifuged at 1600rpm for 2 min. 50µl of the supernatant was added to 1ml of aqueous

counting scintillant, placed in a scintillation tube. The samples were counted in a scintillation counter for 1 min. The percentage of ^{14}C -serotonin released was calculated as follows:

$$\text{percent release} = \frac{\text{Test sample count per minute} - \text{background}}{\text{Total sample count per minute} - \text{background}} \times 100$$

The background was defined as the supernatant fluid radioactivity from platelets that were treated exactly as the test samples but in the absence of HIT serum (HIT serum was substituted with 20 μl of 2% BSA in PBS). The control platelets were lysed with 100 μl of lysis buffer (150mM NaCl and 0.5% Triton X-100). The total sample was then measured directly without centrifugation. A test result is defined as positive if more than 20% serotonin release is detected with a therapeutic heparin concentration of (0.1 IU/ml) but not with a high dose of heparin (100 IU/ml).

2.2.29. Purification of Platelet Factor 4 (PF4)(212)

15ml of Heparin Sepharose Beads (GE Healthcare) were loaded to an Econo-Column Chromatography Column (Bio-Rad) and equipped to the AKTA purifier chromatography system. Prior to purification, the beads were washed with different buffers (Two CVs for each buffer, flow rate at 1ml/min) in the following order: Washing Buffer (20mM HEPES, 0.5M NaCl, 5mM EDTA, pH 7.5) \rightarrow 6M Guanidine HCl \rightarrow Washing Buffer \rightarrow 70% Ethanol \rightarrow Washing Buffer.

PPP was derived from expired platelet packs (~1200ml) after centrifugation at 5000 rpm for 20 min. PPP which contains PF4 was incubated with the washed heparin sepharose beads in a conical flask, shaking at 150 rpm, 4 $^{\circ}$ C, overnight. The beads were allowed to settle for 1 to 2 h at 4 $^{\circ}$ C before the supernatant was carefully separated without disturbing the beads. The beads were then gradually collected in a 50ml Falcon Tube after resuspension with washing buffer. Centrifugal speed of 500rpm for 10 min was used to separate the beads from the washing buffer which was discarded. This was continued until all the beads from the conical flask were collected.

The Heparin Sepharose Beads were loaded to the Column and equipped to the AKTA chromatography system. After the beads were equilibrated with two CVs of washing

buffer, a crude PF4 extract was eluted (20mM HEPES, 2.0M NaCl, 5mM EDTA, pH 7.5) with two CVs at 1ml/min. The crude PF4 extract was then concentrated to a volume of approximately 300µl and loaded to the gel filtration chromatography column packed with Superdex 75 pg (GE Healthcare). The PF4 was then eluted with the same elution buffer to further separate from other contaminants like antithrombin III to obtain purified PF4. This filtration step was repeated three times until an isolated peak of PF4 was obtained. The protein concentration of PF4 was determined according to the Bradford Assay using BSA as a reference protein and was visualized on SDS-PAGE.

2.2.30. Purification of IV.3 MoAb

The purification of IV.3 MoAb from the spent media of cultured IV.3 producing hybridoma cells was conducted first with ammonium sulphate precipitation (Refer to Appendix, Table A1.1), followed by purification with Protein G Agarose (Roche). The total volume of supernatant collected for purification was 1400ml and 2.9g of ammonium sulphate was added to every 100ml of supernatant to achieve a final concentration of 45% saturation at 0°C. The salt was added in small portions to the supernatant placed on a stirrer at 4 °C. It was allowed to dissolve completely before the next portion was added. The supernatant was then left at 4 °C, overnight to allow precipitation of the MoAb. The pellet was collected after centrifugation at 5000rpm for 20 min and was dissolved in 70ml of starting buffer (20mM sodium phosphate, pH 7.0). This was followed by purification of the IV.3 MoAb with Protein G Agarose. 2ml of Protein G Agarose (Roche) was packed into an empty chromatography column (1.5 x 10cm; Bio-Rad), equipped to the AKTA purifier chromatography system and equilibrated with five CVs of the starting buffer. The resin was divided into two 50ml falcon tube and mixed with 35ml (each tube) of the previously dissolved MoAb sample. Batch binding was conducted on an orbital shaker at 10rpm, 4 °C for 1 h. After allowing the resin to settle for 30 min, the supernatant was removed and the resin was transferred to the chromatography column. The column was placed on the purification system and washed with five CVs of washing buffer at 1ml/min, followed by elution with ten CVs of elution buffer at 1ml/min into tubes containing 30µl/ml of 1.0M Tris-HCl, pH 9.0 to neutralize the solution. The eluted peak fraction was pooled and concentrated using ultracentrifugal unit (10kDa) (Millipore). The concentration of purified MoAb was determined according to the Bradford Assay using BSA as a reference protein.

The Protein G Agarose resin was regenerated in the order of water, starting buffer, 6M Guanidine HCl, 70% Ethanol and reequilibrated with the starting buffer again before conducting another round of purification to ensure maximum purification of IV.3 MoAb from the hybridoma supernatant.

2.2.31. Purification of Total HIT IgG

The purification of total HIT IgG from patients' serum was carried out with Protein G Agarose (Roche). Approximately 2ml of the resin was packed into an empty chromatography column (1.5 x 10cm; Bio-Rad), equipped to the AKTA purifier chromatography system and equilibrated with five CVs of the starting buffer (20mM sodium phosphate, pH 7.0).

The fibrin, if present, from 11.5ml of HIT serum was first removed by centrifugation at 4000rpm (10min at 4°C) and the serum was manually dispensed onto the column. The column was placed on an orbital shaker at 10rpm, 4°C. After 1 h, the serum was allowed to flow through. The column was placed back in the purification system and washed with ten CVs of washing buffer (20mM sodium phosphate, 150mM sodium chloride, 2mM EDTA, pH 7.0) at 1ml/min. Total HIT IgG was then eluted with 15 CVs of elution buffer (100mM glycine, pH 2.7) at 1ml/min into tubes containing 30µl/ml of 1.0M Tris-HCl, pH 9.0 to neutralize the solution. The eluted peak fraction was pooled and concentrated using ultracentrifugal unit (10kDa) (Millipore). The protein concentration of purified total HIT IgG was determined according to the Bradford Assay using BSA as a reference protein.

The Protein G Agarose resin was regenerated (Section 2.2.31) before conducting another round of purification on the same HIT plasma collected earlier on. This was repeated twice to ensure maximum recovery of Total HIT IgG from the HIT plasma.

2.2.32. Establishment of HIT Animal Model using NOD/SCID Mice

2.2.32.1. Subcutaneous Injection of Mice

The mouse was placed on the wire lid on the cage to allow it to hang on with its front paws, it was then restrained with the hand and the skin was lifted over the back to form a tent using the fingers. The needle was then inserted at the tent base at a parallel position to the mouse's body to avoid puncturing internal structures. The plunger was then pulled back a little to confirm it had not entered a blood vessel. The full content was injected at a moderate rate. The syringe was then withdrawn and the skin was pressed gently to seal the penetration site.

2.2.32.2. Intraperitoneal Injection of Mice

To avoid injuring the internal organs, the mouse was restrained with one hand by using the index finger and the thumb to tilt the head facing downward; middle finger and ring finger to restrain the hind leg and the tail, respectively. This allows the abdominal area to be well exposed. The needle was then inserted into the right side of the lower abdominal area (close to the midline) at about 30° angle after the injection site had been disinfected. The shaft of the needle was entered to a depth of about half a centimeter. The plunger was pulled back a little to confirm it had not entered a blood vessel or an organ (i.e. intestine or urinary bladder). The full content was injected if no fluid was aspirated. The syringe was then withdrawn.

2.2.32.3. Tail Vein Injection of Mice (213)

Prior performing the procedure, the mice were warmed under a lamp. This is to dilate the tail vein on both sides. The veins should be clearly visible beneath the skin on the lateral surface of the tail. The mouse was then restrained on a restrainer, but leaving the tail free. The tail was then gently held using both index finger and thumb, at an approximate position of 6cm from the base of the tail. In this context, the tail should rest on the index finger and be restrained with the thumb. The syringe was held with the bevel of the needle facing upwards, and inserted into the vein under the skin. This was conducted in a parallel angle in relation to the tail. The plunger was then depressed to deliver the contents from the syringe into the tail vein. After the contents had been delivered, the needle was removed and pressure was applied for approximately 30 sec on the penetration site to stop the blood flow.

2.2.32.4. Blood Collection from Mice (214)

The mouse was restrained in a 50mL Falcon Tube with its head tucked in the tube and with the hind legs free. The thigh was grasped firmly and the saphenous vein, found on the caudal surface of the thigh, was exposed after the hair was removed with a shaver. Petroleum jelly (Vaseline) was then applied to prevent blood migration into the surrounding hair. The vein was punctured with a 27G x 0.5" needle (BD Diagnostics) and the blood was collected with a Microvette® CB 300 Kalium-EDTA (Sarstedt) blood collection tube via capillary action. Pressure was then applied at the penetration site to stop bleeding.

2.2.32.5. Preparation of Human Platelets and Determination of Human Platelets Survival (215, 216)

Whole human blood was collected into acid-citrate-dextrose tube (BD Diagnostics) and centrifuged at 200xg for 10 min to collect platelet-rich plasma (PRP). The platelets were then spun at 750xg for 10 min and resuspended in human plasma at a concentration of 2.0×10^9 /ml. Platelet concentrates (200 μ l) were injected into the tail vein of NOD/SCID mice (8-12 weeks old, female). Blood samples were then collected at different time points (1, 2, 4, 24, and 48 h) for analysis of the survival rate of human platelets (Bleeding protocols are detailed in the previous section). At the last venesection (48 h), the mice were euthanized with carbon dioxide inhalation and the carcasses were disposed in the hospital waste system.

2.2.32.6. Flow Cytometry Analysis of Human Platelets

For each mouse, 1 μ l of blood was used for control and 2 μ l for human platelet analysis, each suspended in separate tubes in 230 μ l of PBS. The control tube was incubated with anti-mouse IgG1 negative control AF647 (1:10; AbD Serotec) and PE Rat IgG1, κ isotype control (1:100; BD Biosciences); the sample tube was incubated with AF647-conjugated anti-human CD41 (1:10; AbD Serotec) and PE Rat anti-mouse CD41 (1:100; BD Biosciences). After incubation for 30 min at 4°C, 50 μ l of CountBright™ Absolute Counting Beads were added to each tube prior to analysis with the FACSCalibur™ flow cytometer (Becton-Dickinson). A single platelet gate was created based on the forward- and side-scatter profiles of platelets. These platelets were later distinguished based on the different fluorescence marker of the labeling antibodies and the percentage of human platelets determined. 1000 counting beads events were

collected and used to calculate the total number of human platelets according to the formula provided by the manufacturer.

2.2.32.7. *Set up for HIT animal model*

To establish the experimental animal model, several components must be introduced.

Model A

A group of nine mice were separated into three groups. At Day 0, 1.5mg of normal human IgG was injected intraperitoneally to group A, and two different concentrations of total HIT IgG (0.75mg or 1.5mg) to groups B and C. For the next day, human PF4 (80µg/ml, final concentration in mouse)(67) was injected via tail vein together with PRP. After 1 h, blood was collected followed by tail vein injection of heparin (600IU/kg). Blood was again collected at 2nd, 4th and 24th h.

Model B

A group of eight mice were separated into two groups. At Day 0, either normal human IgG or HIT IgG together with PF4 were introduced simultaneously via peritoneal injection to the control/experimental group. The following day, PRP alone was introduced via tail vein, and after 1 h, blood was drawn and heparin (600IU/kg) was injected subcutaneously. Subsequently, blood was collected at 2nd, 4th and 24th h.

2.2.33. *Statistical Analyses*

All statistics were conducted using Microsoft Excel. Data are represented either as mean or mean \pm SEM. Differences in each value between groups were analyzed by Student, unpaired, 1-tailed *t* test (Platelet Aggregation Assay and SRA), or 2-tailed *t* test (HIT animal model).

Chapter 3
Anti-FcγRIIa scFv Inhibits Platelet Activation
Induced by HIT Immune Complexes

3.1. Introduction

MoAbs represent one of the fastest growing areas of biopharmaceutical product development with broad applications in medical research, diagnosis, therapy, and basic science (217, 218). Despite their potential applications, the use of MoAbs is often hampered by issues including immunogenicity (i.e. HAMA response) (181, 219), large molecular size that reduces accessibility to the target sites (i.e. solid tumour mass) (192) and Fc-induced unwanted effector functions (i.e. massive cytokine release associated with toxic effects) (193). These obstacles however, can be largely overcome by producing a smaller version of the antibodies. The antibody fragment that contains a complete antigen binding site is the Fv that comprise of VH and VL domains. Back in 1988, it was first reported that the two variable domains can be connected with a synthetic peptide linker, to create a recombinant molecule known as the single-chain Fv (scFv) antibody fragment (195, 220). This could be assembled in either domain order, as VH-linker-VL or VL-linker-VH. Both arrangements have been shown to retain the binding specificity of the parental MoAb. The peptide that bridges the carboxy-terminus of one domain and the amino-terminus of the other should have a length of approximately 3.5nm to ensure the domains are folded correctly to form an intact antigen binding site (220). An ideal linker should therefore be at least 10 residues in length. Linkers of 15 residues are the most commonly used (221).

3.1.1. Generation of scFv

The coding sequence of the variable region of the MoAb of interest can be cloned from hybridoma cells using PCR technology which was first reported by Chaudhary *et al* (222). The approach omits the need of creating and screening genomic or cDNA libraries, allowing the construction of variable regions of many different MoAbs from hybridoma RNA. After the first-strand of cDNA is obtained by reverse transcription of mRNA, the variable regions can be easily cloned using primers that hybridize to the conserved sequences present in the constant (CH1 or CL) domains which adjoin the variable region (222). The primers that anneal to the 3' end of the variable region are of simple design, since the sequences of the constant domain exons are known (223). The design of primers for the 5' end of the variable region on the other hand, was more laborious due to the sequence variability of different V genes. To create these primers, the early approaches included N-terminal protein sequencing of purified antibodies,

which allowed the variable gene families to be categorized followed by the design of degenerate primers based on framework region 1 (223, 224). In 1989, a more simplified approach was undertaken whereby the conserved portions on the 5' region of the VH and VL genes were identified after alignment with the Kabat database (225). This allows the creation of degenerate oligonucleotide primers containing restriction sites for cloning. Since then, a variety of primers suitable for the amplification of murine variable domains has been available (226, 227).

scFv genes can be efficiently constructed either by sequential cloning of both VH and VL genes and assembled with a linker segment generated from oligonucleotides (220), or by using PCR for direct assembly the scFv gene. The latter approach generates the linker by overlap extension of the two primers, which contain both segments of the linker and of the variable region (228-230). With the introduction of restriction sites at both ends of the final construct, the scFv can then be cloned into any desired plasmid for expression purposes (Figure 3.1).

The production of functional Fv and Fab using *E. coli* was first described by Skerra and Plückthun (231) and Better (232). This was subsequently followed by the successful expression of scFv using the same system (233) and has since been the most widely used method for the production of scFv Abs (201, 234, 235). Although other expression systems such as mammalian (236, 237), yeast (238), plant (239, 240) and insect cells (241) have also been reported, bacterial expression systems are still the preferred option when it comes to high yield production. In addition, *E. coli* requires low cost media for rapid growth, and can be easily scaled-up for large scale production using fermenters (242).

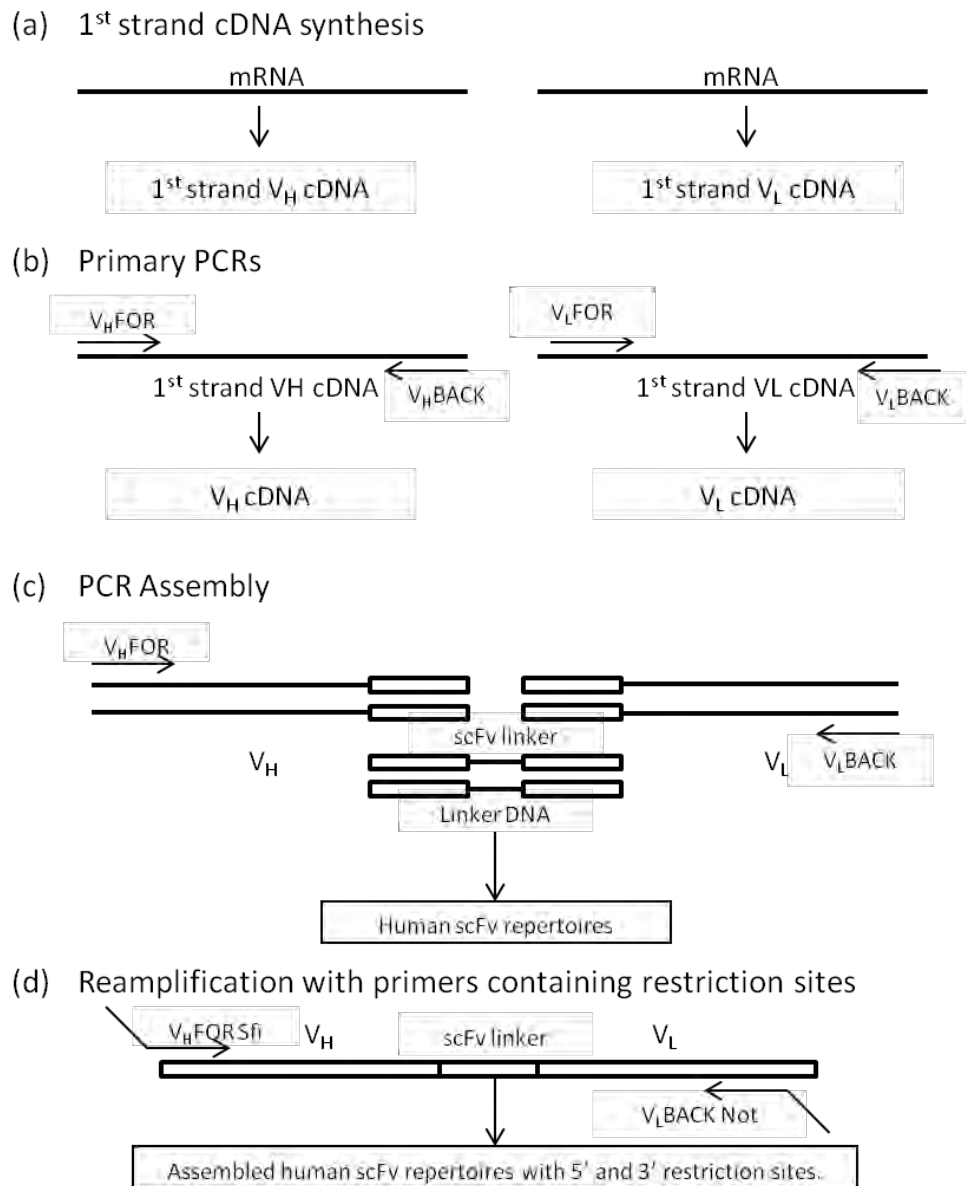


Figure 3.1. PCR assembly of scFv. (a) 1st strand of cDNA is synthesized from mRNA via reverse transcription. (b) 1st strands of cDNA are separately amplified with a mixture of V_H and V_L primers. (c) The V_H and V_L gene are mixed with linker fragment that overlaps C-terminal of V_H and N-terminal of V_L, which is subjected to temperature cycling and PCR amplification (d) The final product of the assembled scFv gene can be reamplified to introduce restriction sites for further cloning. Adapted from Marks et al (229).

The expression of the scFv in *E. coli* can occur via two routes, either by secretion into the periplasmic space (the compartment between inner and outer membrane of the bacteria cell) or into the cytoplasmic space. Proteins secreted into the periplasmic space usually appear to fold properly and are functionally active due to the oxidizing environment that allows correct formation of disulfide bonds (232, 233). This is particularly important for scFvs as the internal disulfide bonds that connects β -sheets of the β -sandwich structure are essential for the folding of VH and VL domains (243).

Currently, there are signal peptides available to direct protein secretion into the periplasm such as OmpA and PelB (244-246). scFvs that are expressed into the cytoplasmic space, are usually misfolded and are present in aggregated form, which leads to the formation of inclusion bodies. In addition to the reducing state of the cytoplasm that strongly prevents the formation of stable disulfide bonds in proteins (247), the formation of protein aggregates can also be due to unwanted intermolecular interactions among partially folded proteins with exposed hydrophobic surfaces. This usually occurs when the proteins are produced at high levels with insufficient amount of chaperones to aid the correct folding of these polypeptides (248). Therefore, several strategies have been developed and established to restore misfolded proteins, as reviewed by Vallejo and Rinas (249). Lastly, to facilitate the affinity purification and detection of these recombinant proteins, polypeptide fusion partners, termed affinity tags can be included. Examples of tags commonly used in scFvs include c-Myc, poly-histidine and FLAG (250-252).

3.1.2. scFv as Therapeutic Molecules

The created scFv serves as the smallest antibody fragment that still contains the complete antigen binding site, presented with a reduced molecular weight relative to a whole antibody (~28000 Da Vs ~150000 Da) (253). This provides a significant advantage in the application of these molecules for treatments such as tumour therapy where the target antigens are often expressed on the surface of the cancer cells. The smaller size bestows the scFvs with unique properties such as better tumour penetration, rapid clearance from the body and no kidney retention, thus allowing efficient localization to the tumours and absence of side effects involving the constant domains (221, 254).

While progress has been made in developing scFvs for tumour therapy, the focus has also shifted to other fields including vascular biology and more specifically, platelets. It is well established that platelets play an important role in normal haemostasis where they adhere and aggregate to form thrombi in response to the site of vascular injury (255). However, in the scenario of ruptured atherosclerotic plaques, platelet activation can lead to thrombotic disorders causing additional tissue damage, which could prove fatal in patients suffering from coronary artery disease (256). These thrombotic disorders led to the development of anti-platelet drug therapy, such as aspirin that inhibits cyclooxygenase, clopidogrel that inhibits adenosine diphosphate receptor and dipyridamole that targets phosphodiesterase (256). In addition, an antibody fragment-chimeric Fab (Abciximab) targeting the receptor GP IIb/IIIa on platelets was created and approved by the FDA for use in patients undergoing percutaneous coronary intervention (257). By inhibiting GPIIb/IIIa, the antibody prevents the last stage of platelet aggregation thus preventing thrombus formation. This pioneer approach has therefore opened up new possibilities for effective platelet targeted treatment using antibodies. Up to date, functional scFvs directed at platelet receptors such as integrin GPIIIa 49-66 and GPVI for thrombus imaging and antithrombotic therapy have been reported (258-260).

Apart from thrombotic events, platelet numbers can also drop due to other causes. Low platelet numbers lead to a bleeding disorder known as thrombocytopenia. The cause of thrombocytopenia could be hereditary due to congenital defects in platelet receptors (70), immune-based (immune thrombocytopenia) caused by autoantibody destruction of platelets, or drug-induced where neoepitopes are formed on the platelet receptors, leading to formation of antibodies or immune complexes that destroy the platelets (261). Drugs that are implicated include penicillin, quinidine, quinine, gold salts, heparin, tirofiban and abciximab (261). This thesis will only deal with heparin-induced thrombocytopenia (HIT).

3.1.3. Limitations of Current Treatment for HIT

Approximately 0.2-5% of patients receiving heparin are at risk of developing HIT, which is a limb- and life-threatening disorder (150). The treatment for HIT consists of the cessation of heparin administration and initiation of nonheparin parenteral anticoagulant treatment such as lepirudin and argatroban (Details discussed in Introduction, Section 1.12). Although the use of these anticoagulants is effective to some extent in controlling existing and preventing new thrombosis, they have not been effective in reducing serious consequences of HIT such as limb loss and death. In HAT-1, HAT-2 and HAT-3 clinical trials, limb amputations and death occurred in 5-7% and 8.6-13.6% of HIT patients treated with lepirudin (262-264); while in ARG-911 and ARG-915 clinical trials, limb amputations and death occurred in 11.1-14.8% and 18.1% - 23.1% of HIT patients treated with argatroban, respectively (265).

The incomplete antithrombotic efficacy observed in HIT patients is probably due to the failure of these anticoagulants to extinguish the strong initiating event in HIT, which is the binding of HIT immune complexes to Fc γ RIIa. This interaction leads to the activation of platelets and the coagulation cascade that generates thrombin, ultimately resulting in serious thrombosis. To treat HIT more effectively, particularly patients with extensive and severe thrombosis, there is still an unmet clinical need for new drugs or therapeutic agents that could block the HIT immune complexes/Fc γ RIIa interaction, consequently preventing the disastrous thromboembolic complications such as limb amputation and death.

Novel drugs targeting the formation of PF4/Heparin complexes and signalling pathways associated with the activation of Fc γ RIIa have been reported (Refer to Introduction, Section 1.13). However, to date, no studies have been published concerning the inhibition of HIT complex interacting with the platelet Fc γ RIIa. This thesis therefore focuses on the generation of an anti-Fc γ RIIa scFv that will block this interaction and thus, may potentially serve as a useful drug for the treatment of HIT.

3.1.4. Hypothesis and Aims

For more than two decades, the IV.3 MoAb has been known to specifically bind to FcγRIIIa. The functionality of the antibody has therefore been applied mainly in the area of HIT diagnosis and medical research. However, with the emergence of antibody engineering, medical treatments focusing on using either MoAb or antibody fragments have been possible. The therapeutic properties of the IV.3 MoAb have not yet been explored. Therefore, by applying the approach of antibody technology, we hypothesized that an antibody fragment, such as a scFv, derived from the IV.3 MoAb will retain the functional properties of the parental antibody. This antibody fragment would bind the FcγRIIIa, block immune complex interaction and prevent HIT-induced platelet activation. Based on this hypothesis, the aims for this chapter are:

- To clone the gene sequence of IV.3 MoAb variable regions using cDNA derived from IV.3 producing hybridoma cells.
- To create a scFv gene construct. The variable sequence of VH and VL will be connected with a flexible peptide linker using PCR. PelB bacterial secretion signal and two affinity tags (FLAG and cMyc) will be introduced at the N- and C-termini, respectively.
- To express the scFv. The protein will be expressed in *E. coli* cells and purified by affinity chromatography.
- To characterize the properties of the scFv. The binding and functional activities of the protein will be evaluated using flow cytometry, platelet aggregation and serotonin release assays.

3.2. Results

3.2.1. *Molecular Cloning and Sequencing of the VH and VL Fragments of IV.3*

As described in Section 3.1.1, hybridoma cells are the primary source to derive the coding sequence of the variable region of MoAbs. We isolated total RNA from the IV.3 MoAb producing hybridoma cells (173) to create cDNA via reverse transcription. The cDNA serves as a template for the amplification of VH and VL (Refer to Table 3.1 and 3.2 for PCR conditions) region using specific primers as previously described (266). These primer sets (Refer to Appendix, Table A2.1) contain the sequence of the constant region (CH1 (Heavy Chain) and CL (Light Chain)) that adjoined to the variable region, thus allowing the annealing of the primers to the template. The resulting amplified VH and VL regions were approximately 360 bp and 342 bp in length (Figure 3.2). This is in agreement with the size obtained by Ohshima et al for a different MoAb (267).

Both fragments were cloned into pCR[®]-Blunt vector (Invitrogen) for sequencing and the results revealed that they possess the basic characteristics of immunoglobulin variable region genes. The DNA sequencing results of VH and VL are shown in Figure 3.3. The sequence analysis of IV.3 variable regions was conducted using <http://www.ncbi.nlm.nih.gov/igblast/> according to NCBI murine database and Kabat classification (223). The analysis indicated that VH chain belongs to the mouse IgG heavy chain family group 9 with 90.8% homologous to murine germline gene VH9.12 [GenBank: AY169688 (268)]. VL chain on the other hand belongs to the mouse IgG kappa light chain family group 2 with 95 % homologous to murine germline gene hf24 [GenBank: AJ231263.1 (269)] (Refer to Appendix, Figure A2.1 for sequence alignment of both variable regions). The CDR regions were determined by referring to Kabat definition.

Table 3.1. PCR conditions for VH amplification

Condition	Temperature/ Duration	Cycle
Initial Denaturation	95 °C/ 5 min	-
Denaturation	94 °C/ 45 sec	35 Cycles
Annealing	50 °C/ 45 sec	
Extension	72 °C/ 90 sec	
Final Extension	72 °C/ 5 min	-

Table 3.2. PCR conditions for VL amplification

Condition	Temperature/ Duration	Cycle
Initial Denaturation	95 °C/ 5 min	-
Denaturation	94 °C/ 45 sec	30 Cycles
Annealing	54 °C/ 45 sec	
Extension	72 °C/ 90 sec	
Final Extension	72 °C/ 5 min	-

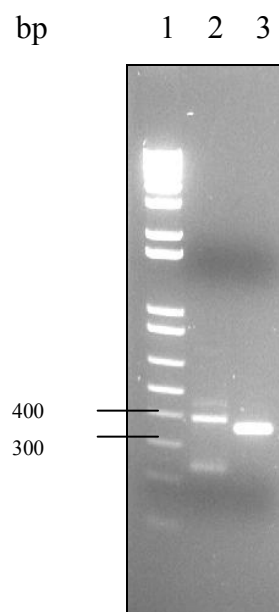


Figure 3.2. PCR amplification of VH and VL regions. Electrophoresis was performed on 1.5% agarose in 1 x TAE buffer. Lane 1: 1kb Plus DNA Ladder (Invitrogen); Lane 2: VH PCR product (360bp); Lane 3: VL PCR product (342bp).

VH chain sequence

```

          9           18           27           36           45           54           63
GAG GTG AAG CTG GTG GAG TCT GGA CCT GAG CTG AAG AAG CCT GGA GAG ACA GTC AAG ATC TCC
E   V   K   L   V   E   S   G   P   E   L   K   K   P   G   E   T   V   K   I   S

          72           81           90           99           108           117           126
TGC AAG GCT TCT GGG TAT ACC TTC ACA AAC TAT GGA ATG AAC TGG GTG AAG CAG GCT CCA GGA
C   K   A   S   G   Y   T   F   T   N   Y   G   M   N   W   V   K   Q   A   P   G
                                CDR-H1

          135          144          153          162          171          180          189
AAG GGT TTA AAG TGG ATG GGC TGG TTA AAC ACC TAC ACT GGA GAG TCA ATA TAT CCT GAT GAC
K   G   L   K   W   M   G   W   L   N   T   Y   T   G   E   S   I   Y   P   D   D
                                CDR-H2

          198          207          216          225          234          243          252
TTC AAG GGA CGG TTT GCC TTC TCT TCG GAA ACC TCT TCC AGC ACT GCC TAT TTG CAG ATC AAC
F   K   G   R   F   A   F   S   S   E   T   S   A   S   T   A   Y   L   Q   I   N

          261          270          279          288          297          306          315
AAC CTC AAA AAT GAG GAC ATG GCT ACA TAT TTC TGT GCA AGA GGG GAC TAT GGT TAC GAC GAC
N   L   K   N   E   D   M   A   T   Y   F   C   A   R   G   D   Y   G   Y   D   D
                                CDR-H3

          324          333          342          351          360
CCT TTG GAC TAC TGG GGT CAA GGA ACC TCA GTC ACC GTC TCC TCA
P   L   D   Y   W   G   Q   G   T   S   V   T   V   S   S

```

VL chain sequence

```

          9           18           27           36           45           54           63
GAT ATT GTG ATG ACG CAG GCT GCA CCC TCT GTA CCT GTC ACT CCT GGA GAG TCA GTA TCC ATC
D   I   V   M   T   Q   A   A   P   S   V   P   V   T   P   G   E   S   V   S   I

          72           81           90           99           108           117           126
TCC TGC AGG TCT AGT AAG AGT CTC CTG CAT ACT AAT GGC AAC ACT TAC TTG CAT TGG TTC CTA
S   C   R   S   S   K   S   L   L   H   T   N   G   N   T   Y   L   H   W   F   L
                                CDR-L1

          135          144          153          162          171          180          189
CAG AGG CCA GGC CAG TCT CCT CAG CTC CTG ATA TAT CGG ATG TCC GTC CTT GCC TCA GGA GTC
Q   R   P   G   Q   S   P   Q   L   L   I   Y   R   M   S   V   L   A   S   G   V
                                CDR-L2

          198          207          216          225          234          243          252
CCA GAC AGG TTC AGT GGC AGT GGG TCA GGA ACT GCT TTC ACA CTG AGC ATC AGT AGA GTG GAG
P   D   R   F   S   G   S   G   S   G   T   A   F   T   L   S   I   S   R   V   E

          261          270          279          288          297          306          315
GCT GAG GAT GTG GGT GTT TTT TAC TGT ATG CAA CAT CTA GAA TAT CCG CTC ACG TTC GGT GCT
A   E   D   V   G   V   F   Y   C   M   Q   H   L   E   Y   P   L   T   F   G   A
                                CDR-L3

          324          333          342
GGG ACC AAG CTG GAA CTG AAA CGG GCT
G   T   K   L   E   L   K   R   A

```

Figure 3.3. Nucleotide and deduced amino acid sequences of VH and VL regions of IV.3. CDR sequences are underlined.

3.2.2. scFv Construct

3.2.2.1. Creating Extended Variable Regions of IV.3 scFv (STG1) Short and Long Linker

To assemble the IV.3 scFv construct (from now on termed STG1), the VH and VL region were linked with a flexible linker. Two different linker sizes consisting of 15 and 30 aa were chosen since the linker of choice is recommended to span the 3.5-nm distance between the variable domains, depicting the architecture of Fv regions. The ideal linker size should therefore be at least 10 residues in length to avoid conformational strain from an overly short connection (270). Since these two linker sizes have been already used in assembling scFvs (203, 267, 271), they were chosen for the current work in order to investigate whether linker length influences the functional properties of the generated scFv.

First, the VH and VL region were extended separately to include necessary components. VH region was amplified by primers designated as F1 and R1/R1.2 (Refer to Appendix, Table A2.2 for primer sequence). Primer F1 introduced an *EcoRV* restriction site, a start codon and a PelB bacterial secretion signal to direct secretion of the protein to the periplasmic space. Primer R1 created part of the Gly₂₃-Ser₇ long linker (30 aa) and primer R1.2 created part of the Gly₁₂-Ser₃ short linker (15aa) (Figure 3.4A).

VL region was amplified by primer F2/F2.2 and R2 (Refer to Appendix, Table A2.3 for primer sequence). Primer F2 added a part of the Gly₂₃-Ser₇ long linker and primer F2.2 introduced a part of the Gly₁₂-Ser₃ short linker respectively. Primer R2 created a FLAG and cMyc tag for detection and purification purposes, followed by a stop codon and an *EcoRI* restriction site at the C-terminal of the sequence (Figure 3.4B).

The PCR for creating the gene segment of VH and VL were conducted at two different stages using KOD DNA Polymerase with conditions listed in Table 3.3. The first stage allows the overlapping region (20bp) of both the primer and the variable region to anneal at a low annealing temperature. The subsequent high annealing temperature at the second stage allows the complete amplification to take place on the partial template created at the first stage. The amplification of the VH and VL segments for the long

linker generated fragments of 486bp and 462bp, respectively (Figure 3.5). For short linker, the VH and VL fragments were of 468bp and 435bp respectively (Figure 3.5).

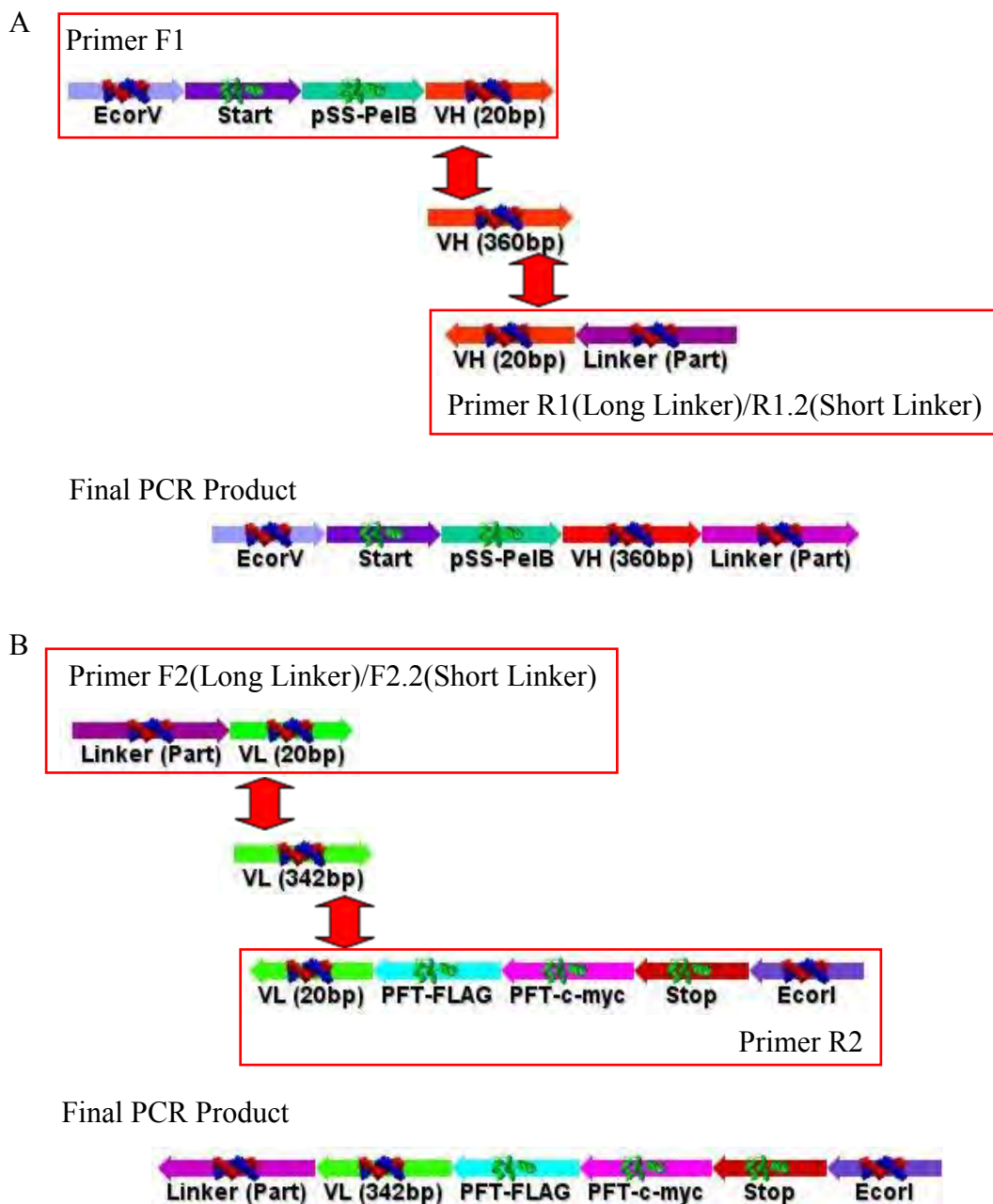


Figure 3.4. Construction of the extended variable regions of STG1. Diagram showing essential components introduced to both variable regions (A. VH and B. VL) conducted over two stages via PCR. The first stage involves annealing of the overlapping region between the template and the primers. The second stage involves amplification of the partial template created at the first stage. PCR conditions are listed in Table 3.3.

Table 3.3. PCR conditions for extension of VH and VL regions.

Stage	Temperature/Duration	Cycle
One	95°C/5 min	-
	94°C/45 sec 36°C (Low Annealing)/10 sec 72°C/5 sec	6
Two	94°C /45 sec 66°C (High Annealing)/2 sec 72°C/ 5 sec	25/30
Final Extension	72°C/5 min	-

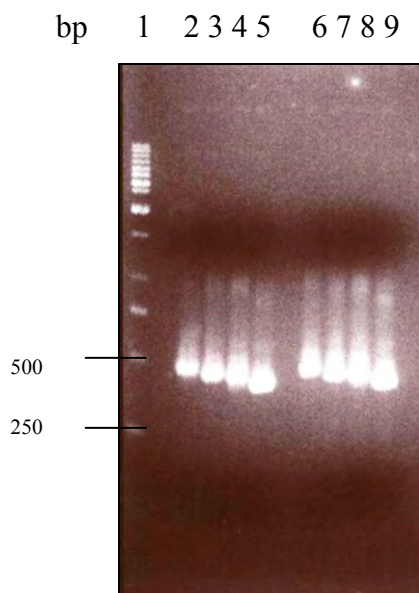


Figure 3.5. PCR amplification of extended VH and VL regions. Electrophoresis was performed on 1.5% agarose in 1 x TAE buffer. A. Lane 1: GeneRuler™ 1kb DNA Ladder (Fermentas); Lanes 2-5: 25 cycles; Lanes 6-9: 30 cycles; Lane 2&6: Amplified VH region for long linker (486bp); Lanes 3&7: Amplified VH region for short linker (468bp); Lanes 4&8: Amplified VL region for long linker (462bp); Lanes 5&9: Amplified VL region for short linker (435bp).

3.2.2.2. Generation of STG1 with Short and Medium Linkers

The 5'-end sequence of the amplified VL segment generated by primer pair F2/F2.2 was complementary to the 3'-end sequence of the VH segment generated by primer pair R1/R1.2. The complete STG1 construct was assembled in a VH-linker-VL manner using overlap extension PCR with conditions listed in Table 3.4. The first stage of the PCR reaction contained only the amplified VH and VL segments which allow the annealing of the overlapping region (18bp). The second stage of the PCR reaction consisted of the addition of primers F1 and R2 for complete amplification to take place (Figure 3.6 and 3.7). The final product was cloned into pCR[®]-Blunt vector (Invitrogen) for sequence analysis.

DNA sequencing showed the correct sequence for STG1 short linker (885bp) (Figure 3.8, Lane 3), however, for STG1 long linker, the fragment size was 903bp (21aa) instead of the expected 930bp (30aa) (Figure 3.8, Lane 2). This was due to a 27bp deletion in the linker region, most likely due to mispairing of the two fragments during the first stage of the PCR overlap extension. The deletion does not lead to a frame shift in the reading frame, thus this accidental version was named STG1 medium linker.

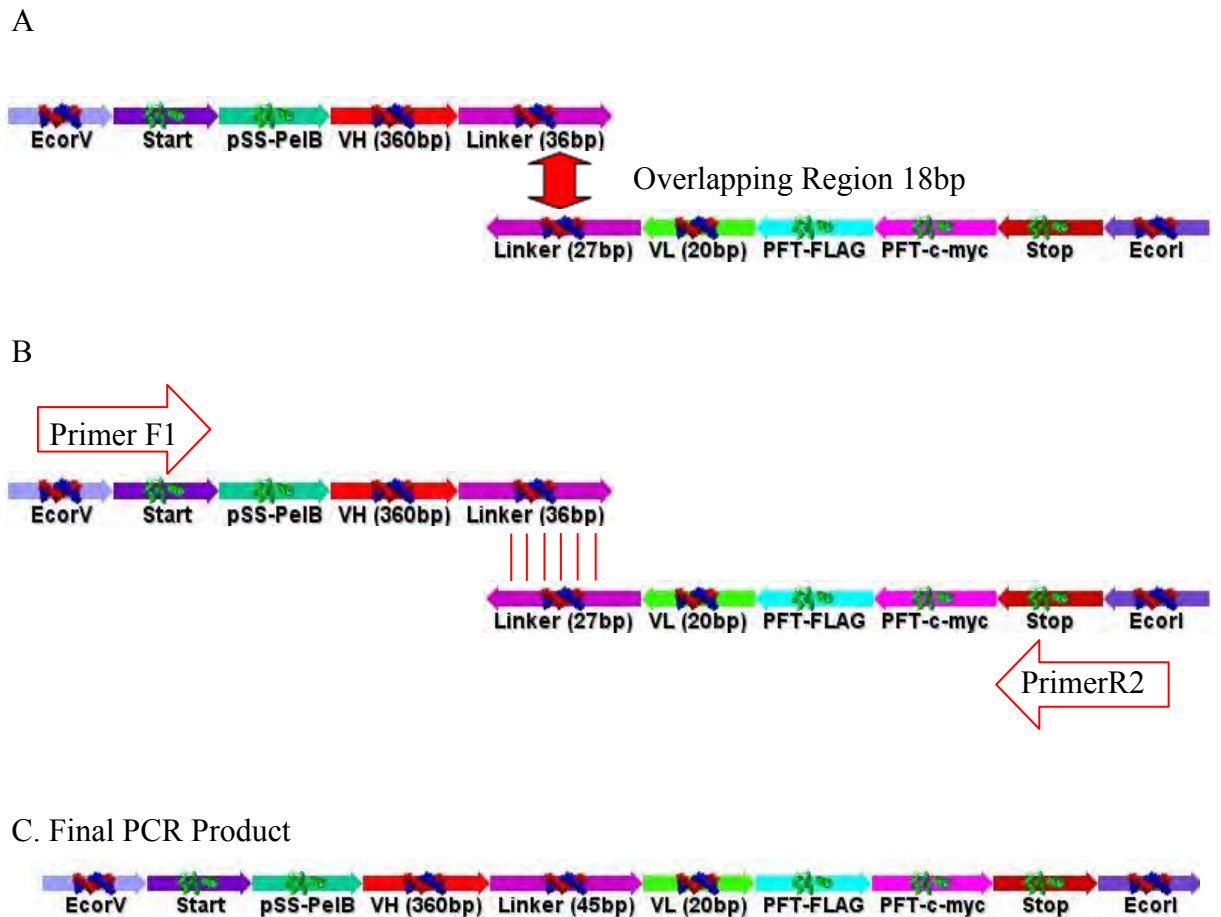


Figure 3.6. An illustrated diagram showing STG1 short linker generated via overlap extension PCR. A. The first stage involves annealing of the overlapping region of the extended VH and VL created previously (Refer to Figure 3.4). B. Complete amplification with two primers on the partial template created at the first stage. C. The final product STG1 short linker with a size of 885bp. PCR conditions listed in Table 3.4.

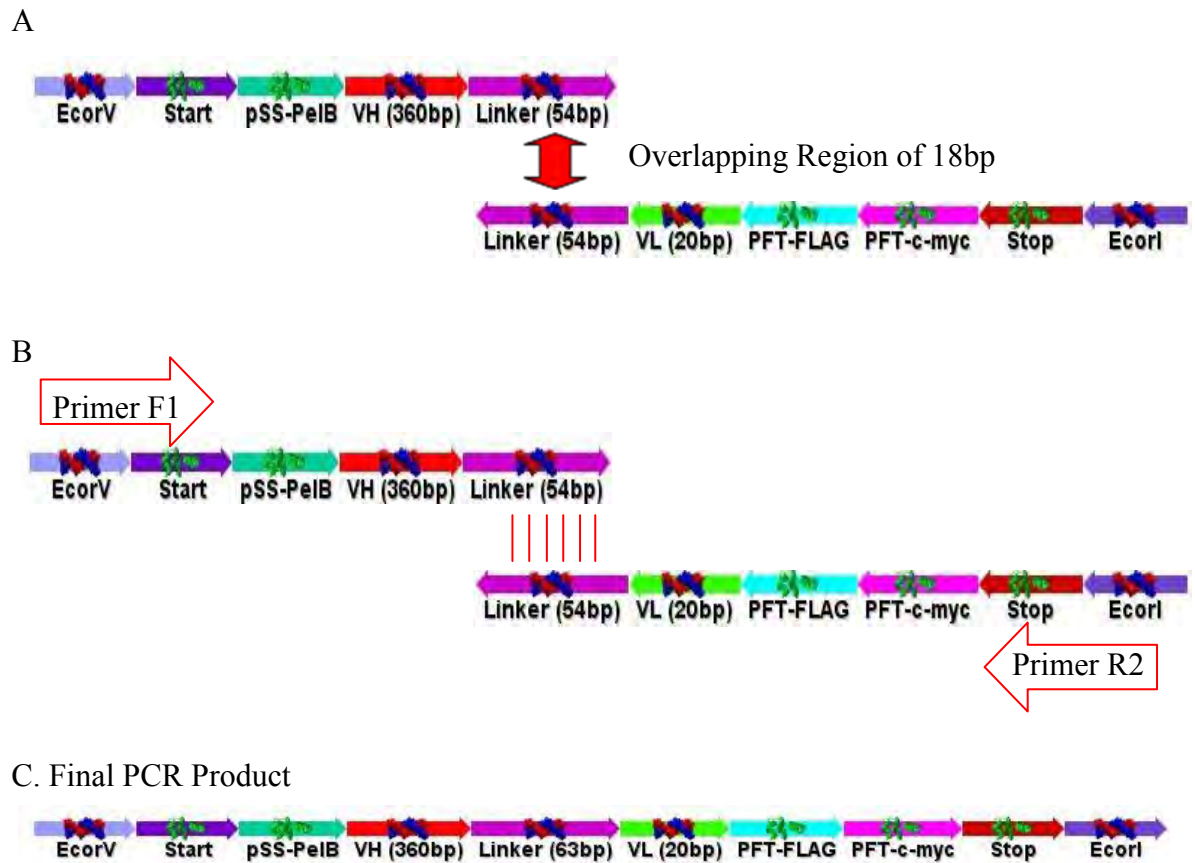


Figure 3.7. An illustrated diagram showing STG1 medium linker generated via overlap extension PCR. A. The first stage involves annealing of the overlapping region of the extended VH and VL created previously (Refer to Figure 3.4). B. Complete amplification with two primers on the partial template created at the first stage. C. The final product of STG1 medium linker with a size of 903bp. PCR conditions listed in Table 3.4.

Table 3.4. PCR conditions for creating STG1 short and medium linker.

Stage	Temperature/Duration	Cycle
One	95°C/5 min	-
	94°C/45 sec 40°C (Low Annealing)/10 sec 72°C/5 sec	6
	94°C /45 sec 66°C (High Annealing)/2 sec 72°C/ 5 sec	30
Final Extension	72°C/5 min	-

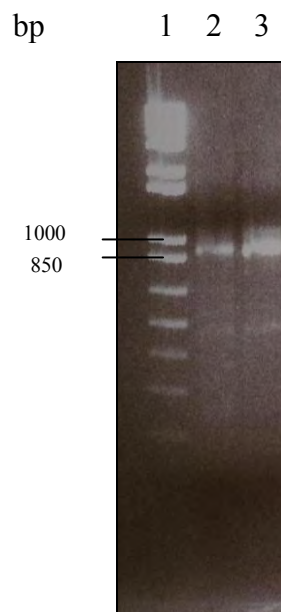


Figure 3.8. Complete construct of STG1 short and medium linker after PCR amplification. Electrophoresis was performed on 1.5% agarose in 1 x TAE buffer. Lane 1: 1kb Plus DNA Ladder (Invitrogen); Lane 2: STG1 with medium linker (903bp); Lane 3: STG1 with short linker (885bp).

3.2.2.3. Creating the Extended Variable Region of STG1 Long Linker

Due to the rich GC nucleotide content of the long linker, the low annealing temperature used in the first stage of PCR led to mispairing of the overlapping region, and instead a linker with a size of 21aa was generated (Section 3.2.2.2). Thus, to create STG1 long linker, the amplified VH and VL segments were each extended separately from the linker region of 5'-end sequence of the amplified VL segment and the linker region of 3'-end sequence of the VH segment (Refer to Appendix, Table A2.4 for primer sequences). These primers (36bp each) have 18bp overlapping the linker region of the initial amplified segment (Figure 3.9). Together with primers F1 for VH and R2 for VL, the PCR conditions to create the additional segment for long linker are listed in Table 3.5. The amplification of the extended VH and VL gene segment for long linker generated a length of 504bp and 478bp (Figure 3.10).

3.2.2.4. Creating STG1 Long Linker

Using overlap extension PCR, the complete construct of STG1 long linker was assembled (Figure 3.11) under the conditions listed in Table 3.6. The construct was ligated into pCR[®]-Blunt vector and the sequence analysis revealed the expected size (930bp) containing the correct long linker (Figure 3.12). The three STG1 constructs (short, medium and long linker) were digested with *EcoRV* and *EcoRI* restriction enzymes and ligated into the periplasmic expression pIG6 vector (Figure 3.14). The DNA sequence of the linkers is shown in Figure 3.13.

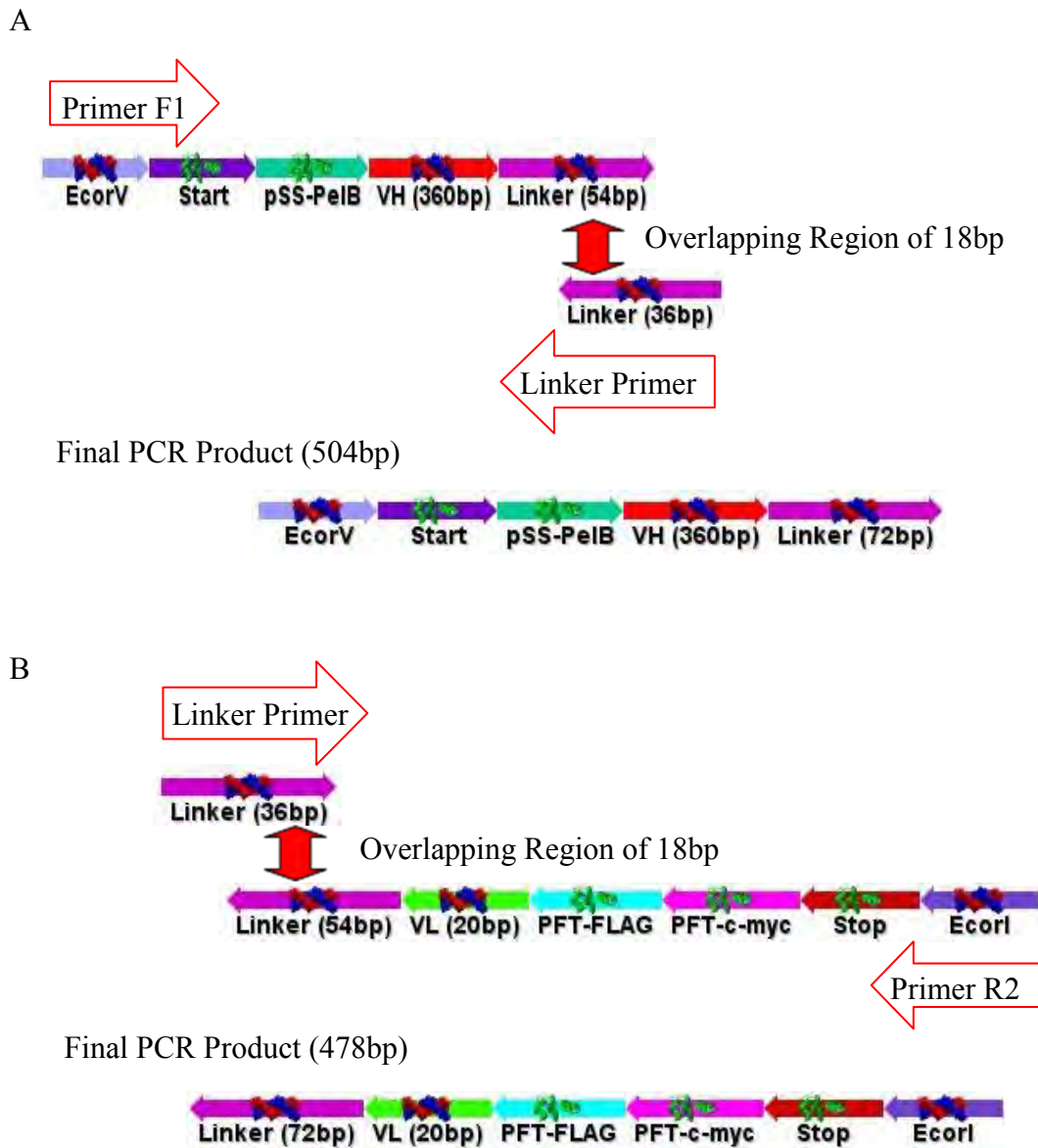


Figure 3.9. Introduction of additional linkers to create STG1 long linker. An additional linker sequence was introduced to the previously extended variable regions (Refer to Figure 3.4). A. VH region and B. VL region. The first stage of PCR involves annealing of the overlapping region between the template and the primers. The second stage involves amplification of the partial template created at the first stage. PCR conditions are listed in Table 3.5.

Table 3.5. PCR conditions to introduce additional segments to both extended variable regions of STG1 long linker.

Stage	Temperature/Duration	Cycle
One	95°C/5 min	-
	94°C/45 sec 36°C (Low Annealing)/10 sec 72°C/5 sec	10
Two	94°C /45 sec 60°C (High Annealing)/2 sec 72°C/ 5 sec	30
Final Extension	72°C/5 min	-

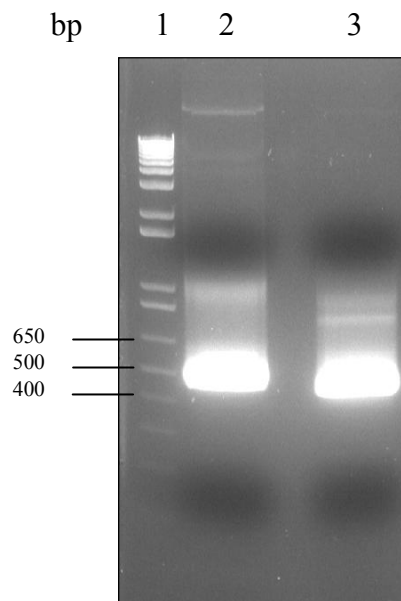
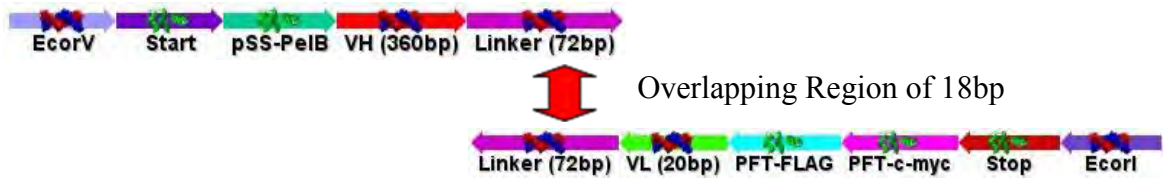
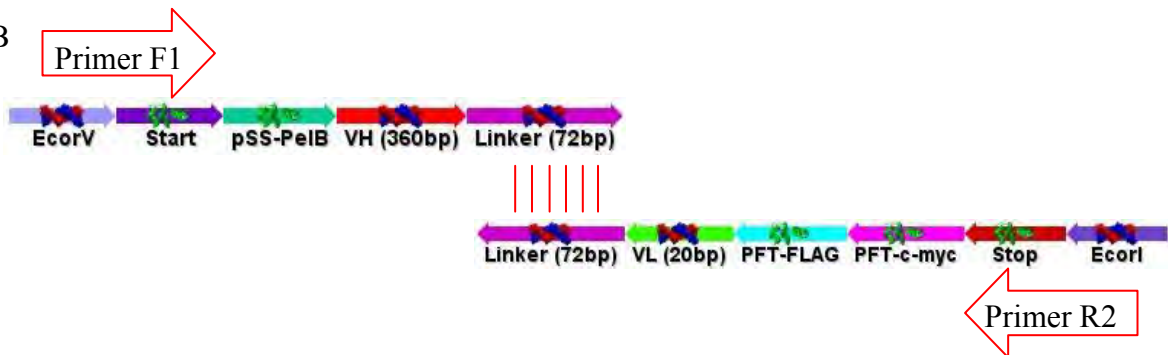


Figure 3.10. PCR amplification of additional linker segment introduced into extended VH and VL regions of STG1 long linker. Electrophoresis was performed on 1.5% agarose in 1 x TAE buffer. Lane 1: 1kb Plus DNA Ladder (Invitrogen); Lane 2: Extended VH region for long linker (504bp); Lane 3: Extended VL region for long linker (478bp).

A



B



C. Final PCR Product



Figure 3.11. Generation of STG1 long linker by overlap extension PCR. A. The first stage involves annealing of the overlapping region of the extended VH and VL created previously (Refer to Figure 3.9). B. Complete amplification with two primers on the partial template created at the first stage. C. The final product of IV.3 scFv long linker with a size of 930bp. PCR conditions listed in Table 3.6.

Table 3.6. PCR conditions to create STG1 long linker.

Stage	Temperature/Duration	Cycle
One	95°C/5 min	-
	94°C/45 sec 65°C (Low Annealing)/10 sec 72°C/5 sec	10
Two	94°C /45 sec 66°C (High Annealing)/2 sec 72°C/ 5 sec	25
Final Extension	72°C/5 min	-

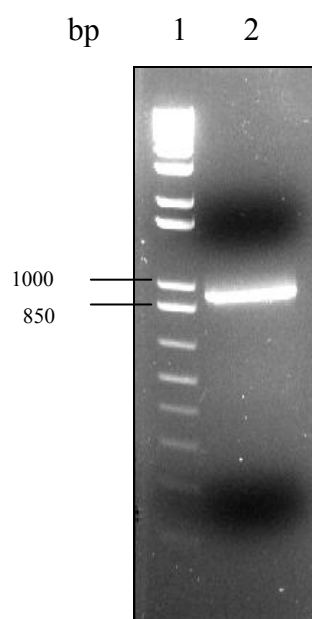


Figure 3.12. STG1 long linker after PCR amplification. Electrophoresis was performed on 1.5% agarose in 1 x TAE buffer. Lane 1: 1kb Plus DNA Ladder (Invitrogen); Lane 2: STG1 with long linker (930bp).

Short Linker

GGT	GGT	GGT	GGT	TCT	GGT	GGC	GGT	GGT	TCC	GGT	GGC	GGT	GGC	AGC
G	G	G	G	S	G	G	G	G	S	G	G	G	G	S

Medium Linker

GGT	GGT	GGT	GGT	TCT	GGT	GGC	GGT	GGT	TCC	GGT	GGC	GGT	GGC	AGC
G	G	G	G	S	G	G	G	G	S	G	G	G	G	S
TCC	GGT	GGC	GGC	GGT	TCT									
S	G	G	G	G	S									

Long Linker

GGT	GGT	GGT	GGT	TCT	GGT	GGC	GGT	GGT	TCC	GGT	GGC	GGT	GGC	AGC
G	G	G	G	S	G	G	G	G	S	G	G	G	G	S
TCC	GGT	GGC	GGC	AGC	GGC	GGT	GGC	GGC	TCC	GGT	GGC	GGC	GGT	TCT
S	G	G	G	S	G	G	G	G	S	G	G	G	G	S

Figure 3.13. Nucleotide and deduced amino acid sequences of short, medium and long linker.

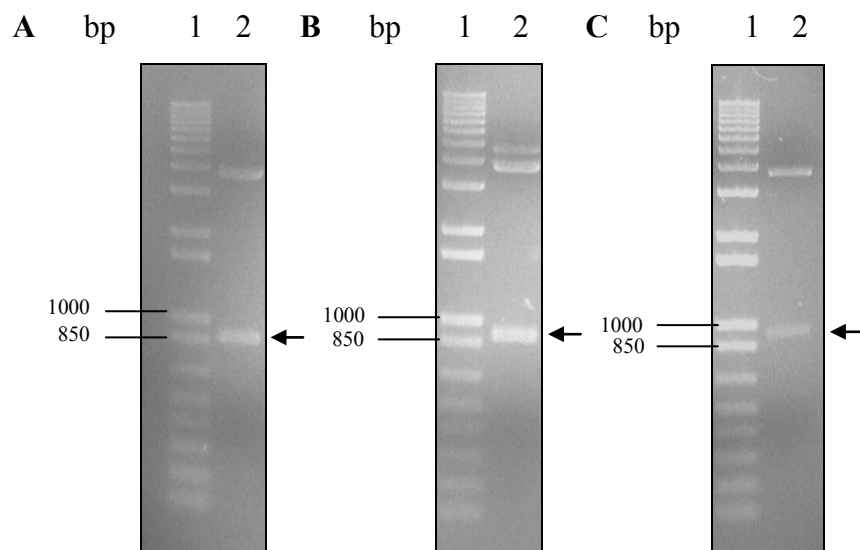


Figure 3.14. Digested pIG6 Vector with STG1 inserts. Electrophoresis was performed on 1.5% agarose in 1 x TAE buffer. A. Lane 1: 1kb Plus DNA Ladder (Invitrogen); Lane 2: STG1 with short linker; B. Lane 1: 1kb Plus DNA Ladder (Invitrogen); Lane 2: STG1 with medium linker; C. Lane 1: 1kb Plus DNA Ladder (Invitrogen); Lane 2: STG1 with long linker. Arrow denotes position of STG1.

3.2.3. Molecular Modeling of STG1

The structural layout of STG1 can be predicted by homology modelling against known protein structures available from the Protein Data Bank (PDB). The VH region of STG1 was modelled against X-ray structures of VH domain of virus-neutralizing anti-idiotypic murine MoAb Fab fragment 409.5.3 [PDB entry 1IAI; 82.93% sequence identity; 2.9Å resolution (272)]. The VL region model of STG1 was based on the structure of estrolytic murine Ab Fab fragment MS6-12 [PDB entry 1MJU; 93.86% sequence identity; 1.22Å resolution (273)]. The two generated templates of the STG1 variable domains were then aligned against X-ray structures of the Anti-Butyrophilin subfamily 3 member A1 Ab fragment 103.2 [PDB entry 4F9P; 50.61% sequence identity to STG1; 3.52Å resolution (274)]. The generated model of STG1 is shown in Figure 3.15.

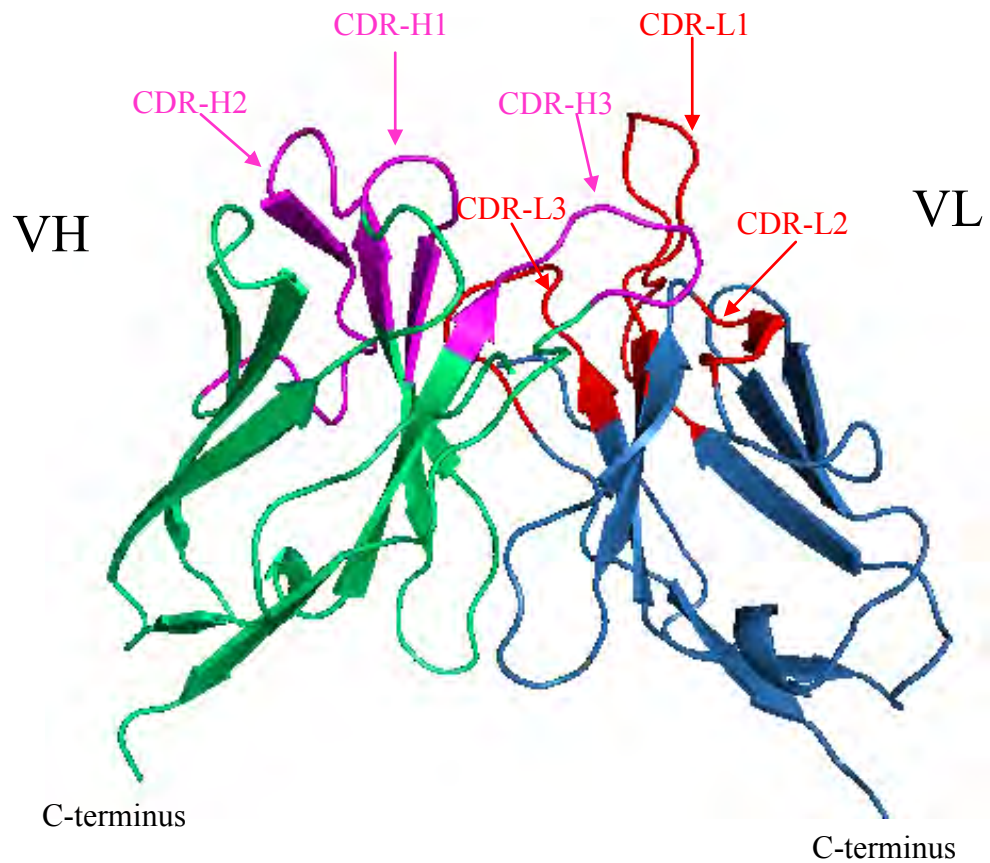


Figure 3.15. Proposed structural model of STG1. The scFv fragment shows the secondary structure of the VH domain (green) and VL domain (blue). The CDRs of VH are shown in magenta and CDRs of VL are shown in red. The linker connecting VH and VL domains is not shown.

3.2.4. Expression and Purification of STG1

All the three recombinant plasmids were chemically transformed into the competent *E. coli* BL21 (DE3) cells and protein expression was induced by IPTG (Figure 3.16). The presence of the protein was confirmed by immunostaining. STG1 expression was not apparent in Coomassie Blue Staining of total cell lysates (Figure 3.17). However, the presence of STG1 proteins was detected using antibodies against the c-Myc and FLAG tags (Figures 3.18). The observed bands (approximately 31 kDa) correspond to the predicted molecular weight of STG1 short, medium and long linker (31.9, 32.5 and 33.5 kDa, respectively).

The soluble and insoluble fraction prepared as described in Chapter 2, were also analyzed by SDS-PAGE and Western blotting. The results showed that the expressed STG1 proteins were mainly found in the insoluble fraction, indicating that they were present as inclusion bodies. Nevertheless, small amounts of STG1 were also present in soluble form (Figure 3.20).

The soluble fraction of the STG1 proteins secreted into the periplasmic space was purified by affinity chromatography using ANTI-FLAG[®] M2 Affinity Gel. The fraction of the soluble supernatant before purification, unbound fraction after purification and the purified STG1 were analyzed on SDS-PAGE and Western blotting. The affinity chromatography provided a partially purified STG1 as shown in Figure 3.21A (Lanes 3&6) and 3.22A (Lane 3) with some contaminating proteins still present in the preparations. Western blot using an anti-FLAG antibody showed that STG1 was enriched by the purification step (Figure 3.21B (Lanes 3&6) and 3.22B (Lane 3)). The yield of the partially purified STG1 of three different linkers was between 200µg-300µg per litre of bacterial culture. The partially purified protein was dialyzed with PBS and used for binding assays.

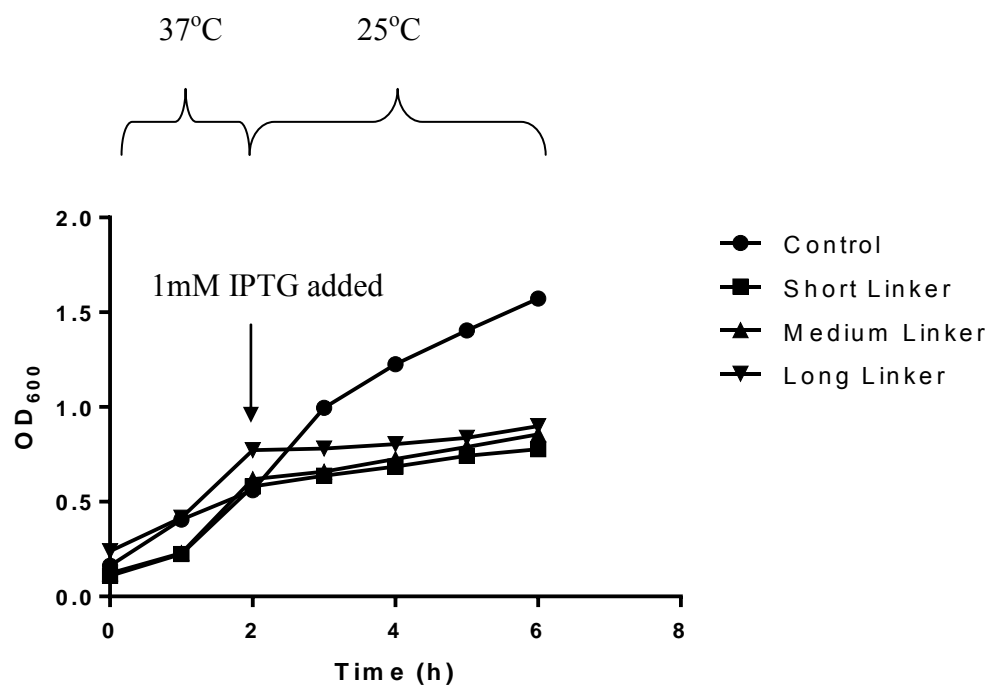


Figure 3.16. Bacterial growth curve of *E. coli* BL21(DE3) expressing STG1 of different linkers. Non-transformed *E. coli* BL21(DE3) was used as control.

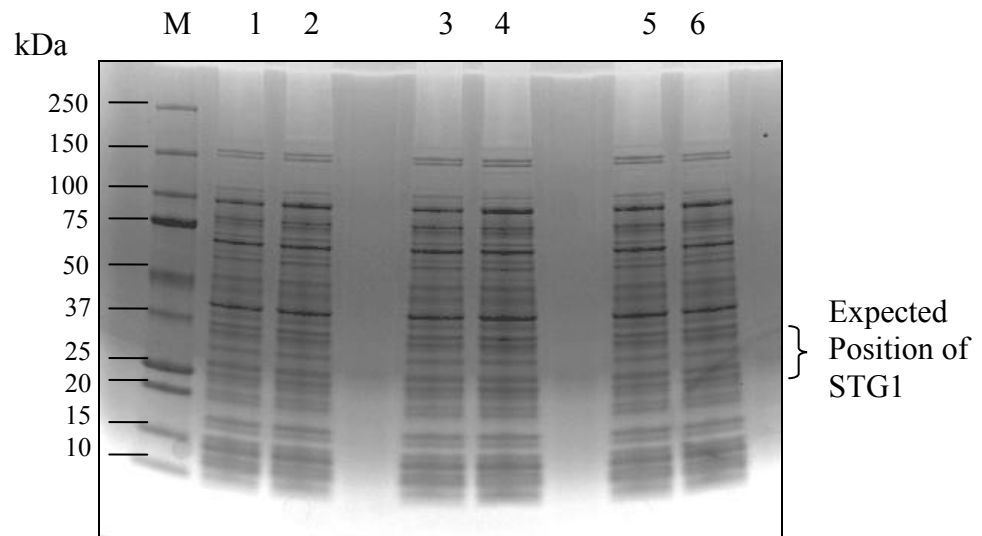


Figure 3.17. Coomassie Blue Staining of *E.coli* cell lysates-before and after induction. Lane M: Molecular weight marker (Bio-Rad); Lanes 1&2: STG1 short linker; Lanes 3&4: STG1 medium linker; Lanes 5&6: STG1 long linker.

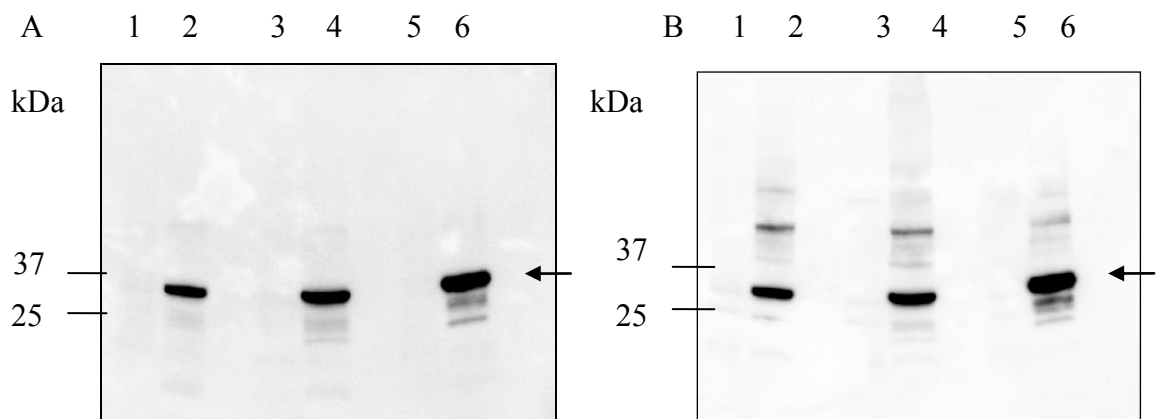


Figure 3.18. Western Blotting of *E.coli* total cell lysates-before and after induction. A. Immunostaining with Anti-cMyc antibody and B. Immunostaining with Anti-FLAG antibody. Lanes 1&2: STG1 short linker; Lanes 3&4: STG1 medium linker; Lanes 5&6: STG1 long linker. Arrow denotes position of STG1. The scFvs carried both cMyc and FLAG tag, which allows visualization of the recombinant protein on Western Blot. Lanes 1, 3 & 5, before induction; lanes 2, 4 & 6, after induction.

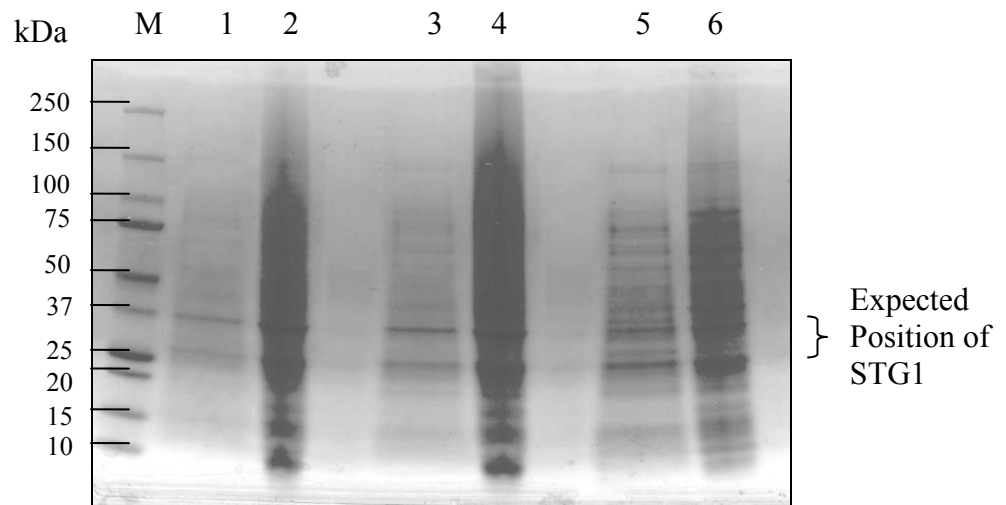


Figure 3.19. Coomassie Blue Staining of *E. coli* total cell lysates-soluble and insoluble fractions. Lane M: Molecular weight marker (Bio-Rad); Lanes 1&2: Soluble and insoluble fraction of STG1 short linker; Lanes 3&4: Soluble and insoluble fraction of STG1 medium linker; Lanes 5&6: Soluble and insoluble fraction of STG1 long linker.

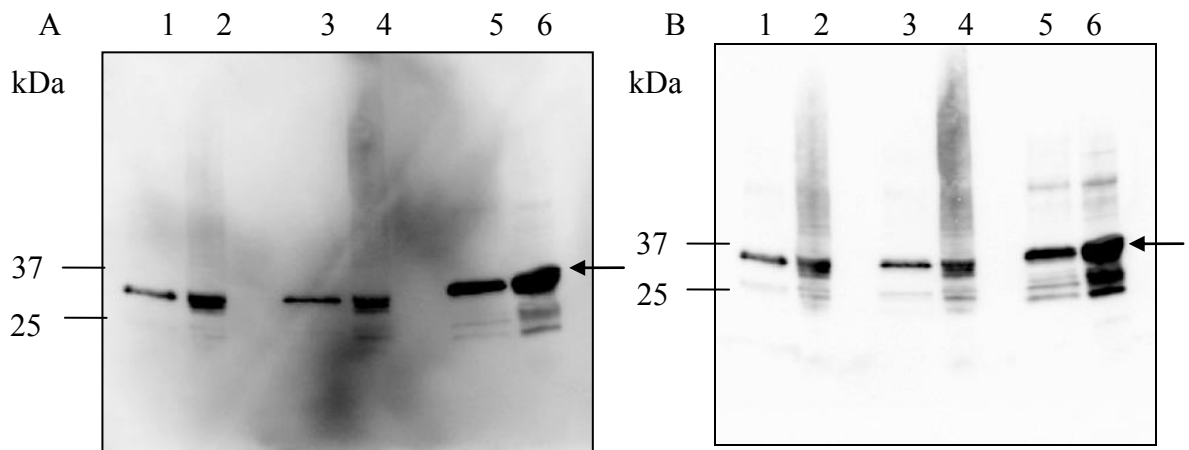


Figure 3.20. Western Blotting of *E. coli* total cell lysates-soluble and insoluble fraction. A. Immunostaining with Anti-cMyc antibody and B. Immunostaining with Anti-FLAG antibody. Lanes 1&2: Soluble and insoluble fraction of STG1 short linker; Lanes 3&4: Soluble and insoluble fraction of STG1 medium linker; Lanes 5&6: Soluble and insoluble fraction of STG1 long linker. Arrow denotes position of STG1.

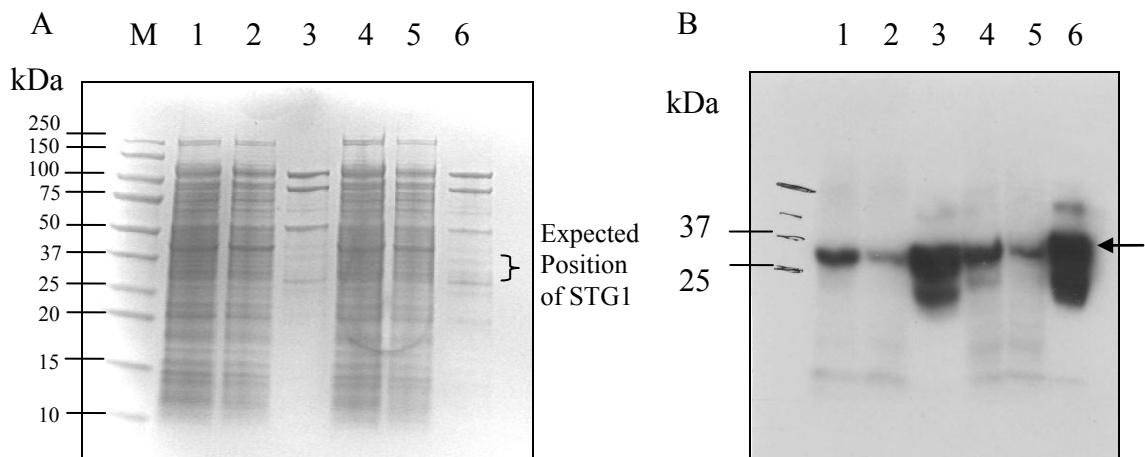


Figure 3.21. STG1 short and medium linker purified with ANTI-FLAG M2 affinity resin. A. Coomassie Blue staining and B. Western Blotting. Lane M: Molecular weight marker (Bio-Rad); Lanes 1-3: STG1 short linker; Lane 4-6: STG1 medium linker. Lanes 1&4: Soluble supernatant before purification; Lane 2&5: Unbound fraction; Lanes 3&6: Purified STG1. Arrow denotes STG1.

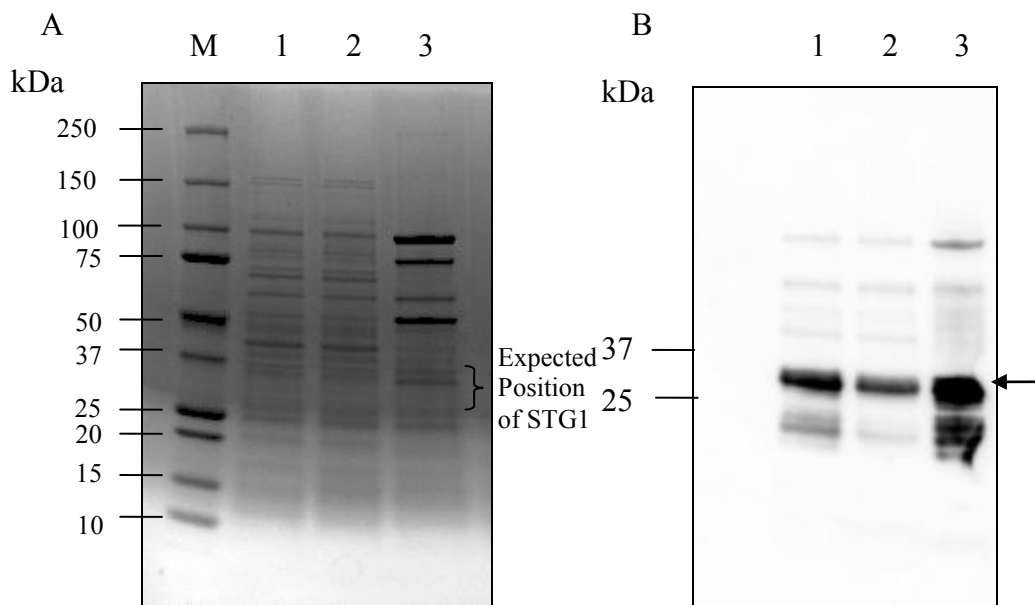


Figure 3.22. STG1 long linker purified with ANTI-FLAG M2 affinity resin. A. Coomassie Blue staining and B. Western Blot. Lane M: Molecular weight marker (Bio-Rad); Lane 1: Soluble supernatant before purification; Lane 2: Unbound fraction; Lane 3: Purified STG1. Arrow denotes STG1.

3.2.5. STG1 Recognizes the Fc γ RIIa on Human Platelets

To determine the antigen binding properties and specificity of the affinity purified STG1, direct immunofluorescence was performed using human platelets and the degree of fluorescence was analyzed by flow cytometry. The presence of Fc γ RIIa receptors on human platelets was first confirmed with the IV.3 MoAb (Refer to Appendix, Section 2.3 for purification profile of the MoAb) and a secondary AF488-conjugated anti-mouse IgG. As shown in Figure 3.23, the highest binding percentage of IV.3 MoAb was seen at a concentration of 500nM (83.02%) and with fluorescence intensity (Y Geo Mean) of 75.25.

To test the binding of STG1 with three different linkers, these samples were incubated with human platelets followed by staining with AF488-conjugated anti- c-Myc antibody. The secondary antibody alone was used as negative control. The binding was tested on platelets with STG1 concentrations of 2.5 μ M (Figure 3.24). STG1 medium linker gave the highest percentage of binding (58.9%) and fluorescence intensity (Y Geo Mean=67.0), this was followed by STG1 short linker (Binding=40.8%; Y Geo Mean=33.3) and STG1 long linker (Binding=31.4%; Y Geo Mean=14.0).

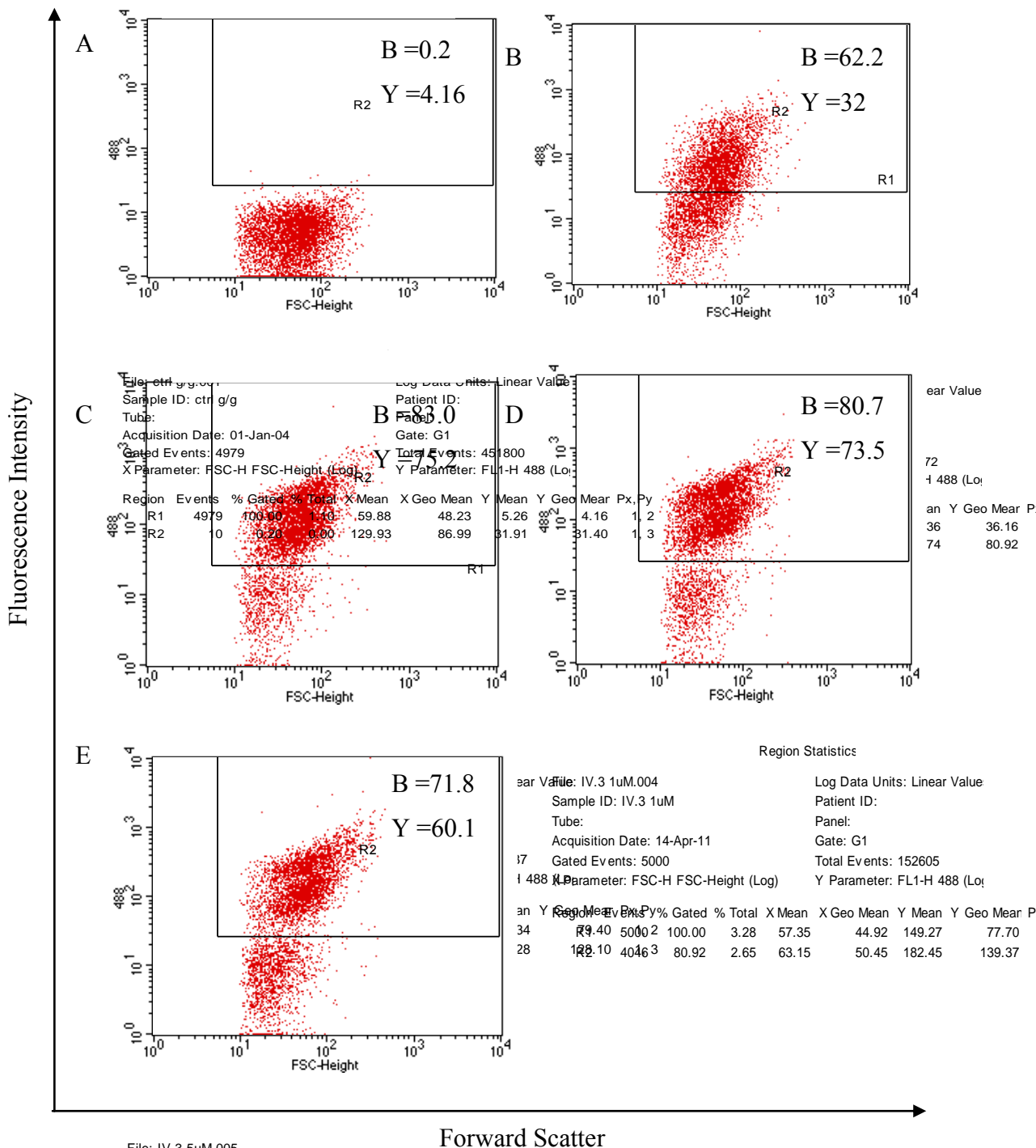


Figure 3.23. Binding of IV.3 MoAb to human platelets. A. Negative Control-Simultaneous control $\alpha_{\text{v}}/\gamma_1$. B-E. IV.3 MoAb tested at various concentrations (50nM, 300nM, 1µM and 5µM). Abbreviations in figure: B, Binding %; Y, Y Geometric Mean.

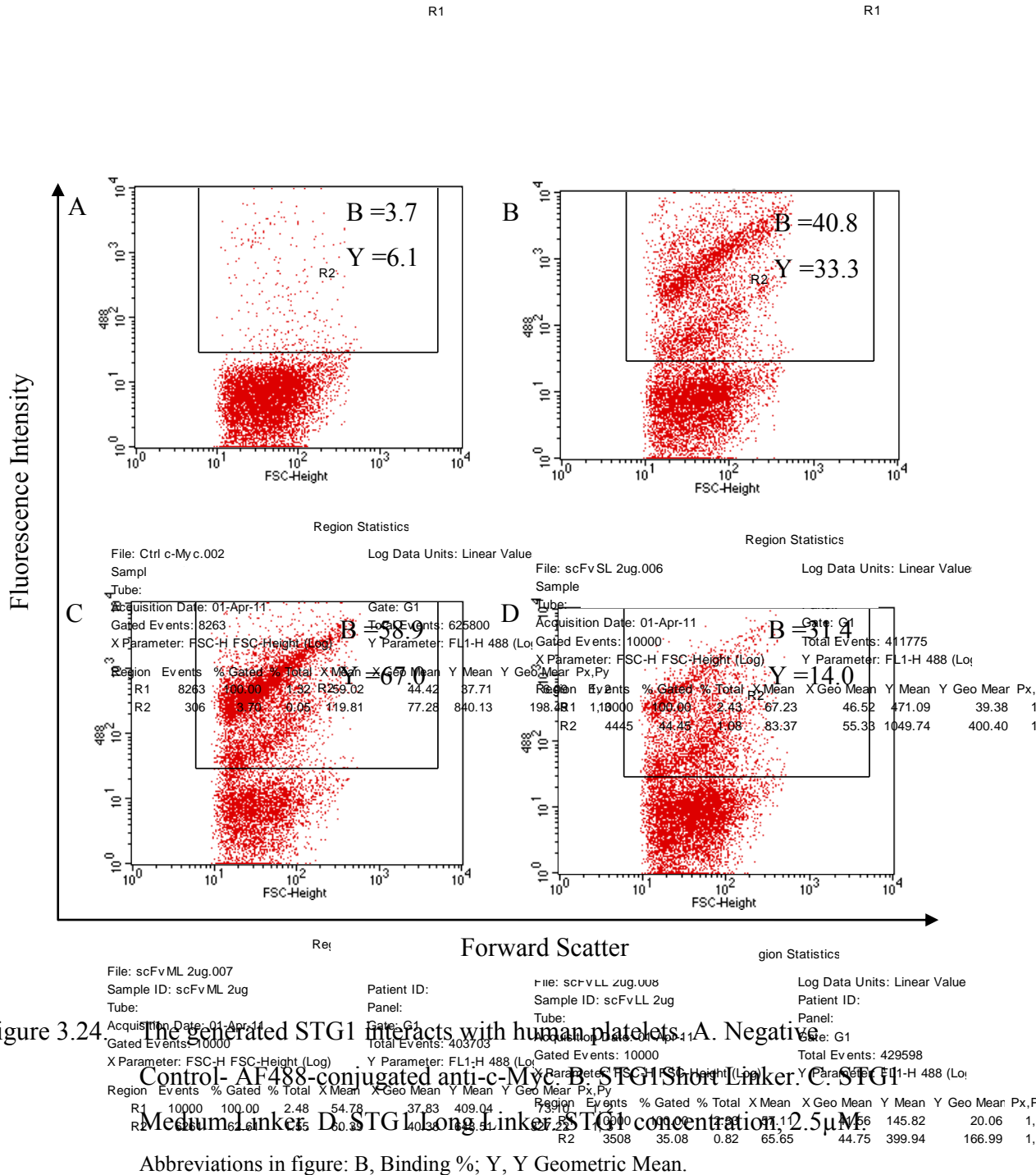


Figure 3.24

The generated STG1 interacts with human platelets. A. Negative Control- AF488-conjugated anti-c-Myc. B. STG1 Short Linker. C. STG1 Medium Linker. D. STG1 Long Linker. STG1 concentration: 2.5 μM.

Abbreviations in figure: B, Binding %; Y, Y Geometric Mean.

3.2.6. STG1 Inhibits Platelet Aggregation in the presence of HIT IgG and Heparin

Light transmission aggregometry was used to investigate the inhibition of HIT IgG-induced platelet aggregation by STG1. The extent of platelet aggregation is measured quantitatively by continuous recording of light transmission across the platelet suspension. As the extent of aggregation increases, more light transmission is detected. If more than 20% of platelet aggregation is recorded, it is considered as a positive end point (77). In this assay, the PRP from a healthy donor was used. To assess the ability of STG1 to inhibit platelet aggregation induced by HIT immune complexes, HIT IgG (Refer to Appendix, Section A2.4 for purification profile) and heparin were added to PRP either in the absence (negative control) or in the presence (positive control) of IV.3 MoAb. Platelet aggregation was observed in the former (Figure 3.25A) but not in the latter where IV.3 inhibited platelet aggregation at a concentration of ≥ 10 nM (Figure 3.26).

Following the set up of the controls, the affinity purified STG1 was then tested at various concentrations ranging from 300nM to 700nM. STG1 was able to inhibit HIT IgG induced aggregation up to 90% or more at concentrations of ≥ 400 nM (Figure 3.27). These results show that STG1 at submicromolar concentrations is a functional molecule able to block platelet aggregation induced by HIT IgG and heparin.

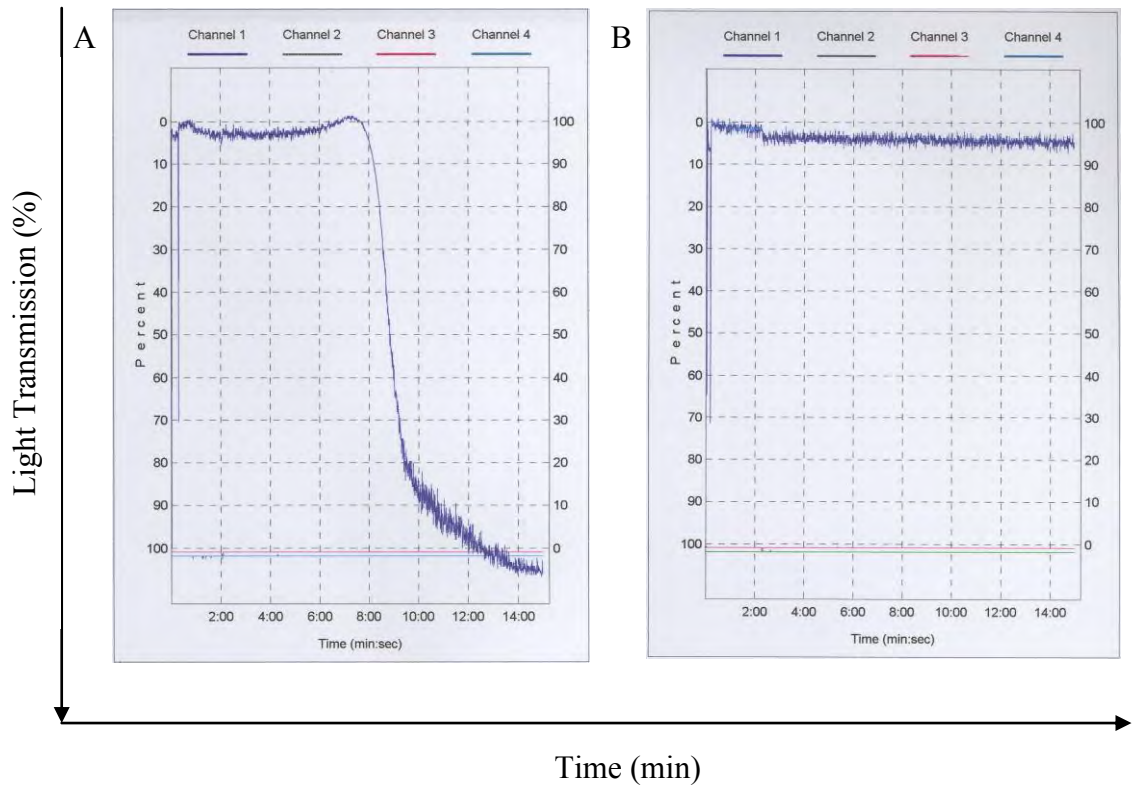


Figure 3.25. Platelet aggregation curves. A. Platelet aggregation induced with HIT IgG and heparin in the absence of IV.3 MoAb. B. The presence of IV.3 MoAb inhibits platelet aggregation induced by HIT IgG and heparin.

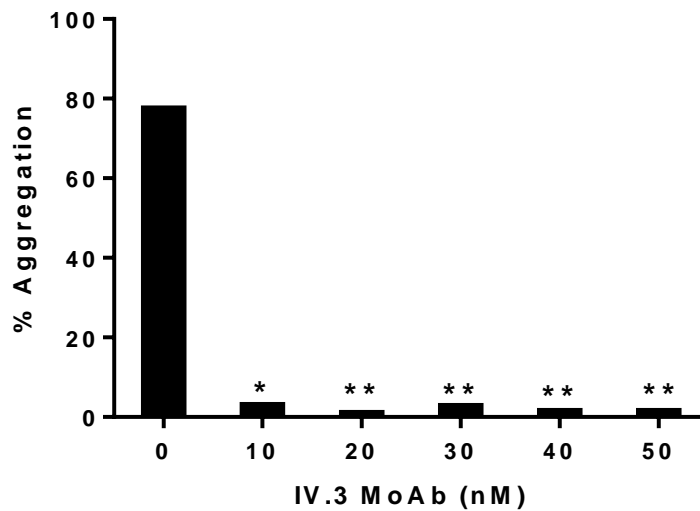


Figure 3.26. IV.3 MoAb inhibits platelet aggregation induced by HIT IgG. In the absence of the IV.3 MoAb, HIT IgG and heparin induced platelet aggregation to the extent of ~80%. However, IV.3 MoAb at a concentration of 10nM or greater inhibits platelet aggregation by about 90%. Data represent the mean from two independent experiments. * $0.05 > P > 0.01$. ** $0.01 > P > 0.001$.

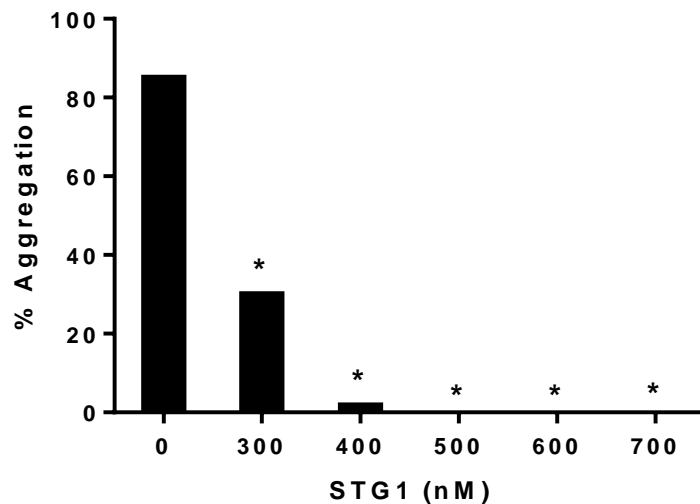


Figure 3.27. STG1 inhibits platelet aggregation induced by HIT IgG. In the absence of STG1, HIT IgG and heparin induced platelet aggregation of ~80%. Platelet aggregation was inhibited by ~90% in the presence of STG1 at concentrations of 400nM or greater. Data represent the mean from two independent experiments. * $0.05 > P > 0.01$.

3.2.7. STG1 Inhibits Serotonin Release in the presence of HIT Serum and Heparin

The ability of STG1 to block platelet activation induced by HIT serum was also examined using SRA. The assay was established by Sheridan et al (130) and remains a widely used functional assay for detection of the HIT Ab. As a positive control, IV.3 MoAb (1 and 2 μ M) inhibited serotonin release when normal PRP was incubated with HIT serum and heparin (0.1 IU/ml) (Figure 3.28).

As shown in Figure 3.29, HIT serum in the presence of 0.1 IU/ml heparin induced strong 14 C-serotonin release (Control). The release of 14 C-serotonin was not observed in the presence of 100 IU/ml of heparin. Importantly, the presence of STG1 at 1 and 2 μ M reduced 14 C-serotonin release to less than 20% for the heparin concentrations of 0.1 IU/ml. This result indicates that STG1 can inhibit HIT IgG-induced platelet activation.

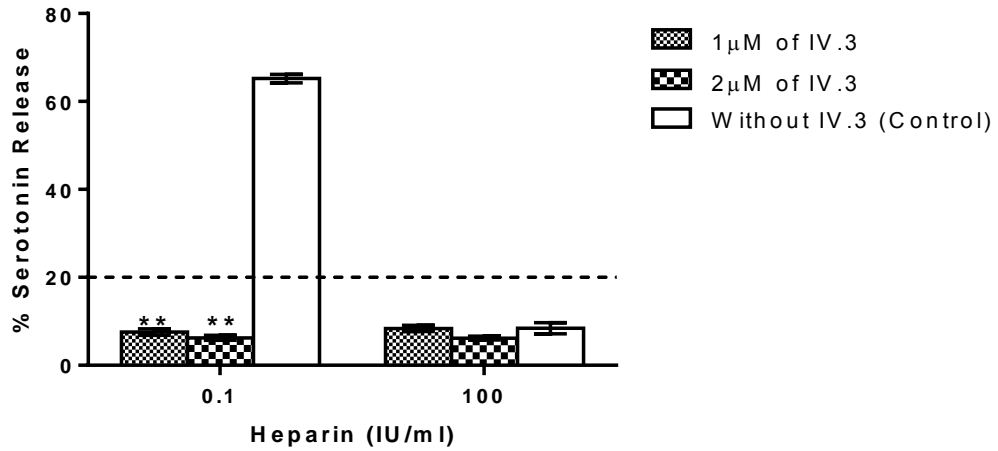


Figure 3.28. IV.3 MoAb inhibited platelet activation induced by HIT serum and heparin. Serum which gave with >20% serotonin release at 0.1IU/ml of heparin, compared with <20% serotonin release at 100IU/ml of heparin were considered as positive serum. When 1 or 2μM IV.3 scFv was added, ¹⁴C-serotonin release was strongly inhibited at both concentrations of heparin. No IV.3 MoAb was present in the control. Data are mean ± SEM; n=4. **0.01 > P > 0.001.

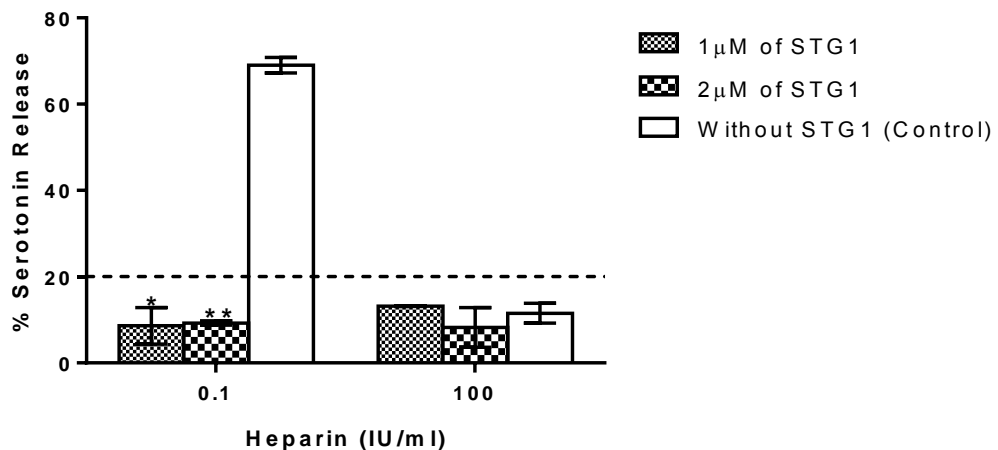


Figure 3.29. STG1 blocked platelet activation induced by HIT serum and heparin. When 1 and 2μM of STG1 scFv was added, the serotonin release was inhibited at both concentrations of heparin. No STG1 was present in the control. Data are mean ± SEM; n=4. *0.05 > P > 0.01. **0.01 > P > 0.001.

3.3. Discussion

HIT is a serious adverse effect of anticoagulant therapy with heparin and is caused by antibodies targeting the PF4/heparin immune complex. The interaction of the immune complex with the Fc γ RIIa on platelets is a key initiating event leading to the pathogenesis of HIT (107). The subsequent platelet activation leads to PF4 release that enhances formation of more immune complexes and generation of platelet microparticles that are highly thrombogenic (75). In addition, direct activation of endothelial cells (78) and monocytes (79, 80) by HIT antibodies triggers the expression of cell surface tissue factor, initiating the coagulation cascade. All these effects weigh in to produce hypercoagulability and thrombotic complications in HIT patients, such as DVT, myocardial infarction, stroke and even death (48).

The current clinical management of HIT comprises heparin withdrawal and its replacement with parenteral non-heparin anticoagulants. While these treatments were deemed effective in reducing new thrombosis in HIT patients, it seems clear that patients still suffer serious clinical consequences such as limb amputation and death. This highlights the inadequate efficacy of current anticoagulant treatments for HIT. Without concomitantly inhibiting the initiation of HIT (i.e. HIT immune complexes interacting with Fc γ RIIa), anticoagulant therapies alone are insufficient to prevent limb gangrene and death. In this context, a strategy that involves extinguishing the initiating event would be an attractive therapeutic option.

The anti-Fc γ RIIa IV.3 MoAb has been widely used in *in vitro* studies as a blocker to prevent HIT IgG mediated platelet activation that initiates Fc γ RIIa signalling (174, 275, 276). In addition, the role of IV.3 is also to prevent the binding of IgG to Fc γ RIIa (176). These findings emphasize the central role of Fc γ RIIa in the pathogenesis of HIT and the likely therapeutic efficacy upon receptor inhibition.

In view of the functional properties of IV.3 MoAb, the aim of this current work was to clone the coding sequence of the variable domain of IV.3 to create a scFv antibody fragment. The scFv derived from IV.3 should be able to retain the original binding properties and block Fc γ RIIa on platelets, thus preventing activation by HIT immune complexes and achieving a similar inhibitory effect as the original antibody. In

comparison to its parental antibody, the establishment of a functional scFv is important for several reasons. The molecule serves as the smallest functional unit that preserves the complete antigen binding activity. Due to its reduced size, the scFv can be easily cleared from the system, reducing potential side effects (277). In relation to platelets, the absence of the Fc portion in the scFv avoids the issue of thrombocytopenia due to complement-mediated platelet lysis (278). While functional antibody fragments such as Fab and F(ab')₂ without the Fc region can be generated by papainolysis, the approach is not always reproducible and does not produce molecules as small as scFvs (253).

In this study, we cloned the immunoglobulin genes from the IV.3 MoAb secreting hybridoma cells. To amplify the VH and VL region of the antibody, primer sets designed on the basis of the commonly present variable domain in murine monoclonal antibodies were used (266). After the variable region was obtained with confirmed sequence matching with the NCBI murine database, these regions were individually extended to include restriction sites, secretion signal, tags, and part of the linker. This was carried out with overlapping extension PCR, incorporating two stages of different annealing temperature.

The scFvs with three different linker sizes of 15-, 21- and 30-aa were constructed. These linkers were more than 12aa in length to allow both variable domains to be positioned in a similar manner as the Fv domain of the parental antibody to form the antigen binding site (279, 280). This is also important to prevent possible formation of bivalent dimer (diabody) between two scFv molecules. Formation of diabodies has been reported in scFvs with linkers between 5 to 12 residues in length (281, 282).

The STG1 constructs with different linkers were subsequently ligated into pIG6 periplasmic expression vector which places these genes under *lac* promoter control. After IPTG induction, the expressed target protein wasn't present as a dominant band as determined by Coomassie Blue Staining. However, its presence was revealed on Western blotting and it was noted that the protein expression levels were similar for the three STG1 proteins (Figure 3.18). In addition, no differences in the bacterial growth patterns were observed (Figure 3.16). The periplasmic expression of the scFvs in *E. coli* relies on the N-terminal PelB leader peptide that directs the proteins towards periplasmic space. The presence of protein disulfide isomerase and chaperones aids the

correct formation of disulfide links in the oxidizing atmosphere of the periplasmic space and produce folded antibody fragments (283, 284). These protein soluble fractions were released after the osmotic shock procedure removed the outer membrane of *E. coli*. However, due to high protein concentrations and overproduction, the protein may not be correctly folded and aggregation may still occur (285). In addition, some proteins that are present in the cytoplasmic space also tend to aggregate due to reducing environment, forming inclusion bodies. These inclusion bodies were observed in the bacterial pellet in the three STG1 construct (Figure 3.20).

The soluble fraction of the three recombinant proteins was isolated with affinity purification. On SDS-PAGE analysis, the isolated protein fraction showed the presence of other contaminant proteins. The partially purified fraction was then tested for binding activity. Like IV.3 MoAb, STG1 proteins showed significant binding to FcγRIIIa receptors on human platelets, with the medium linker exhibiting the strongest binding at 2.5 μM.

The three STG1 constructs show similar binding activity, expression levels and ease of purification. Only one STG1 protein was chosen for subsequent analysis. It has been reported that long linkers are more stable than short linkers (286). In addition, the long linker used in STG1 was engineered with a disulfide bond in the scFv fragment for stabilization (203). For these reasons, STG1 with the long linker was chosen for subsequent work.

In aggregation studies, STG1 with long linker at ≥ 400 nM potently inhibited platelet aggregation induced by HIT IgG. The inhibiting concentrations of STG1, however, were over an order of magnitude higher than those of IV.3 MoAb (400 nM versus 10 nM). Nevertheless, the inhibitory activity of STG1 is still within the nM range. In addition, SRA studies showed that platelet activation was strongly inhibited by STG1. The results obtained from these two assays demonstrated that the created scFv possesses functional activity in inhibiting platelet activation induced by HIT IgG. These findings are consistent with the observations of Reilly et al and Lhermusier et al. These authors showed that by inhibiting the phosphorylation of Syk (signalling molecule involved in the FcγRIIIa signalling pathway), platelet aggregation and serotonin release can be inhibited (118, 167).

The successful production of STG1 opens up a new therapeutic window of opportunity for treating HIT. STG1 not only demonstrates strong binding affinity and specificity for FcγRIIIa receptor, but the protein is also capable of inhibiting platelet aggregation and activation induced by HIT IgG. These results support the hypothesis proposed at the beginning of this chapter that a scFv derived from IV.3 MoAb would be able to retain the original functional properties of the parental antibody and to be potentially beneficial for HIT treatment. For HIT treatment, STG1 must be humanized since the recombinant protein is derived from a murine MoAb. Humanization is essential to prevent immunogenicity when administered to HIT patients. Thus, the humanization of STG1 along with characterization of its properties is the main aim for the next chapter of this thesis.

Chapter 4

Humanized Anti-FcγRIIIa scFv Inhibits Platelet Activation Induced by HIT Immune Complexes

4.1. Introduction

As highlighted in Chapter 1, the introduction of hybridoma technology in 1975 (177) ushered in a new chapter in the development of scientific research for medical diagnostic and therapeutic applications. While many monoclonal antibodies have been generated and characterized, their clinical utility is often hampered by issues of immunogenicity which limits the antibody's therapeutic efficiency. Known as the potent human anti-murine antibody (HAMA) response, the administered murine antibodies are rapidly cleared from the system, thus blocking the therapeutic effect, and causing hypersensitivity reactions (181, 219). While some of these antibodies exhibit the potential to treat various ailments, their unwanted immunogenicity has to be overcome for successful administration into patients. This prompted the development of a process known as humanization. This approach aims to modify antibodies from non-human sources, such as murine hybridomas to resemble human immunoglobulins (287), thus reducing their immunogenic potential.

4.1.1. Approaches to Humanization

The first generation of humanized antibodies includes the construction of murine-human chimeric antibodies. Using recombinant immunoglobulin genes, the murine variable regions are linked to the human constant region. When administered, these chimeric antibodies were found to be less immunogenic and were effective in treating several diseases (Refer to Chapter 1, section 1.15). However, with the presence of the murine variable region in the antibody construct, a human anti-chimeric antibody (HACA) response was observed in patients (181, 219). This indicates that additional modifications are required to further decrease the immunogenicity of monoclonal antibodies, leading to the second generation of humanized antibodies using a CDR grafting approach (Figure 4.1). CDRs or hypervariable domains are present as three polypeptide chain loops in each VH and VL domain (288, 289). These CDRs from both domains form the antigen binding sites and are surmounted by the packing of β -sheets, which are referred to as the Framework Region (FR) (Figure 4.2) (290).

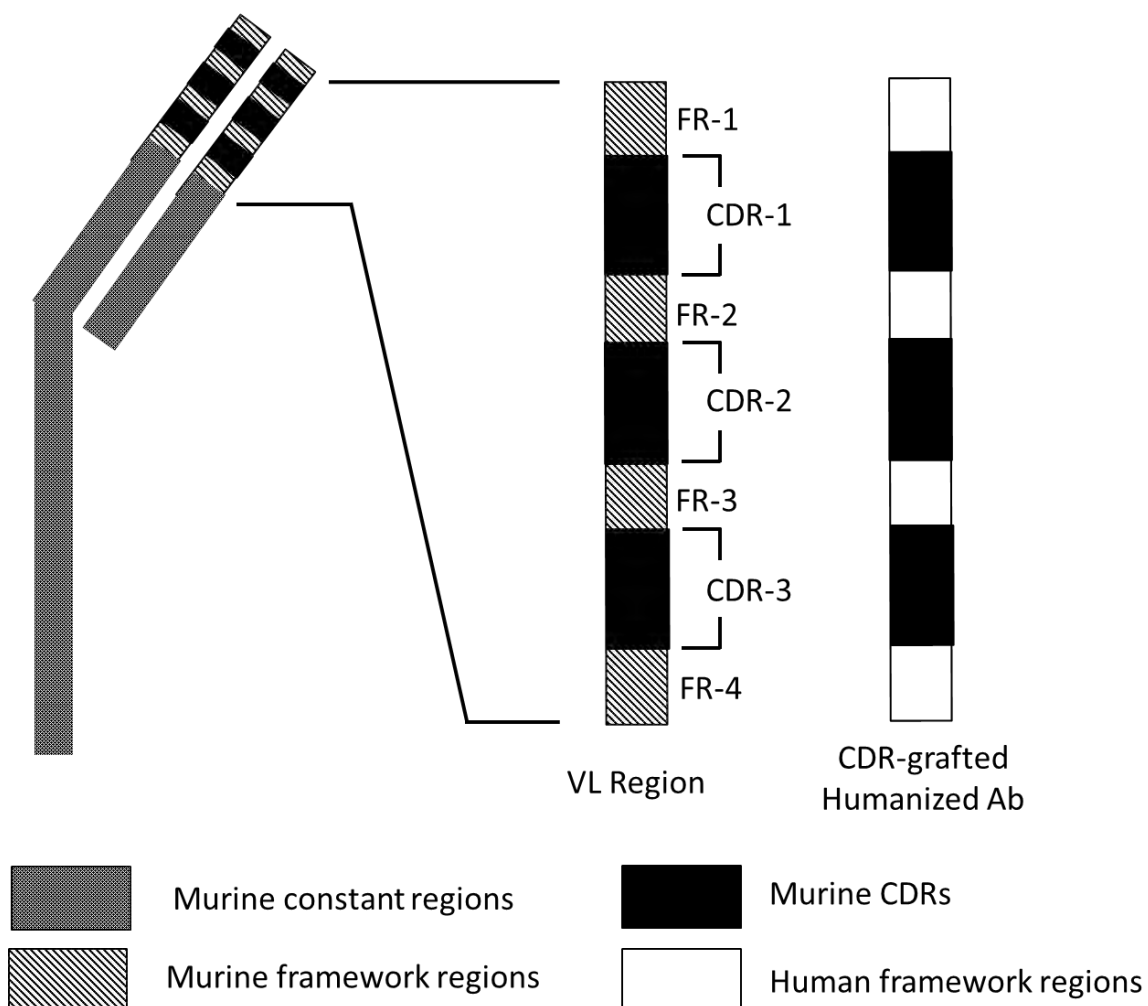


Figure 4.1. Illustration of the humanization of the VL region of a murine antibody. Each variable region contains four FRs and three CDRs. CDRs from the antibody of murine origin were retained and grafted onto the framework of a human antibody. Adapted from Kashmiri et al (291). Abbreviations: CDR, Complementarity Determining Region; FR, Framework Region.

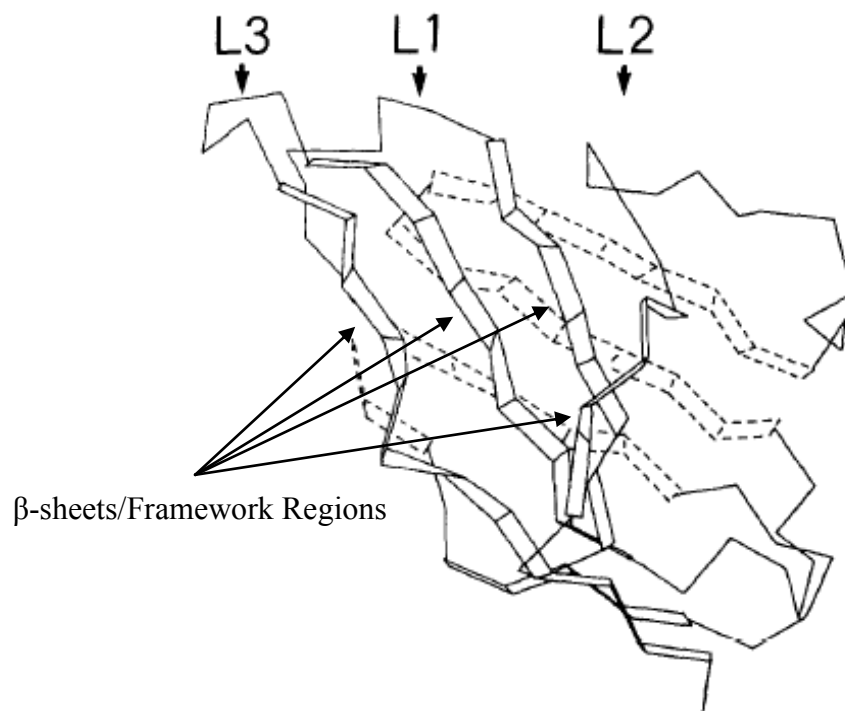


Figure 4.2. The structure of a variable domain of VL. The β -sheets, also known as framework regions are represented as ribbons. The three polypeptide chain loops (CDRs) are noted as L1, L2 and L3 (H1, H2 and H3 in the case of VH). L2 and L3 link adjacent β -sheet strands while L1 links two strands of β -sheets from different variable domains. Reprinted with permission from Chothia et al (288).

CDR grafting consist of transferring the CDRs from a murine antibody onto a human antibody framework, thus creating antibodies with greater homology to human sequences than chimeric antibodies, while preserving the specificity and affinity of the parental murine antibody (185). While CDR grafted antibodies were reported to be functional in some cases (292, 293), the approach often leads to a large reduction in the antigen-binding affinity of the humanized antibody compared to the parental murine antibody. This is because there are certain framework residues that interact with CDR residues in the variable domains, which further support the conformation of these antigen binding loops (217). The transfer of the murine CDR residues to the human framework alone could therefore lead to alterations in the antibody structure. Thus, it was proposed that these key framework residues are important in maintaining the integrity of the antigen binding site (294).

Using a computer-guided modeling approach, these key framework residues were subsequently identified by Queen and coworkers (294). Transferring the CDR and key framework murine residues onto a high homology human template, enables the creation of humanized antibodies that maintain the binding activity of the original murine immunoglobulin. The success of this approach has led to the generation of a large number of a humanized antibodies (295). In addition, these findings also propelled the diversification of humanization methods such as specificity-determining residues (SDRs) grafting (291), germ-line humanization (296) and point mutations (201).

SDRs grafting consists of the insertion of only crucial CDR residues involved in the antibody-ligand interaction from murine to human antibodies (291). Germline humanization refers to the matching of murine CDRs to the human CDRs that have the highest structural similarity, resulting in the use of framework sequences of those human variable genes to construct a humanized antibody (296). Point mutations on the other hand, aim to alter amino acid residues in the murine framework towards a human framework sequence for stability and solubility purposes while retaining intact murine CDRs (201). Currently, there are 11 humanized antibodies that have been approved by the FDA (The list of humanized monoclonal antibodies is shown in Chapter 1, Figure 10) for therapeutic applications in humans, which indicates that these antibodies are safe and well tolerated compared to the previous two generations of humanized antibodies that adopted the chimera and CDR grafting approach, respectively.

4.1.2. *Generation of Humanized scFv*

To express humanized antibodies, several factors must be taken into account. These include the form of the antibody to be expressed (i.e. whole antibody, Fab, or scFv), the choice of host organisms including prokaryotes like *E. coli* and eukaryotes like yeast or mammalian cells, and the amount required since large doses are needed for therapeutic purposes (217). Thus, a production system that is tailored to all these requirements must be optimized to ensure the target antibodies are manufactured efficiently and effectively. While mammalian cells are often the platform of choice for the production of whole humanized antibodies, *E. coli* is still the preferred option to produce small non-glycosylated antibody fragments such as scFvs (297). *E. coli* cell lines not only generate antibodies much faster and easier compared to mammalian cell lines, but also facilitate the progression from antibody characterization to large-scale manufacturing (298).

Using the *E. coli* bacterial expression system, the scFv is either secreted into the periplasmic space as native active proteins or accumulated within the cytoplasmic compartment forming aggregates known as inclusion bodies. The formation of this protein precipitates is due to the reducing environment that disfavours formation of disulfide bonds (247). In addition, high levels of protein expression in bacteria could also lead to the formation of insoluble inclusion bodies (285). This is possibly due to the rapid production rate that surpasses the native folding rate of the target protein (299). Although the production of an inactive target protein is an important drawback, the expression of inclusion bodies has several advantages. These include higher degree of purity of the target protein in aggregated form, high expression level, protection from proteolytic degradation by host cell enzymes compared to the soluble counterpart, and easy separation from the soluble proteins by means of centrifugation, filtration or size-exclusion chromatography (249, 300).

4.1.3. Protein Refolding from Inclusion Bodies

By placing the inclusion bodies under favourable conditions, the aggregated proteins can be subsequently renatured into an active form. This process involves two important aspects: solubilisation and refolding. The solubilisation of proteins is often conducted using strong denaturant such as guanidine HCl, urea or strong ionic detergent such as *N*-lauroylsarcosine, which render the protein flexible and in a state of disordered, unfolded structure (301). In addition to the solubilisation agent, the buffer should also contain reducing agents such as DTT or β -ME to prevent cysteine oxidation (302).

Protein refolding involves a change in conditions that allows the native protein conformation to be restored from the denatured state. It requires the decrease of high concentrations of denaturant and reducing agents that will force the protein molecules to collapse into a compact structure. However, the correct refolding pathway often competes with misfolding and aggregation of the target protein (Figure 4.3). Thus, it is important that the intermediate concentration of the denaturant be determined to induce correct folding of the protein molecules, while still allowing flexibility for structural reorganization. Various refolding protocols are available such as dilution, dialysis, or on-column refolding that gradually remove the denaturant.

4.1.3.1. Approaches to Protein Refolding

The simplest refolding method is by direct dilution, whereby the solubilized protein at high denaturant concentration is delivered into the renaturant buffer (249). Upon addition, the unfolded sample is brought into rapid collapse, bypassing the intermediate denaturant concentration. This allows the formation of the native structure of the protein. Although refolding by dilution can be ideal at small laboratory scale, the technique has its drawbacks especially during scale up as it is time-consuming and costly, with extensive concentration steps required after renaturation (249, 300). However, a different dilution approach known as “pulsed renaturation” has been developed. This is where denatured, solubilised protein is added in pulses into the refolding buffer. This approach has been shown to give about 10% higher yield compared with batch dilution (303, 304).

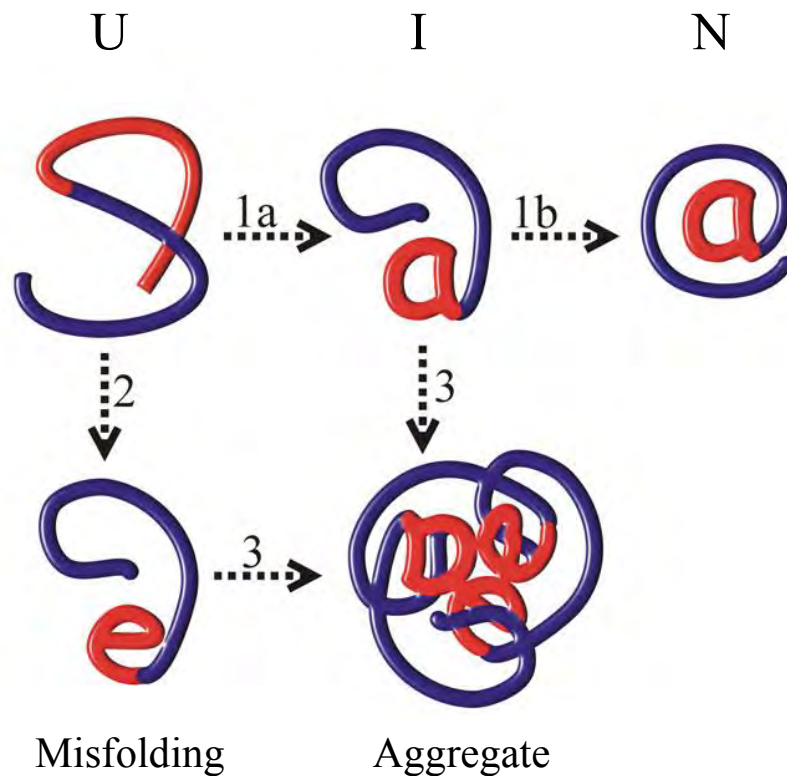


Figure 4.3. Diagram of protein refolding course. The (1) correct protein folding pathway competes with (2) misfolding and (3) aggregation. Aggregation occurs among the intermediates that expose the hydrophobic region. (U, unfolded; I, intermediate; N, native; Blue Lines, hydrophilic solvent-exposed region; Red Lines, hydrophobic region). Reprinted with permission from Vallejo and Rinas (249).

Another refolding technique involves dialysis of the denatured protein samples against a refolding buffer for removal of denaturant. Unlike the direct dilution method, the concentration of the denaturant decreases gradually and the rate of folding into the intermediate and native structures increases. The protein passes through different regimes of denaturant concentrations and the intermediates, which are prone to aggregation may be greatly enhanced (249). However, for some proteins, high refolding yields can be achieved if the rate of denaturant removal is adapted to the requirements of the target protein. Dialysis can be conducted either by one-step or step-wise. In one-step dialysis, the concentration of denaturant decreases with time to the concentration of refolding solvent; in step-wise dialysis, the unfolded protein sample passed through high, middle and low denaturant concentration allowing it to establish equilibrium at each denaturant concentration (301).

In recent years, refolding using chromatographic processes is gaining popularity as it is easily automated using commercially available preparative chromatography systems (305). One of the approaches to chromatographic refolding involves reversible adsorption of the denatured protein onto a matrix with subsequent denaturant dilution to promote refolding. This could be conducted using ion-exchange chromatography (IEC) or immobilized metal ion affinity chromatography (IMAC). In comparison to IEC, IMAC allows efficient simultaneous purification and refolding of those proteins engineered with polyhistidine tags (306, 307).

4.1.3.2. Protein Refolding in the form of Nanoparticles

A method that has previously been used to purify membrane proteins has recently been shown to be applicable for the purification and refolding of inclusion bodies. SMA copolymer is a chemical entity that is used in the plastics industry (308) and for drug delivery (309). The polymer is made with hydrophilic maleic acid and hydrophobic styrene moieties, making it amphipathic (308). For purification of membrane proteins, SMA copolymer is first added to destabilize the membrane. Together with exogenous lipids, the polymer encapsulates both lipids and membrane proteins forming soluble nanometer-sized particles (Figure 4.4.) (310). These are stable particles that can be easily purified and analysed. The same approach has since been adopted to purify bacterial cytoplasmic inclusion bodies like the outer membrane enzyme PagP (211).

In this chapter, we will focus on the humanization of STG1 created by experiments described in Chapter 3. The humanized construct was expressed, purified, and characterized in relation to its binding and functional properties. This will be followed by testing the efficacy of humanized STG1 (termed STG2) in an animal model of HIT.

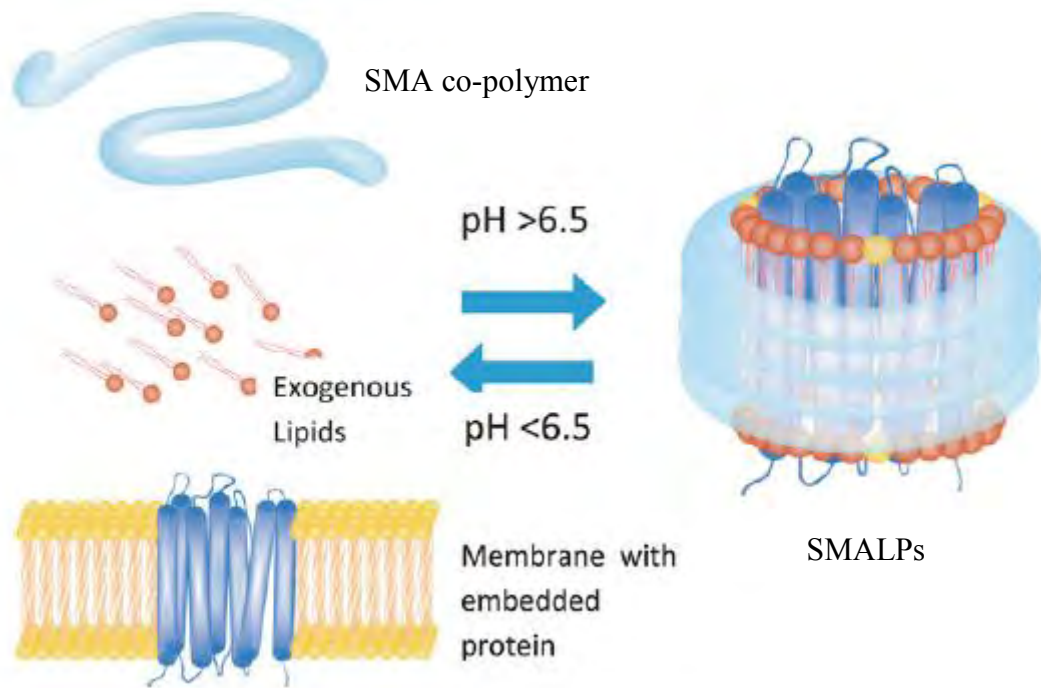


Figure 4.4. Schematic illustration of both lipid and membrane protein encapsulated with SMA co-polymer. The addition of SMA co-polymer to membrane protein leads to the formation of SMALPs. At neutral pH, the protein encapsulated in a disc-like structure can be easily purified. At an acidic pH, the polymer disassociates from the particle leaving behind the membrane containing the membrane protein. Reprinted with permission from Jamshad et al (308).

4.1.4. Animal Models for HIT

As highlighted in Chapter 1 (Section 1.7), the establishment of HIT animal models has advanced the understanding of how HIT occurs *in vivo*. The transgenic animal that expresses human FcγRIIIa and human PF4 recapitulates the mechanism of HIT once heparin and HIT IgG like antibody-KKO are administered (107, 108). This results in the events of HIT which are thrombocytopenia and thrombosis. Using these transgenic mice, new possible treatments for HIT such as the Syk inhibitors (i.e. PRT318 and R406) (Chapter 1, Section 1.14) targeting the signalling pathway of FcγRIIIa have been tested (118, 167). Both inhibitors have demonstrated encouraging results as new approaches to HIT treatment.

While the transgenic mice have largely contributed to the understanding of HIT, it is essential to note that the platelet biology may still be different between mice and humans. These include smaller size of mouse platelet (0.5μM vs humans-1-2μM) that leads to lower expression of surface antigens; higher platelet count for mouse (1000-1500 X 10⁹/L vs humans-150-400 X 10⁹/L); and shorter platelet lifespan for mouse (3-4 days vs 8-9 days) (311). These differences have to be taken into considerations when the data obtained from the HIT animal models are extrapolated to humans. Thus, an animal model that evaluates human platelets would still be advantageous to fully assess the physiological events of HIT. This can be conducted by expression of human platelets via transplantation of human cord blood CD34⁺ cells or by injection of human platelet rich plasma into non-obese diabetic/severe combined immunodeficient (NOD/SCID) mice (215, 216).

The model of human platelets circulating in NOD/SCID mice has been successfully used to study ITP. The detrimental effect of platelet destruction caused by anti-GPIIb/IIIa and anti-GPVI antibodies was observed in the depletion of human platelets and the model has proved valuable in recapitulating the events of ITP in mice (215).

4.1.5. Hypothesis and Aims

As the work in Chapter 3 shows, the created murine scFv successfully demonstrates binding to platelets and is able to prevent platelet activation in the presence of HIT IgG *in vitro*. This suggests that the recombinant protein could be of therapeutic potential for the treatment of HIT. However, to avoid the issues of immunogenicity as highlighted earlier, it is essential that the murine scFv be humanized to improve its applicability as a future therapeutic agent.

We hypothesize that a humanized scFv (termed STG2) will retain the functional properties demonstrated by STG1. In addition, the humanized molecule is expected to inhibit platelet activation in the presence of the HIT-Immune Complexes both *in vitro* and *in vivo*. To address these hypotheses, the aims of this chapter are:

- To construct a humanized scFv based on the murine STG1 antibody.
- To express the humanized scFv in *E. coli* and to purify the protein by affinity chromatography.
- To characterise the humanized scFv. The binding and functional activities of the protein will be evaluated using flow cytometry and platelet aggregation and activation assays.
- To establish a mouse model of HIT.
- To evaluate the activity of the humanized scFv in the mouse model of HIT.

4.2. Results

4.2.1. Humanization of STG1

In Chapter 3, the murine scFv STG1 demonstrated antigen binding properties by interacting with FcγRIIa on platelets. The recombinant protein also exhibited a functional role by preventing platelet aggregation and activation induced by HIT IgG. Based on these observations, STG1 could emerge as a potential treatment for HIT. To improve the properties of the molecule for possible clinical application in HIT patients, a humanized version of the STG1 was designed. This is essential to prevent likely HAMA response (219). STG1 was humanized by adopting the CDR-grafting and point mutation approach. As mentioned in the previous chapter, the subgroup of VH and VL genes of STG1 belong to murine(mu)VH9 and V_K2, respectively. By comparison to the human germ line sequences in <http://www.ncbi.nlm.nih.gov/igblast/>, the VH domain of murine IV.3 closely resembles that of human germline VH domain IGHV7-81*01 with 69.4% identity and the VL domain closely resembles IGKV2-18*01 with 76% identity based on IMGT database (312)(Refer to Appendix, Figure A3.1 for sequence alignment).

For the humanization of STG1, the sequence of the donor CDR was preserved while the FRs underwent several amino acid substitutions with human germline residues. This is likened to the CDR-grafting approach where the murine CDRs are grafted onto a human acceptor framework. The changes were conducted by comparing to the chart of human germline family sequences extracted from the IMGT database which are available on the website (<http://www.bioc.uzh.ch/antibody/>). Based on these sequences, it was decided to change selected amino acid residues to closely reflect the subgroup of the VH and VL human scaffold. For VH, this resulted in the subgroup of human (hu)VH3&5 in FR1, huVH2 in FR2, huVH7 in FR3 and huVH3 in FR4. For VL, all the FRs were changed to huV_K2 (Figure 4.5). Using the search engine <http://www.ncbi.nlm.nih.gov/igblast/>, the comparison of the huVH with the most homologous human germ line sequences yielded 74.5% identity to the IGHV7-4-1*01 and huVL with 88% sequence identity to IGKV2-28*01 retrieved from the IMGT database (312) (Refer to Appendix, Figure A3.2 for sequence alignment). This was similar to the amino acid identity between STG1 and STG2 (excluding CDRs) which exhibits 76% and 87% on the VH and VL domain respectively.

A. VH

Mouse: EVKLVESGPELKKPGETVKISCKASGYTFTNYGMNWWKQAPGKGLKWMGWL
 Human: EVQLVESGPGGLVKPGETLKISCKGSGYSFTNYGMNWWRQAPGKGLEWVSWL

Human VH Group 3 and 5
Human VH Group 2

Mouse: NTYTGESIYPDDFKGRFAFSSETSASTAYLQINNLKNEDMATYFCARGDYG
 Human: NTYTGESIYPDDFKGRF**V**F**S**LDT**S**VSTAYLQ**I**CSL**K**AED**T**A**V**Y**Y**CARGDYG

Human VH Group 7

Mouse: YDDPLDYWGQGTSVTVSS
 Human: YDDPLDYWGQGT**L**VTVSS

Human VH Group 3

B. VL

Mouse: DIVMTQAAPSVPVTPGESVSISCRSSKSLHTNGNTYLHWFLQRPQGSPQL
 Human: DIVMTQ**S**PL**S**L**P**VTPG**E**PA**S**ISCRSSKSLHTNGNTYLHW**Y**LQ**K**PGQSPQL

Human Vk Group 2
Human Vk Group 2

Mouse: LIYRMSVVLASGVPDRFSGSGSGTAFTLSISRVEAEDVGVFYCMQHLEYPLT
 Human: LIYRMSVVLASGVPDRFSGSGSG**T**D**F**TL**K**ISRVEAEDVGV**Y**YCMQHLEYPLT

Human Vk Group 2

Mouse: FGAGTKLELKRA
 Human: FGAGTKLELKRA

Human Vk Group 2

Figure 4.5. Amino acid sequence alignment between the variable regions of STG1 and STG2. (A) VH and (B) VL. CDR residues are underlined. Letters in bold indicate amino acid changes that were made in the FRs. The original STG1 belongs to subgroups muVH9 and muVk2 (VH9Vk2). The humanized sequence in the FR categorized as huVH subgroups of 2, 3, 5 and 7, while the huVL falls under subgroup 2 (VH35273Vk2). In total, 32 amino acids were changed.

4.2.2. Construction of STG2

The sequence encoding the humanized VH and VL domain, fused with a long flexible linker Gly₂₃-Ser₇ was chemically synthesized by DNA2.0 (Menlo Park, CA) with codon optimization for increased protein expression in bacteria (313)(Figure 4.6). The construct did not include a secretion signal, but included cMyc and HIS₆-tags at the C-terminus for detection and purification purposes. The final construct with a size of 852bp was digested from the commercial standard pJa vector (Figure 4.7A) and ligated into pET11a vector for bacterial expression (Figure 4.7B).

VH Chain Sequence

```

          9           18           27           36           45           54           63
GAA GTA CAA CTG GTG GAG AGC GGC CCT GGC CTG GTG AAA CCT GGA GAA ACC CTC AAG ATT TCC
E   V   Q   L   V   E   S   G   P   G   L   V   K   P   G   E   T   L   K   I   S

          72           81           90           99           108           117           126
TGC AAG GGC TCG GGC TAT TCG TTC ACA AAC TAC GGC ATG AAT TGG GTC CGG CAG GCA CCG GGC
C   K   G   S   G   Y   S   F   T   N   Y   G   M   N   W   V   R   Q   A   P   G
                                CDR-H1

          135          144          153          162          171          180          189
AAG GGC CTG GAA TGG GTG AGC TGG CTG AAC ACC TAT ACC GGC GAG TCG ATC TAC CCG GAC GAC
K   G   L   E   W   V   S   W   L   N   T   Y   T   G   E   S   I   Y   P   D   D
                                CDR-H2

          198          207          216          225          234          243          252
TTC AAG GGA CGC TTC GTT TTT AGC CTC GAC ACG TCT GTT TCA ACG GCC TAT CTG CAG ATT TGC
F   K   G   R   F   V   F   S   L   D   T   S   V   S   T   A   Y   L   Q   I   C

          261          270          279          288          297          306          315
AGT CTG AAG GCG GAG GAT ACG GCA GTC TAT TAC TGT GCC CGT GGT GAC TAT GGC TAC GAT GAC
S   L   K   A   E   D   T   A   V   Y   Y   C   A   R   G   D   Y   G   Y   D   D
                                CDR-H3

          324          333          342          351          360
CCC CTG GAC TAC TGG GGA CAG GGT ACC CTC GTG ACG GTA AGC TCT
P   L   D   Y   W   G   Q   G   T   L   V   T   V   S   S

```

VL Chain Sequence

```

          9           18           27           36           45           54           63
GAT ATC GTC ATG ACG CAG TCA CCG CTG TCC TTG CCC GTG ACC CCA GGC GAG CCG GCC TCA ATC
D   I   V   M   T   Q   S   P   L   S   L   P   V   T   P   G   E   P   A   S   I

          72           81           90           99           108           117           126
TCG TGT CGC TCT TCT AAG AGC CTG CTG CAC ACC AAT GGC AAC ACG TAC CTG CAT TGG TAT CTG
S   C   R   S   S   K   S   L   L   H   T   N   G   N   T   Y   L   H   W   Y   L
                                CDR-L1

          135          144          153          162          171          180          189
CAG AAA CCG GGG CAG AGT CCG CAG CTT CTT ATC TAT CGC ATG TCC GTC TTG GCG TCC GGG GTT
Q   K   P   G   Q   S   P   Q   L   L   I   Y   R   M   S   V   L   A   S   G   V
                                CDR-L2

          198          207          216          225          234          243          252
CCG GAT CGT TTC TCC GGG TCC GGC TCC GGT ACG GAT TTC ACA CTC AAG ATC AGC CGC GTC GAG
P   D   R   F   S   G   S   G   S   G   T   D   F   T   L   K   I   S   R   V   E

          261          270          279          288          297          306          315
CGC GAA GAT GTC GGC GTC TAC TAC TGC ATG CAG CAT CTG GAA TAT CCC CTC ACG TTC GGC GCT
A   E   D   V   G   V   Y   Y   C   M   Q   H   L   E   Y   P   L   T   F   G   A
                                CDR-L3

          324          333          342
GGC ACA AAG CTC GAA CTT AAG CGT GCC
G   T   K   L   E   L   K   R   A

```

Figure 4.6. Nucleotide and deduced amino acid sequences of VH and VL regions of STG2. CDR sequences are underlined.

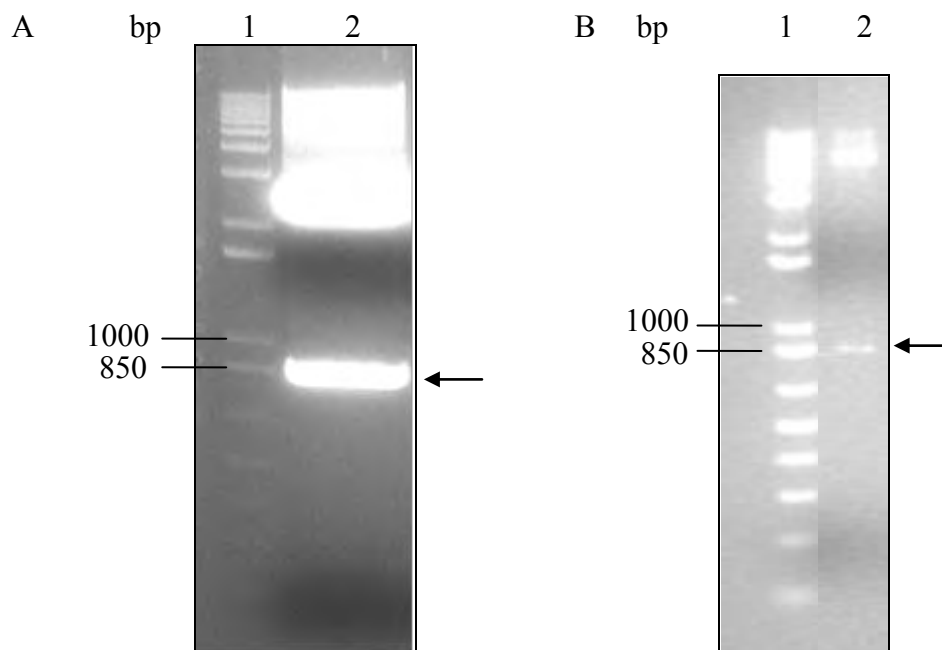


Figure 4.7. Digested (A) pJa Vector and (B) pET11a with STG2 insert. Electrophoresis was performed on 1.5% agarose in 1 x TAE buffer. A. Lane 1: 1kb Plus DNA Ladder; Lane 2: Digested pJa vector with STG2 insert (852bp) (Arrow). B. Lane 1: 1kb Plus DNA Ladder; Lane 2: Digested pET11a vector with STG2 insert (852bp) (Arrow).

4.2.3. Molecular Modeling of STG2

The VH region of STG2 was modeled against X-ray structures of anti-CD20 Fab fragment GA101 [PDB entry 3pp4; 87.61% sequence identity; 1.6Å resolution (314)]. The VL region of STG2 was modeled against inhibitor of alternative complement pathway anti-factor D Fab fragment [PDB entry 4d9q; 75.21% sequence identity; 2.28 Å resolution (315)]. Both regions of STG2 were then superimposed with STG1 as previously generated (Figure 3.15) to compare the structural homology of both scFvs. As shown in Figure 4.8, the overall structure of STG2 was well superposed with STG1 except for VH-CDR-H3. The CDR-H3 of STG2 deviates as compared to STG1. However, it has to be noted that the structure of both STG1 and STG2 was deduced by homology modeling against the database of known protein structures, thus, they may not be an exact representation of the true structure. However, the modeled STG2 structure was overall almost identical or similar to STG1 and it has been demonstrated that distortion of CDR did not lead to a reduced antigen binding affinity (316), we therefore proceeded with the production and evaluation of STG2.

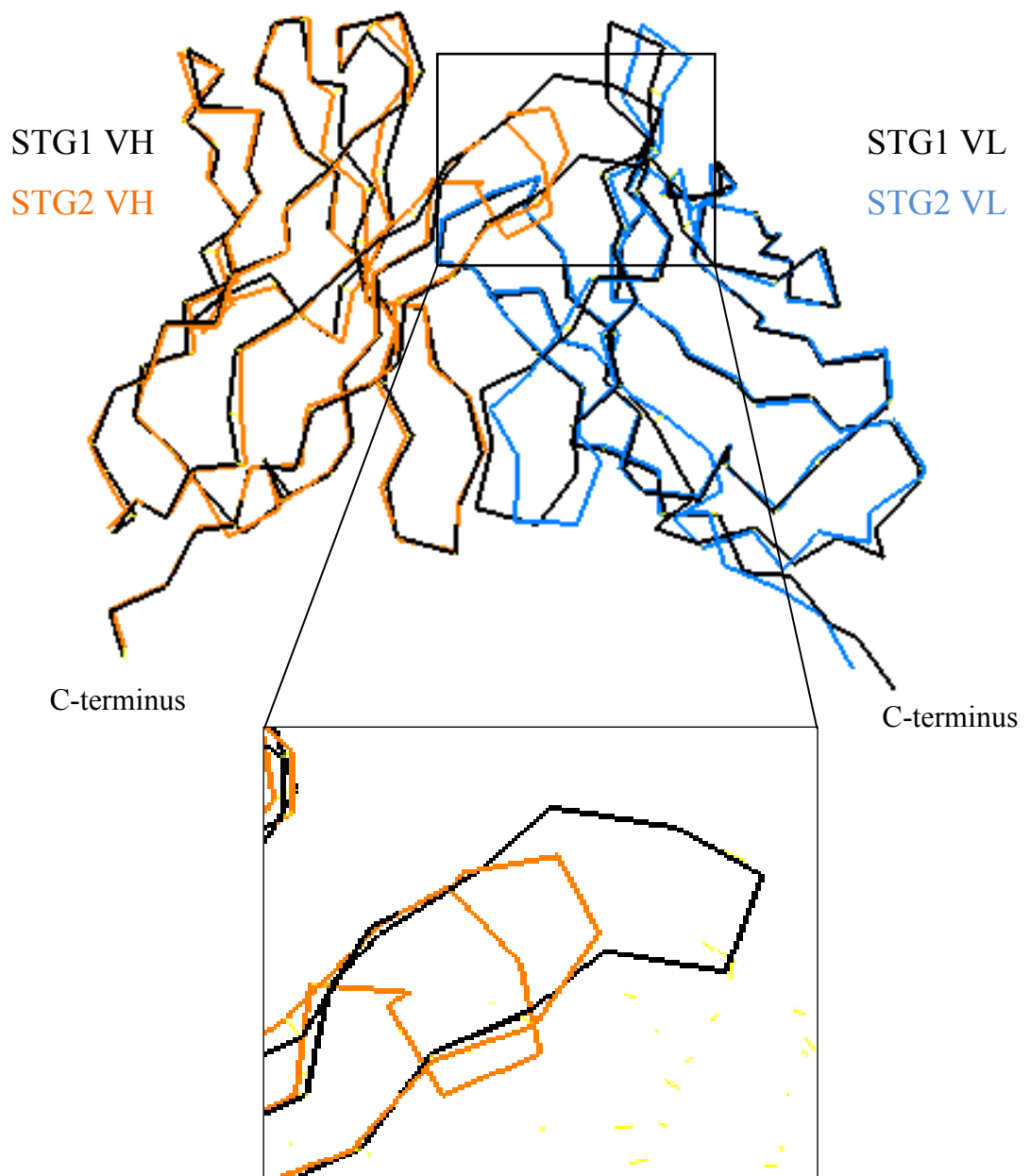


Figure 4.8. Superimposed diagram of STG1 and STG2 in lateral view. STG1 (black) and STG2 (orange for VH and blue for VL) were displayed as a ribbon model. The structure of VH-CDR-H3 of STG2 and STG1 was magnified (Inset). The linker connecting the VH and VL domain is not shown.

4.2.4. Expression of STG2

The recombinant pET11a-STG2 vector was chemically transformed into competent *E. coli* BL21 (DE3) bacterial cells and protein expression was induced by IPTG (Figure 4.9). As shown on SDS-PAGE, a protein of approximately 30 kDa, corresponding to the expected molecular weight of STG2 (30.91kDa), was highly expressed after IPTG induction (Figure 4.10A). The identity of the protein was confirmed by Western blot with anti-cMyc and anti-Penta-HIS antibodies (Figure 4.10B). The protein was harvested from the bacterial pellet by osmotic shock and the soluble and insoluble fractions were evaluated by SDS-PAGE analysis and Western blotting. Figure 4.11 shows that the protein (30.91kDa) was present mainly in the insoluble fraction (Figure 4.11, lane 3), indicating that STG2 was largely expressed as inclusion bodies in *E. coli*.

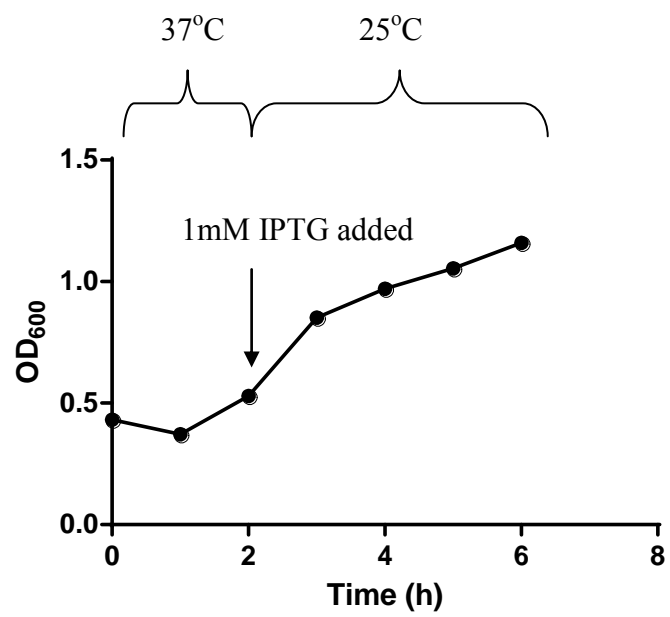


Figure 4.9. Bacterial growth pattern of *E. coli* BL21(DE3) expressing STG2.

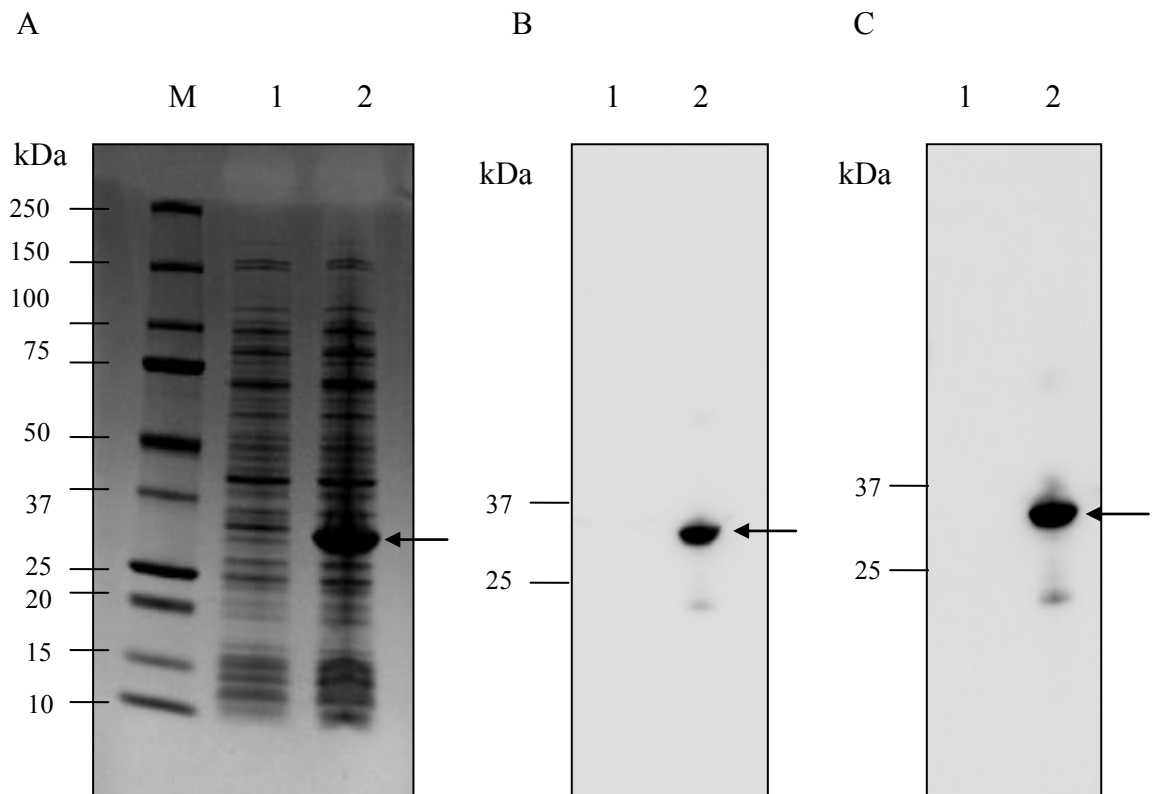


Figure 4.10. Gel analysis of pET11a-STG2 expressed in *E. coli* BL21 (DE3).
A. Coomassie Blue Staining and Western Blot (Immunostaining with B. Anti-cMyc antibody and C. Anti-Penta-HIS antibody). Lane M: Molecular weight marker (Bio-Rad). Lane 1: Total protein of STG2 before induction; Lane 2: Total protein of STG2 after induction. Arrow denotes STG2.

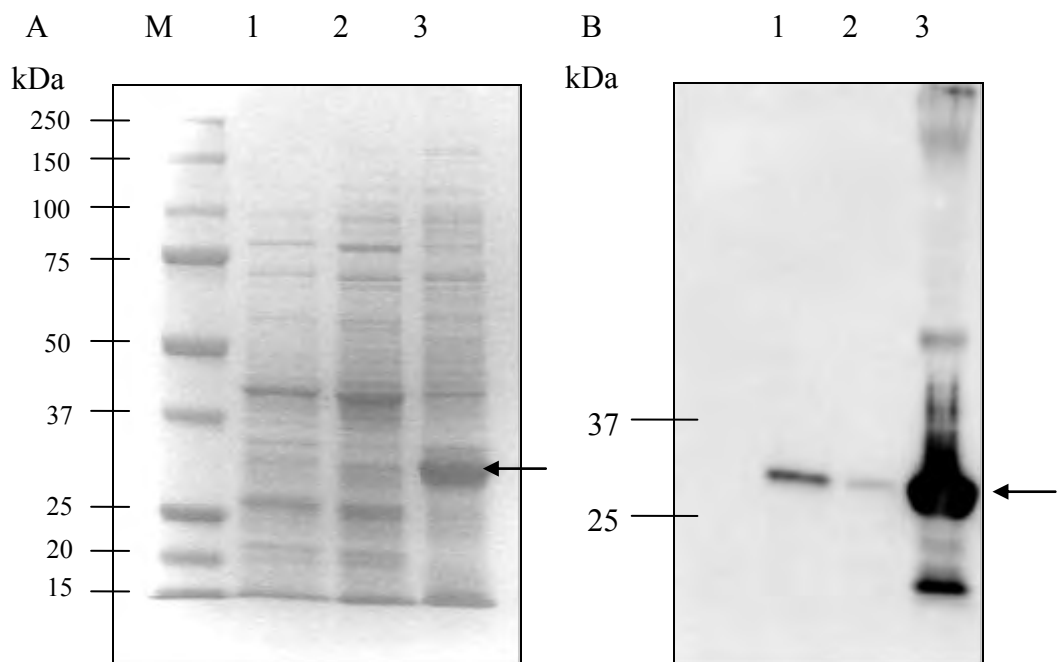


Figure 4.11. Gel analysis of soluble and insoluble fractions of pET11a-STG2. A. Coomassie Blue staining and B. Western Blot (Immunostaining with Anti-cMyc antibody). Lane M: Molecular weight marker (Bio-Rad). Lane 1: Soluble Fraction (In Osmotic Shock Solution); Lane 2: Soluble Fraction (In MgCl_2 Solution); Lane 3: Insoluble Fraction. Arrow denotes STG2.

4.2.5. Purification and One-Step Dialysis Refolding of STG2

The STG2 inclusion bodies were readily solubilized in 8M urea. Prior to this step, the inclusion bodies were washed with 2M urea combined with 2% Triton X-100 during the washing phase to remove contaminant proteins as it has been reported that hydrophobic membrane proteins would precipitate simultaneously with the inclusion bodies (317). To renature the recombinant protein into its native form, an *in vitro* refolding system using a one-step dialysis approach was attempted. STG2 solubilized in 8M urea was purified by IMAC by binding onto Nickel-Chelating Resin in the presence of 10mM imidazole (STG2 is expected to bind nickel resins due to the presence of a polyhistidine tail).

As shown in Figure 4.12, the subsequent elution phase revealed the presence of a minor peak eluting at around 72.5mM imidazole, and a main peak eluting at around 140mM imidazole. The presence of the target protein after the purification was detected by SDS-PAGE and Western blotting (Figure 4.13). After affinity chromatography, it was observed that the majority of the target protein was present in peak 2, with a low concentration present in peak 1. In peak 2, while a high concentration of the target protein was obtained, the purity was unsatisfactory with some contaminating proteins still present in the eluted sample. These higher MW bands above STG2 could represent multimers (corresponding to 61.82 and 92.73kDa for dimers and trimers, respectively) of the scFv since they are recognized by both MoAbs (anti-cMyc and anti-Penta-HIS); while the lower MW bands may reflect the presence of degradation products.

The presence of different forms of scFv is a common phenomenon and has been previously reported for other scFv constructs (256, 279, 318). These could be attributed to the association of VH and VL of different molecules (319) or to the sequence of the molecule itself (320). For the eluted sample in peak 2, the majority of the scFv was present as a monomer (~75%) and this was deemed appropriate for functional testing, therefore further refinement was not conducted. In addition, transition of multimers to monomer has been observed, demonstrating the instability of these larger forms of scFv (256). Therefore, peak 2 with a total pooled fraction of 16ml was concentrated to a volume of 6ml and subjected to one-step dialysis as described in the materials and methods section. The dialyzed STG2 was further concentrated to a volume of 1ml to be used in functional assays.

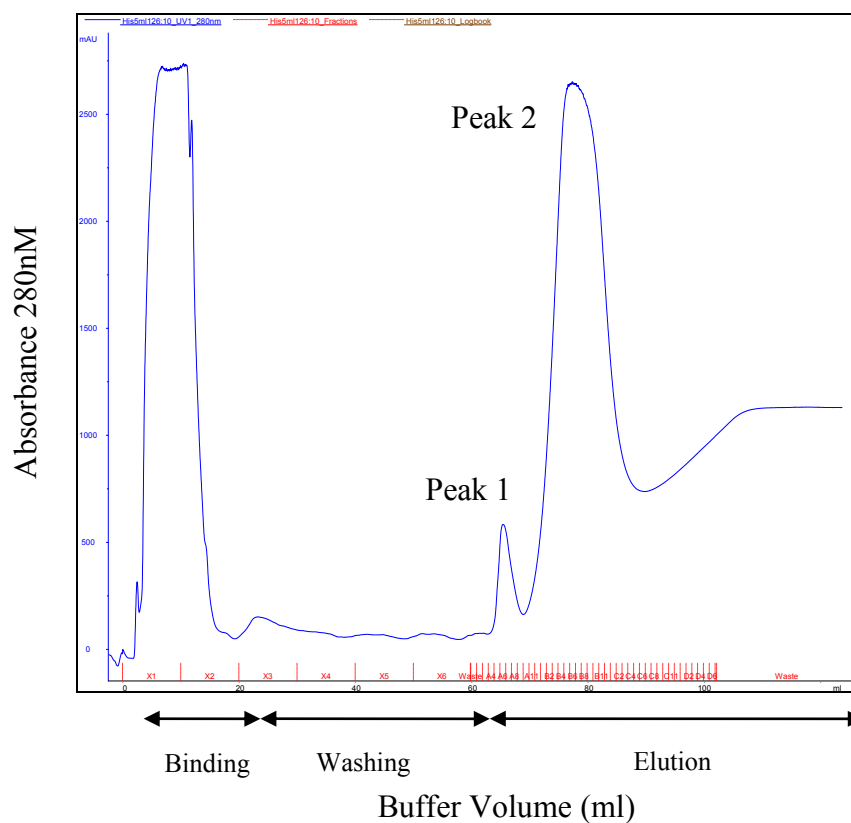


Figure 4.12. Purification profile of solubilized STG2. The sample was applied to a column of Nickel-Chelating Resin with a gradual increase of imidazole during stages of binding (10mM), washing (20mM) and gradient elution (20mM-500mM). Peak 1 was eluted at 72.5mM imidazole and peak 2 at 140mM imidazole during the elution phase.

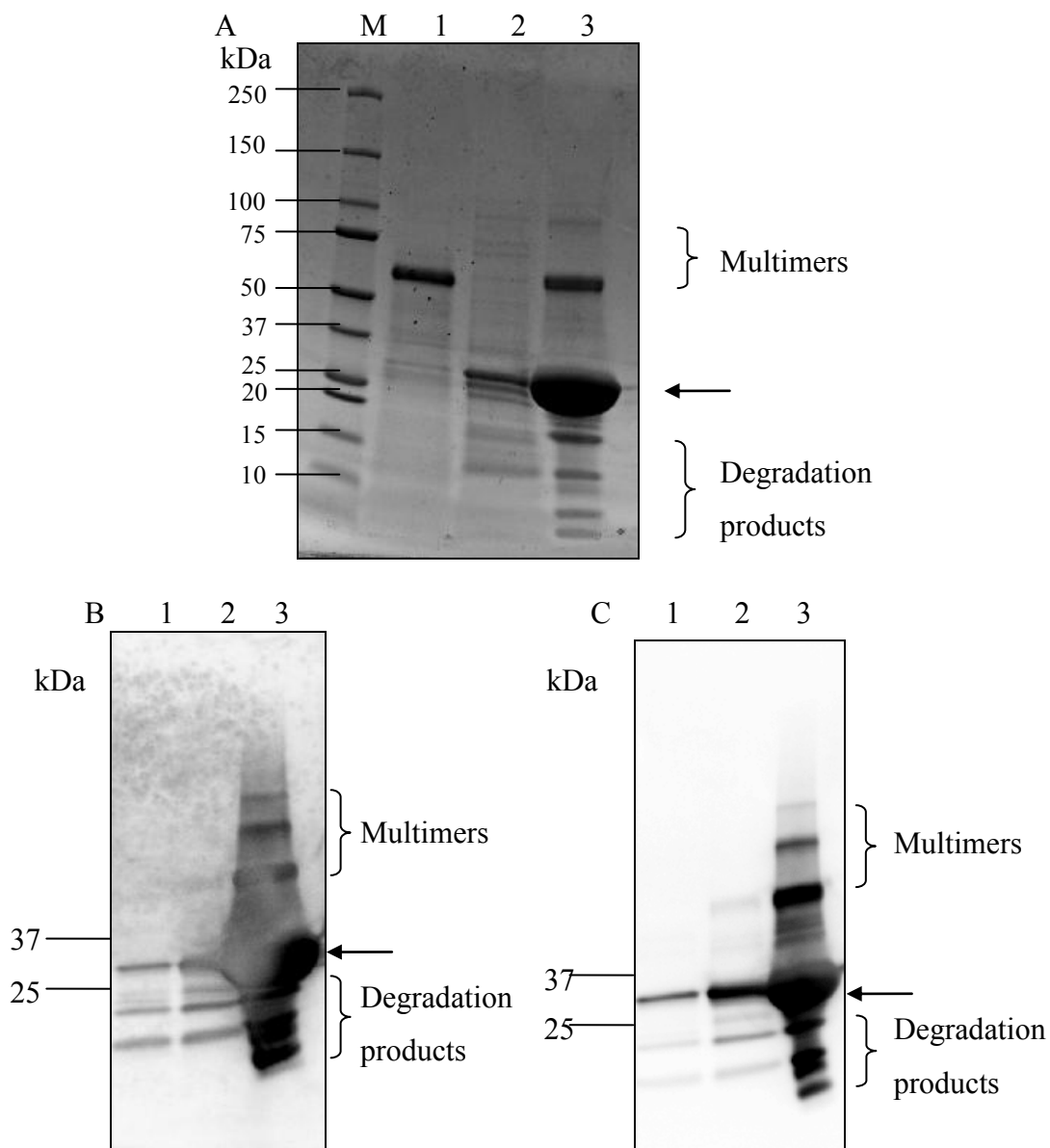


Figure 4.13. Gel analysis of solubilized STG2 purified with Nickel-Chelating Resin. A. Coomassie Blue staining and Western Blot (Immunostaining with B. Anti-Penta-HIS Antibody and C. Anti-cMyc Antibody). Lane M: Molecular weight marker (Bio-Rad); Lane 1: Solubilized inclusion body before purification; Lane 2: Purified protein in peak 1; Lane 3: Purified protein in peak 2. Arrow indicates position of STG2. Multimers and degradation products were observed in peak 2.

4.2.6. STG2 Refolded with One-Step Dialysis Fails to Inhibit Platelet Aggregation

The purified refolded STG2 added at 30μM was not able to inhibit platelet aggregation induced by HIT IgG (Figure 4.14(1)). This high concentration was chosen as the first initial attempt to test the functional properties of the protein. As demonstrated, the inhibition property exhibited by STG2 is much lower in comparison to the parental antibody IV.3 (10nM) (Figure 3.26) and STG1 (400nM) (Figure 3.27). This could be attributed to either the improper refolding of STG2 or disruption of STG2 structure due to the humanization approach. However, a conclusion could not be reached at this stage.

To ensure the proper refolding of STG2, the recombinant protein was subjected to a second round of overnight dialysis against 1L of PBS and 0.5mM of GSSG for oxidation of free thiol groups to encourage disulfide bond formation (321). The attempt to restore the correct folding of the protein was unsuccessful as it didn't exhibit any functional activity in preventing platelet aggregation in the presence of HIT IgG (Figure 4.14(2)).

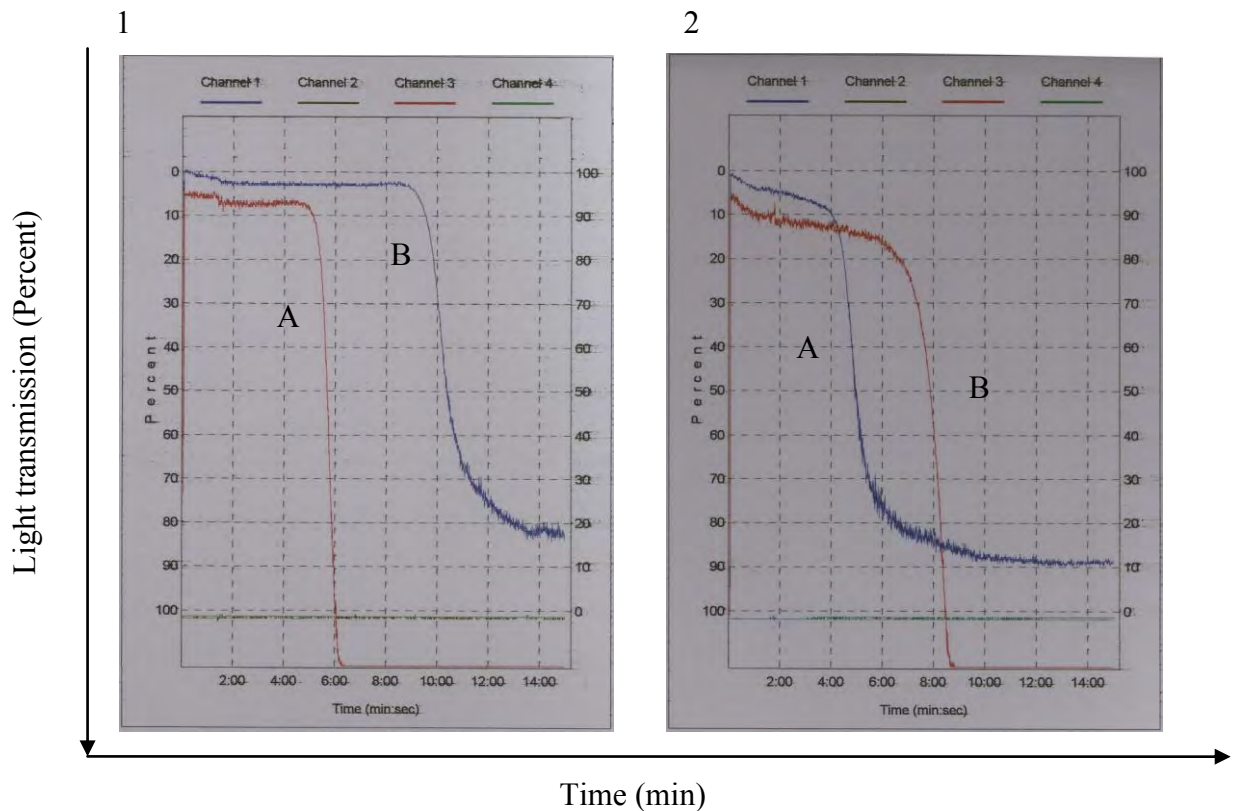


Figure 4.14. STG2 refolded with one-step dialysis fails to inhibit platelet aggregation induced by HIT IgG and heparin. (1). A. Negative Control- Platelet aggregation in the presence of HIT IgG and heparin (0.5IU/ml), but in the absence of STG2. B. 30 μ M of STG2 failed to inhibit platelet aggregation in response to HIT IgG and heparin (0.5IU/ml). (2). Second attempt of dialysis. A. Negative Control- Platelet aggregation in the presence of HIT IgG and heparin (0.5IU/ml), but in the absence of STG2. B. 30 μ M of STG2 failed to inhibit platelet aggregation in response to HIT IgG and heparin (0.5IU/ml) after second dialysis step.

4.2.7. Purification and Step-Wise Dialysis Refolding of STG2

It is likely that the proper refolding of the protein didn't take place during the *in vitro* refolding process. The dialysis stage that involves only one-step change of buffer from 8M to 1M of urea may not be sufficient for the protein to be correctly refolded.

Therefore, in the subsequent experiment, refolding was attempted using stepwise dialysis. This approach involves placing the protein at different intermediate, decreasing concentrations of urea to promote refolding.

As before (section 4.2.5), STG2 inclusion bodies were solubilized in 8M urea and purified with Nickel affinity chromatography. The target protein was subsequently eluted at around 170mM imidazole during the gradient elution phase (Figure 4.15). A total of 12ml was collected and dialyzed against a linear decreasing urea concentration from 3M to 1M. 0.5M L-Arginine and 0.5M GSSG were added at the 1M urea stage. The sample was finally dialyzed in PBS and subjected to further analysis. Approximately 50mg of total protein was harvested from 1L of bacterial culture.

4.2.8. STG2 Refolded with Step-Wise Dialysis Exhibits Partial Activity

The ability of STG2 to inhibit HIT IgG-induced platelet aggregation was tested by light transmission aggregometry. Previously, 30μM of STG2 (section 4.2.6) that was refolded with one-step dialysis did not exhibit any functional property and failed to inhibit platelet aggregation induced by HIT IgG. Therefore, 30μM of STG2 refolded via stepwise dialysis was tested. The protein inhibits platelet aggregation for only 30 min after addition in the presence of HIT IgG (data not shown). After examining several concentrations, STG2 was able to fully inhibit platelet aggregation in the presence of HIT IgG at a concentration of 110μM (Figure 4.16). This important observation is the first indication that STG2 is capable of blocking the HIT immune complexes from activating the platelets. This also shows that the humanization approach may not have affected the structure of STG2 required for the interaction with platelets. However, the high concentration (110μM) required for the protein to exert its inhibitory function denotes that the majority of the STG2 is not present in a correct conformation, and further optimization of the refolding procedure is thus required.

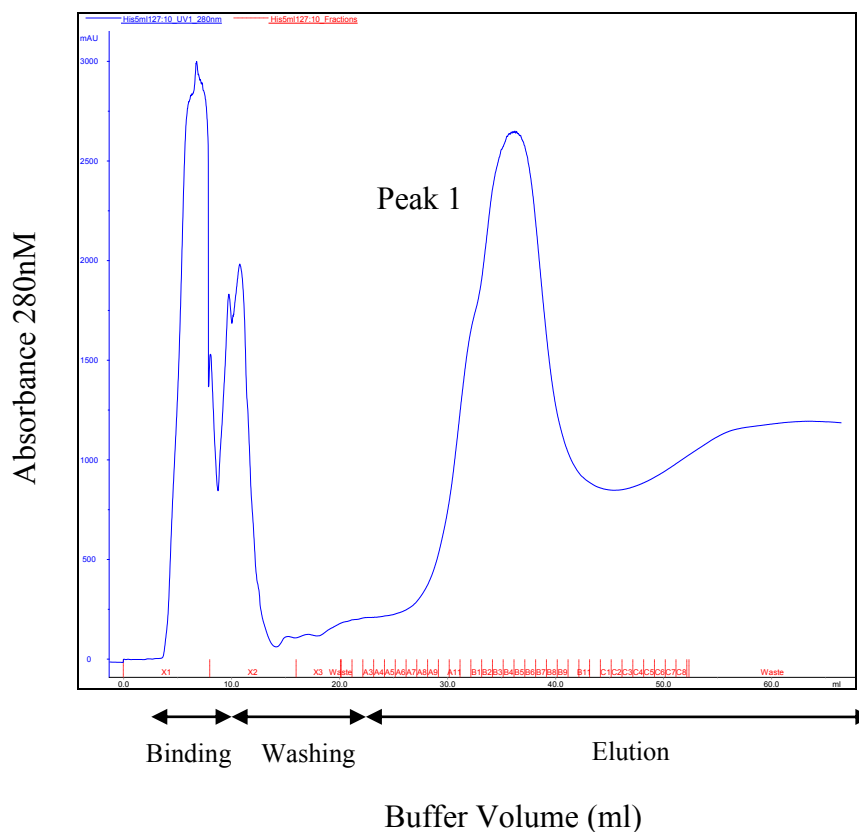


Figure 4.15. Purification profile of solubilized STG2. The sample was applied to a column of Nickel-Chelating Resin with a gradual increased of imidazole during stages of binding (10mM), washing (20mM) and gradient elution (20mM-500mM). Peak 1 was eluted at 170mM Imidazole and these fractions were collected.

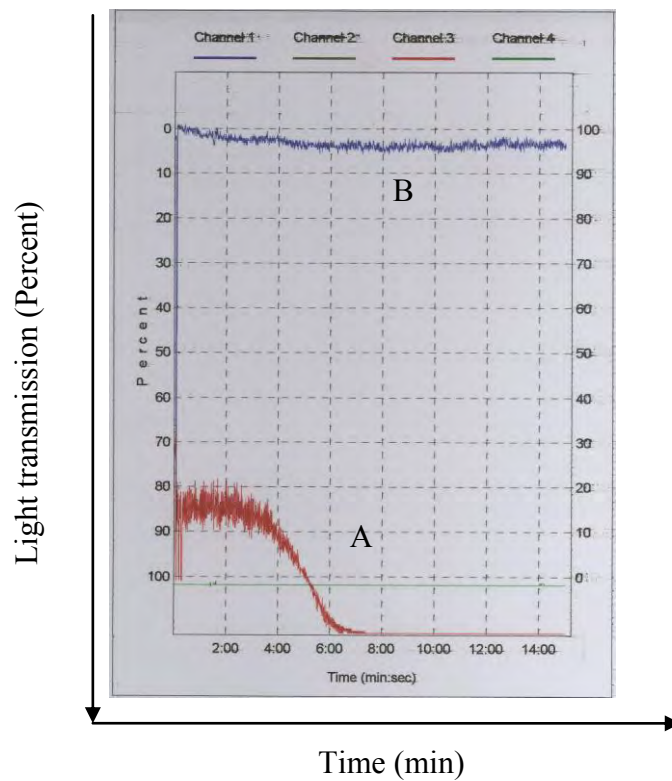


Figure 4.16. STG2 refolded with step-wise dialysis inhibits platelet aggregation induced by HIT IgG and heparin. A. Negative Control- Platelet aggregation in the presence of HIT IgG and heparin (0.5IU/ml), but without STG2. B. Platelet aggregation was inhibited in the presence of 110 μ M of refolded STG2.

4.2.9. STG2 Refolded with Step-Wise Dialysis Did Not Bind to Human Platelets

In the previous section, STG2 was observed to inhibit platelet aggregation induced by HIT IgG. To determine the interaction of STG2 with Fc γ RIIa on platelets, the antigen binding capability of the recombinant protein was evaluated by flow cytometry. The flow cytometric analysis showed that STG2 (tested at three different concentrations of 100, 300, 600 μ M) detected with AF 488-conjugated anti-c-Myc antibody did not interact with human platelets (Figure 4.17). These results suggest that STG2 does not recognize Fc γ RIIa on platelets. However, the observations from the platelet aggregation assay (Figure 4.16) may suggest that a minimal portion of the protein has an active conformation. This was shown by the ability of 110 μ M STG2 to inhibit platelet aggregation in the presence of HIT IgG. These observations indicate that the humanization step may not have abolished the specificity of STG2, and that the low activity detected may be due to protein misfolding.

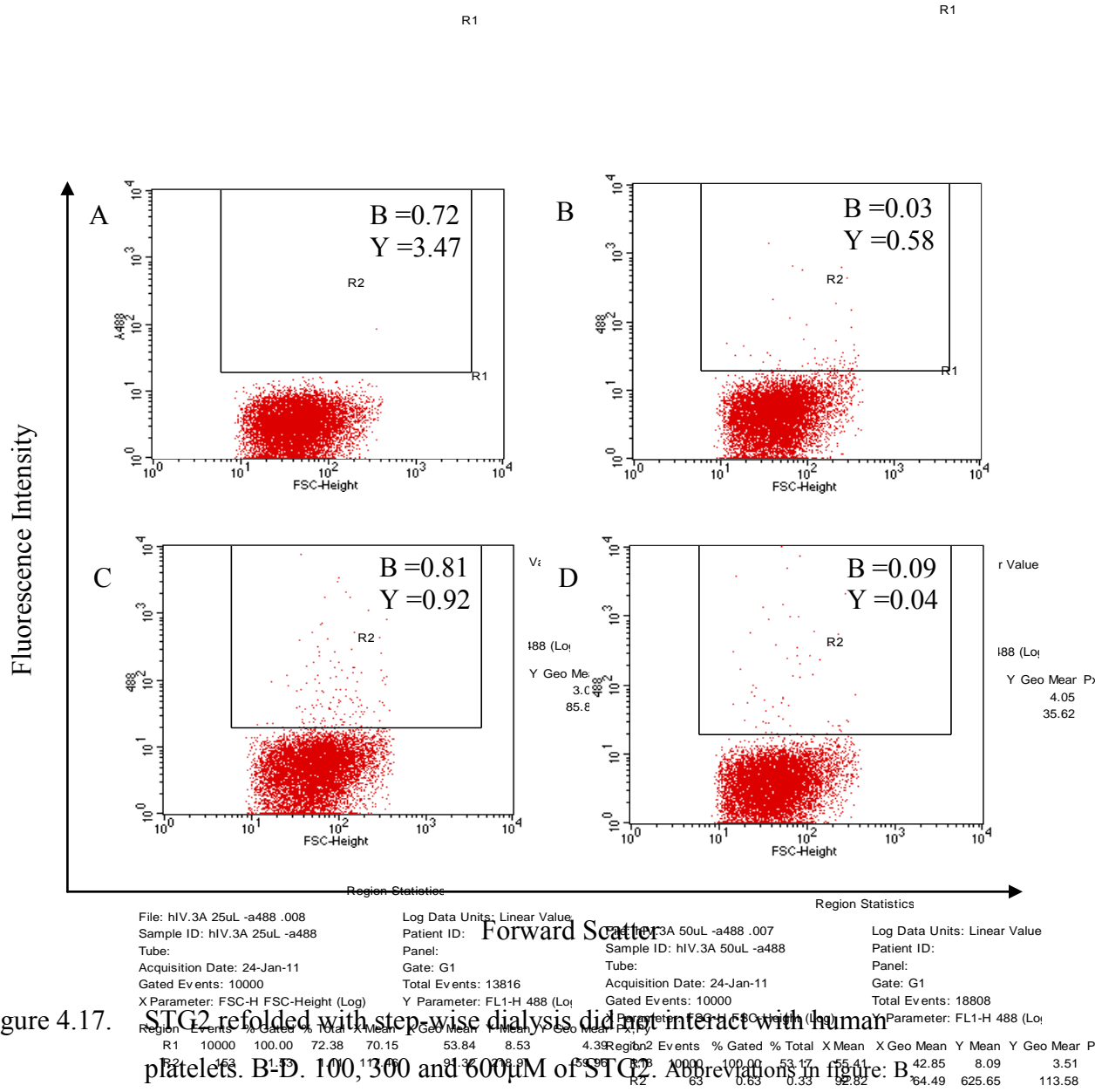


Figure 4.17. STG2 refolded with step-wise dialysis did not interact with human platelets. B-D. 100, 300 and 600 μM of STG2. Abbreviations in figure: B, Binding %; Y, Y Geometric Mean.

4.2.10. Purification and On-Column Refolding of STG2

The solubilized STG2 refolded using the stepwise dialysis system didn't yield a high proportion of functional protein as examined in both binding and functional assays (Figures 4.16 and 4.17). Therefore, another approach was undertaken to attempt the refolding of the protein into an active conformation. Instead of decreasing the concentration of the denaturant by gradual reduction of dialysis buffer concentration, an on-column refolding system was applied and conducted on affinity chromatography. STG2 denatured with 8M urea was loaded and bound onto 1ml of Nickel-Chelating Resin under reducing conditions. After the washing step, the concentration of urea was gradually decreased by the introduction of urea free refolding buffer. The slow removal of denaturant from the system is expected to promote on-column protein refolding. At the end of the refolding process, the elution of the protein was observed at around 250mM imidazole (Figure 4.18). The presence of the target protein in the eluted fraction was examined on SDS-PAGE and by Western blotting (Figure 4.19). Approximately 15mg of purified refolded STG2 was obtained from 1 L of culture (Table 4.1).

4.2.11. STG2 Refolded On-Column Binds to Fc γ RIIIa on Platelets

To evaluate the antigen binding activity of the refolded protein using the on-column refolding system, direct immunofluorescence was carried out on human platelets. The flow cytometry results (Figure 4.20) demonstrate that the refolded STG2 was able to bind to human platelets in a concentration dependent manner. The highest binding capacity of STG2 was observed at concentration of 5 μ M (Binding %=59.8; Y Geo Mean=122.6).

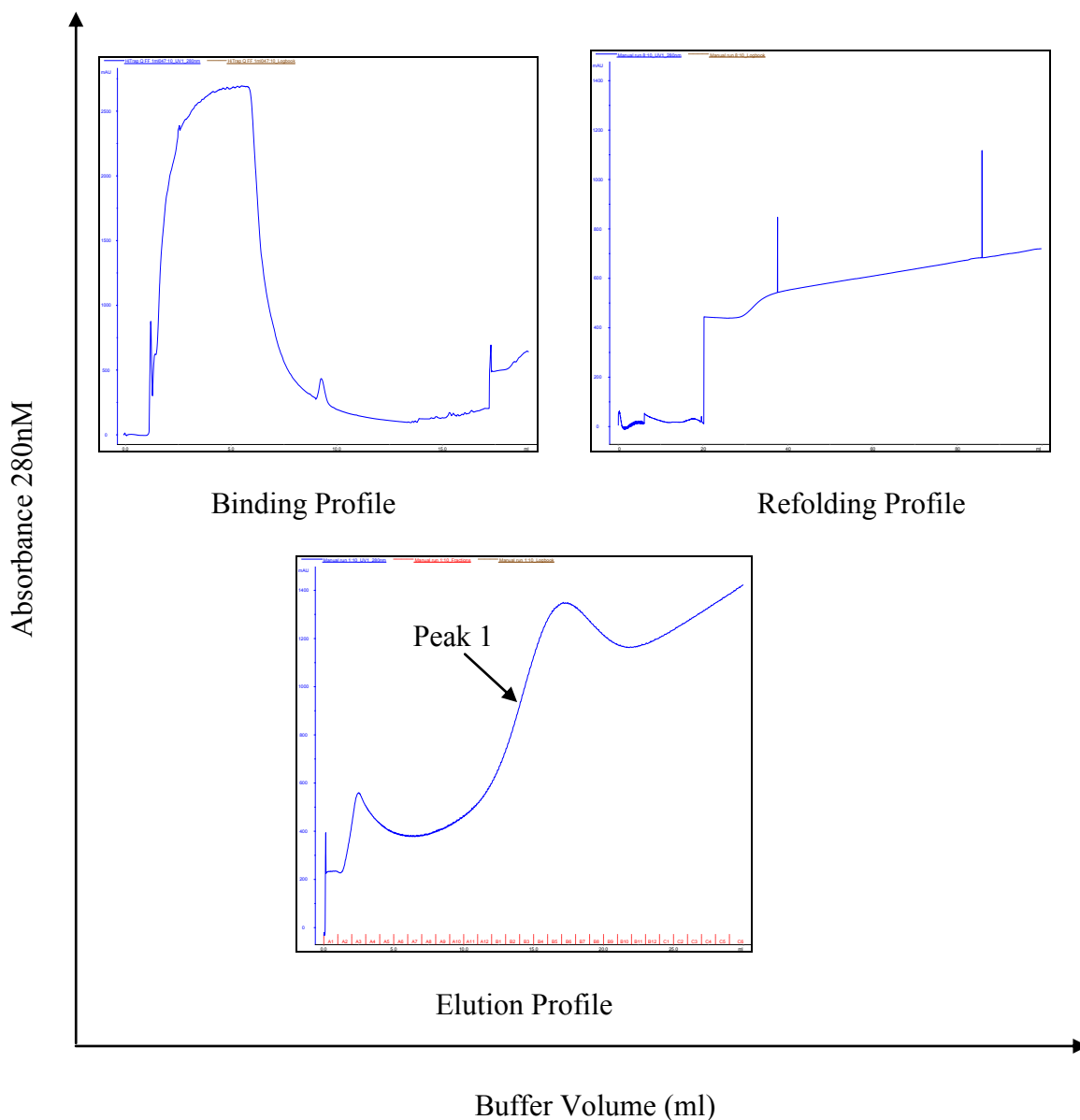


Figure 4.18. Purification and on-column refolding profile of solubilized STG2. The denatured sample was loaded onto a column filled with 1ml Nickel-Chelating Resin. STG2 bound to the resin in a denatured form was slowly refolded as the urea concentration was gradually reduced during the refolding phase. The subsequent increase in the concentration of imidazole prompted the elution of the target protein at around 250mM imidazole.

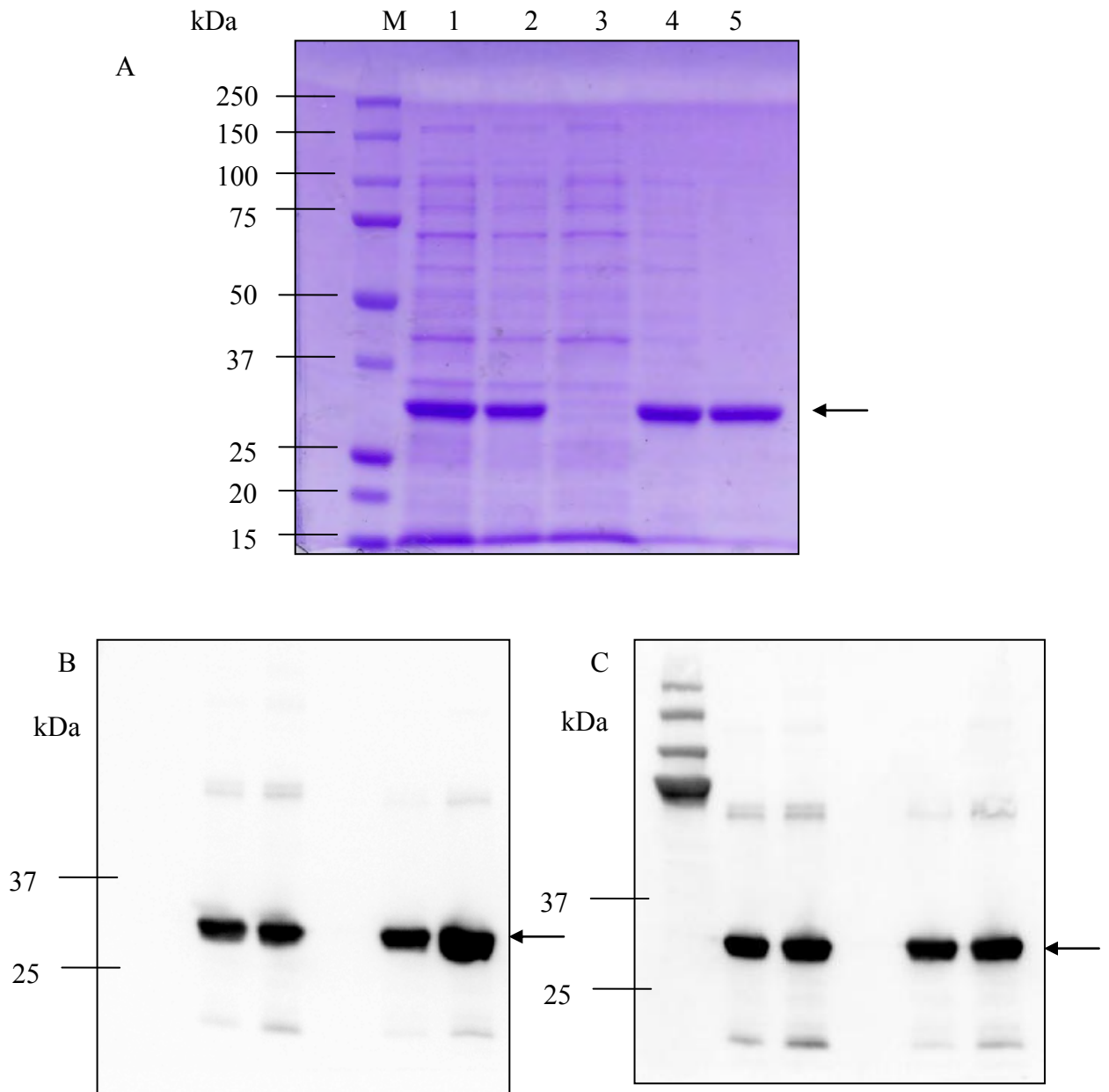


Figure 4.19. Gel analysis of the purified refolded STG2. A. Coomassie Blue Staining and Western Blot (Immunostaining with B. Anti-cMyc antibody and C. Anti-Penta-HIS antibody). Lane M: Molecular weight marker (Bio-Rad); Lane 1: Total cell lysate; Lane 2: Pellet after sonication; Lane 3: Soluble fraction; Lane 4: Solubilized inclusion body with 8M urea before purification; Lane 5: Purified inclusion body in peak 1 after on-column refolding. Arrow denotes STG2.

Table 4.1. Summary on purification and refolding of STG2

Procedure	Total protein (mg)
Total cell lysate ^a	273
Pellet after sonication	150
Soluble fraction	100
Solubilized inclusion bodies	90
Purified and refolded	15

^a From about 5g of wet-weight cells obtained from 1 L cell culture

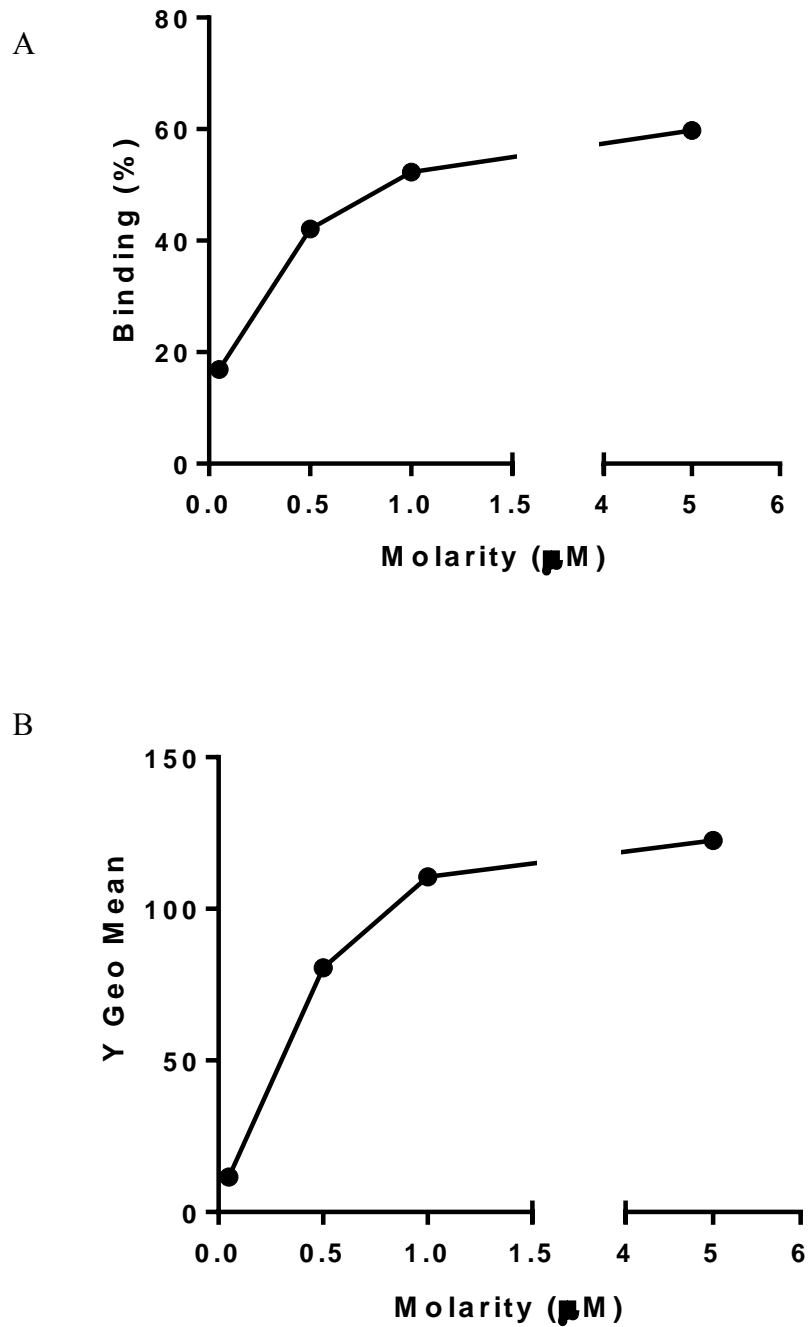


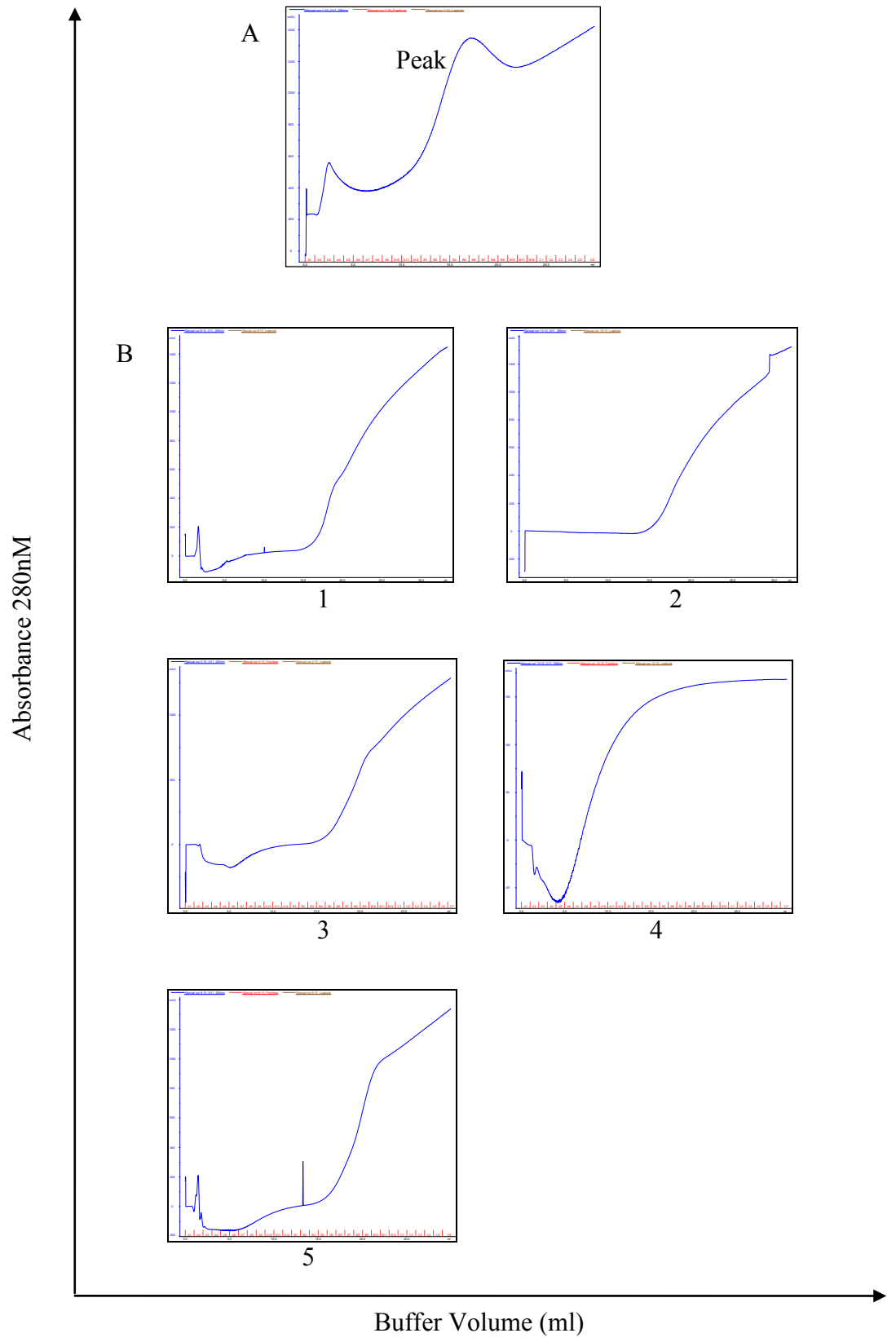
Figure 4.20. STG2 refolded on-column interacts with human platelets. Different concentrations of STG2 (50nM, 500nM, 1μM and 5μM) were incubated with human platelets followed by detection with Alexa Fluor 488-conjugated anti-c-Myc. Binding efficiency is measured by A. Percentage of bound platelets. B. Y Geometric Mean, which represents the binding intensity.

4.2.12. Optimization of STG2 Purification

The procedure to obtain a purified and functional STG2 protein after on-column refolding was successfully established as the protein demonstrated binding to human platelets. The protocol was repeated to obtain sufficient protein for the required assays. This time, however, problems were encountered in the elution phase during the purification step. Unlike the initial elution profile (Figure 4.21A), no elution of the target protein was observed after numerous attempts (Figure 4.21B). A control run was tested consisting of only the elution buffer (500mM imidazole), which was introduced gradually onto the column in the absence of the protein. As the concentration of imidazole gradually increased, a corresponding absorbance signal was also recorded (Figure 4.21C). This suggested that the STG2 protein peak might be masked by the background absorbance produced by the elution buffer. Protein elution at a lower imidazole concentration (350mM) allowed the recovery STG2 at around 240mM imidazole (Figure 4.21D). This protocol was successfully applied in subsequent rounds of STG2 purification.

4.2.13. Incomplete On-Column Refolding of STG2

The binding activity of the purified STG2 was evaluated with flow cytometry analysis. The results indicate that the on-column refolding protocol is not able to produce antibody of a consistent level of activity. Figure 4.22 shows the platelet binding profile of five STG2 protein batches. The binding activity ranged from 58% to 0%, indicating that the on-column refolding methodology is not suitable for the reliable refolding and purification of STG2. Additional refinement of the refolding protocol will be required to produce sufficient amounts of active STG2 antibody.



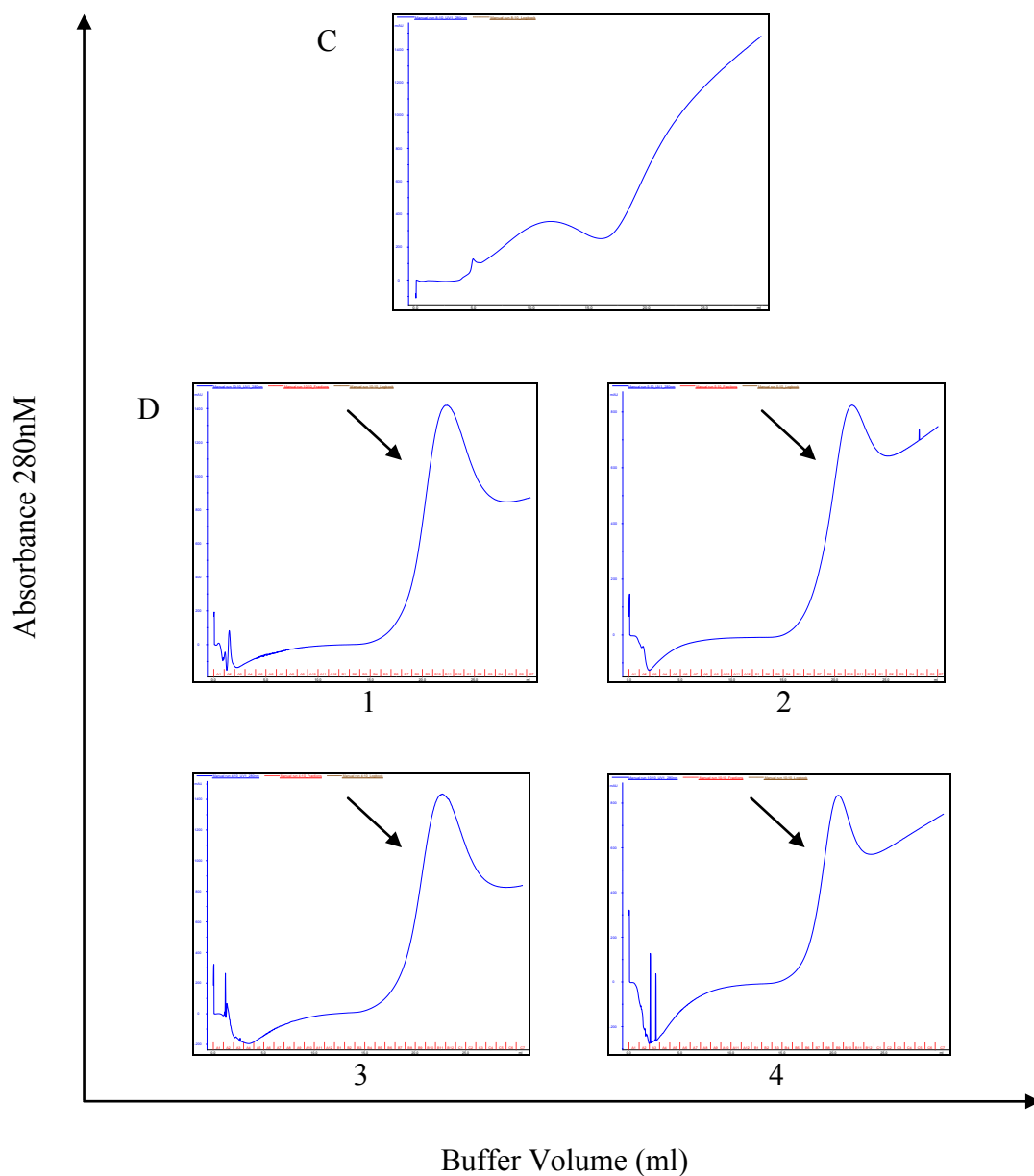


Figure 4.21. Elution profile of STG2 after on-column refolding. A. Target protein eluted with buffer containing 500mM imidazole. B. No elution peak observed during subsequent purifications (Number denotes attempts conducted). C. A control run of 500mM imidazole without STG2. D. Elution peak of the STG2 (Arrow) at around 240mM imidazole observed after the concentration of imidazole in the elution buffer was lowered from 500mM to 350mM (Number denotes attempts conducted).

R1

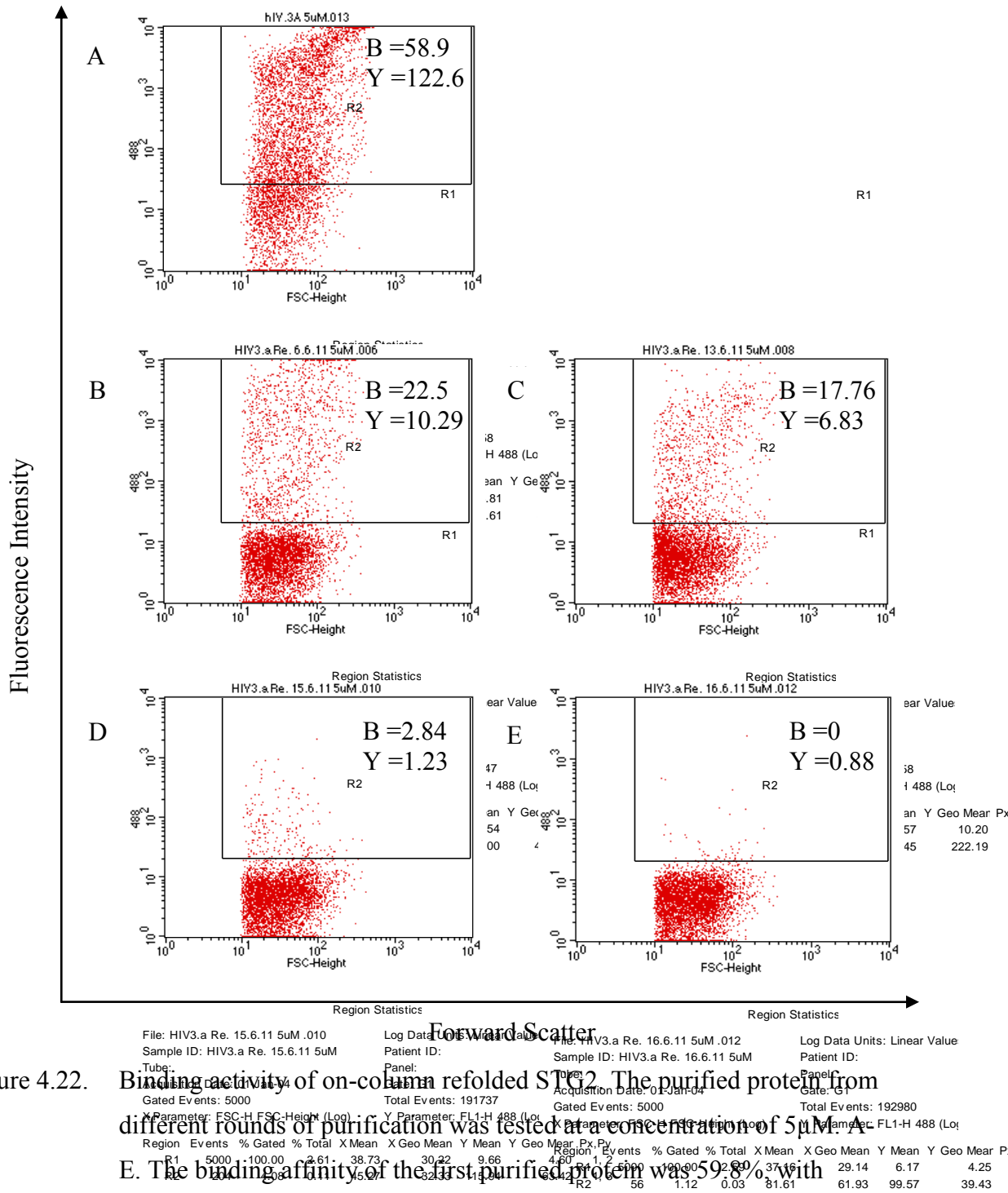


Figure 4.22.

Binding activity of on-column refolded STG2. The purified protein from different rounds of purification was tested at a concentration of 5 μM. A-E. The binding affinity of the first purified protein was 59.8% with

fluorescence intensity of 122.6. However, the protein purified in subsequent attempts showed a gradual decrease in binding capacity. Abbreviations in figure: B, Binding %; Y, Y Geometric Mean.

4.2.14. Purification and Refolding of STG2 with SMALPs

As shown in the previous section, on-column refolding did not produce consistent levels of active STG2. This prompted the evaluation of a different approach to obtain a pure and functional STG2 from the inclusion bodies. In the new protocol, the solubilization of the inclusion bodies was conducted with 5% SDS instead of 8M urea. The SDS was removed from the sample via dialysis against 50mM Tris.HCl (pH 8.0), followed by the addition of β -OG for further solubilization of the sample. The solubilized protein was integrated into a nanoparticle structure with the assistance of both DMPC and SMA copolymer. The resulting particles were then subjected to purification with nickel affinity chromatography. An elution peak was observed at around 250mM of imidazole of the gradient elution phase (Figure 4.23). The pooled fraction was analyzed by SDS-PAGE and Western blotting. Figure 4.24 shows a single band corresponding to the expected size of STG2 (30.91kDa). Immunostaining revealed the presence of two other bands at around 62kDa and 20kDa. This suggests that a fraction of the protein may be present in a dimer form (61.8kDa). The 20kDa band is most likely a degradation product of STG2.

4.2.15. STG2 Incorporated into SMALPs Binds to Fc γ RIIIa on Platelets

To evaluate the binding capacity of the purified STG2 integrated into SMALPs, direct immunofluorescence staining was performed and the fluorescence intensity was evaluated by flow cytometry. As shown in Figure 4.25, various concentrations of the target protein were tested showing that the binding to human platelets occurred in a concentration dependent manner. The highest binding activity was observed at a concentration of 1.5 μ M.

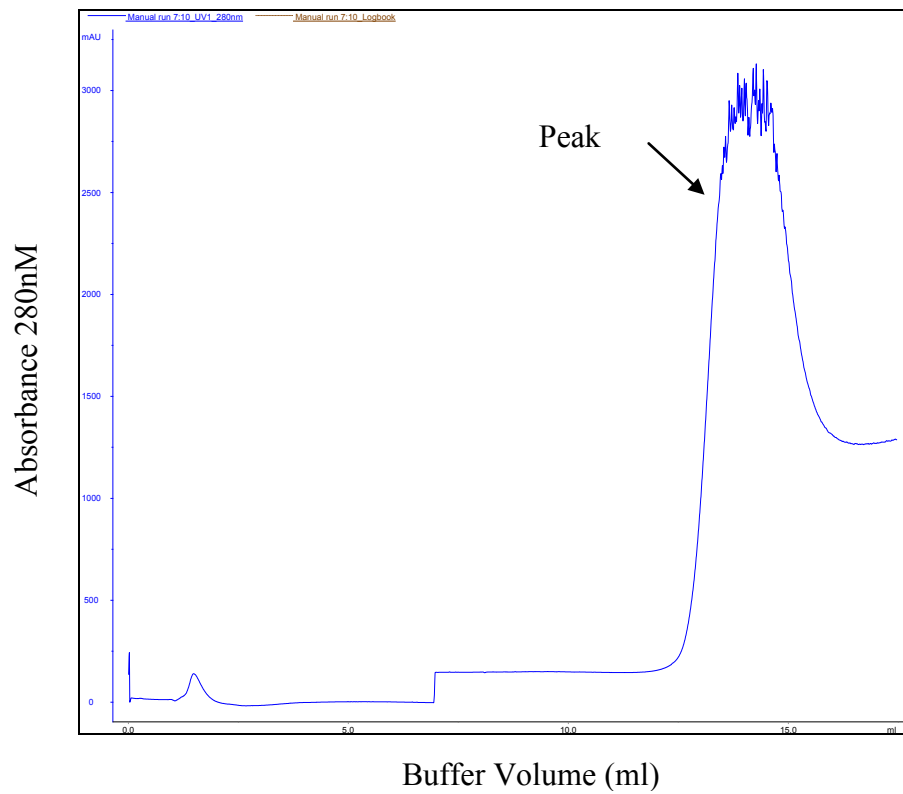


Figure 4.23. Elution profile of STG2 after incorporation into SMALPs. The protein was eluted at around 250mM imidazole.

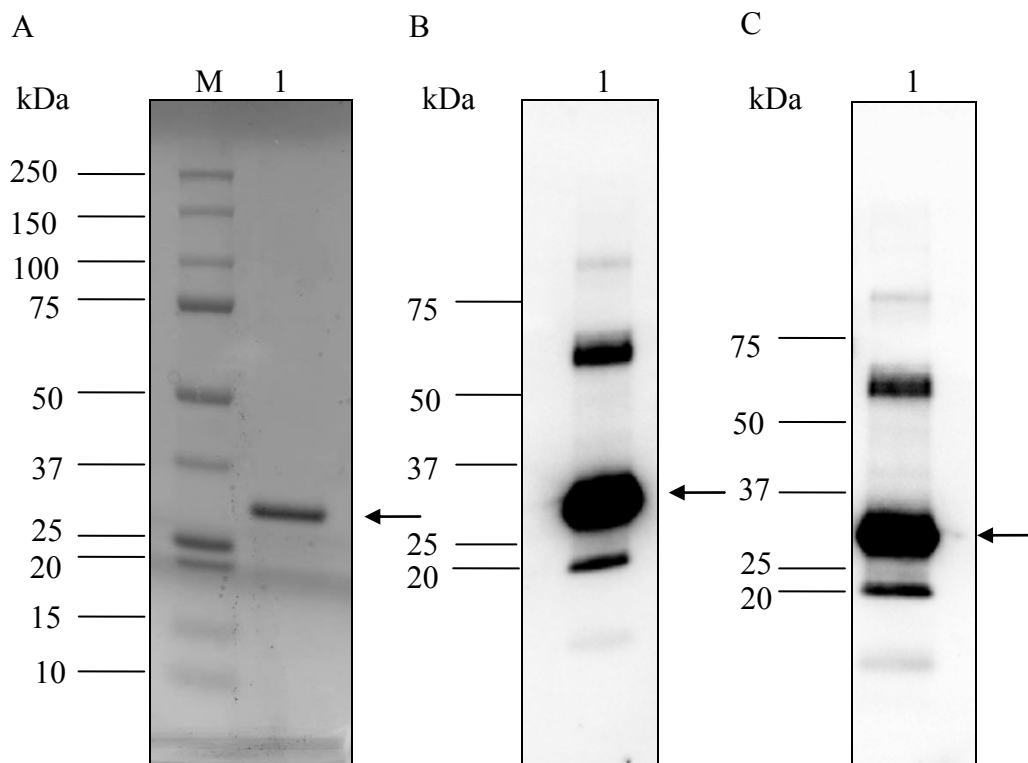
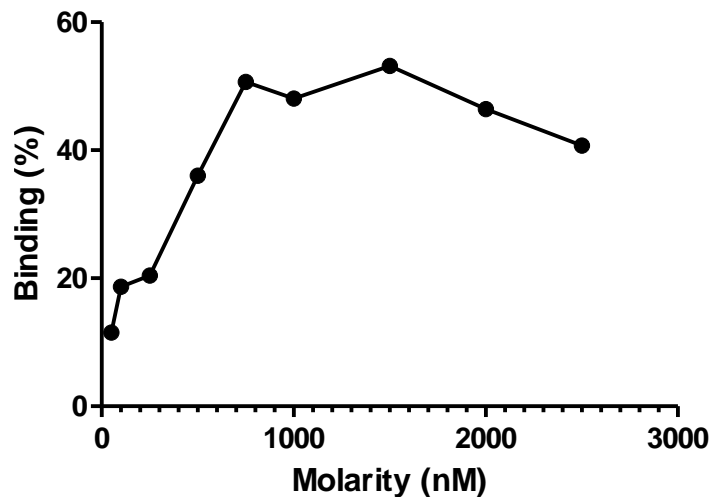


Figure 4.24. Gel analysis of purified STG2 incorporated into SMALPs.

A. Coomassie Blue Staining. B & C. Western Blot immunostaining with Anti-cMyc Antibody and Anti-Penta-HIS Antibody. Arrow denotes STG2.

A



B

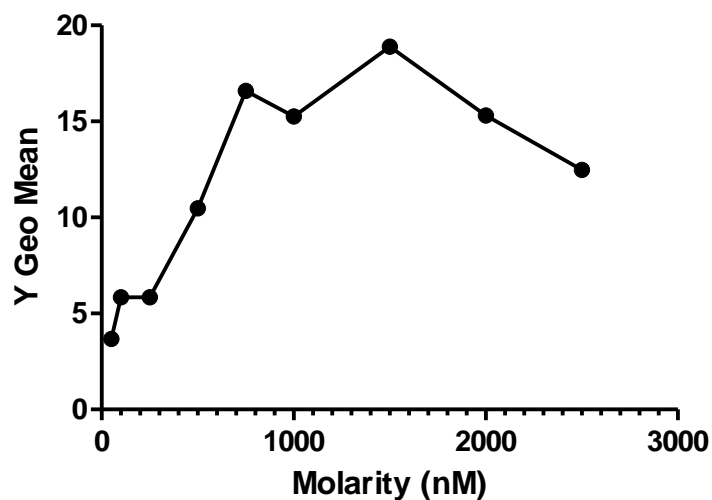


Figure 4.25. STG2 (incorporated into SMALPs) interacts with human platelets. Different concentrations of STG2 (50nM, 100nM, 250nM, 500nM, 750nM, 1 μ M, 1.5 μ M, 2 μ M, and 2.5 μ M) were incubated with human platelets followed by detection with AF 488-conjugated anti-c-Myc. Binding efficiency is measured by A. Percentage of bound platelets and, B. Y Geometric Mean, which represents the binding intensity.

4.2.16. Purified STG2 (Incorporated into SMALPs) Leads to Spontaneous Platelet Aggregation

Having shown the STG2 incorporated in SMALPs interacted efficiently with human platelets, we sought to evaluate its functional capacity in a platelet aggregation assay. When STG2 was tested for its inhibitory activity (at a concentration of 6μM), the protein not only failed to inhibit the aggregation of platelets in the presence of HIT IgG (Figure 4.26A), but it also caused spontaneous platelet aggregation even in the absence of HIT IgG (Figure 4.26B). These results were validated against the negative control (platelet aggregation occurred in the presence of HIT IgG and heparin, with no inhibitor); and positive control (platelet aggregation did not occur in the presence of HIT IgG and heparin, in the presence of 10nM of IV.3 MoAb). We ruled out the possibility that SMALPs (which wrapped around STG2) as the cause of spontaneous platelet aggregation since no platelet aggregation was observed with other proteins that were prepared using the same approach (data not shown). Therefore, we proposed that the spontaneous platelet aggregation might be due to the presence of dimers present in the purified fraction of STG2 (Figure 4.24).

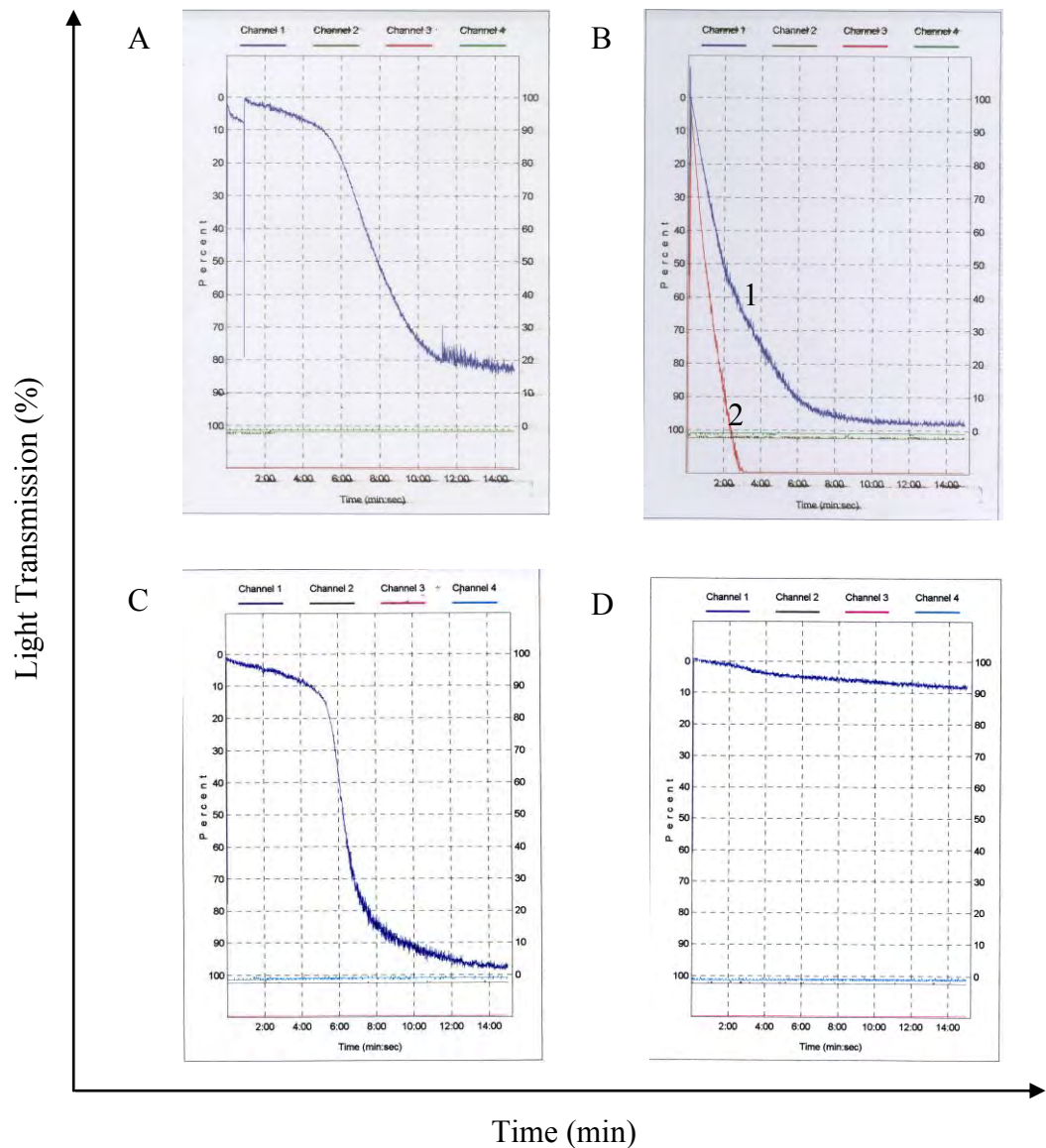


Figure 4.26. Purified STG2 (incorporated into SMALPs) leads to spontaneous platelet aggregation. A. Purified STG ($6\mu\text{M}$) added to PRP, HIT IgG and heparin (0.5IU/ml) failed to inhibit platelet aggregation. B. Purified STG2 added at a concentration of (1) $6\mu\text{M}$ or (2) $10\mu\text{M}$ to PRP led to spontaneous platelet aggregation in the absence of HIT IgG and heparin (0.5IU/ml). C. Negative Control-No inhibition of platelet aggregation in the presence of PRP, HIT IgG and heparin (0.5IU/ml); D. Positive Control-Inhibition of platelet aggregation with 10nM of IV.3 MoAb when it was added to PRP, HIT IgG and heparin (0.5IU/ml).

4.2.17. Purification of Soluble STG2

In view of the unsuccessful attempts to refold functional STG2 from inclusion bodies, we decided to purify the protein present in the soluble fraction. The soluble fraction containing STG2 was collected by disruption of the bacterial pellet in the presence of lysis buffer followed by centrifugation. This was then applied to 1ml of HiTrap HP column for purification by affinity chromatography. As shown in Figure 4.27, a peak was observed during the gradient elution phase when the concentration of imidazole reached 230mM. Evaluation on SDS-PAGE and by Western blotting showed that the pooled fraction contained the target protein (Figure 4.28). Approximately 1mg of soluble STG2 was obtained from 1 L of bacterial culture.

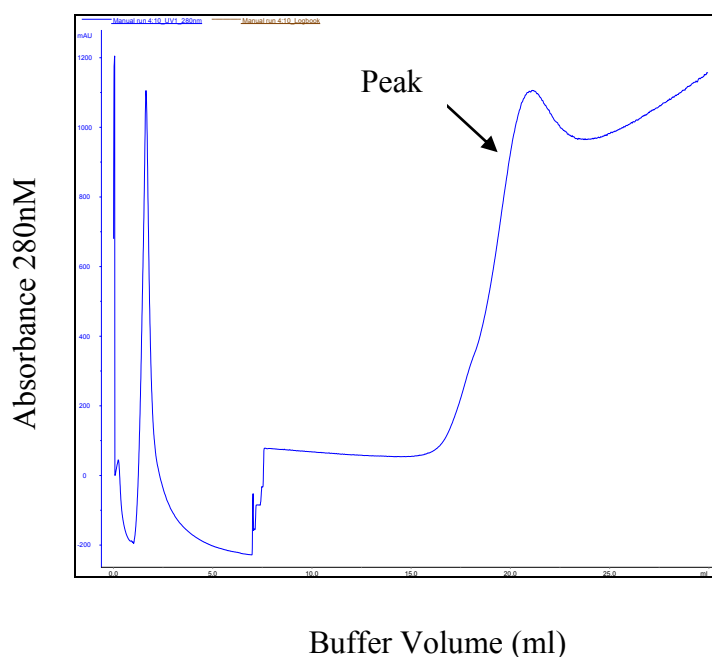


Figure 4.27. Elution profile of soluble STG2. The protein was eluted at around 230mM imidazole.

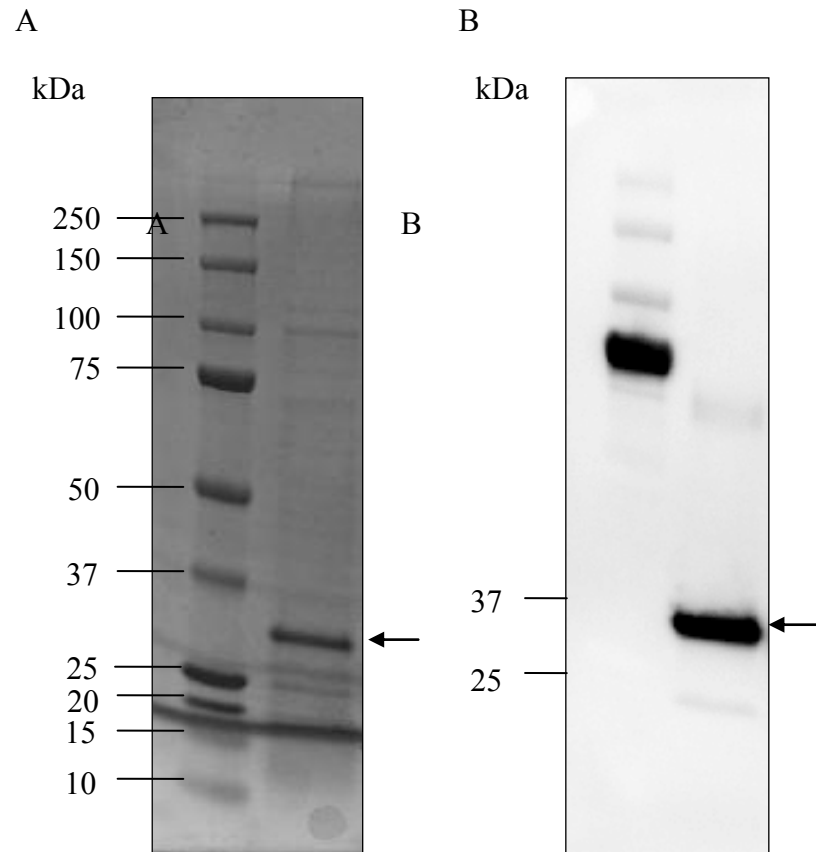


Figure 4.28. Gel analysis of purified soluble STG2. A. Coomassie Blue Staining. B. Western Blot Immunostaining with Anti-Penta HIS Antibody. Arrow denotes STG2.

4.2.18. Soluble STG2 Binds to FcγRIIIa on Platelets

Three different concentrations of soluble STG2 (1μM, 5μM and 10μM) were evaluated by flow cytometry and the binding was observed to be dose dependent (Figure 4.29). The binding capacities of the tested concentrations were > 20% higher than the negative control. The binding capacity of STG2, however, was lower than the parental IV.3 MoAb (500nM=83.02%, Y Geo Mean=75.24, Figure 3.23).

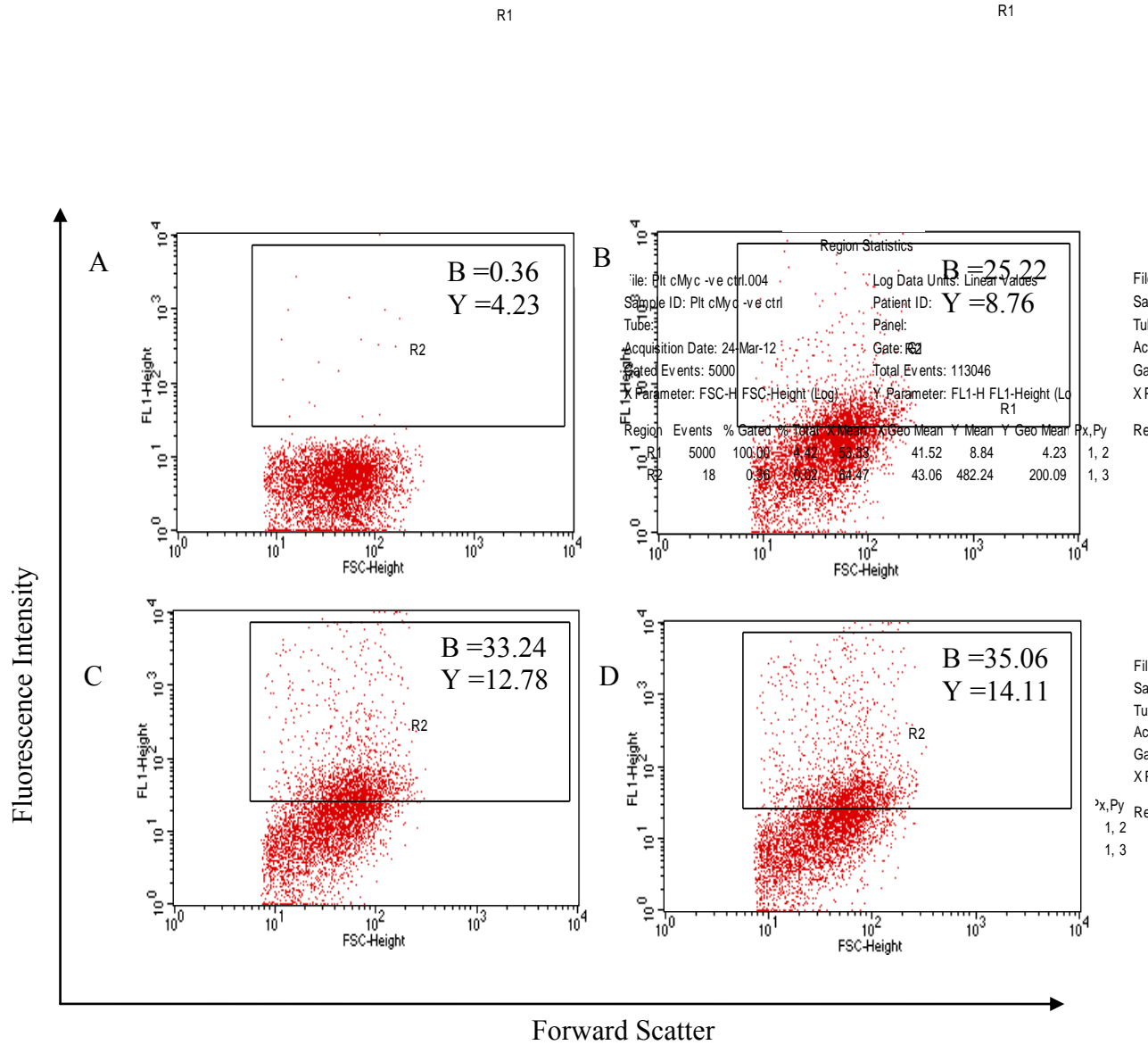


Figure 4.29. Soluble STG2 interacts with human platelets. A. Negative Control-AF 488-conjugated anti-human c-Myc (Binding %=0.36; Y Geo Mean=4.23). B-D. 1μM, 5μM and 10μM of STG2. Abbreviations in figure: B, Binding %; Y, Y Geometric Mean.

4.2.19. Soluble STG2 Inhibits Platelet Aggregation in the presence of HIT IgG and Heparin

The functional ability of STG2 to inhibit HIT IgG-induced platelet aggregation was then evaluated by light transmission aggregometry. As demonstrated in the previous chapter, IV.3 MoAb inhibited platelet aggregation at a concentration of ≥ 10 nM (Figure 3.26). The inhibitory capability of purified STG2 was then tested with various concentrations starting from 100nM and gradually titrated to determine the minimum concentration required to inhibit platelet aggregation. Significantly, STG2 inhibited HIT IgG induced aggregation by 90% or more at a concentration of ≥ 10 nM (Figure 4.30). These results showed that STG2 was able to prevent HIT IgG-induced platelet aggregation at nanomolar concentrations. In addition, the results demonstrate that STG2 retains comparable inhibitory properties as the original antibody, IV.3.

4.2.20. Soluble STG2 Inhibits Serotonin Release in the presence of HIT Serum and Heparin

The efficacy of STG2 to prevent platelet activation in the presence of HIT serum and heparin (0.1IU/ml) was examined using SRA. Though STG2 (2 μ M and 3 μ M) was able to decrease platelet activation substantially (32.23% and 21.48%, respectively) at a heparin concentration of 0.1IU/ml (Figure 4.31), it's above the required 20% mark. This suggests that the tested concentration of STG2 was still not able to fully inhibit the activation of platelets. Nevertheless, this experiment shows that STG2 possesses promising functional properties, but concentrations $>3\mu$ M may be required to inhibit platelet activation and to ensure serotonin release is kept under 20%.

The attempts to purify more STG2 to conduct extra serotonin release assays were only partially successful. The expression of soluble protein was variable and the yields obtained after purification were unsatisfactory (data not shown). It's likely that the humanization process has introduced structural changes that preclude the expression of properly re-folded STG2. We therefore decided to refine the humanized molecule with the purpose of increasing its solubility and functional characteristics.

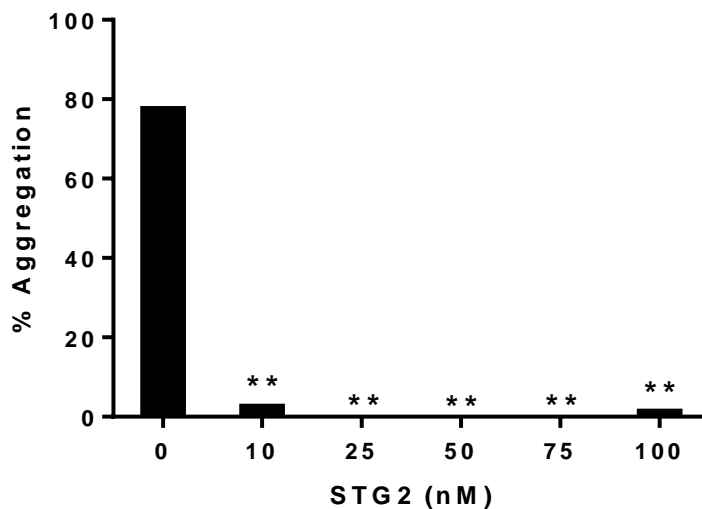


Figure 4.30. STG2 inhibits platelet aggregation induced by HIT IgG and heparin. In the absence of the STG2, the HIT IgG-induced aggregation in human PRP was close to 80%. However, when STG2 was present at a concentration of ≥ 10 nM, more than 90% of platelet aggregation was prevented. Data represent the mean from two independent experiments. $**0.01 > P > 0.001$.

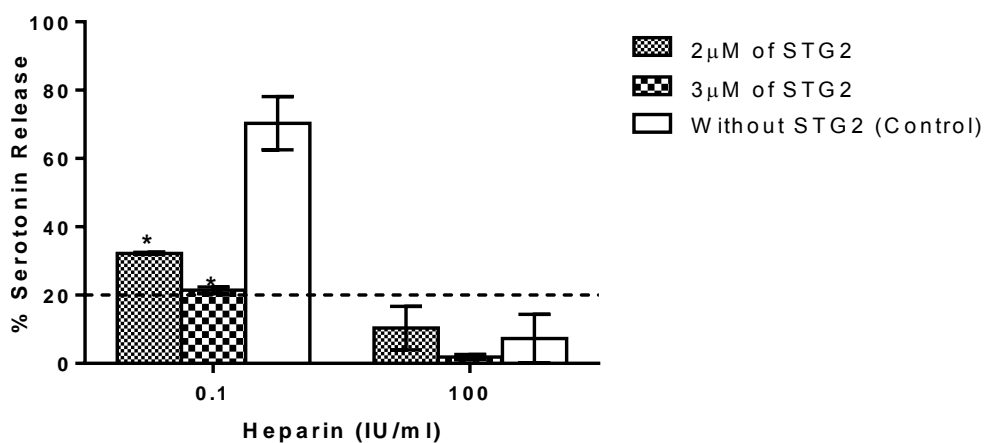


Figure 4.31. Soluble STG2 inhibits platelet activation induced by HIT serum and heparin. Positive results are defined as $>20\%$ serotonin released at 0.1 IU/ml of heparin, compared with $<20\%$ serotonin released at 100 IU/ml of heparin. The added STG2 substantially inhibited the release of serotonin at a heparin concentration of 0.1 IU/ml. Data are mean \pm SEM; $n=4$. $*0.05 > P > 0.01$.

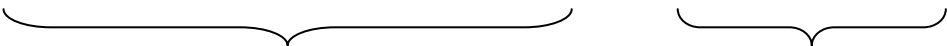
4.2.21. Refinement of the Humanized scFv

For the construction of the second humanized molecule based on STG1, we adopted a strategy that consisted of less amino acid changes in the FRs and, as before, no changes in the CDRs sequences. Moreover, a bacterial secretion signal for periplasmic expression of soluble protein was also included in the construct. The second humanized version of STG1 was termed STG3. In total, only 7 amino acids were replaced (32 amino acids were mutated to generate STG2). For VH, 3 residues were replaced in FR3 reflecting a subgroup of huVH7, while the sequence in FR1, 2 and 4 remained unchanged reflecting a subgroup of huVH1 and 3. For VL, 1 residue was changed in each FR, reflecting a subgroup of huVk2 for all FRs (Figure 4.32). The comparison of STG3 with the human germline database available on <http://www.ncbi.nlm.nih.gov/igblast/> reveals a 70.4% sequence similarity to human germline VH domain IGHV7-4-1*02 and a 77% sequence similarity to human germline VL domain IGKV2-18*01 based on IMGT database (312) (Refer to Appendix, Figure A3.3 for sequence alignment). A sequence alignment between STG1 and STG3 shows 97% and 95% sequence identity for both VH and VL domains respectively.

4.2.22. Construction of STG3

The sequence encoding the humanized VH and VL domain, fused with a short linker Gly₁₂-Ser₃ was chemically synthesized by Genscript (New Jersey,US) with codon optimization for increased protein expression in bacteria (Figure 4.33). The construct includes a secretion signal at the N-terminus; cMyc and HIS₆-tags at the C-terminus for detection and purification purposes. The construct with a size of 876bp was placed in pET11a vector for bacterial expression.

A. VH

Mouse: EVKLVESGPELKKPGETVKISCKASGYTFTNYGMNWVKQAPGKGLKWMGWL
 Human: EVKLVESGPELKKPGETVKISCKASGYTFTNYGMNWVKQAPGKGLKWMGWL

 Human VH Group 1 Human VH Group 1
 Mouse: NTYTGESIYPDDFKGRFAFSSETSASTAYLQINNPKNEDMATYFCARGDYG
 Human: NTYTGESIYPDDFKGRFAFS**L**ETSASTAYLQINNPK**S**ED**T**ATYFCARGDYG

 Human VH Group 7
 Mouse: YDDPLDYWGQGTSVTVSS
 Human: YDDPLDYWGQGTSVTVSS

 Human VH Group 3

B. VL

Mouse: DIVMTQAAPSVPVTPGESVSISCRSSKSLLHTNGNTYLHWFLQRPQSPQL
 Human: DIVMTQA**P**PSVPVTPGESVSISCRSSKSLLHTNGNTYLHWFLQRPQSP**R**L

 Human *Vk* Group 2 Human *Vk* Group 2
 Mouse: LIYRMSVLASGVPDRFSGSGSFTAFTLSISRVEAEDVGVFYCMQHLEYPLT
 Human: LIYRMSVLASGVPDRFSGSGSFTAFTLSISRVEAEDVGV**Y**CMQHLEYPLT

 Human *Vk* Group 2
 Mouse: FGAGTKLELKRA
 Human: FGAGTKLE**I**KRA

 Human *Vk* Group 2

Figure 4.32. Amino acid sequence alignment between the variable regions of STG1 and STG3. (A) VH and (B) VL. CDR residues are underlined. Letters in bold indicate amino acid changes that were made in the FRs. The original STG1 belongs to subgroups muVH9 and muVk2 (VH9Vk2). The humanized sequence in the FR is categorized as huVH subgroups of 1, 7 and 3, while the huVL falls under subgroup 2 (VH173Vk2). In total, 7 amino acids were changed.

VH chain sequence

```

          9           18           27           36           45           54           63
GAA GTG AAA CTG GTG GAA AGT GGC CCG GAA CTG AAA AAA CCG GGT GAA ACC GTT AAA ATT AGT
E   V   K   L   V   E   S   G   P   E   L   K   K   P   G   E   T   V   K   I   S

          72           81           90           99           108           117           126
TGC AAA GCA TCC GGT TAT ACC TTT ACG AAC TAC GGC ATG AAT TGG GTC AAA CAG GCT CCG GGC
C   K   A   S   G   Y   T   F   T   N   Y   G   M   N   W   V   K   Q   A   P   G
                                CDR-H1

          135          144          153          162          171          180          189
AAA GGT CTG AAA TGG ATG GGT TGG CTG AAC ACC TAT TAC ACG GGC GAA TCC ATT TAC CCG GAT GAC
K   G   L   K   W   M   G   W   L   N   T   Y   T   G   E   S   I   Y   P   D   D
                                CDR-H2

          198          207          216          225          234          243          252
TTT AAA GGC CGT TTT GCA TTC TCA CTG GAA ACC TCA GCG TCG ACG GCC TAT CTG CAA ATC AAC
F   K   G   R   F   A   F   S   L   E   T   S   A   S   T   A   Y   L   Q   I   N

          261          270          279          288          297          306          315
AAT CTG AAA TCT GAA GAT ACC GCA ACG TAC TTC TGC GCT CGC GGT GAT TAT GGC TAC GAT GAC
N   L   K   S   E   D   T   A   T   Y   F   C   A   R   G   D   Y   G   Y   D   D
                                CDR-H3

          324          333          342          351          360
CCG CTG GAC TAT TGG GGC CAG GGT ACC AGT GTG ACG GTT AGC TCT
P   L   D   Y   W   G   Q   G   T   S   V   T   V   S   S

```

VL chain sequence

```

          9           18           27           36           45           54           63
GAT ATT GTC ATG ACC CAA GCG CCG CCG TCG GTC CCG GTG ACC CCG GGT GAA AGC GTG TCT ATC
D   I   V   M   T   Q   A   P   P   S   V   P   V   T   P   G   E   S   V   S   I

          72           81           90           99           108           117           126
AGT TGT CGT AGT TCC AAA TCA CTG CTG CAT ACC AAC GGT AAT ACG TAT CTG CAC TGG TTT CTG
S   C   R   S   S   K   S   L   L   H   T   N   G   N   T   Y   L   H   W   F   L
                                CDR-L1

          135          144          153          162          171          180          189
CAG CGT CCG GGT CAA AGC CCG CGT CTG CTG ATT TAC CGC ATG TCA GTG CTG GCG TCG GGT GTT
Q   R   P   G   Q   S   P   R   L   L   I   Y   R   M   S   V   L   A   S   G   V
                                CDR-L2

          198          207          216          225          234          243          252
CCG GAT CGT TTT TCC GGC TCA GGT TCG GGT ACC GCA TTC ACG CTG AGC ATC TCT CGC GTG GAA
P   D   R   F   S   G   S   G   S   G   T   A   F   T   L   S   I   S   R   V   E

          261          270          279          288          297          306          315
GCC GAA GAC GTT GGC GTC TAT TAC TGT ATG CAG CAT CTG GAA TAT CCG CTG ACC TTC GGT GCC
A   E   D   V   G   V   Y   Y   C   M   Q   H   L   E   Y   P   L   T   F   G   A
                                CDR-L3

          324          333          342
GGC ACG AAA CTG GAA ATT AAA CGC GCT
G   T   K   L   E   I   K   R   A

```

Figure 4.33. Nucleotide and deduced amino acid sequences of VH and VL regions of STG3. CDR sequences are underlined.

4.2.23. Molecular Modelling of STG3

The VH region of STG3 was modeled against X-ray structures of a Fab fragment with steroid-binding affinity [PDB entry 2o5x; 81.82% sequence identity; 2.05 Å resolution (322)]. The VL region of STG3 was modeled against the structure of estrolytic murine Ab Fab fragment MS6-12 [PDB entry 1mju; 92.11% sequence identity; 1.22 Å resolution (273)]. Both regions of STG3 were then superimposed with STG1 as previously generated (Figure 3.15) to compare the structural homology of both scFvs. Overall, the generated model of STG3 was well superposed with STG1, except for the VH-CDR-H3 that showed a slight deviation (Figure 4.34). Nevertheless, this should not deter CDR-H3 from interacting with the antigen as its surface structure is well presented, furthermore, the general structure of STG3 showed a higher degree of similarity to STG1 when compared to the previously generated STG2.

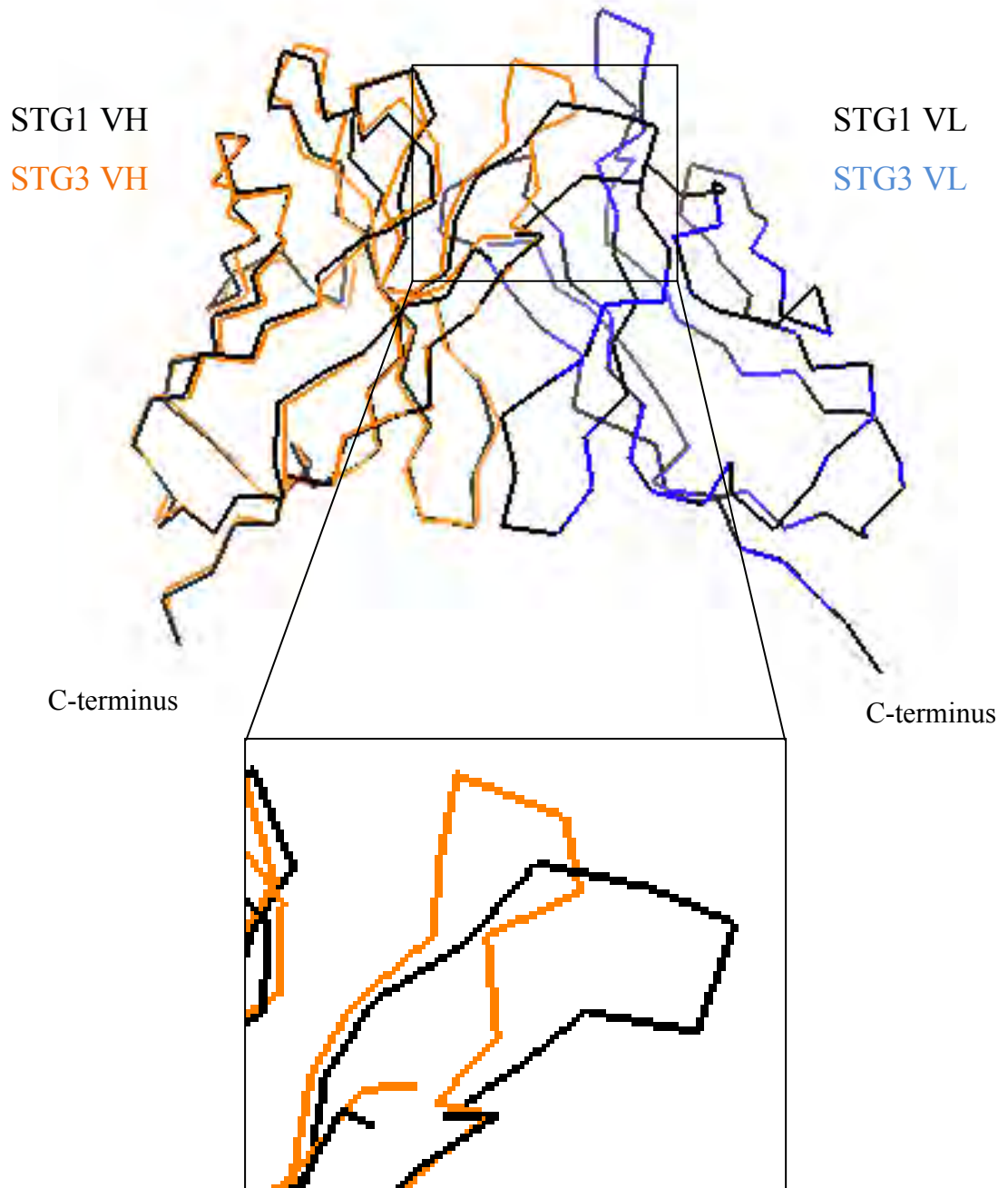


Figure 4.34. Superimposed diagram of STG1 and STG3 in lateral view. STG1 (black) and STG3 (orange for VH and blue for VL) were displayed as a ribbon model. The structure of VH-CDR-H3 of STG3 and STG1 was magnified (Inset). The linker connecting the VH and VL domain is not shown.

4.2.24. Expression of STG3

STG3 was expressed as previously described (Section 4.2.4). A thick band of approximately 30kDa corresponding to the expected molecular weight of STG3 (31.57kDa), was observed after induction with IPTG (Figure 4.36).

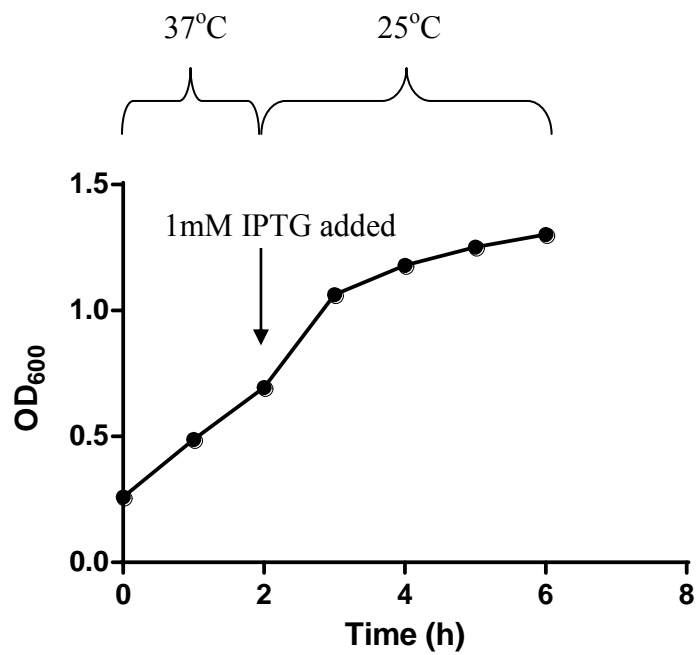


Figure 4.35. Bacterial growth pattern of *E. coli* BL21(DE3) expressing STG3.

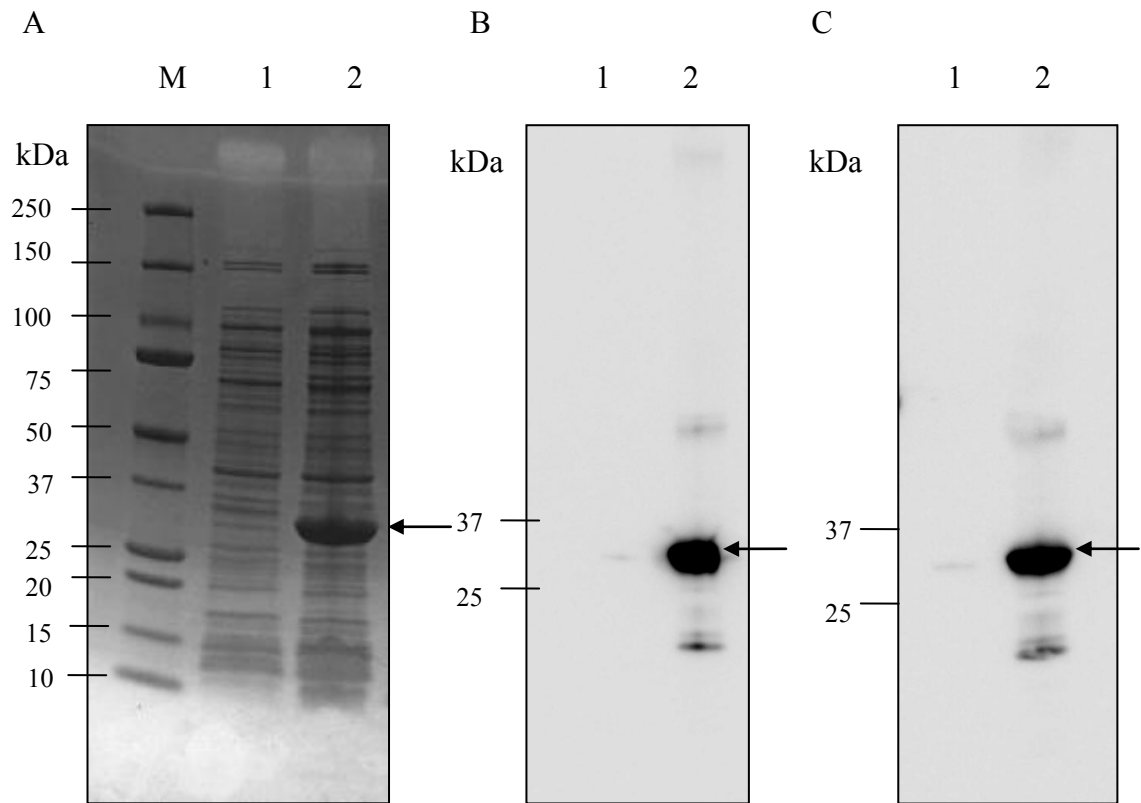


Figure 4.36. Gel analysis of pET11a-STG3 expressed in *E. coli* BL21 (DE3). A. Coomassie Blue Staining and Western Blot (Immunostaining with B. Anti-cMyc antibody and C. Anti-Penta-HIS antibody). Lane M: Molecular weight marker (Bio-Rad). Lane 1: Total protein of STG2 before induction; Lane 2: Total protein of STG3 after induction. Arrow denotes STG3.

4.2.25. Purification of STG3

The soluble fraction of STG3 was purified after the bacterial pellet was treated with an osmotic shock procedure that gently disrupts the outer membrane of *E. coli*, releasing proteins from the periplasmic space. This fraction was then collected and purified via Nickel-chelating resin. As shown in Figure 4.37, two major peaks were observed during the elution phase, both eluted fractions were pooled and examined on SDS-PAGE. The 1st peak contained an irrelevant protein (data not shown) while the 2nd peak consisted of a partially purified STG3 as confirmed by Western blotting (Figure 4.38).

Approximately 250µg of partially purified STG3 was obtained from 1 L of bacterial culture.

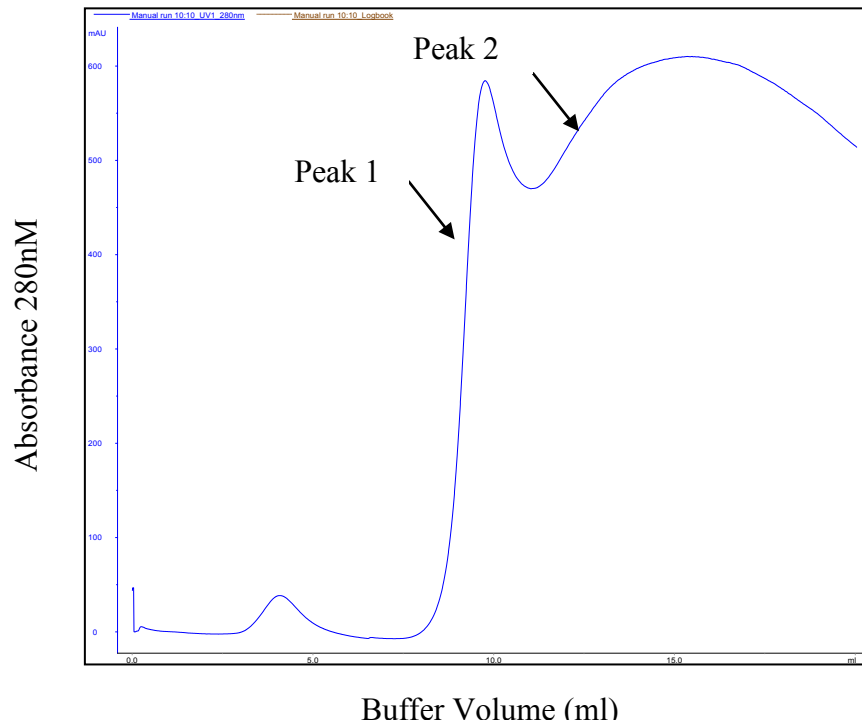


Figure 4.37. Elution profile of soluble STG3. The protein was eluted at around 150mM imidazole.

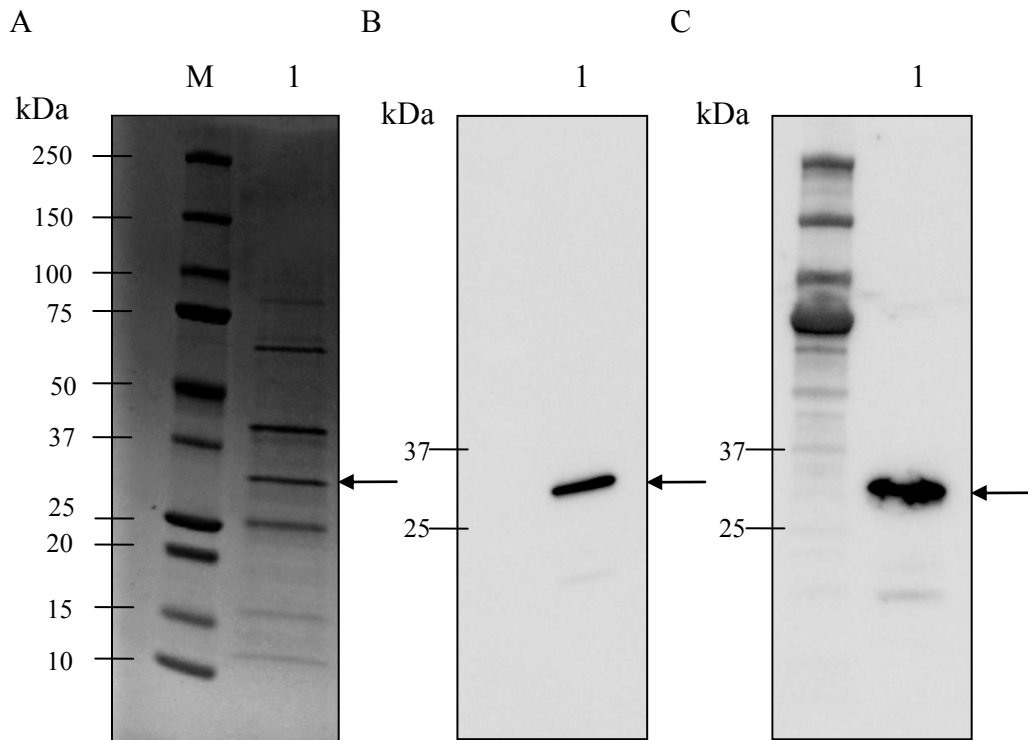


Figure 4.38. Gel analysis of purified soluble STG3. A. Coomassie Blue Staining and Western Blot (Immunostaining with B. Anti-cMyc antibody and C. Anti-Penta-HIS antibody). Lane M: Molecular weight marker (Bio-Rad). Lane 1: Purified STG3 from periplasmic fraction. Arrow denotes STG3.

4.2.26. Soluble STG3 Binds to FcγRIIa on Platelets

The purified soluble form of STG3 was tested for its binding capacity to human platelets. This was conducted by fluorescence immunostaining and the fluorescence intensity was recorded by flow cytometry. A concentration of 1 μM of STG3 was tested and an increased in fluorescence intensity was observed in comparison to the negative control-AF488-conjugated anti-c-Myc antibody (Figure 4.39).

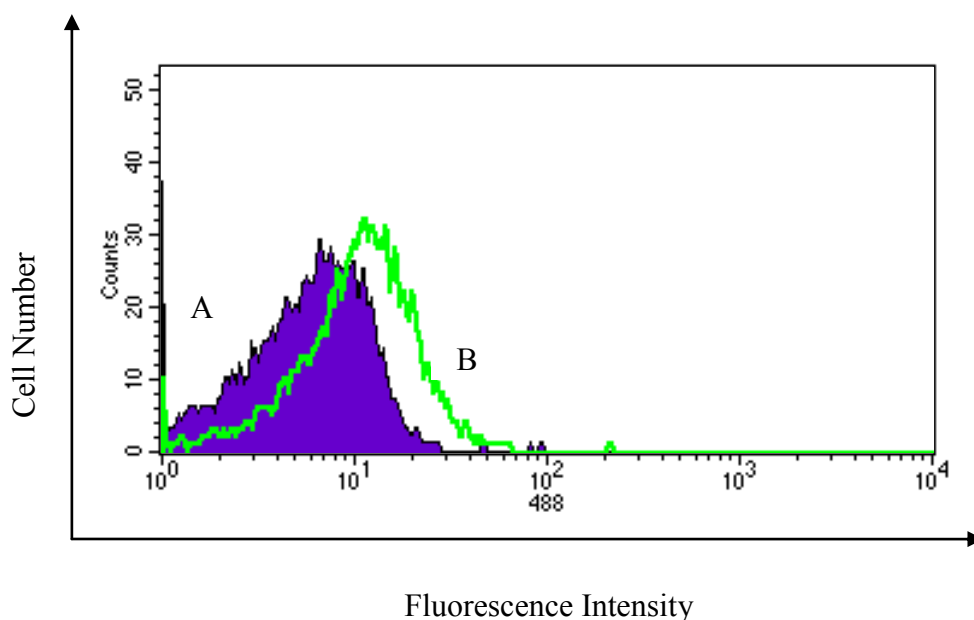


Figure 4.39. Soluble STG3 interacts with human platelets. A. Negative Control- AF 488-conjugated anti-human c-Myc (solid histogram). B. 1 μM of STG3 (open histogram).

4.2.27. Soluble STG3 Inhibits Platelet Aggregation in the presence of HIT IgG and Heparin

The functional capacity of this humanized antibody fragment was evaluated by light transmission aggregometry. This is to demonstrate its function in inhibiting platelet aggregation induced by HIT IgG and heparin (0.5IU/ml). The purified STG3 was tested at various concentrations starting from 100nM and gradually titrated until the minimum concentration needed to inhibit platelet aggregation was obtained. STG3 was observed to inhibit HIT IgG-induced platelet aggregation by 90% or more at a concentration of \geq 70nM (Figure 4.40).

4.2.28. Soluble STG3 Inhibits Platelet Activation in the presence of HIT Serum and Heparin

The functional property of STG3 was further evaluated with SRA. $>20\%$ of serotonin released was initially observed at a concentration of 1 μ M of STG3, nevertheless, the following two concentrations of STG3 (2 and 3 μ M) successfully decreased the activation of platelets with serotonin release levels of less than 20% (17.4% and 12.75%, respectively) at a heparin concentration of 0.1IU/ml, and serotonin release levels of less than 20% observed for heparin concentration of 100IU/ml (Figure 4.41). This shows that the STG3 is fully functional in inhibiting platelet activation.

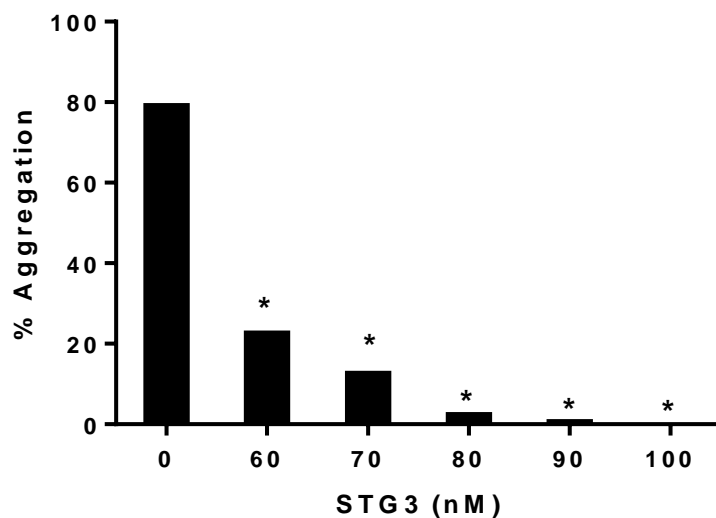


Figure 4.40. STG3 inhibits platelet aggregation induced by HIT IgG. In the absence of the STG3, the HIT IgG-induced aggregation in human PRP was close to 80%. However, when STG3 was present at a concentration of ≥ 70 nM, HIT IgG-induced platelet aggregation was inhibited by $\sim 90\%$ or more. Data represent the mean from two independent experiments. $*0.05 > P > 0.01$.

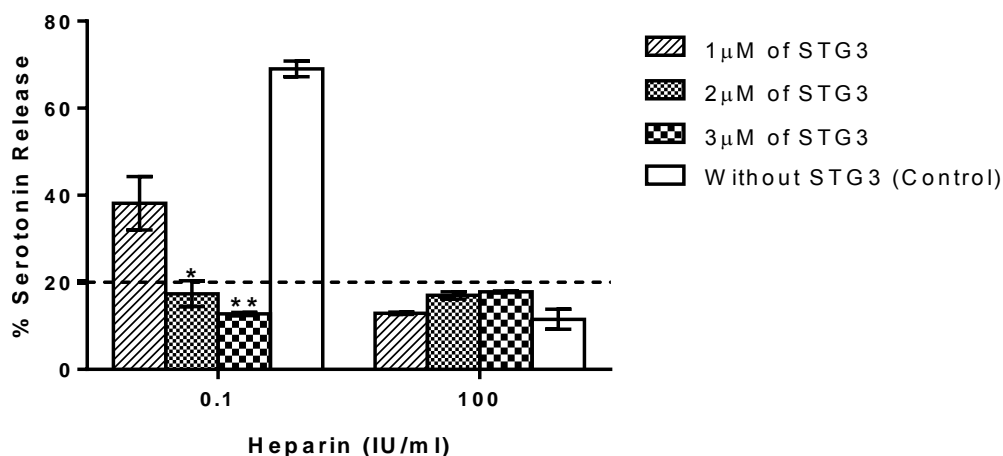


Figure 4.41. Soluble STG3 inhibits platelet activation induced by HIT Serum and heparin. Positive results are defined as $>20\%$ serotonin released at 0.1 IU/ml of heparin, compared with $<20\%$ serotonin released at 100 IU/ml of heparin. The added STG3 at $\geq 2 \mu$ M inhibits the release of serotonin at a heparin concentration of 0.1 IU/ml. Data are mean \pm SEM; $n=4$. $*0.05 > P > 0.01$. $**0.01 > P > 0.001$.

4.2.29. Establishing HIT Animal Model in NOD/SCID Mice

4.2.29.1. Calculation of the Number of Circulating Human Platelets using CountBright™ Absolute Counting Beads

We sought to generate a HIT animal model using immune-deficient NOD/SCID mice. The initial step was to establish circulation of human platelets into the animals. To this end, we adopted the approach described by Boylan et al (215). Here, approximately 200µl of concentrated human platelet-rich plasma (2×10^9 platelets/ml) was introduced into the circulation of the mice via tail vein injection. The level of human platelets circulating in the system is gated (Figure 4.42) and calculated with reference to the counting beads and the formula provided (Figure 4.43). The total numbers of platelets are later normalized to be presented in percentage.

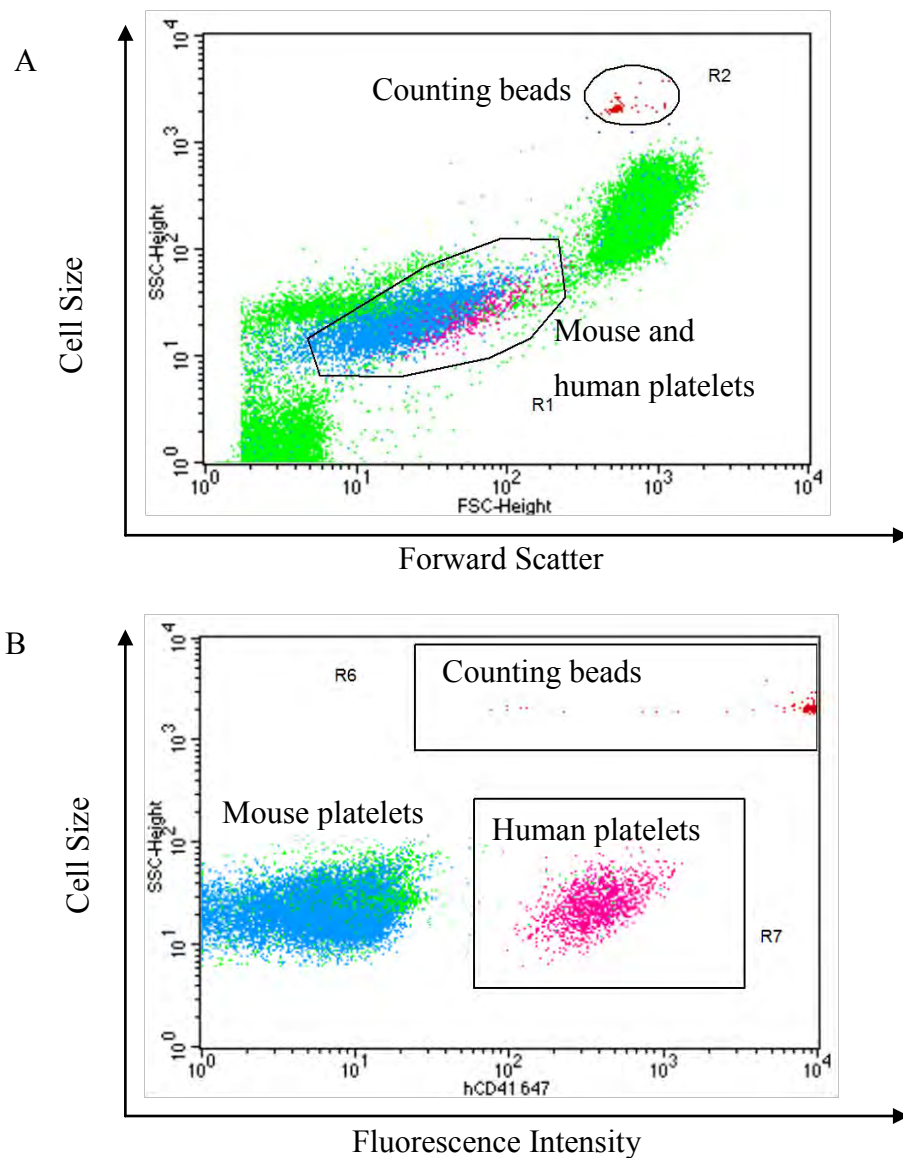


Figure 4.42. Determination of circulating human platelet numbers using counting beads. Blood collected from mice injected with human platelets was stained with PE Rat anti-mouse CD41 and AF647-conjugated anti-human CD41. A. A logarithmic side scatter versus logarithmic forward scatter plot was used to gate the region of the counting beads and platelets. The beads are distinguished from the platelets due to their distinct light scattering properties. B. A plot of logarithmic side scatter versus human CD41-positive cells clearly distinguished human platelets from other cells.

A

Calculation of cell concentration:

$$\frac{A}{B} \times \frac{B}{D} = \text{concentration of sample as cell}/\mu\text{L}$$

Where:

A = number of cell events

B = number of bead events

C = assigned bead count of the lot (beads/50μL)

D = volume of sample (μL)

B

Example of calculation of the concentration of human platelets:

2μL of mouse whole blood was added into a final volume of 250μL
(Dilution Factor of 1:125)

Events collected for human platelets = 6565

Events collected for counting beads = 1006

$$\frac{6442}{1006} \times \frac{51,000}{250} = 1306$$

1306 human platelets x 125 Dilution Factor = 163250 of human
platelets/μL

Figure 4.43. Calculation of the concentration of human platelets circulating in mice using counting beads. A. Formula provided by the CountBright™ Absolute Counting Beads manufacturer (Invitrogen). B. Sample calculation of human platelet numbers in mouse circulation.

4.2.29.2. *Human Platelets Injected into NOD/SCID Mice are Detected in the Circulation*

Prior to establishing a HIT animal model using NOD/SCID mice, a platelet survival study was conducted. This is to ensure that the circulating human platelets can be detected in the mouse model system. The mouse blood was collected at designated time intervals and the circulating level of human platelets was analyzed as described in the previous section. As shown in Figure 4.44, the platelet survival rate was over 60%, 4 h after human PRP was injected, and gradually decreased to a level of approximately 30% after 24 h. This most likely corresponds to the kinetic profile of normal clearance due to platelet aging (215).

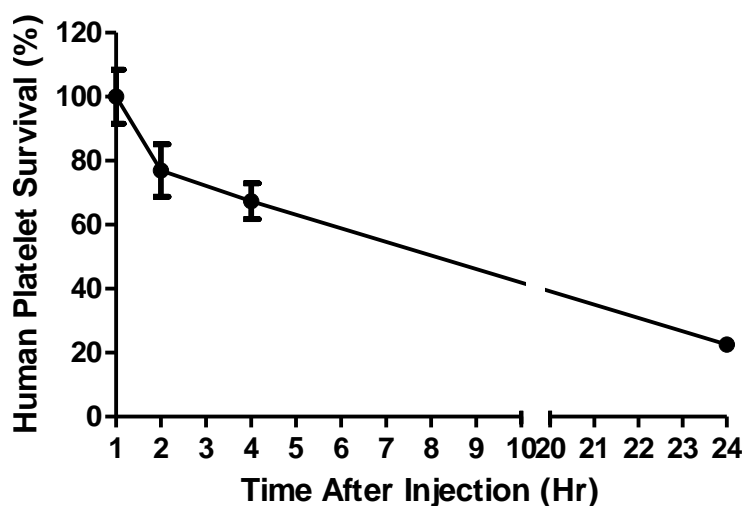


Figure 4.44. Human platelets detected in NOD/SCID mice over a period of 24 h. Human platelet numbers were determined by flow cytometry using CountBright™ Absolute Counting Beads. 4 h after human PRP was injected, more than 60% of the injected human platelets were observed to be circulating in the system. The levels of human platelets decreased gradually over the next 24 h. Each data point represent the mean \pm SEM; n=4.

4.2.29.3. The NOD/SCID Animal Model Did Not Recapitulate the Features of HIT

To establish the HIT animal model, two groups of mice were injected with two concentrations of HIT IgG. Normal human IgG was used in the control group. The concentration of the HIT IgG needed to induce platelet aggregation was first determined in *in vitro* platelet aggregation assays (Refer to Appendix, Figure A2.6). IgG was injected via intraperitoneal route on Day 0 (107). On Day 1, PF4 and human PRP were introduced simultaneously via the tail vein. The amount of injected PF4 was based on the circulating level of human PF4 in transgenic mice reported to induce thrombocytopenia (67). The heparin concentration was determined in reference to the human therapeutic dose range (600IU/kg) (67). After injection, blood was collected at four different time points. As shown in Figure 4.45A, the animals pre-treated with HIT IgG and PF4 did not exhibit a drastic drop in the percentage of human platelets after receiving heparin at the 1st hour (a fast drop in human platelet numbers was expected after heparin administration). In addition, the circulating level of the human platelets was somewhat higher (but not statistically significant with $P>0.05$) in the HIT experimental group compared to the control group over the period of 24 h.

The protocol described above consisted of tail vein injection of human platelets followed by tail vein administration of heparin. We found that this procedure caused agitation in the animals, thus making heparin injection via this route impractical. For this reason, the protocol was modified as follows: Day 0, intraperitoneal injection of IgG (HIT or normal) and PF4; Day 1, injection of human PRP via tail vein followed by subcutaneous administration of heparin. Analysis of human platelet survival rates in the HIT animal model showed no significant drop of human platelets over 24 h post heparin treatment (Figure 4.45B). All time points were not significant ($P>0.05$) except for 2nd hour, however, this does not change the conclusion of this experiment.

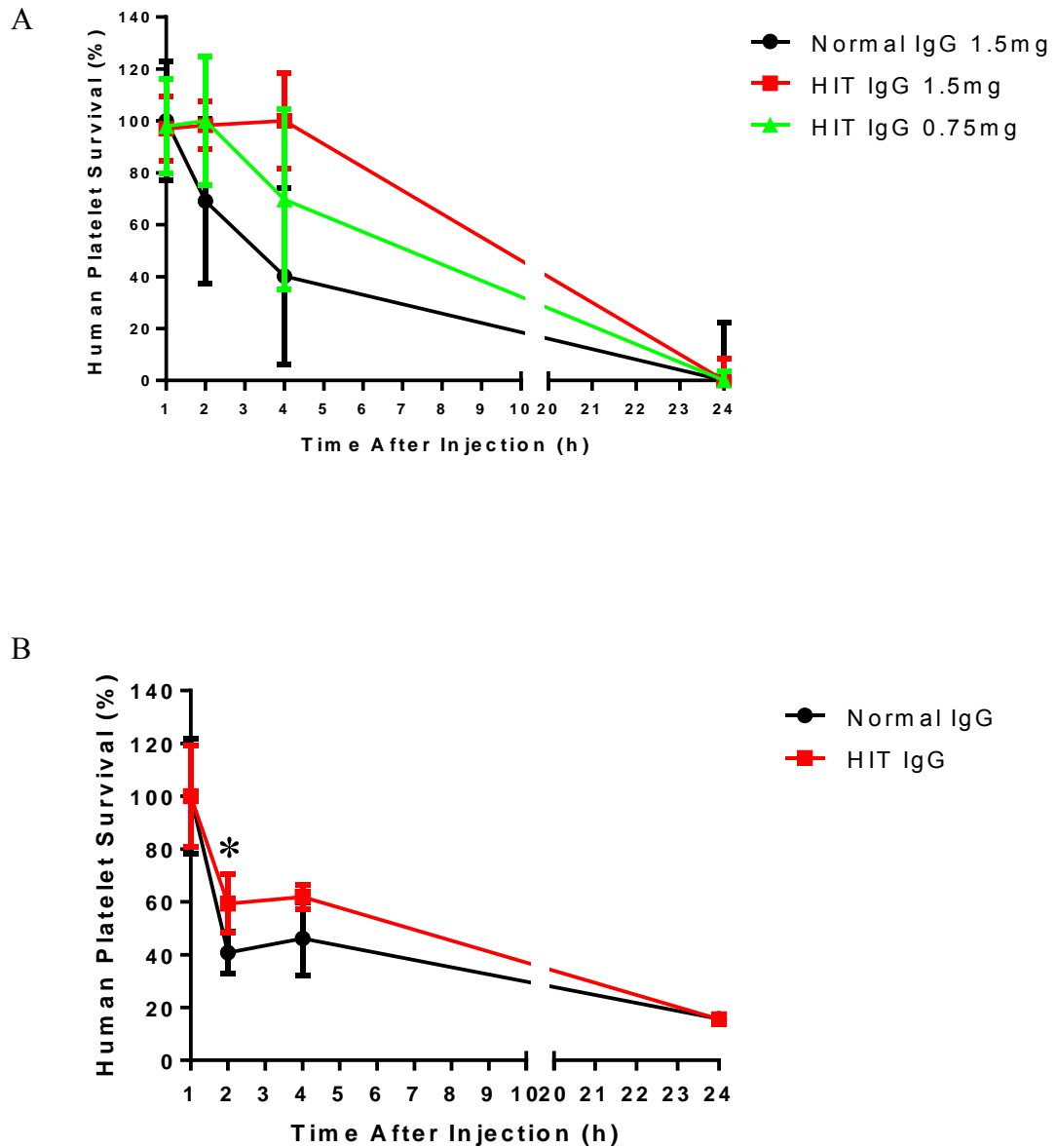


Figure 4.45. Survival of human platelets in NOD/SCID mice after introduction of HIT IgG, PF4 and Heparin. A. Human platelet survival rate in the experimental HIT animal model following exposure to heparin did not decrease over a period of 24 h relative to the control. $P > 0.05$. B. Modification of the protocol did not affect the platelet survival profile. $P > 0.05$. $0.05 > P > 0.01$. Each data point represent the mean \pm SEM; $n=4$.

4.3. Discussion

The work presented in Chapter 3 clearly demonstrates the capacity of STG1 to prevent the events of HIT *in vitro*. The recombinant protein binds to FcγRIIIa on platelets and inhibits platelet aggregation and activation in the presence of HIT IgG. STG1 therefore possesses potential therapeutic properties that could be of benefit in the treatment of HIT. However, since it is well known that murine antibodies are highly immunogenic when administered to humans, it is essential that the molecule be modified by humanization to facilitate human therapeutic applications (323). This chapter therefore aimed to adopt the humanization approach to improve the usefulness of STG1. We proposed that the binding and functional capacity of the modified antibody would be retained even after humanization.

CDR-grafting represents one of the conventional methods for humanization of murine antibodies. It involves the transfer of the antigen binding loops from the murine antibodies with desired antigen specificity to the scaffolds of corresponding human variable region FRs (185). However, simple CDR-grafting often decreases the affinity of the donor antibody because some FRs are in direct contact with the antigen or support the conformation of the CDR-loops. This led to the development of other humanization methodologies (Mentioned in section 4.1.1). To humanize the STG1, both CDR-grafting and point mutation approaches were adopted. While the CDRs from the parental murine antibody were preserved, a total of 32 residues in the framework of STG1 were mutated to increase similarity to the human framework. This was conducted based on the large database of human germline variable gene sequence available through the website (<http://www.bioc.uzh.ch/antibody/>).

The humanized molecule (STG2) was produced in bacteria by the pET11a expression vector, which uses the bacteriophage T7 RNA polymerase and T7 promoter to initiate protein transcription (169). The production host *E. coli* BL21(DE3) carries an IPTG-inducible *lacUV5* promoter (324), leading to the synthesis of large amount of mRNA, thus, high-yield of the desired protein. Unlike STG1, a leader sequence was not included in STG2 to favour accumulation of considerable amounts of the target protein as misfolded non-disulfide-linked cytoplasmic inclusion bodies. The production of inclusion bodies is advantageous as these aggregated proteins are protected from proteolytic degradation and are present at higher degrees of purity (249, 325). As shown

in this Chapter, substantial amounts of STG2-containing inclusion bodies were easily obtained with at least 50-60% purity (Figure 4.11A, Lane 3).

The inclusion bodies of STG2 were first denatured with 8M urea to form a monomolecular dispersion (301). This occurs because of increase in solubility of polar molecules via hydrogen bonding (326). Prior to refolding, the solubilized scFv denatured with 8M urea was purified since these solubilized inclusion bodies contain impurities that may associate with the expressed protein and interfere with its refolding (301). In addition, it has been reported that higher refolding yields can be obtained with purified solubilized inclusion bodies (327, 328). The histidine-tag fused to the C-terminal end of STG2 allows the protein to be purified in the denatured state on a Nickel-Chelating Resin. While immobilized IMAC is generally considered to be highly efficient as a single-step purification method (329), other contaminants were also observed in the purified sample of STG2. Nevertheless, the purified sample comprised approximately 80% of the target protein (Figure 4.13, Lane 3).

One-step refolding method was utilized to refold the recombinant STG2, however, the protein did not exhibit inhibitory properties on platelet aggregation assays, suggesting that it was either not properly folded or that the humanization process had rendered the scFv inactive. It is more likely, however, that the lack of activity was due to ineffective refolding of the protein. This might be due to protein collapse and formation of a compact structure caused by the drastic change from high denaturant concentration (8M urea) to 1M urea and then to aqueous buffer. Once these proteins collapse, they may misfold or aggregate and have no flexibility to refold into the native structure in the absence of denaturants (301).

Subsequently, a stepwise-dialysis approach was adopted based on the protocol described by Umetsu and coworkers to refold scFvs from inclusion bodies expressed in *E. coli* (208). STG2 inclusion bodies denatured with 8M urea were refolded by low reduction of the denaturant's concentration. The gradual alteration in the concentration of denaturant allows the unfolded protein sample to establish equilibrium at each stage. The protein molecules are therefore able to reorganize their structures, yet still allow proper folding to take place with correct disulfide bond formation (301).

Disulfide exchange and suppression of protein aggregation were promoted by addition of 0.5M GSSG and 0.5M L-Arginine at the final refolding stages (321). The oxidizing reagent GSSG aims to oxidize free thiol groups to control the refolding of the scFv while L-Arginine effectively stabilizes the exposed hydrophobic areas on the scFv (208). Thus, throughout the stepwise dialysis procedure, no aggregate formation was observed.

Step-wise refolding was partially successful. The refolded STG2 inhibited platelet aggregation in the presence of HIT serum in the μM range ($30\mu\text{M}$). This compares unfavourably with the nM concentrations required for the IV.3 MoAb. In addition, the recombinant antibody fragment did not exhibit antigen binding properties as shown by flow analysis. The high concentrations required to inhibit platelet aggregation and the undetectable binding by flow cytometry indicate that the majority of the scFv was not successfully refolded.

While the expression of the target protein in *E. coli* was satisfactory, the attempts to refold the denatured STG2 were met with little success. In addition, the refolding techniques employed so far are labour and time intensive, involving the use of large volumes of buffers and generation of chemical waste. In recent years, a chromatographic refolding approach has been used successfully (209, 306). The denatured protein can be reversibly adsorbed onto a matrix, this is followed by subsequent dilution of the concentration of the denaturant to promote on-column refolding. For the histidine-tag-containing STG2, the refolding was conducted using IMAC since this allows efficient simultaneous purification and refolding (306, 307).

For the formation of disulfide bonds in the protein, the thiol reagent glutathione in oxidized (GSSG) and reduced form (GSH) was included in the refolding buffer as the refolding yields are strongly dependent on the redox environment (297, 330). The methodology yielded purified STG2 (Figure 4.19, Lane 5) that demonstrated antigen binding properties as determined by flow cytometry analysis. This suggests that for STG2 a slow and gradual removal of urea in on-column refolding is more efficient than the dialysis approach, resulting in higher recovery yields and properly refolded protein.

Despite the advantages of on-column refolding and the initial success of this methodology when applied to STG2, further evaluation indicated that STG2 could not be consistently refolded and purified using this technique. Assessment of a number of parameters (including preparation of fresh transformants since plasmid instability may occur in the glycerol stock of transformed *E. coli* (331), use of fresh buffers and columns) did not lead to improvements in the preparation of sufficient amounts of active STG2. The variation of the refolding outcome from different purification attempts could well suggest that inappropriate disulfide-linkage formation within the molecule may still occur during the refolding process. Therefore, we conjectured that the nature of the protein might play a more important role than the refolding conditions, affecting its tendency to renature into an active conformation.

A new technique was adopted to solubilize the inclusion bodies followed by purification using the SMALPs. The solubilization was first conducted in the harsh and mild detergent micelles-SDS and β -OG that presents a largely hydrophobic environment (332). STG2 was then integrated in SMALPs by adding SMA which is an amphipathic polymer in the presence of synthetic phospholipid-DMPC (211). The resulting nanoparticles were purified by Nickel-Chelating Resin. Examination of the purified nanoparticles showed that STG2 was effectively incorporated into the polymer and was able to recognize the Fc γ RIIa on human platelets. This properly folded scFv, however, proved inadequate in functional assays. The presence of STG2 nanoparticles led to spontaneous platelet aggregation both in the presence and absence of HIT serum. This may be due to the formation of nanoparticles that include several STG2 molecules in a single disc. The binding of each nanoparticle could, therefore, engage simultaneously with several Fc γ RIIa receptors, leading to cross-linking of the receptors thus causing platelet activation and aggregation. It is well known that cross-linking of Fc γ RIIa causes platelet aggregation (333). Cross-linking of Fc γ RIIa was previously illustrated by incubation of platelets with IV.3 MoAb followed by the addition of antimouse IgG (Fab')₂ (334). Moreover, nanoparticles containing multiple STG2 molecules could also link Fc γ RIIa from different platelets, also favouring platelet aggregation.

Since the attempts to refold STG2 from inclusion bodies using several refolding approaches did not yield sufficient active protein, we therefore focused on purifying the soluble fraction of the antibody fragment from the cytoplasmic compartment of the *E.coli*. It has been reported that some scFvs are able to retain the correct conformation in the reducing environment of the cytoplasmic compartment (335, 336). The results of the flow cytometry analysis showed that the purified soluble STG2 was in its native conformation and was able to recognize FcγRIIIa on platelets. Importantly, the recombinant protein also exhibited functional properties by inhibiting platelet aggregation in the presence of HIT IgG and heparin (0.5IU/ml) with a concentration as low as 10nM. This is comparable to the concentration of the original IV.3 antibody needed to inhibit HIT IgG-induced platelet aggregation (Figure 3.26). This finding demonstrates that the activity of STG2 was well preserved and the humanization changes did not affect significantly the structural conformation of the molecule, allowing it to execute a potent inhibitory function against HIT antibodies. Thus, STG2 is able to prevent platelet aggregation by blocking the FcγRIIIa on platelets and interfering with the binding of the HIT immune complexes.

Despite the strong activity of STG2 in platelet aggregation assays, it could not prevent platelet activation effectively in serotonin release assay. The serotonin release reduction, though statistically significant, was still over 20% at a STG2 concentration of $\geq 2\mu\text{M}$. Moreover, further STG2 expression attempts resulted in insufficient amounts of soluble protein, which precluded the performance of further experiments.

With the aim of improving the production of soluble STG2, a second humanized version of STG1 (termed STG3) was therefore designed. This more refined scFv construct included a minimal number of amino acid changes in the FRs and was devised with a PelB bacterial secretion signal at the N-terminus for secretion of native STG3 into the periplasmic space. The improvements introduced to STG3 allowed successful purification of soluble protein from the bacterial pellet. Moreover, the antibody fragment was in an active conformation and demonstrated both binding and functional properties, at efficacies comparable to the IV.3 MoAb. Thus, STG3 was able to execute its functions at nM concentration in platelet aggregation assays and at μM concentrations in SRA, successfully preventing platelet aggregation and activation in the presence of HIT IgG and Heparin.

Recently, our laboratory showed that the condition known as quinine-induced thrombocytopenia can be recapitulated in NOD/SCID mice (337). We sought to establish a similar HIT animal model using NOD/SCID mice. The platelets were introduced into the circulation based on the mouse model established by Boylan et al (215). The human platelets were clearly detected one hour after administration into the system with the level of circulating platelets decreasing by about 50% after 24 h. To create the events of HIT *in vivo*, several additional components were introduced into the system: IgG (HIT or normal control), human PF4 and heparin. However, as shown in Figure 4.45, no reduction in the number of circulating human platelets was observed in the presence of HIT IgG and heparin. This suggests that the introduced components may have not reached the critical concentrations to recapitulate HIT in these animals. It is likely that the low percentage of circulating human platelets (about 12% of total platelets) and/or insufficient human PF4 in plasma did not favour the formation of HIT immune complexes. Future evaluation of STG3 will be done using the double transgenic mice generated by our collaborators, Dr. Steven McKenzie, Philadelphia, USA (108).

In conclusion, this chapter demonstrates that the humanization attempt did not hamper the binding and functional properties of the humanized scFv in comparison to STG1 and IV.3 MoAb. To humanize STG1, we retained the sequence of all CDR regions that bind to the receptor FcγRIIIa and mutated selected residues on the FRs to reflect a more humanlike sequence. To purify STG2 from the bacterial culture, we focused on the refolding of scFv in the inclusion bodies, with the aim of obtaining a high yield of pure and properly refolded scFv. The refolding of the protein, however, was met with modest success since these procedures did not consistently yield a functional protein.

Nevertheless, the refolded STG2 obtained gave an initial indication that the molecule was able to recognize and bind to the FcγRIIIa receptor and was able to inhibit platelet aggregation in the presence of HIT IgG and heparin (0.5IU/ml).

Subsequently, purified soluble STG2 was able to exhibit binding at μM range and to inhibit platelet aggregation at nM range. Although STG2 significantly inhibited platelet activation, the release of serotonin was substantially but not completely inhibited. This prompted the construction of STG3 that has less residue changes in the FRs, with better structural resemblance to STG1, and a bacterial secretion signal included for expression

into the soluble fraction. The purified STG3 successfully showed both binding and functional properties (inhibition of platelet aggregation at nM range and platelet serotonin release at μM range).

An attempt to establish a HIT animal model using NOD/SCID mice was not successful, probably because of the complexity involved in introducing several components to produce HIT events *in vivo* in these mice. Therefore, in future, we will focus our effort on testing the efficacy of STG3 *in vivo* using transgenic HIT animal model (kindly provided by Dr S. McKenzie).

Chapter 5
Generation & Characterization of BsAb with
Specificity for GPIb α and Fc γ RIIIa

5.1. Introduction

With the establishment of MoAbs as important therapeutic agents, the rapid progress in antibody engineering technologies has led to the creation of different types of antibody formats with more powerful therapeutic potential. Apart from introducing modifications that include chimerization, humanization, and fusion with toxic payloads, these antibodies can also be further refined to form fragments of monovalent Fab, Fv or scFv which serve as alternatives to the bivalent full length MoAbs. Furthermore, Fabs or scFvs with different antigenic targets can be fused together, creating another class of antibody derivatives (193). With the promise of improved potency, this new range of molecules is known as bispecific antibodies (BsAbs).

5.1.1. *The Different Forms of BsAbs*

BsAbs differ from conventional MoAbs by the fact that they possess two distinct antigen binding specificities. Aligned in a single molecule, the construct can either bind to two adjacent epitopes on a single target antigen or alternatively, it can also cross-link to two different antigens (338). BsAbs have been designed in a number of different formats (Figure 5.1). The first attempt to produce BsAbs employed the quadroma cell technology, which relies on the somatic fusion of two different hybridomas expressing murine MoAbs with desired specificities (339-341). However, hampered by the random pairing of two different immunoglobulin heavy and light chain that often yield non-functional by-products, a modification was introduced by selecting hybridomas that express IgG subclasses that would have a higher tendency for preferential pairing (342).

The structure of quadroma-derived BsAbs resembles that of MoAbs, thus, to avoid potential undesirable effects triggered by the constant fragment-Fc, the region could be removed by enzymatic digestion to create the bispecific F(ab')₂ fragment (343). Without using quadroma technology, alternative recombinant strategies have also been used to produce similar bispecific constructs. For instance the natural ability of certain protein domains to associate as heterodimers has been utilized to create these constructs. Examples include the introduction of adhesive amino acid sequences or replacement of complementary protein pairs (e.g. constant Ig domains C_K and C_{H1}, the leucine zipper domains of transcription factors Fos and Jun) that could join to the variable domains (344, 345).

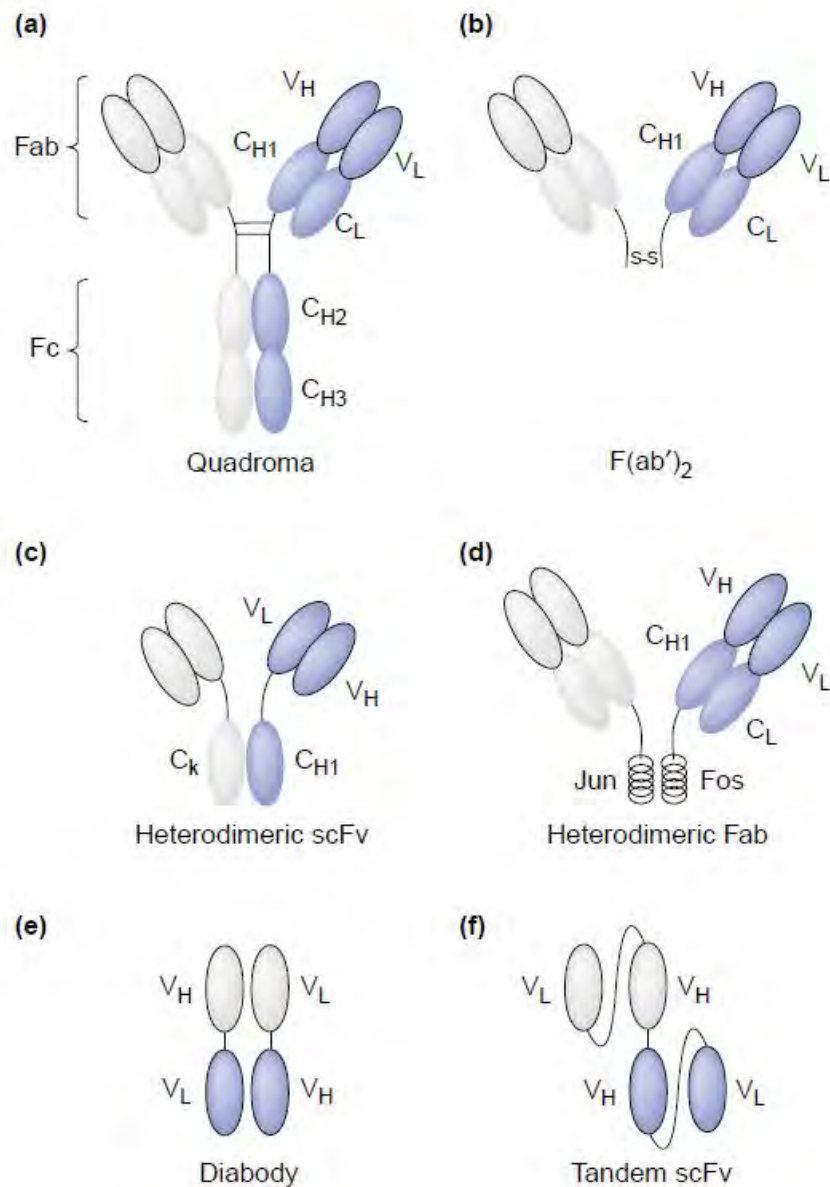


Figure 5.1. Diagrammatic representation of different formats of BsAb. (a) Quadroma-derived BsAb, resembling monospecific MoAbs in structure and size. (b-d) Heterodimeric BsAbs of medium size, comprising constant immunoglobulin regions and/or heterodimerization domains. (e-f) BsAbs of minimal size, consisting of only variable immunoglobulin regions. The different colours represent different binding specificities. Reprinted with permission from Kufer et al (346). Abbreviations: C_{H1-3}, constant regions of Ig-heavy chain; C_L, constant regions of Ig-light chain; Fab, antigen binding fragment; Fc, constant fragment; V_H, variable heavy chain; V_L, variable light chain.

Using recombinant DNA technology, much smaller BsAbs such as diabodies and tandem scFvs can be constructed, which comprise only two VH and VL domains from different antibodies within a single molecule. To create diabodies, a very short linker is used to link VH and VL domains with opposing antigen specificity on the same chain (282, 347). The coexpression of the VH-VL fusions in *E. coli* forces the complementary pairing of the domains of two chains to form stable BsAbs heterodimers. Based on scFvs, tandem scFvs can also be constructed. Here, two scFvs can be connected with a flexible polypeptide linker of varying length on a single polypeptide chain (348). In comparison to diabodies that have two separate linkers between native scFv domains, tandem scFv have high flexibility with only one glycine-serine linker. This allows the tandem scFv with two binding sites to rotate freely, facilitating simultaneous binding of two epitopes that are less accessible on different cell surfaces (349). Like other recombinant proteins, tandem scFvs were first produced using *E. coli* systems (350, 351). Although studies have shown that the bacterial expression of the functional antibody was often low even after renaturation processes, the issue can be resolved by choosing to express the molecules in mammalian cells where the proteins are secreted directly into culture media in functional and folded conformations (352).

5.1.2. BsAbs in Clinical Applications

The majority of the BsAbs developed so far are used in cancer immunotherapy (Refer to Table 5.1) that aims to cross-link tumour cells to immune cells such as cytotoxic T cells, natural killer cells and macrophages. By doing so, the molecule concentrates these effector cells in the vicinity of the target and induces a potent cytotoxic event (192). In addition, studies have shown that these intermediate sized BsAbs have rapid tissue penetration, high target retention and rapid blood clearance (193). Besides tumour therapy, BsAbs have also been developed to target platelets for antithrombotic treatment via dissolution of platelet thrombi. This involves the platelet receptor integrin GPIIb/IIIa which is the most abundant receptor on the platelet's surface and plays a role in binding von Willebrand factor (vWF) or fibrinogen to mediate platelet aggregation under shear conditions (103, 353). Examples of these BsAbs include proteins binding to GPIIIa49-66 epitope and plasminogen first kringle (258, 354) or to integrin GPIIb/IIIa and tissue plasminogen activator (355).

Table 5.1. BsAbs developed for clinical usage.

Brand Name	Format	Specificity	Indication	Reference
MDX-H210	F(ab) ₂	HER2/neu x CD64 (γFcRI)	Breast cancer	(356, 357)
Catumaxomab	Quadroma	EpCAM x CD3	Malignant ascites and ovarian cancer	(358-360)
Ertumaxomab	Quadroma	HER2/neu x CD3	Breast cancer	(361)
Blinatumomab	Tandem scFv	CD19 x CD3	B cell lymphoma	(362)
r28M	Tandem scFv	CD28 x MAP	Melanoma	(363)
No name	Tandem scFv	GPIIIa49-66 epitope x plasminogen first kringle	Thrombus	(258, 354)
No name	Tandem scFv	GPIIb/IIIa and tissue plasminogen activator	Thrombus	(355)

5.1.3. GPIb-IX-V Complex

The GPIb- IX-V complex is another platelet receptor which serves as an adhesion receptor for the multimeric adhesive ligand vWF in the arterial circulation. This mediates platelet adhesion to sites of blood vessel injury in the subendothelium. In addition, the complex also provides a high affinity binding site for thrombin during platelet activation. The GPIb-IX-V complex contains four polypeptides (GPIb α , GPIb β , GPIX and GP V) which are present in a stoichiometry of 2:2:2:1 on the platelet plasma membrane (364) (Figure 5.2). GPIb α is the major ligand-binding region of GPIb-IX-V. It is a membrane spanning subunit that contains the N-terminal globular domain (residues 1-282) providing non-contiguous binding sites for different ligands and epitopes for several anti-GPIb α monoclonal antibodies (Figure 5.3).

While several MoAbs are known to bind to the N-terminal domain of GPIb α , only AK2 will be highlighted in this Chapter. The AK2 epitope on GPIb α was mapped using immunoprecipitation by Berndt et al (365) and is localized to residues 35-60 of human GPIb α . AK2 was further used to demonstrate the binding sites of vWF and P-selectin by inhibiting the binding of these ligands to GPIb α . For studies of HIT, AK2 was able to inhibit the binding of the HIT immune complexes on normal platelets but not on the Bernard-Soulier Syndrome (BSS) platelets that lack the GPIb- IX-V complex (71). This shows that the binding of AK2 to GPIb α leads to steric interference due to the close proximity of GPIb α and Fc γ RIIa (366, 367), thus preventing the binding of the immune complex to platelets.

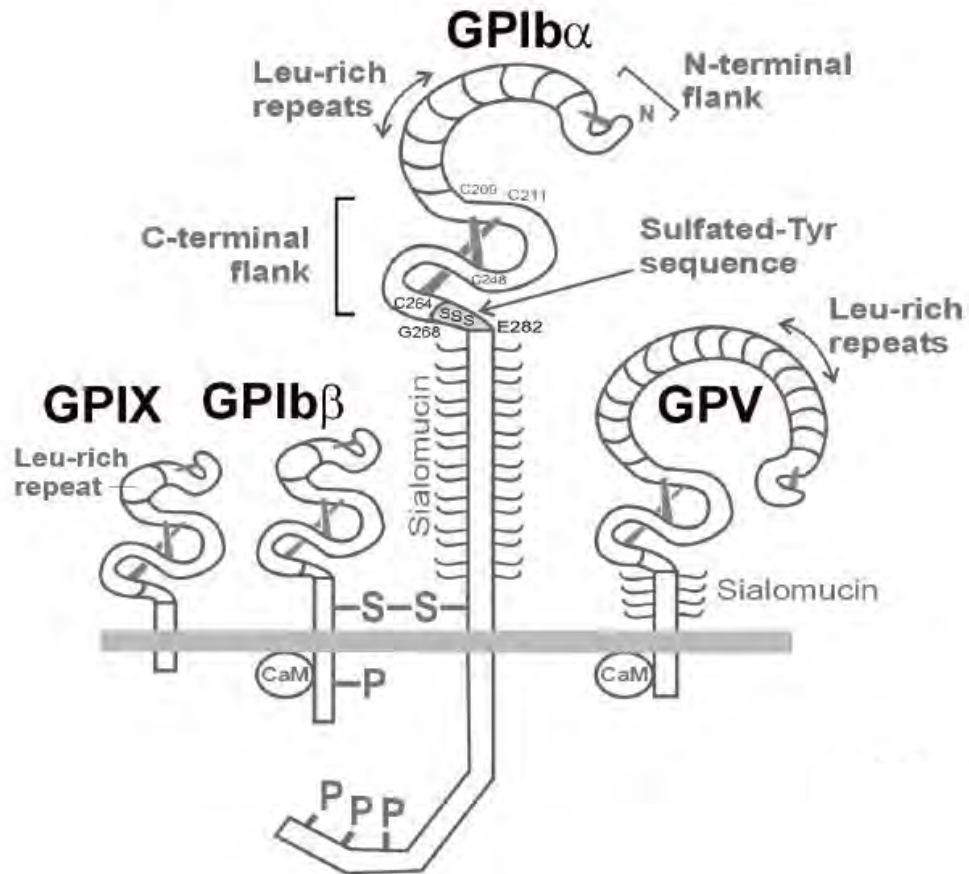


Figure 5.2. Diagram of the GPIb-IX-V complex. The subunits of the complex, which are GPIb α , GPIb β , GPIX and GPV contain extracellular leucine-rich repeats and disulfide-loops at the N- and C- terminal respectively. The cytoplasmic tails of both GPIb β and GPIb α contain phosphorylation sites while the cytoplasmic tails of GPIb β and GPV contain calmodulin binding sites. Sialomucin core is present in both GPIb α and GPV. Reprinted with permission from Andrews et al (368).

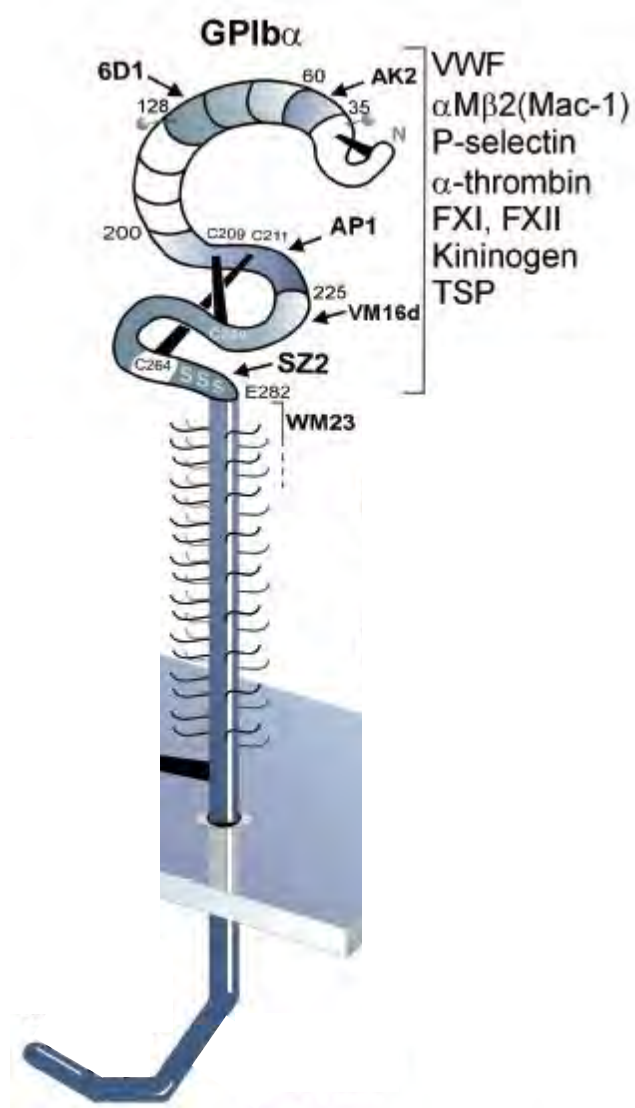


Figure 5.3. Functional binding sites located on GPIb α . The N-terminal 282 residues contain binding sites for the listed ligands, and epitopes for several MoAbs that include AK2, 6D1, AP1, VM16d, SZ2 and WM23. Reprinted with permission from Andrews et al (368).

5.1.4. Hypothesis and Aims

The creation of different forms of BsAbs provides the opportunity of targeting distinct antigenic sites simultaneously. In some contexts, this provides a huge advantage over conventional MoAbs that are monovalent and monospecific. Most of the BsAbs described to date have been designed for cancer treatment whereby these molecules can direct immune effector cells to tumours or for radionuclide pre-targeting to tumours. For platelets, BsAbs have also been developed for dissolution of thrombi.

In Chapter 4, we showed that STG2 retained the capacity to bind Fc γ RIIa and was able to prevent engagement of the HIT immune complexes with human platelets *in vitro*. Compared to other receptors, such as GPIb α (over 25,000 copies per platelet), Fc γ RIIa is present at low levels on the platelet's surface (400-2000 copies per platelets) (82, 364). We sought to increase the affinity of STG2 by designing a BsAb that, apart from binding to Fc γ RIIa, will be directed to platelets by interacting with an abundant receptor (GPIb α). Therefore, we hypothesize that a BsAb targeting both GPIb α and Fc γ RIIa will have high affinity for platelets, and will inhibit HIT immune complexes binding with increased efficacy, thus, conferring better antiplatelet properties upon STG2. Based on the proposed hypothesis, the aims for this chapter would be:

- To construct the BsAb in the form of tandem scFv based on the MoAbs AK2 and IV.3. This molecule will be denoted as STGK2 throughout this thesis. The peptide sequence will be designed and the DNA will be chemically synthesized by DNA2.0.
- To express STGK2. The recombinant protein will be expressed in bacteria *E. coli* and purified using affinity chromatography.
- To characterize the properties of the STGK2. The binding and functional activities of the protein will be evaluated using flow cytometry and platelet aggregation assays.

5.2. Results

5.2.1. Humanization of muAK2 scFv

As demonstrated in Chapter 4, the humanized anti-Fc γ RIIa scFv (STG2) exhibits antigen binding and functional properties that prevented platelet aggregation and activation in the presence of HIT IgG. However, in consideration of the low copy number of Fc γ RIIa (400-2000 per platelet) (82) compared to other platelet receptors such as GPIb α (25,000 per platelet) (364), the delivery rate of STG2 to platelets might not be efficient when administered. To enhance the delivery properties of STG2, a BsAb in the form of Tandem scFv was therefore designed by coupling STG2 to huAK2 scFv. This novel antibody was denoted as STGK-2. HuAK2 scFv (Jiang, X-M, unpublished) recognizes GPIb α receptors and was humanized from muAK2 scFv, adopting the CDR-grafting and point mutation approach.

Sequence analysis using <http://www.ncbi.nlm.nih.gov/igblast/> shows that the subgroup of VH and VL genes of muAK2 belonged to muVH2 and V κ 3, respectively. The DNA sequences of muAK2 VH and VL are shown in Figure 5.4. The CDR regions were determined by referring to Kabat definition. Furthermore, the comparison of the sequence to the human germ line database using the same search engine revealed a similarity of 62.9% to IGHV4-59*01 for VH domain and 76.8% to IGKV7-3*01 for VL domain. For the humanization of AK2, the murine CDRs were preserved (except for one residue changed in CDR-H3) while selected FRs residues were substituted to obtain a higher similarity to human sequences. This was conducted by comparing to the human germline sequences extracted from the IMGT database available on the AAAAA website (<http://www.bioc.uzh.ch/antibody/>). The FRs of the murine VH domain were changed to closely reflect human subgroup VH3 while the FRs of the murine VL domain were changed to reflect human V κ 1 and 2 (Figure 5.5). The comparison of the huVH with the most homologous human germ line sequences yielded 77.3% identity to the IGHV3-66-1*01 and huVL with 82.8% sequence identity to IGKV1-39*01.

VH Chain Sequence

```

          9           18           27           36           45           54           63
CAG GTG CAG CTG AAG GAG TCA GGA CCT GGC CTG GTG GCG CCC TCA CAG AGC CTG TCC ATC ACA
  Q  V  Q  L  K  E  S  G  P  G  L  V  A  P  S  Q  S  L  S  I  T

          72           81           90           99           108           117           126
TGC ACC GTC TCT GGG TTC TCA TTA ATC GGC TAT AGT GTA AAC TGG GTT CGC CAG CCT CCA GGA
  C  T  V  S  G  F  S  L  I  G  Y  S  V  N  W  V  R  Q  P  P  G
                                CDR-H1

          135           144           153           162           171           180           189
AAG GGT CTG GAG TGG CTG GGA ATG ATA TGG GGT GAT GGA AGC ACA GAC TTT AAT TCA GCT CTC
  K  G  L  E  W  L  G  M  I  W  G  D  G  S  T  D  F  N  S  A  L
                                CDR-H2

          198           207           216           225           234           243           252
AAA TCC AGA CTG AGC ATC AGC AAG GAC AAC TCC AAG AGC CAA GTT TCC TTA GAA ATG AAC AGT
K  S  R  L  S  I  S  K  D  N  S  K  S  Q  V  S  L  E  M  N  S

          261           270           279           288           297           306           315
CTG CAA ACT GAT GAC ACA GCC AGG TAC TAT TGT GCC AGA GAT CGG AGG GGG TCC CAT GCT ATG
  L  Q  T  D  D  T  A  R  Y  Y  C  A  R  D  R  R  G  S  H  A  M
                                CDR-H3

          324           333           342           351
GAC TAC TGG GGT CAA GGA ACC TCA GTC ACC GTC TCC TCA
D  Y  W  G  Q  G  T  S  V  T  V  S  S
    
```

VL Chain Sequence

```

          9           18           27           36           45           54           63
GAC ATT GTG CTG ACC CAA TCT CCA GCT TCT TTG GCT GTG TCT CTA GGG CAG AGG GCC ACC ATA
  D  I  V  L  T  Q  S  P  A  S  L  A  V  S  L  G  Q  R  A  T  I

          72           81           90           99           108           117           126
TCC TGC AGA GCC AGT GAA AGT GTT GAT AGT TAT GGC AAT AGT TTT ATG CAC TGG TAC CAG CAG
  S  C  R  A  S  E  S  V  D  S  Y  G  N  S  F  M  H  W  Y  Q  Q
                                CDR-L1

          135           144           153           162           171           180           189
AAA CCA GGA CAG CCA CCC AAA CTC CTC ATC TAT CGT GCA TCC AAC CTA GAA TCT GGG ATC CCT
  K  P  G  Q  P  P  K  L  L  I  Y  R  A  S  N  L  E  S  G  I  P
                                CDR-L2

          198           207           216           225           234           243           252
GCC AGG TTC AGT GGC AGT GGG TCT AGG ACA GAC TTC ACC CTC ACC ATT AAT CCT GTG GAG GCT
  A  R  F  S  G  S  G  S  R  T  D  F  T  L  T  I  N  P  V  E  A

          261           270           279           288           297           306           315
GAT GAT GCT GGA GCC TAT TAC TGT CAG CAA AGT AAT GAG GAT CCA TTC ACG TTC GGC TCG GGG
  D  D  A  G  A  Y  Y  C  Q  Q  S  N  E  D  P  F  T  F  G  S  G
                                CDR-L3

          324           333
ACA AAG TTG GAA ATA AAA
  T  K  L  E  I  K
    
```

Figure 5.4. Nucleotide and deduced amino acid sequences of VH and VL regions of muAK2. CDR sequences are underlined.

A. VH

Mouse: QVQLKESGPGLVAPSQSL SITCTVSGFSLIGYSVNWVRQPPGKGLEWLGMI
 Human: **EVQLVESG**PGLVQ**PG**SL**RLS**CAASGFSLIGYSVNWVRQ**AP**GKGLEW**VAMI**

Human VH Group 3
Human VH Group 3

Mouse: WGDGSTDFNSSALKSRLSISKDNSKSQVSLEMNSLQTDDTARYYCARRRGS
 Human: WGDGSTDFNSSALKSR**FT**ISKDNSK**N**TLYLQMNSL**RAE**DTAVYYCARRRGS

Human VH Group 3

Mouse: HAMDYWGQGTSVTVSS
 Human: **H**VMDYWGQGT**L**VTVSS

Human VH Group 3

B. VL

Mouse: DIVLTQSPASLAVSLGQRATISCRASESVDSYGNSFMHWYQQKPGQPPKL
 Human: DI**Q**MTQSP**S**SL**SAS**VGDRVTI**T**CRASESVDSYGNSFMHWYQQ**PGKA**PKL

Human V k Group 1
Human V k Group 2

Mouse: LIYRASNLESGIPARFSGSGSRTDFTLTINPVEADDGAYYCQQSNEDPF
 Human: LIYRASNLESG**V**PS**R**FSGSGS**G**TDFTLTTI**S**SL**Q**PE**D**FA**T**YYCQQSNEDPF

Human V k Group 1

Mouse: TFGSGTKLEIK
 Human: TFG**Q**GTK**V**EIK

Not categorized

Figure 5.5. Amino acid sequence alignment between the variable regions of muAK2 and huAK2. (A) VH and (B) VL. CDR residues are underlined. Letters in bold demonstrate amino acid changes that were made in the FW region. The original muAK2 belongs to subgroup of muVH2 and muV k 3 (VH2V k 3). The humanized sequence in the FW region categorized as huVH subgroups 3, while the huVL falls under subgroup 1 and 2 (VH2V k 121). In total, 52 amino acids were changed.

5.2.2. Cloning of *STGK2*

STGK2 was designed by coupling *STG2* to the humanized AK2 scFv described in section 5.2.1. A short linker (Gly₄Ser)₃ was chosen to link the variable domains of each scFv in a VH-linker-VL orientation, and long linker Gly₂₃-Ser₇ was selected to join scFvs in a huAK2-linker-*STG2* manner to form a Tandem scFv (*STGK2*) (See diagram f, Figure 5.1.). The nucleotide sequence of *STGK2* was chemically synthesized with codon optimization for protein expression in bacteria by DNA2.0, CA, USA (Figure 5.6). The final construct with a size of 1659bp including two tags (c-Myc and Penta-HIS) was digested from the commercial standard pJa vector and ligated into the pET11a vector (Figure 5.7).

5.2.3. Expression of *STGK2*

The recombinant pET11a-*STGK2* plasmid was chemically transformed into competent *E. coli* host BL21 (DE3) and the protein was expressed after induction with 1mM IPTG (Figure 5.8). As shown on SDS-PAGE, a protein of approximately 62.5 kDa that corresponds to the predicted molecular weight of *STGK2* (60.28 kDa) was highly expressed after induction (Figure 5.9A). The identity of the protein was further confirmed on Western blot by immunostaining with Anti-cMyc and anti-Penta-HIS antibodies (Figure 5.9B). A bacterial secretion signal was not included in the construct to prompt the *STGK2* protein to accumulate as inclusion bodies. The inclusion bodies were subjected to the solubilisation protocol.

VH Chain Sequence

```

          9           18           27           36           45           54           63
GAA GTT CAA CTG GTA GAG AGC GGC GGC GGC CTG GTA CAA CCT GGC GGC AGC CTG CGC CTG AGC
E   V   Q   L   V   E   S   G   G   G   L   V   Q   P   G   G   S   L   R   L   S

          72           81           90           99           108           117           126
TGT GCC GCG TCC GGC      81 TTT TCC CTG ATC GGC TAC AGC GTG AAT      108 TGG GTC CGT      117 CAA GCA CCG GGC
C   A   A   S   G   F   S   L   I   G   Y   S   V   N      W   V   R   Q   A   P   G
                                CDR-H1

          135           144           153           162           171           180           189
AAG GGT CTG GAG TGG TTG GGT ATG ATC TGG GGT GAT GGT AGC ACT GAC TTC AAT AGC GCG CTG
K   G   L   E   W   L   G   M   I   W   G   D   G   S   T   D   F   N   S   A   L
                                CDR-H2

          198           207           216           225           234           243           252
AAA AGC CGT TTC ACG ATT AGC AAG GAC ACC AGC AAA AAC ACC GTG TAT CTG CAA ATG AAT AGC
K   S   R   F   T   I   S   K   D   T   S   K   N   T   V   Y   L   Q   M   N   S

          261           270           279           288           297           306           315
CTG CGT GCT GAG GAC ACC GCG GTT TAC TAT TGC GCA CGC GAT CGC CGT GGC AGC CAC GCG ATG
L   R   A   E   D   T   A   V   Y   Y   C   A   R   D   R   R   G   S   H   A   M
                                CDR-H3

          324           333           342           351
GAC TAT TGG GGT CAA GGC ACC CTG GTT ACC GTT TCT TCG
D   Y   W   G   Q   G   T   L   V   T   V   S   S

```

VL Chain Sequence

```

          9           18           27           36           45           54           63
GAC ATT CAA ATG ACT CAG AGC CCT AGC AGC CTG TCT GCG AGC GTG GGT GAT CGT GTC ACG ATC
D   I   Q   M   T   Q   S   P   S   S   L   S   A   S   V   G   D   R   V   T   I

          72           81           90           99           108           117           126
ACG TGT CGC GCT AGC GAG AGC GTG GAT TCT TAT GGT AAT AGC TTT ATG CAC TGG TAT CAG CAG
T   C   R   A   S   E   S   V   D   S   Y   G   N   S   F   M   H      W   Y   Q   Q
                                CDR-L1

          135           144           153           162           171           180           189
AAA CCG GGT AAA GCG CCG AAG CTG CTG ATT TAC CGC GCA AGC AAC CTG GAA TCG GGC GTC CCG
K   P   G   K   A   P   K   L   L   I   Y   R   A   S   N   L   E   S      G   V   P
                                CDR-L2

          198           207           216           225           234           243           252
TCC CGT TTC TCT GGT TCC GGT TCC GGT ACC GAT TTT ACG CTG ACC ATT TCT AGC CTG CAG CCG
S   R   F   S   G   S   G   S   G   T   D   F   T   L   T   I   S   S   L   Q   P

          261           270           279           288           297           306           315
GAA GAT TTT GCG ACC TAT TAC TGC CAG CAG AGC AAT GAG GAC CCG TTC ACG TTC GGC CAG GGC
E   D   F   A   T   Y   Y   C   Q   Q   S   N   E   D   P   F   T      F   G   Q   G
                                CDR-L3

ACC AAA
T   K

```

Figure 5.6. Nucleotide and deduced amino acid sequences of VH and VL regions of humanized AK2. CDR sequences are underlined.

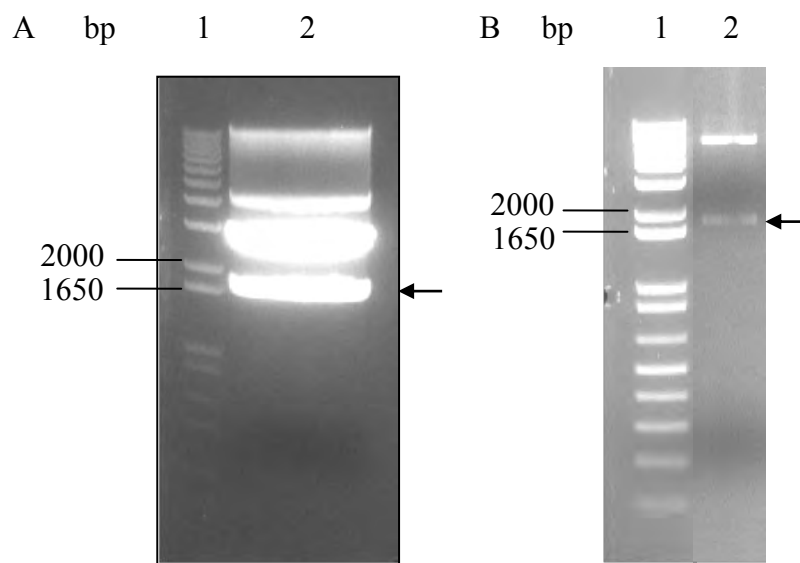


Figure 5.7. Cloning of STGK2 into pET11a. Electrophoresis was performed on 1.5% agarose in 1 x TAE buffer. A. Lane 1: 1kb Plus DNA Ladder; Lane 2: Digested pJa vector with STGK2 insert (Arrow). B. Lane 1: 1kb Plus DNA Ladder; Lane 2: Digested pET11a vector with STGK2 insert (Arrow).

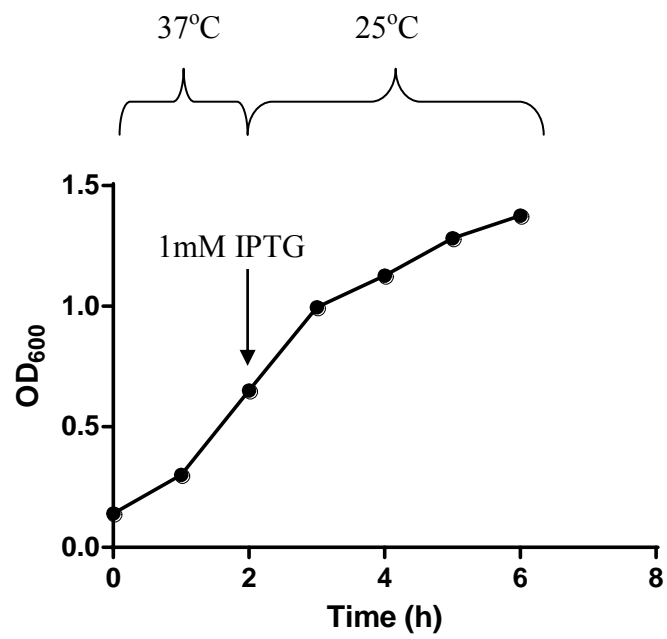


Figure 5.8. Bacterial growth pattern of *E. coli* BL21(DE3) producing STGK2.

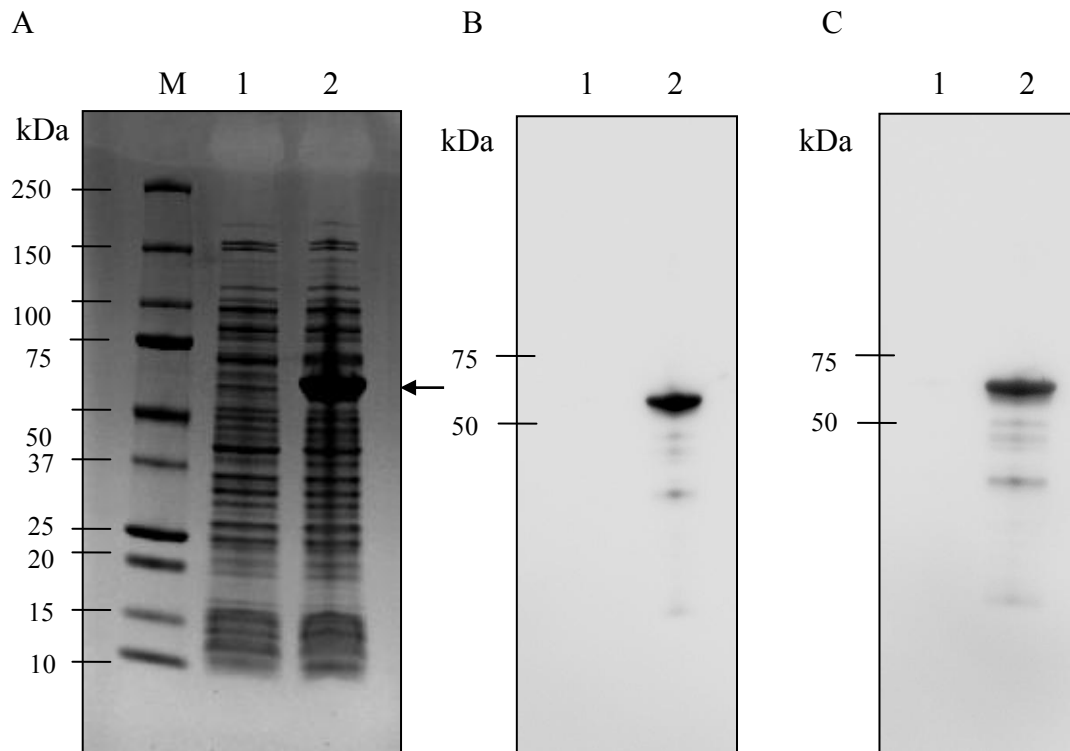


Figure 5.9. Gel analysis of STGK2 expressed in *E. coli* BL21 (DE3).
A. Coomassie Blue Staining and B & C. Western blot (Immunostaining with Anti-cMyc antibody and Anti-Penta-HIS antibody, respectively). Lane M: Molecular weight marker (Bio-Rad). Lane 1: Total protein before induction; Lane 2: Total protein after induction. A prominent band of the expected molecular weight (60.28kDa) is observed after induction (Arrow).

5.2.4. Purification and On-Column Refolding of Solubilized STGK2

The STGK2 inclusion bodies were first solubilised with denaturant (8M urea). An on-column refolding approach was conducted on affinity chromatography coupled with purification. The protein was loaded and bound onto the 1ml Nickel-Chelating Resin under denaturing conditions. This was followed by a washing step to remove nonspecific proteins, and the refolding step that gradually decreases the concentration of urea from 8M to 0M to encourage protein refolding. At the end of the refolding process, the elution of the protein was observed at 250mM of imidazole (Figure 5.10). The collected elution peak was analyzed by SDS-PAGE and Western blot. Figure 5.11 (Lane 5) shows that purified STGK2 was obtained after purification. Approximately 11 mg of highly purified refolded STGK2 was obtained from 1 L of culture (Table 5.2).

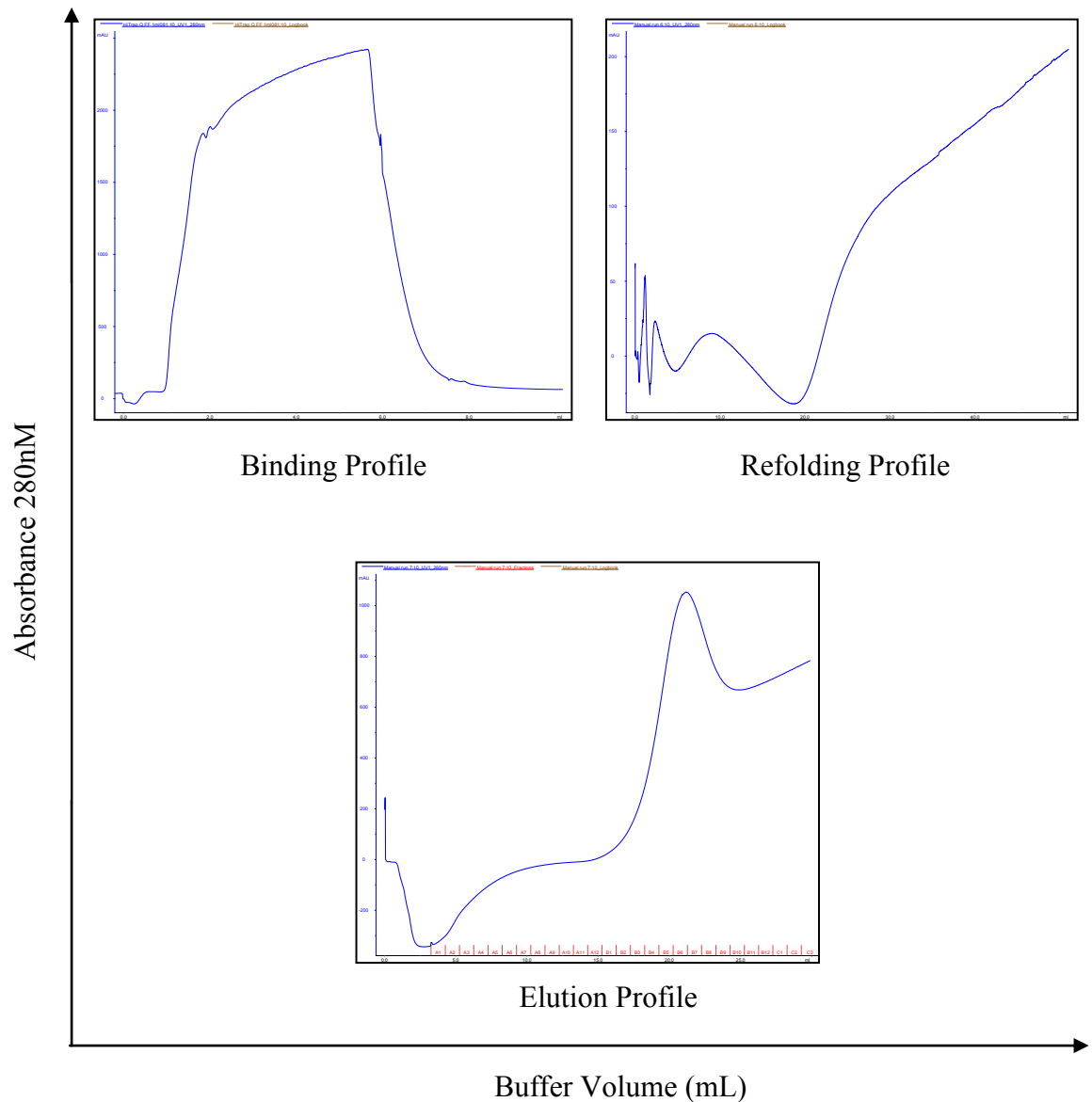


Figure 5.10. Affinity chromatography of purification and on-column refolding of solubilized STGK2. The denatured sample was loaded onto a Nickel-Chelating Resin Column. The STGK2 bound to the resin in a denatured form was slowly refolded by gradually decreasing the urea concentration during the refolding phase. The subsequent increase in the concentration of imidazole prompted the elution of the target protein at around 250mM imidazole.

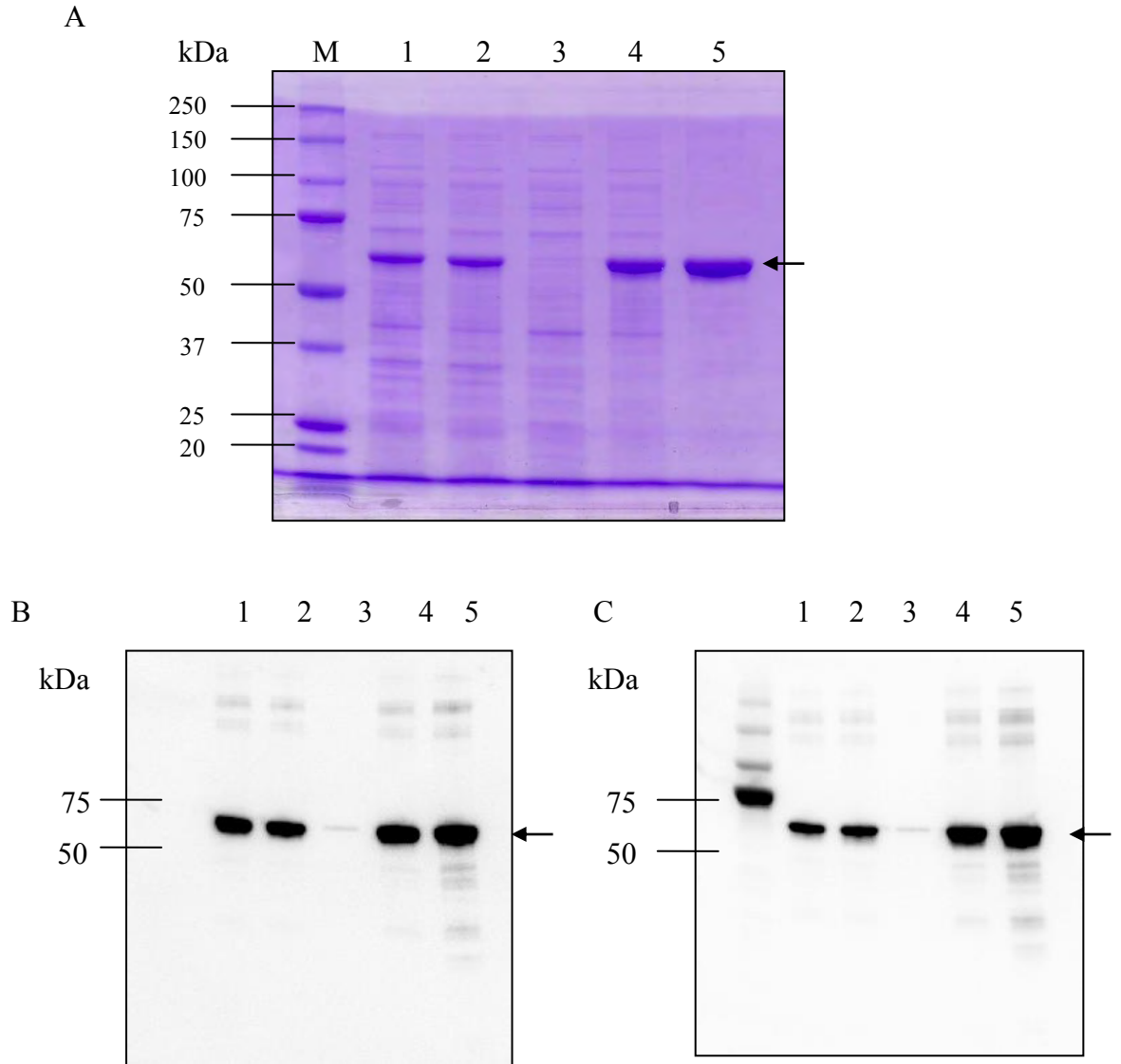


Figure 5.11. Gel analysis of the purified refolded STGK2. A. Coomassie Blue Staining. B & C. Western blot (Immunostaining with Anti-cMyc and Anti-Penta-HIS antibodies, respectively) (2 μ g loaded for each lane). Lane 1: Total Cell Lysate; Lane 2: Pellet after sonication; Lane 3: Soluble fraction; Lane 4: Solubilized fraction (8M urea); Lane 5: Purified STGK2 (Arrow).

Table 5.2. Summary on purification and refolding of STGK2

Procedure	Total protein (mg)
Total cell lysate ^a	600
Pellet after sonication	460
Soluble fraction	175
Solubilized inclusion bodies	165
Purified and refolded	11

^a From about 5g of wet-weight cells obtained from 1 L cell culture

5.2.5. STGK2 Refolded On-Column Binds to Platelets

The antigen binding activity of the refolded STGK2 to human platelets was evaluated using the direct immunofluorescence approach. The presence of GPIb α on platelets was first confirmed with AK2 MoAb revealed with AF488-conjugated anti-mouse IgG (Figure 5.12). While no significant differences were observed between the three concentrations tested (Figure 5.12), the highest fluorescence intensity was exhibited at a concentration of 100nM of AK2.

The binding of STGK2 was tested at different concentrations ranging from 50nM to 1000nM by incubating with human platelets followed by staining with AF488-conjugated anti-c-Myc MoAb. The binding was compared with a negative control sample, containing the secondary antibody alone. The flow cytometry analysis (Figure 5.13) demonstrates that refolded STGK2 was able to bind to the platelets in a dose-dependent manner. The binding capacity reaches a plateau at a concentration of ≥ 500 nM (approximately 75% binding), however, the highest fluorescence intensity (Y Geo Mean=170.9) was exhibited at a concentration of 750nM. Higher concentrations of STGK2 led to a decreased in the fluorescence intensity.

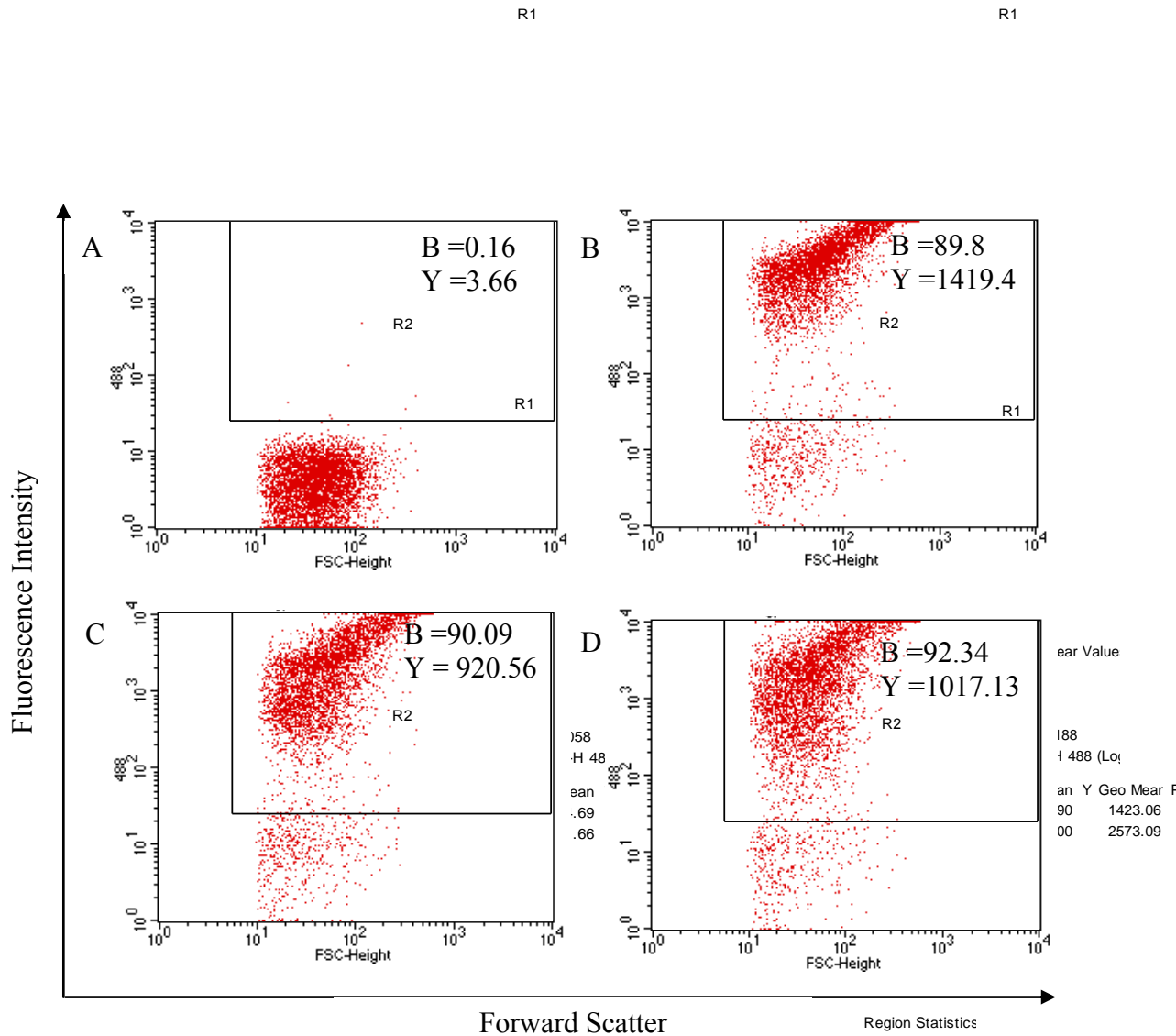


Figure 5.12: Binding of AK2 MoAb to human platelets. A: Negative control. B-D: AK2 MoAb tested at various concentrations of 100, 250 and 500nM. Abbreviations in figure: B, Binding %; Y, Y Geometric Mean.

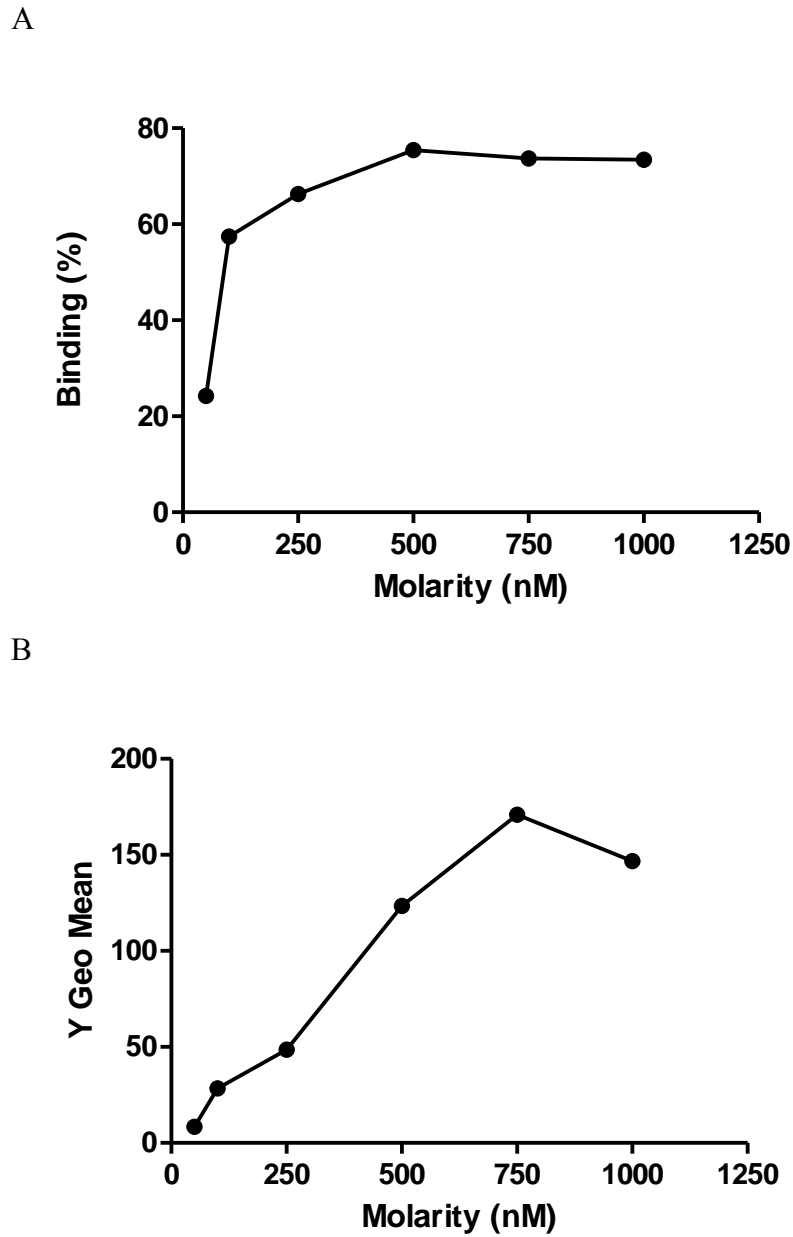


Figure 5.13. Refolded STGK2 interacts with human platelets. Different concentrations of STGK2 (50nM, 100nM, 250nM, 500nM, 750nM and 1000nM) were incubated with human platelets followed by detection with AF488-conjugated anti-c-Myc antibody. Binding efficiency is measured with A. Percentage which represents the number of platelets bound by the antibody. B. Y Geo Mean which represents the binding intensity.

5.2.6. STGK2 Leads to Spontaneous Platelet Aggregation

As STGK2 was observed to bind to platelets efficiently, the ability of the protein to inhibit HIT IgG-induced platelet aggregation was tested by light transmission aggregometry. Unexpectedly, spontaneous platelet aggregation occurred once STGK2 was added to platelets. The spontaneous aggregation caused by STGK2 was dose dependent as shown in Figure 5.14. Aggregation of <20% was observed for STGK2 concentrations of ≤ 75 nM (Data not shown), while complete aggregation was observed in the presence of 750nM of STGK2 (Figure 5.14B). STGK2-induced platelet aggregation depends on Fc γ RIIIa interaction. As shown in Figure 5.14C, pre-incubation of platelets with the IV.3 MoAb neutralized the capacity of 750nM STGK2 to induce spontaneous platelet aggregation. Taken together, these results indicate that STGK2 possesses intrinsic platelet activation capacity and is therefore of no practical use for our purposes.

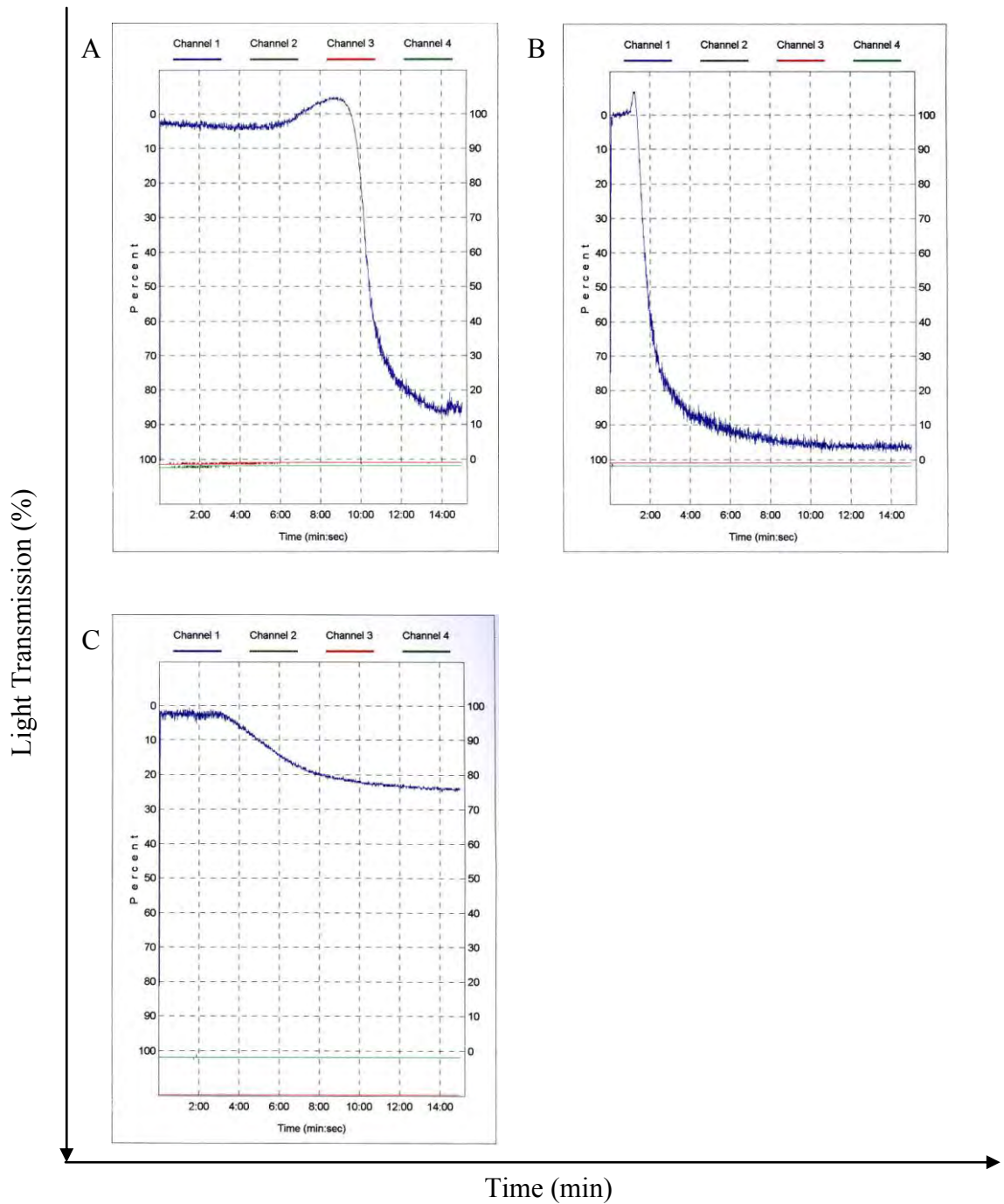


Figure 5.14. STGK2 leads to platelet aggregation in the absence of HIT IgG.
 A. Control, HIT IgG and heparin (0.5 IU/ml) induced platelet aggregation at a level of 80%. B. STGK2 induced complete spontaneous aggregation at a concentration of 750nM. C. The addition of IV.3 MoAb abolished the spontaneous platelet aggregation exerted by 750nM STGK2.

5.3. Discussion

scFv antibodies such as STG2 (Chapter 4) are artificial molecules not found in nature. Nevertheless, they share a crucial similarity with natural immune antibodies: they are specific for a single antigen. Antibody engineering has allowed the creation of other types of antibodies, such as BsAbs, with specificity for more than one target antigen. In Chapter 4, we demonstrated *in vitro* that the humanized anti-Fc γ RIIa scFv (STG2) has significant binding and functional activity. It recognizes Fc γ RIIa on platelets and inhibits HIT IgG induced platelet aggregation and activation. In this Chapter, we aimed to improve the functional activity of STG2 by generating a BsAb with the capacity to interact with platelets more efficiently.

BsAbs which have dual specificity, confer better selectivity and efficacy for targeted therapy. These molecules are therefore advantageous in comparison to both the whole antibody and scFv antibody fragments. In terms of cancer treatment, a large molecule like IgG (150kDa) has low tumour penetration rate and toxicity due to subsequent accumulation in the serum; scFv (30kDa) on the other hand are cleared rapidly and have low tumour retention properties due to its much smaller size (193). Therefore, BsAbs with an intermediate molecular weight of around 55kDa have the ideal characteristics of rapid tissue penetration, high target retention and rapid clearance from the system. Most of the BsAbs created for tumour therapy aims to redirect immune effector cells (i.e. T-cells, natural killer cells and macrophages) against tumours leading to the destruction of these cancerous cells (Refer to section 5.1.2). The BsAb created in this study presented in the form of Tandem scFv, will specifically target platelets, and comprises STG2 that binds to Fc γ RIIa and huAK2 scFv that binds to GPIb α .

The refolding of STGK2 from inclusion bodies yielded active protein that recognizes either GPIb α or Fc γ RIIa receptors. Unlike STG2, the refolding of STGK2 was effective, which demonstrates that refolding approaches must be optimized empirically for different protein constructs. Upon testing STGK2 on platelet aggregation assay, it was revealed that the recombinant protein caused unwanted spontaneous aggregation in the absence of both HIT IgG and heparin. To confirm that the aggregation was caused by the BsAb, the platelets were pre-incubated with the anti-Fc γ RIIa MoAb IV.3. Subsequent addition of STGK2 did not induce platelet aggregation. This shows that the

STGK2-induced platelet aggregation can be blocked by an anti-Fc γ RIIa MoAb, indicating that the aggregation of platelets by STGK2 relies on the activation of Fc γ RIIa. Since no spontaneous platelet aggregation was observed when platelets were incubated with both IV.3 and AK2 MoAbs (Data not shown), this suggests that activation of the platelets is due to cross-linking of GPIb α and Fc γ RIIa .

GPIb α , which is a subunit of GPIb-IX-V complex, has been reported to have functional interaction with Fc γ RIIa. One study showed that by targeting GPIb α with either AK2 MoAb or its F(ab')₂ fragment, the aggregation of normal human platelets induced by HIT IgG was inhibited. This inhibition was not observed on BSS platelets that lack the GPIb-IX-V complex (Figure 5.15 C) (71). This shows that AK2 does not interact directly with Fc γ RIIa but exerts its inhibitory effect from steric interference. This is further supported by reports showing that both GPIb-IX-V and Fc γ RIIa lie in close proximity, are co-localized on the platelet membrane and may mediate some signalling events (367, 369).

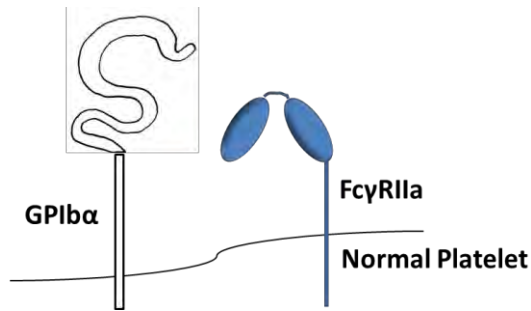
Based on the data of the platelet aggregation study, spontaneous platelet aggregation induced by STGK2 suggests that some form of interaction may have taken place between GPIb α and Fc γ RIIa. The binding of AK2 scFv to GPIb α and binding of the other arm STGK2 to the Fc γ RIIa induces cross-linking of the receptors, and this leads to platelet activation (Figure 5.15D). This is further supported by the fact that addition of IV.3 MoAb prevented the aggregation induced by STGK2 (Figure 5.15E); which implies that the activation response requires binding of STGK2 to Fc γ RIIa.

This can be likened to the experiment in which cross-linking of Fc γ RIIa was induced by simply incubating the platelets with IV.3 MoAb followed by the addition of anti-mouse IgG F(ab')₂ (133, 334, 370). IV.3 serves as the primary antibody that binds to the Fc receptor via its variable region without triggering platelet activation. Next, the secondary antibody links the two MoAbs. This action results in the cross-linking of the Fc receptors, triggering intracellular signalling events, ultimately leading to platelet activation. A similar scenario occurs with ultralarge immune complexes that cause HIT. These complexes comprising heparin, PF4, and HIT IgG cross-link Fc γ RIIa on the platelet surface, activating the platelets and initiating the coagulation cascade (371).

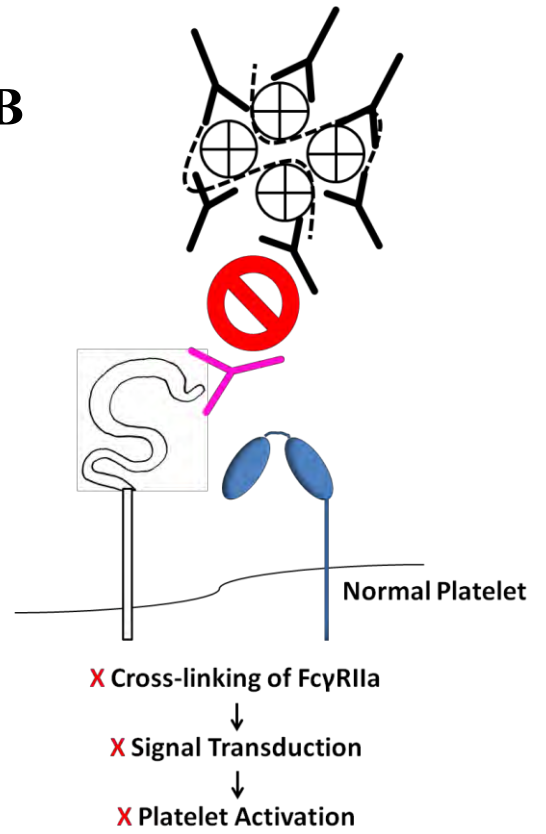
The cross-linking of the Fc γ RIIa receptors can be confirmed via immunoprecipitation approach. As mentioned in Chapter 1, under section 1.13., the engagement of the Fc receptor leads to phosphorylation of ITAM that recruits signalling proteins such as Syk. The activation of Syk leads to recruitment of enzymes that include phospholipase C γ 2, phosphatidylinositol 3-kinase, protein kinase C and etc, with platelet aggregation and activation as the end point (104, 133, 370, 372, 373). These phosphorylated signalling molecules can therefore be immunoprecipitated on Protein A/G agarose beads after labelling with the respective antibodies and detected by Western Blot. However, since the experimental data did not support the proposed hypothesis for this study, which is to inhibit platelet aggregation induced by the HIT immune complexes more effectively than STG2, these additional experiments are therefore not warranted.

In conclusion, a humanized BsAb that recognizes both GPIb α and Fc γ RIIa was designed, expressed and purified. The antibody showed strong binding affinity to human platelets at nanomolar concentrations. However, and contrary to our hypothesis, STGK2 did not inhibit HIT immune complexes-induced platelet aggregation, but rather initiated spontaneous platelet aggregation. Thus, bivalent antibodies directed towards Fc γ RIIa and another platelet receptors may not be experimentally or therapeutically useful due to the likelihood of receptor cross-linking and ensuing platelet activation.

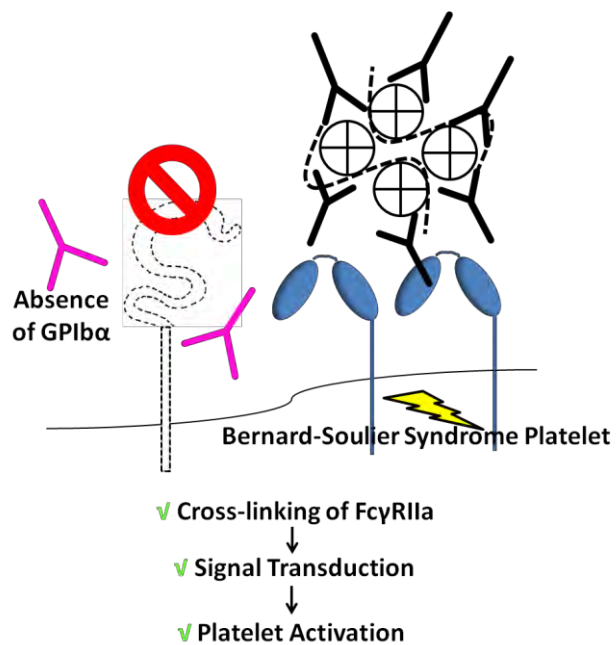
A



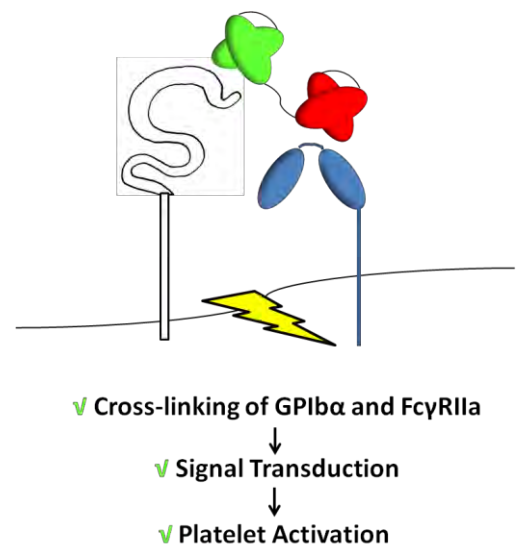
B



C



D



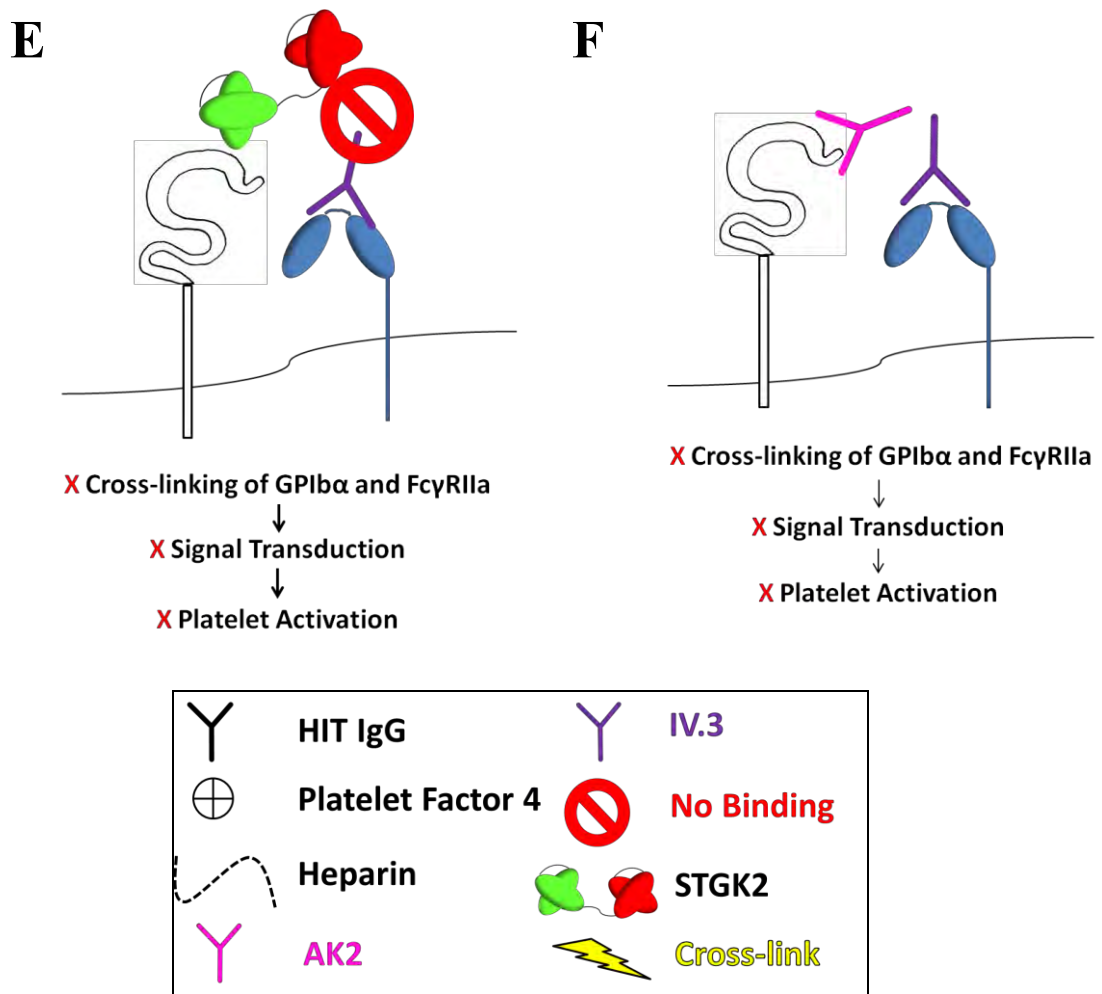


Figure 5.15. Diagrams illustrating the interactions between GPIb α and Fc γ RIIa in the presence of different molecules. A. Both receptors at resting stage. B. The binding of AK2 to GPIb α leads to steric hindrance that prevents HIT immune complexes from binding to Fc γ RIIa, thus, no platelet activation is observed. C. AK2 did not prevent the HIT immune complexes from interacting with Fc γ RIIa in the absence of GPIb α . D. STGK2 interacts with both receptors simultaneously. This leads to cross-linking of both receptors and subsequent platelet activation. E. The binding of IV.3 MoAb to Fc γ RIIa prevents STGK2 from interacting with the Fc receptor and no platelet activation is observed. F. The binding of IV.3 and AK2 MoAbs together does not lead to platelet activation.

Chapter 6

Final Summary and Future Work

6.1. Final Summary

Heparin-induced thrombocytopenia (HIT) is a life threatening thrombotic complication of heparin treatment. HIT occurs when immune complexes consisting of heparin, platelet factor 4 (PF4) and specific HIT IgG (374) are formed following sensitization of the patients by heparin. These ultralarge immune complexes interact with platelets via Fc γ RIIa receptors, inducing receptor cross-linking, thus leading to platelet activation (333). The activated platelets subsequently release PF4 which amplifies the immune-complex-mediated platelet activation events and also generates procoagulant microparticles which initiate the downstream coagulation pathway (44). The serious clinical sequelae include venous thrombosis such as deep vein thrombosis and pulmonary embolism; arterial thrombosis such as myocardial infarction, stroke and limb gangrene requiring amputation (77). The current treatments for HIT mainly focus on inhibiting the coagulation pathway. These interventions have been shown to improve the conditions of these patients to a certain extent. However, these treatments are still inadequate in tackling issues of disabling morbidity such as limb amputation and mortality, thus, justifying the need to search for better therapeutic options for HIT.

The overall aim of this thesis was therefore to seek a different alternative to treat HIT. Since it is well established that Fc γ RIIa plays a key role in initiating HIT, we focused on constructing an anti-Fc γ RIIa antibody fragment in the form of a scFv and on assessing the feasibility of this recombinant protein to block activation and aggregation of platelets induced by HIT immune complexes. The principal findings from this project are:

- The creation of a scFv derived from an anti-Fc γ RIIa MoAb which retained the capacity to interact with human platelets.
- The recombinant scFv was able to inhibit platelet aggregation and activation in the presence of HIT IgG/serum and heparin.
- The conservation of Fc γ RIIa blocking properties after humanization of the scFv.

The subsequent sections will provide a brief summary of each finding.

The variable region of the anti-Fc γ RIIa MoAb (IV.3) serves as the antigen binding site that interacts and blocks the Fc receptor. In Chapter 3, the sequence of the variable region was cloned and confirmed by sequencing to create the antibody fragment scFv, which we termed STG1. The expressed protein was purified from the periplasmic fraction of *E. coli* in a soluble form. The yield was ~0.5mg/L of bacterial culture, which was comparable to the reported yield for scFv purified from the periplasmic fraction (1-2mg/L) (318). Upon testing, STG1 retained the capacity to recognize Fc γ RIIa on platelets. The binding affinity was lower than the parental IV.3 MoAb (1-2 fold lower), however, this is generally expected and similar findings have been reported for other scFvs (297, 375). This may be due to the absence of the Fc region and the constant domain of the variable regions that affects the stability, and also distorts the conformation of the scFv antigen binding site (376). The initial findings that STG1 interacted with Fc receptor on platelets suggest that the recombinant protein might also possess receptor-blocking activity. When the functional properties of STG1 were tested on both platelet aggregation and SRA, it was observed that it successfully inhibited platelet activation induced by the HIT immune complexes. While the concentrations of STG1 were comparable to IV.3 tested in SRA (1 to 2 μ M), the concentration of the protein needed in platelet aggregation assays was approximately 10-fold higher compared to its parental MoAb. Nevertheless, it still falls within the satisfactory nM range. This main finding from Chapter 3 therefore demonstrated that the monovalent STG1 retained the same effective properties as the parental Ab.

By demonstrating that STG1 possessed functional characteristics, the next aim was to design and develop a functional humanized version of this scFv. Shown in Chapter 4, humanization was conducted on STG1, based on CDR-grafting and point mutation approach which have been conducted for other humanized scFvs (201, 256, 296). This new molecule was termed STG2. During humanization, the CDRs that form the crucial antigen binding site were retained while selected framework residues were mutated to reflect a more humanlike sequence. We proceeded to purify the insoluble form of STG2, also known as inclusion bodies, after expression in the bacterial system. The purification of the inclusion bodies under denaturing conditions allowed us to obtain a purity of up to 80% and a high yield of 50mg per 1L of bacterial culture. The ease of purification is possibly aided by the C-terminal His₆-tag that was exposed to the solvent under denaturing condition, which facilitates the purification process in comparison to

soluble, non-denatured proteins. The purified denatured STG2 was then refolded by means of one-step and step-wise dialysis, however both approaches failed to fully restore the functional conformation of STG2. Nevertheless, the latter step-wise dialysis approach yielded a fraction of functional STG2 that inhibits platelet aggregation tested at a high concentration of 30 μ M.

Subsequently, STG2 refolding was conducted on IMAC column under more stringent conditions. A functional STG2 was refolded and purified, and the protein demonstrated a slightly higher binding affinity in comparison to STG1, possibly due to higher sample purity. However, subsequent attempts to produce more functional STG2 using the same purification approach were not consistently successful, suggesting that the nature of the protein may play an unpredictable role in preventing the correct refolding and disulfide bond formation. This was evident as the other recombinant protein-STGK2 (Chapter 5) was effectively refolded using the same on-column refolding approach and demonstrated satisfactory binding capacity.

The above issues thus prompted us to purify the soluble fraction of STG2. Although a much lower yield was obtained (\sim 1mg/L), the protein demonstrated both binding and functional properties on platelet aggregation but was less effective on SRA, indicating suboptimal inhibitory capacity. To obtain a more functional STG2, a humanized STG3 with less aa changes in the framework residues and with more structural similarity to STG1 was constructed, fitted with bacterial secretion signal to increase the secretion of the protein into the oxidizing environment of periplasmic fraction. Finally, soluble STG3 that retains its original conformation exhibited the desired binding capacity to Fc γ RIIa receptors on platelets and functional properties in inhibiting platelet aggregation and activation induced by HIT IgG and heparin, at a concentration much closer to the IV.3 MoAb.

When STG2 demonstrated inhibition of HIT events *in vitro*, we sought to further improve the affinity and antiplatelet properties of the molecule. A scFv directed against GPIIb α was fused to STG2 to create a BsAb. As shown in Chapter 5, the binding capacity of STGK2 was between 60-80% at concentrations of 0.1-1 μ M and exhibited higher binding properties in comparison to the other scFvs. This was possibly due to the binding of the bivalent STGK2 to both GPIIb α and Fc γ RIIa that prompts better

interaction with platelets, especially to the more abundant GPIIb/IIIa receptor (25,000 copies per platelet) (82). Nevertheless, the higher binding capacity of STGK2 did not prove advantageous for the blockage of the Fc receptor. Binding of this BsAb led to receptor cross-linking, ultimately causing spontaneous platelet activation and aggregation in the absence of the HIT IgG/heparin immune complexes.

The establishment of a HIT animal model using NOD/SCID mice was attempted. This was based on a previously published study where quinine-induced thrombocytopenia was successfully recapitulated in NOD/SCID mice (337). In our study, the introduction of human platelets into the mice's circulation was clearly detected for a time frame of 24 h. However, the introduction of several components essential to induce HIT was not sufficient to establish HIT in the animals and a drop in human platelet numbers was not observed after the administration of heparin. This may be attributed to reasons where the levels of these components and the injected human platelets did not meet the required ratio for the formation of the HIT immune complexes, since the amount introduced was solely based on the data generated *in vitro*. Furthermore, it has been clearly shown that after being injected with KKO and heparin, the different levels of human PF4 expressed in HIT transgenic mice correlate to the severity of thrombocytopenia. On these observations, the generation of a NOD/SCID model of HIT appears to be impractical (67).

In conclusion, we successfully proposed that it is possible to develop a treatment for HIT via inhibition of FcγRIIIa to prevent platelet activation by the HIT immune complexes. This was achieved by constructing an antibody fragment in the form of scFv, derived from the variable regions of IV.3 MoAb. The scFv not only recognizes FcγRIIIa on platelets, but it also blocks the receptor from being activated by the HIT immune complexes as demonstrated on both platelet aggregation and serotonin release assays. This shows that the recombinant protein was able to retain the binding and functional properties of the parental antibody. The molecule was then humanized by changing selected murine residues on the FW region to reflect a more humanlike sequence. This is important to decrease immunogenicity for potential therapeutic application. The humanization approach did not affect the binding and functional properties of the original scFv as the new molecule was successful in preventing platelet activation induced by HIT IgG and heparin. To further improve the characteristics of this

humanized scFv, the molecule was fused to a humanized scFv derived from AK2 that targets GPIIb α , to create a BsAb in a form of Tandem scFv with dual specificity.

Unfortunately, this molecule leads to spontaneous platelet aggregation in the absence of HIT immune complexes, thus we did not proceed further with the BsAb molecule.

6.2. Future Work

This thesis demonstrates a new possible approach to treat HIT by targeting Fc γ RIIa with a recombinant scFv derived from a known Fc receptor blocking MoAb. However, some aspects need to be addressed to realize the full potential of the humanized scFv. Though soluble scFv can be purified from the periplasmic environment of *E. coli*, due to the narrow space and inefficient secretion of the target protein into the periplasm, only low yields can be achieved. To improve the yield, scFv can be co-expressed with chaperones which bind and assist with the refolding of proteins to reach the native conformations. Notable examples are cytoplasmic chaperones such as GroELS (377) and periplasmic chaperones such as Skp and FkpA (378, 379). Furthermore, the cytoplasmic expression of soluble scFv can be enhanced using fusion partners such as glutathione S-transferase (GST) (380), thioredoxin (Trx) (377, 381) and maltose-binding protein (MBP) (382).

A different expression system that allows expression of recombinant proteins at low temperature can also be utilized to increase the yield of disulfide containing proteins. The inclusion of a cold shock promoter *cspA* (383), together with the fusion partners mentioned previously have been reported to be successful in producing soluble proteins (384, 385). The purification of scFv can be further improved by optimizing several parameters. The purity of the scFv can be refined with gel filtration chromatography that separates the target protein from other contaminants. In addition, for better purification outcomes, the scFv can be conferred a Protein L recognition site by a single point mutation in the FR1 of the variable light chain, thus providing the means for a single step purification (260).

Once the antibody fragment has been purified, the affinity of the scFv against Fc γ RIIa can then be determined by surface plasmon resonance (SPR) that measures the kinetic (k_{on} , k_{off}) and equilibrium dissociation (K_D) constants (386). The approach utilizes a chip in which antigen is immobilized on the surface, and uses polarized light to detect the

antigen interaction with flow through analytes (i.e. scFv) (387). A comparison in terms of affinity can therefore be made with the parental MoAb IV.3.

During platelet activation in the events of HIT, microparticles are released and serve as an important implication of the thrombotic complication. These submicron vesicles are easily distinguished from human platelets and can be detected by flow cytometry via expression of surface antigens such as Annexin V and CD41 (388). Based on this, the inhibition properties of scFv can be confirmed if the recombinant protein is able to prevent the release of microparticles in the presence of HIT-IgG and heparin. The function of scFv can be further elucidated using other functional assays such as the flow chamber-based assay which allows the viewing of platelet events in real time (389). The latest semi-automated microfluidic platform (Venaflux, Cellix, Ireland) has already been purchased by our School and will be installed soon. Using the system, HIT-IgG induced platelet aggregation and thrombus formation can be recreated and viewed using whole blood in a fluidics chamber, and the inhibition properties of scFv can therefore be assessed.

Though the half-life of the scFvs constructed in the project has not been determined, we speculated that it might be short lived under *in vivo* condition. In general, the half-life of scFv has been reported to be much shorter (minutes to several hours) than normal IgG (three weeks) (390). This is due to the absence of the Fc domain where the scFv does not interact with Fc receptors leading to fast clearance from the circulation, and is much smaller in size in comparison to normal antibody. In the context of HIT treatment, these properties may be unfavourable for the antibody fragment to execute its therapeutic function, since the occurrence of HIT events usually spanned over a few days after initiation of heparin therapy. The design of these scFvs can therefore be improved through several amendments. To prolong its presence in the circulation, the antibody fragment can be fused to a human constant domain (CL to VL and CH1 to VH) to create a Fab portion (344). The Fab portion can also be covalently conjugated to polyethylene glycol (PEG) singly, or by linking two Fabs to create an antigen binding fragment similar to the MoAb (391). This approach termed PEGylation has been commonly used to extend half-life of protein of interest and clinically proven to be effective and safe (392). All these created antibody fragments have to be tested experimentally for their efficacy.

Lastly, to confirm the efficacy and the stability of the antibody fragment *in vivo*, the recombinant molecule needs to be tested in an animal model. As demonstrated in Chapter 4, the establishment of a HIT animal model using NOD/SCID mice wasn't successful. While similar models have been used to study the events of drug-induced thrombocytopenia (215, 216, 393), more parameters are involved to induce HIT in the mouse model (i.e. platelets expressing human Fc γ RIIa, PF4, heparin and HIT IgG). Furthermore, due to the short period of circulation of injected human platelets in the mouse model, it was only possible to monitor the level of platelet count but insufficient to establish thrombotic events. Therefore, we propose to test the scFvs in HIT transgenic mice. This animal model endogenously expresses human PF4 and Fc γ RIIa (108). By introducing HIT IgG/HIT-IgG like MoAb KKO and heparin, the events of HIT can be easily observed. Therefore, we anticipate that the antibody fragment of STG1/STG3 would be able to abolish the events of HIT.

Appendix

A1. Appendix for Chapter 2

A1.1. Ammonium Sulphate Precipitation

Solid ammonium sulphate is added to solution for protein precipitation. The amount to be added is based on Table A1.1 to achieve the desired percentage saturation.

Table A1.1. Weight of ammonium sulphate (grams) added per 100ml of solution.

* #	20	25	30	35	40	45	50	55	60	65	70	75	80	85	90	95	100
0	10.6	13.4	16.4	19.4	22.6	25.8	29.1	32.6	36.1	39.8	43.6	47.6	51.6	55.9	60.3	65	69.7
5	7.9	10.8	13.7	16.6	19.7	22.9	26.2	29.6	33.1	36.8	40.5	44.4	48.4	52.6	57	61.5	66.2
10	5.3	8.1	10.9	13.9	16.9	20	23.3	26.6	30.1	33.7	37.4	41.2	45.2	49.3	53.6	58.1	62.7
15	2.6	5.4	8.2	11.1	14.1	17.2	20.4	23.7	27.1	30.6	34.3	38.1	42	46	50.3	54.7	59.2
20	0	2.7	5.5	8.3	11.3	14.3	17.5	20.7	24.1	27.6	31.2	34.9	38.7	42.7	46.9	51.2	55.7
25		0	2.7	5.6	8.4	11.5	14.6	17.9	21.1	24.5	28	31.7	35.5	39.5	43.6	47.8	52.2
30			0	2.8	5.6	8.6	11.7	14.8	18.1	21.4	24.9	28.5	32.3	36.2	40.2	44.5	48.8
35				0	2.8	5.7	8.7	11.8	15.1	18.4	21.8	25.4	29.1	32.9	36.9	41	45.3
40					0	2.9	5.8	8.9	12	15.3	18.7	22.2	25.8	29.6	33.5	37.6	41.8
45						0	2.9	5.9	9	12.3	15.6	19	22.6	26.3	30.2	34.2	38.3
50							0	3	6	9.2	12.5	15.9	19.4	23	26.8	30.8	34.8
55								0	3	6.1	9.3	12.7	16.1	19.7	23.5	27.3	31.3
60									0	3.1	6.2	9.5	12.9	16.4	20.1	23.9	27.9
65										0	3.1	6.3	9.7	13.2	16.8	20.5	24.4
70											0	3.2	6.5	9.9	13.4	17.1	20.9
75												0	3.2	6.6	10.1	13.7	17.4
80													0	3.3	6.7	10.3	13.9
85														0	3.4	6.8	10.5
90															0	3.4	7
95																0	3.5
100																	0

* Final concentration of ammonium sulphate at 0°C.

Initial concentration of ammonium sulphate at 0°C.

A2. Appendix for Chapter 3

A2.1. List of Primers

Table A2.1. Primers for the amplification of both VH and VL of IV.3 MoAb (IgG_{2b})

Heavy Chain Variable Region

Forward Primer

5'-GGCCAGTGGATAGTCAGATGGGGGTGTCGTTTTGGC-3'

Reverse Primer

5'-GAGGTGAAGCTGGTGGAGTC-3'

Light Chain Variable Region

Forward Primer

5'-GGATACAGTTGGTGCAGCATC-3'

Reverse Primer

5'-GATATTGTGATGACGCAGGCT-3'

Table A2.2. Primers for construction of STG1 (Heavy Chain).

Extension for Heavy Chain Variable Region

Forward Primer-F1 (EcoRV site, Start Codon, PelB bacterial secretion signal).

5'-GCC GATATC ATG
AAGTCTCTGATTACTCCTATTACTGCTGGTCTGCTGCTGGC
ACTGTCTCAGCCGCTGCTGGCGAGGTGAAGCTGGTGGAGTC-3'

Reverse Primer-R1 (for long linker extension).

5'-
GCCACCGAGCTGCCACCGCCACCGGAACCACCGCCACCAGAACCACCACC
A CCTGAGGAGACGGTGACTGAGG-3'

Reverse Primer-R1.2 (for short linker extension).

5'-
GCCACCGGAACCACCGCCACCAGAACCACCACCCTGAGGAGACGGTGAC
T GAGG-3'

Table A2.3. Primers for construction of STG1 (Light Chain).**Extension for Light Chain Variable Region**

Forward Primer-F2 (for long linker extension).

5'-

GGTGGCAGCTCCGGTGGCGGCAGCGGCGGTGGCGGCTCCGGTGGCGGCGGT
TCTGATATTGTGATGACGCAGGC-3'

Forward Primer-F2.2 (for short linker extension).

5'-GGCGGTGGTTCCGGTGGCGGTGGCAGCGGATATTGTGATGACGCAGGC-3'

Reverse Primer-R2 (EcoRI site, Stop Codon, cMyc and FLAG tag).

5'-GC GAATTC TTA CAGATCTTCCTCAGAGATCAGTTTCTGCTC
ACCTTTGTCATCA TCGTCTTTGTAATCAGCCCGTTTCAGTTCCAGCT-3'**Table A2.4. Primers for creating long linker in STG1.****Extension for Heavy Chain Variable Region**

Reverse Primer (additional segment for long linker extension)

Paired Primer (F1)

5'-GCCGCCACCGCCGCTGCCGCCACCGGAGCTGCCACC-3'

Extension for Light Chain Variable Region

Forward Primer (additional segment for long linker extension)

5'-GGCGGTGGTTCCGGTGGCGGTGGCAGCTCCGGTGGC-3' Paired Primer (R2)

A2.2. Sequence Analysis of Variable Regions of IV.3 MoAb with Murine Germline Sequence

VH

```

IV.3 VH 1  EVKLVESGPELKKPGETVKISCKASGYTFTNYGMNWVKQAPGKGLKWMG 49
VH9.12 1  QIQ..Q..... 49

IV.3 VH 50 WLNTYTGESIYPDDFKGRFAFSSETSASTAYLQINNLLKNEPMATYFCAR 98
VH9.12 50 .I.....PT.A.....L..... 98

```

VL

```

IV.3 VL 1  DIVMTQAAPSVPVTPGESVSI SCRSSKSL LHTNGNTYLHWFLQRPQSPQLLIY 54
hf24 1  .....S.....Y..... 54

IV.3 VL 55 RMSVLAGV PDRFSGSGSGTAFTLSISRVEAEDVGVFYCMQHLEYP 100
hf24 55 ...N.....R.....Y..... 100

```

Figure A2.1. Sequence analysis of the variable regions of IV.3 MoAb against murine germline gene sequence from the NCBI murine database. (.) indicates residues identical to the aligned germline gene sequence. CDRs are shaded.

A2.3. Purification of IV.3 MoAb

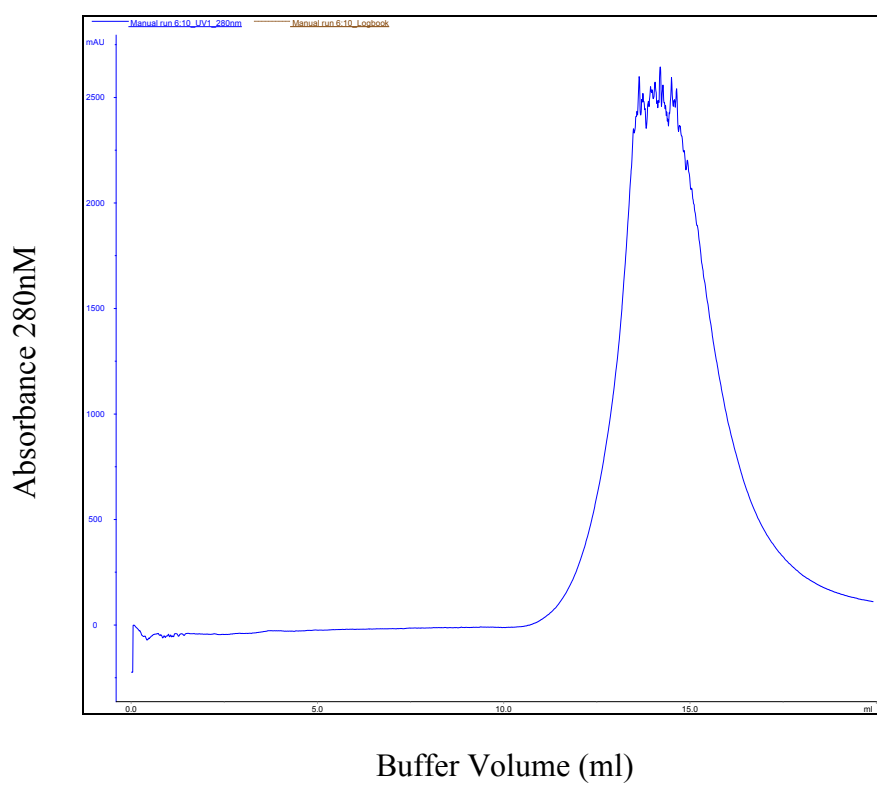


Figure A2.2. Elution profile of IV.3 MoAb purified from supernatant of hybridoma culture.

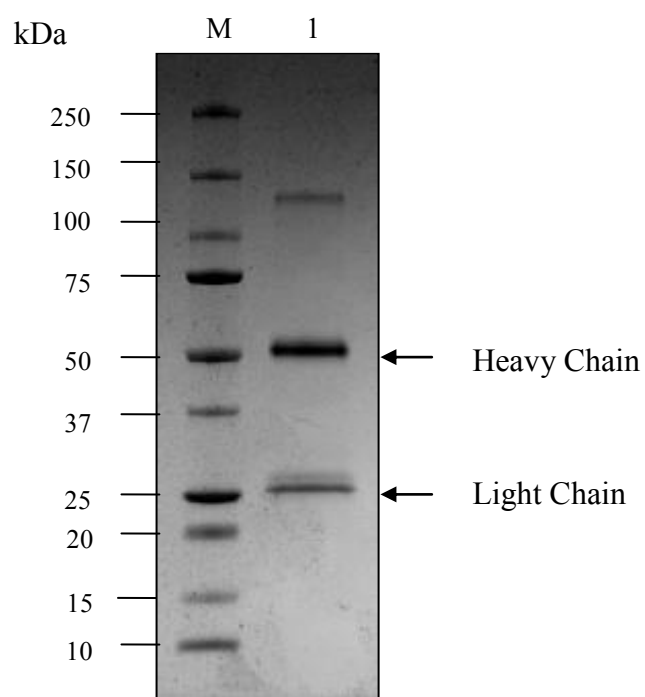


Figure A2.3. Coomassie Blue Staining of purified IV.3 MoAb. Lane M: Molecular weight marker (Bio-Rad); Lane 1: Purified IV.3 MoAb (Heavy Chain, 50 kDa; Light Chain, 24 kDa).

A2.4. Purification of Total HIT IgG

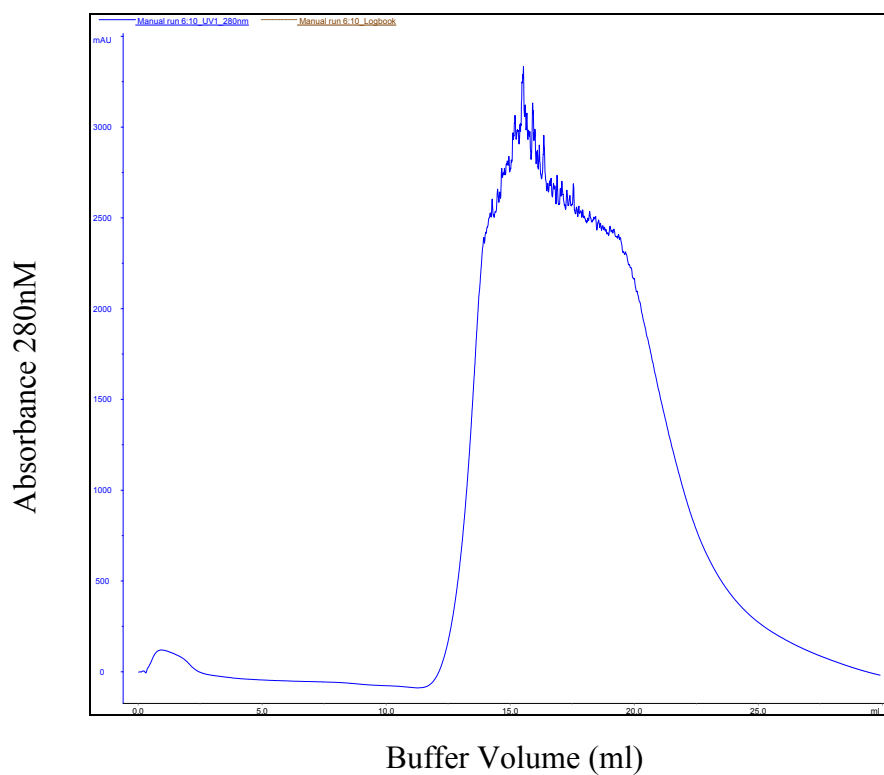


Figure A2.4. Elution profile of Total HIT IgG purified from patient HIT serum. Purification was conducted using Protein G Agarose resin. A total of 43.2mg of Total HIT IgG was purified from 11.5ml of HIT serum.

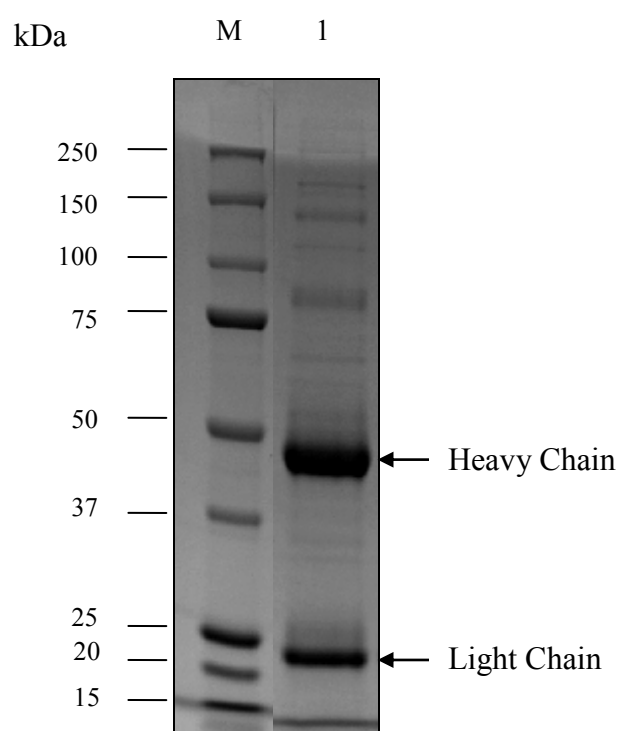


Figure A2.5. Coomassie Blue Staining of purified Total HIT IgG. Lane M: Molecular weight marker (Bio-Rad); Lane 1: Purified HIT IgG (Heavy Chain, 50 kDa; Light Chain, 24 kDa).

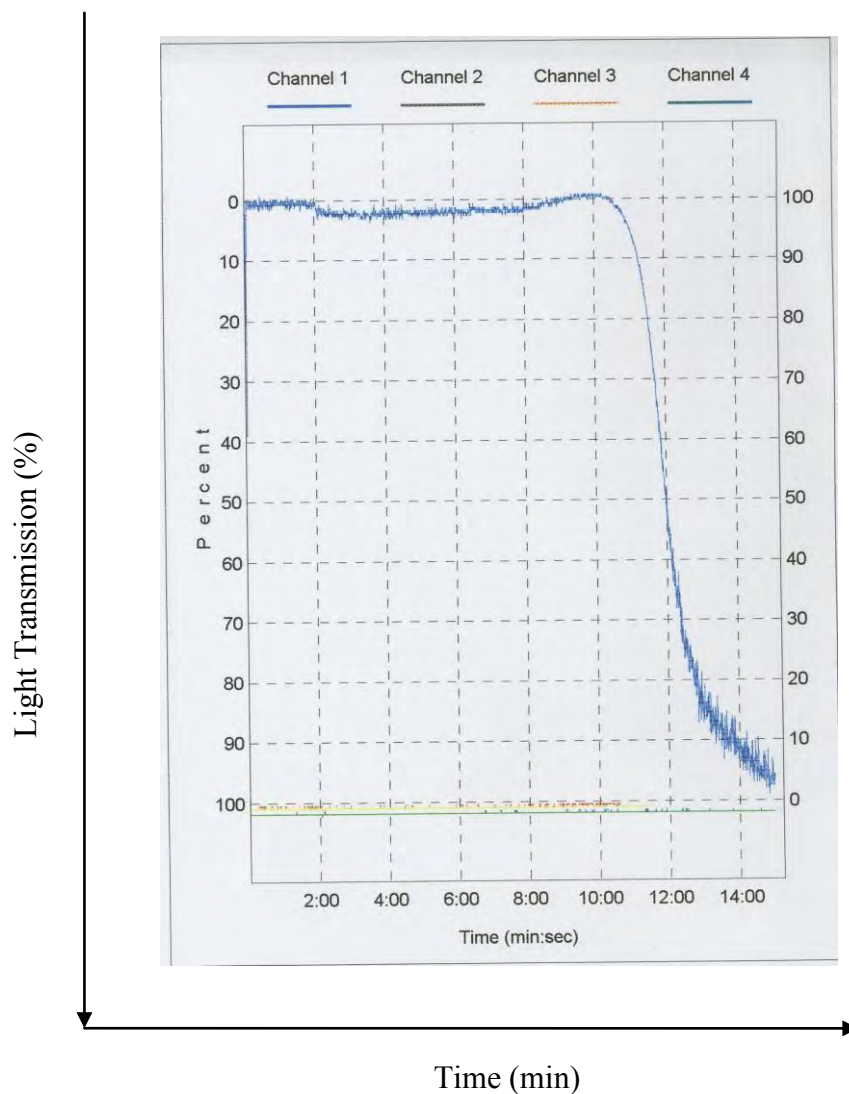


Figure A2.6. Platelet aggregation plot generated after induction with Total HIT IgG (500 μ g/ml). The total blood volume of mice is 6-8% per 100g of body weight (214), for the NOD/SCID mice used in this project, the average weight was approximately 25g, thus total blood volume would be 1.5-2ml. Based on this, we therefore decided to test two different concentrations of HIT IgG at 1.5mg and 0.75mg.

A3. Appendix for Chapter 4

A3.1. Sequence Analysis of Variable Regions of IV.3 MoAb with Human Germline Gene Sequence

VH

IV.3 VH	1	EVKLVESGPELKKPGETVKISCKASGYTFTNYGMN	WVKQAPGKGLKWMG	49
IGHV7-81*01	1	Q.Q..Q..H.V.Q..AS..V.....S..T.....P....Q..E...		49
IV.3 VH	50	WLNTYTGESIYPDDFKGRFAFSSETSASTAYLQINN	LKNEDMATYFCAR	98
IGHV7-81*01	50	.F.....NPT.AQG.T...V..MD.....SS..A....M.Y...		98

VL

IV.3 VL	1	DIVMTQAAPSVPVTPGESVVISCRSSKSL	LHTNGNTYLH	39
IGKV2-18*01	1TP..L..N...PA.....Q....S..Y....		39
IV.3 VL	40	WFLQRPQSPQLLIYRMSV	LASGVPDRFSGSGS	GTAFTLSISRVEAE 86
IGKV2-18*01	40	.Y..K.....V.NHL.....SD...K..W....		86
IV.3 VL	87	DVGVFYCMQHLEYP		100
IGKV2-18*01	87Y....ATQF.		100

Figure A3.1. Sequence analysis of the variable regions of IV.3 MoAb against human germline gene sequence from the IMGT database. (.) indicates residues identical to the aligned germline gene sequence. CDRs are shaded.

A3.2. Sequence Analysis of Humanized Variable Regions (STG2) with Human Germline Gene Sequence

VH

huVH	1	EVQLVESGPGPLVKPGETLKI	SCKGSGYSFTNYGMN	WVRQAPGKGLEWVS	49
IGHV7-4-1*01	1	Q.....Q..SE.K...ASV.V...A...T..S.A.....Q.....MG			49
huVH	50	WLNTYTGESIYPDDFKGRFV	FSLDTSVSTAYLQICSLKAEDTAVYYCAR		98
IGHV7-4-1*01	50	.I..N..NPT.AQG.T.....			98

VL

huVL	1	DIVMTQSPLSLPVT	PGEPASISCRSSKSL	LLHTNGNTYLH	39
IGKV2-28*01	1Q.....S..YN..D		39
huVL	40	WYLQKPGQSPQLLIYR	MSVLAGVPDRFSGSGSGTDFTLKISRVEAE		86
IGKV2-28*01	40LG.NR.....			86
huVL	87	DGVVYYCMQHLEYP			100
IGKV2-28*01	87A.QT.			100

Figure A3.2. Sequence analysis of the humanized variable regions STG2 against human germline gene sequence from the IMGT database. (.) indicates residues identical to the aligned germline gene sequence. CDRs are shaded.

A3.3. Sequence Analysis of Humanized Variable Regions (STG3) with Human Germline Gene Sequence

VH

```

huVH          1  EVKLVESGPELKKPGETVKISCKASGYTFTNYGMNWKQAPGKGLKWMG 49
IGHV7-4-1*02  1  Q.Q..Q..S.....AS..V.....S.A....R....Q..E... 49

huVH          50  WLNTYTGESIYPDDFKGRFAFSLETSASTAYLQINNLSKEDTATYFCAR 98
IGHV7-4-1*02  50  .I..N..NPT.AQG.T...V...D..V.....SS..A....V.Y... 98

```

VL

```

huVL          1  DIVMTQAPPSVPVTPGESVSISSCRSSKSLHTNGNTYLH 39
IGKV2-18*01  1  .....T...L..N...PA.....Q....S..Y.... 39

huVL          40  WFLQRPQSPRLLIYRMSVLASGVPDRFSGSGSGTAFTLISIRVEAE 86
IGKV2-18*01  40  .Y..K.....Q.....V.NHL.....SD...K..W.... 86

huVL          87  DVGVYYCMQHLEYP 100
IGKV2-18*01  87  .....ATQF. 100

```

Figure A3.3. Sequence analysis of the humanized variable regions (STG3) against human germline gene sequence from the IMGT database. (.) indicates residues identical to the aligned germline gene sequence. CDRs are shaded.

A3.4. Purification of PF4

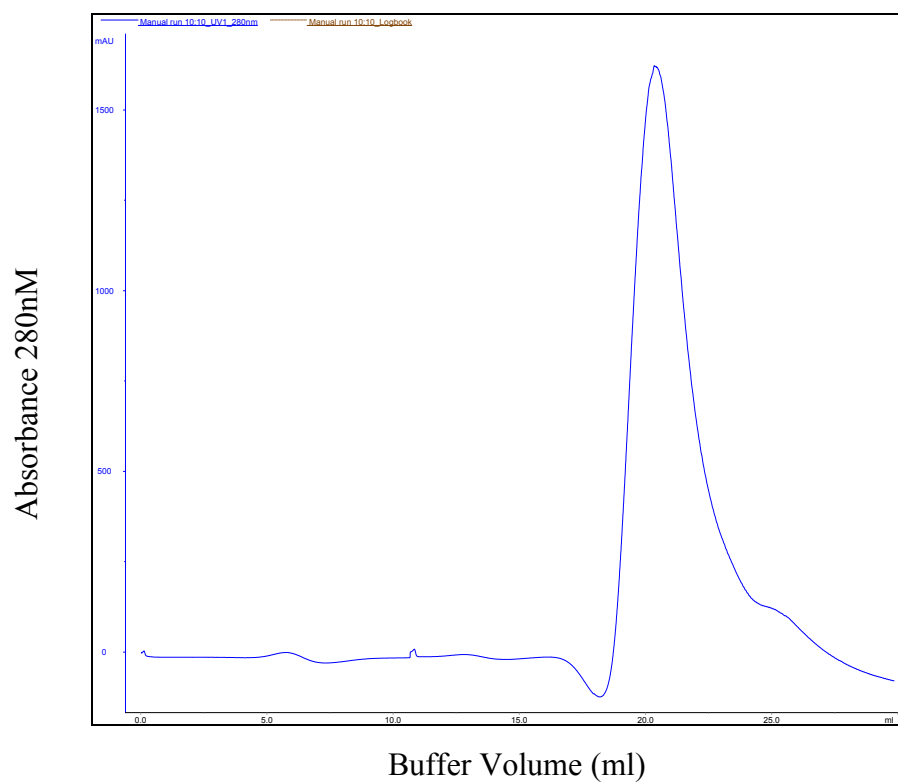


Figure A3.6. Elution profile of crude PF4 extract from expired human platelets. Purification was first conducted on Heparin Sepharose Column before proceeding to Gel filtration Column.

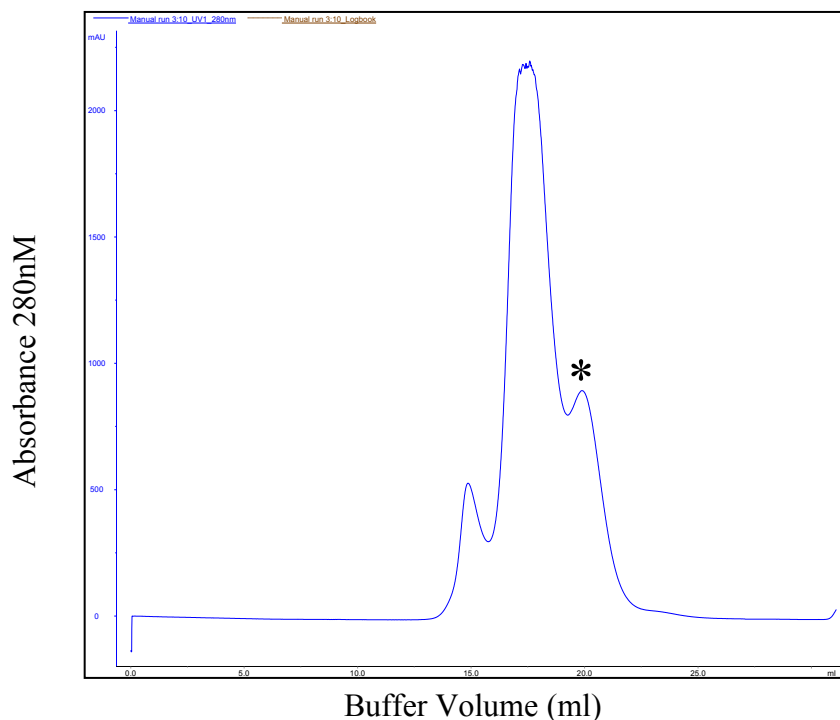


Figure A3.7. Gel filtration elution profile of crude PF4 (*) extract (1st Round). Purification was conducted on gel filtration column. The peak noted with asterisk was collected and subjected to a 2nd round of purification.

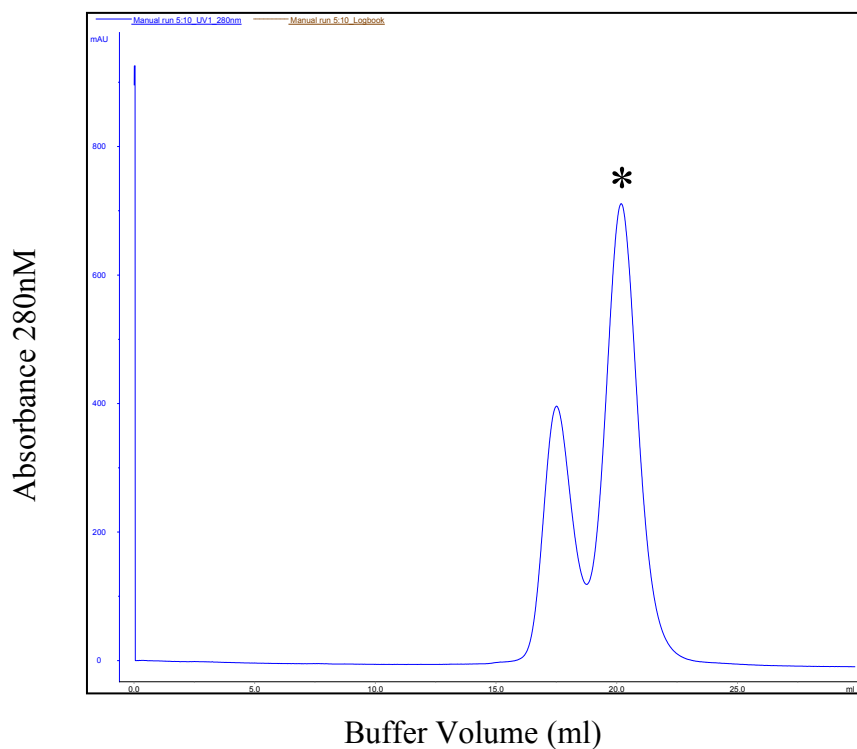


Figure A3.8. Gel filtration elution profile of crude PF4 (*) extract (2nd Round). Purification was conducted on gel filtration column. The peak noted with asterisk was collected and subjected to a 3rd round of purification.

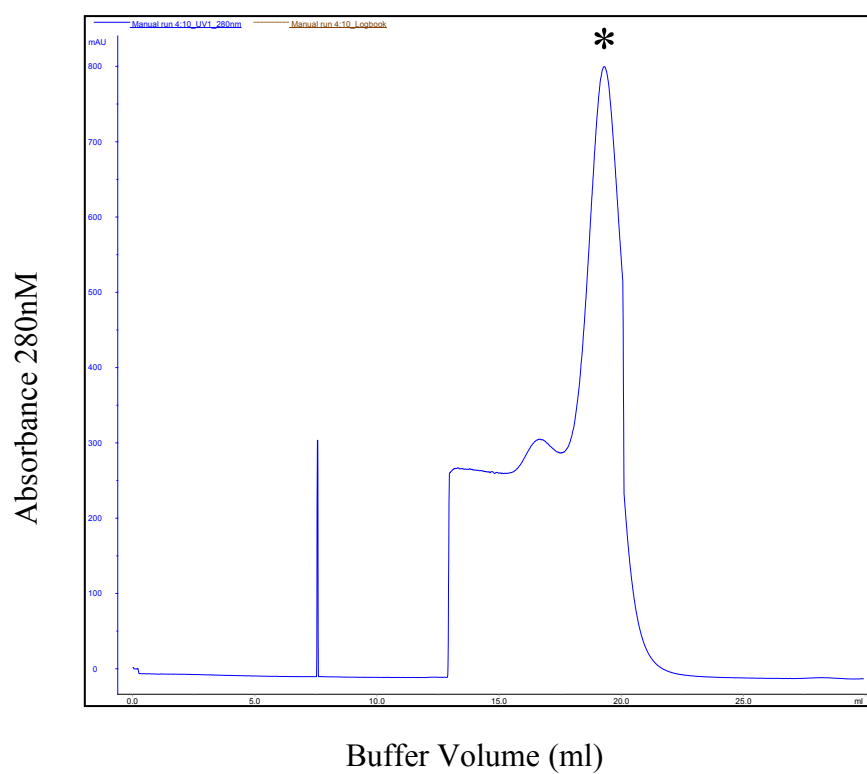


Figure A3.9. Gel filtration elution profile of crude PF4 (*) extract (3rd Round). Purification was conducted on gel filtration column. The peak noted with asterisk was collected.

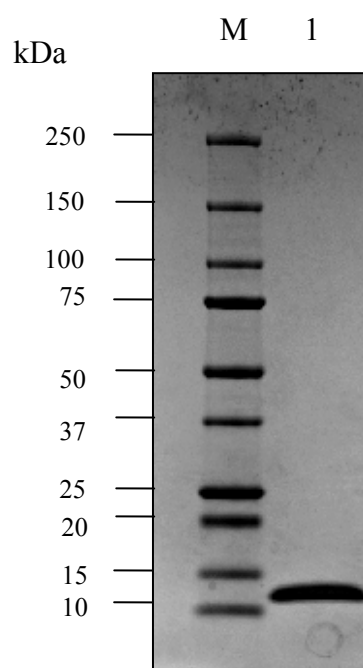


Figure A3.10. Coomassie Blue Staining of purified PF4. Lane M: Molecular weight marker (Bio-Rad); Lane 1: Purified PF4 (7.7kDa).

References

1. McLean J. The Thromboplastic Action of Cephalin. *Am. J. Physiol.* -- Legacy Content. 1916;41(2):250-7.
2. Howell WH, Holt E. Two New Factors in Blood Coagulation—Heparin and Proantithrombin. *Am. J. Physiol.* -- Legacy Content. 1918;47(3):328-41.
3. Mason EC. A note on the use of heparin in blood transfusion. *J. Lab. Clin. Med.* 1924;10:203-6.
4. Hedenius P, Wilander O. The influence of intravenous injections of heparin in man on the time of coagulation. *Acta Med. Scand.* 1936;88:443-9.
5. Jorpes E. The chemistry of heparin. *Biochem. J.* 1935;29(8):1817-30.
6. Crafoord C. Preliminary report on postoperative treatment with heparin as a prevention of thrombosis. *Acta Chir. Scand.* 1937;79:407.
7. Murray D, Jaques L, Perrett T, Best C. Heparin and the thrombosis of veins following injury. *Surgery.* 1937;2:163.
8. Liu J, Lindhardt RJ. A Simpler, Safer Synthetic Heparin. Chapel Hill, North Carolina, America. : University of North Carolina, Eschelmann School of Pharmacy; 2011 [cited 2012 31/10/2012]. Available from: <http://pharmacy.unc.edu/heparin2011>.
9. Hirsh J, Anand SS, Halperin JL, Fuster V. Guide to Anticoagulant Therapy: Heparin : A Statement for Healthcare Professionals From the American Heart Association. *Arterioscler. Thromb. Vasc. Biol.* 2001;21(7):e9-e33.
10. Neri Serneri GG, Modesti PA, Gensini GF, Branzi A, Melandri G, Poggesi L, Rostagno C, Tamburini C, Carnovali M, Magnani B. Randomised comparison of subcutaneous heparin, intravenous heparin, and aspirin in unstable angina. *Studio Epopoquine Sottocutanea nell'Angina Instabile (SESAIR) Refrattorie Group. Lancet.* 1995;345(8959):1201-4.
11. Nowak G. Heparin-induced thrombocytopenia (HIT II)-A drug-associated autoimmune disease. *Thromb. Haemost.* 2009;102:887-91.
12. Ouseph R, Ward RA. Anticoagulation for intermittent hemodialysis. *Semin. Dial.* 2000;13(3):181-7.
13. Basu D, Gallus A, Hirsh J, Cade J. A Prospective Study of the Value of Monitoring Heparin Treatment with the Activated Partial Thromboplastin Time. *N. Engl. J. Med.* 1972;287(7):324-7.
14. Li W, Johnson DJD, Esmon CT, Huntington JA. Structure of the antithrombin-thrombin-heparin ternary complex reveals the antithrombotic mechanism of heparin. *Nat. Struct. Mol. Biol.* 2004;11(9):857-62.
15. Brieger DB, Mak K-H, Kottke-Marchant K, Topol EJ. Heparin-Induced Thrombocytopenia. *J. Am. Coll. Cardiol.* 1998;31(7):1449-59.
16. Frangos SG, Chen AH, Sumpio B. Vascular drugs in the new millennium. *J. Am. Coll. Surg.* 2000;191(1):76-92.
17. Kakkar VV, Djazaeri B, Fok J, Fletcher M, Scully MF, Westwick J. Low-Molecular-Weight Heparin And Prevention Of Postoperative Deep Vein Thrombosis. *Br. Med. J. (Clin. Res. Ed.).* 1982;284(6313):375-9.
18. Gray E, Mulloy B, Barrowcliffe TW. Heparin and low-molecular-weight heparin. *Thromb. Haemost.* 2008;99:807-18.
19. Nutescu E, Racine E. Traditional versus modern anticoagulant strategies: Summary of the literature. *Am. J. Health. Syst. Pharm.* 2002;59(20) Supplement(6):S7-S14.
20. Copley A, Robb T. Studies on platelets III: The effect of heparin in vivo on the platelet count in mice and dogs. *Am. J. Clin. Pathol.* 1942;12:563-70.

21. Natelson EA, Lynch EC, Alfrey CP, Jr., Gross JB. Heparin-induced thrombocytopenia. An unexpected response to treatment of consumption coagulopathy. *Ann. Intern. Med.* 1969;71(6):1121-5.
22. Weismann RE, Tobin RW. Arterial embolism occurring during systemic heparin therapy. *AMA Arch. Surg.* 1958;76(2):219-25; discussion 25-7.
23. Roberts B, Rosato E. A cause of arterial emboli. *Surgery.* 1964;55:803-8.
24. Rhodes GR, Dixon RH, Silver D. Heparin induced thrombocytopenia with thrombotic and hemorrhagic manifestations. *Surg. Gynecol. Obstet.* 1973;136(3):409-16.
25. Rhodes GR, Dixon RH, Silver D. Heparin induced thrombocytopenia: eight cases with thrombotic-hemorrhagic complications. *Ann. Surg.* 1977;186(6):752-8.
26. Fratantoni JC, Pollet R, Gralnick HR. Heparin-induced thrombocytopenia: confirmation of diagnosis with in vitro methods. *Blood.* 1975;45(3):395-401.
27. Nelson JC, Lerner RG, Goldstein R, Cagin NA. Heparin-induced thrombocytopenia. *Arch. Intern. Med.* 1978;138(4):548-52.
28. Cimo PL, Moake JL, Weinger RS, Ben-Menachem YB, Khalil KG. Heparin-induced thrombocytopenia: association with a platelet aggregating factor and arterial thromboses. *Am. J. Hematol.* 1979;6(2):125-33.
29. Babcock RB, Dumper CW, Scharfman WB. Heparin-induced immune thrombocytopenia. *N. Engl. J. Med.* 1976;295(5):237-41.
30. Bell WR, Tomasulo PA, Alving BM, Duffy TP. Thrombocytopenia occurring during the administration of heparin. A prospective study in 52 patients. *Ann. Intern. Med.* 1976;85(2):155-60.
31. Chong BH, Pitney WR, Castaldi PA. Heparin-Induced Thrombocytopenia: Association of Thrombotic Complications with Heparin-Dependent IgG Antibody that Induces Thromboxane Synthesis and Platelet Aggregation. *The Lancet.* 1982;320(8310):1246-9.
32. Chong BH, Berndt MC. Heparin-induced thrombocytopenia. *Blut.* 1989;58(2):53-7.
33. Burgess JK, Chong BH. The platelet proaggregating and potentiating effects of unfractionated heparin, low molecular weight heparin and heparinoid in intensive care patients and healthy controls. *Eur. J. Haematol.* 1997;58(4):279-85.
34. Chong BH. Heparin-induced thrombocytopenia. *J. Thromb. Haemost.* 2003;1(7):1471-8.
35. Chong BH. Heparin-induced thrombocytopenia. *Aust. N. Z. J. Med.* 1992;22:145-52.
36. Warkentin TE, Roberts RS, Hirsh J, Kelton JG. An Improved Definition of Immune Heparin-Induced Thrombocytopenia in Postoperative Orthopedic Patients. *Arch. Intern. Med.* 2003;163(20):2518-24.
37. Rice L, Attisha WK, Drexler A, Francis JL. Delayed-Onset Heparin-Induced Thrombocytopenia. *Ann. Intern. Med.* 2002;136(3):210-5.
38. Warkentin TE, Kelton JG. Delayed-Onset Heparin-Induced Thrombocytopenia and Thrombosis. *Ann. Intern. Med.* 2001;135(7):502-6.
39. Warkentin TE. Clinical picture of heparin-induced thrombocytopenia. In: Warkentin TE, Greinacher A, editors. *Heparin-induced thrombocytopenia*. 3rd ed. New York: Marcel Dekker, Inc. ; 2004. p. 53-106.
40. Kelton JG, Warkentin TE. Heparin-induced thrombocytopenia: a historical perspective. *Blood.* 2008;112(7):2607-16.
41. Warkentin TE, Kelton JG. A 14-year study of heparin-induced thrombocytopenia. *Am. J. Med.* 1996;101(5):502-7.

42. Greinacher A, Farner B, Kroll H, Kohlmann T, Warkentin TE, Eichler P. Clinical features of heparin-induced thrombocytopenia including risk factors for thrombosis. A retrospective analysis of 408 patients. *Thromb. Haemost.* 2005;94(1):132-5.
43. Warkentin TE, Elavathil LJ, Hayward CPM, Johnston MA, Russett JI, Kelton JG. The Pathogenesis of Venous Limb Gangrene Associated with Heparin-Induced Thrombocytopenia. *Ann. Intern. Med.* 1997;127(9):804-12.
44. Warkentin TE. Heparin-Induced Thrombocytopenia: IgG-Mediated Platelet Activation, Platelet Microparticle Generation, and Altered Procoagulant/Anticoagulant Balance in the Pathogenesis of Thrombosis and Venous Limb Gangrene Complicating Heparin-Induced Thrombocytopenia *Transfus. Med. Rev.* 1996;10(4):249-58.
45. Lewis BE, Wallis DE, Leya F, Hursting MJ, Kelton JG. Argatroban anticoagulation in patients with heparin-induced thrombocytopenia. *Arch. Intern. Med.* 2003;163(15):1849-56.
46. Hong AP, Cook DJ, Sigouin CS, Warkentin TE. Central venous catheters and upper-extremity deep-vein thrombosis complicating immune heparin-induced thrombocytopenia. *Blood.* 2003;101(8):3049-51.
47. Rosenberger LH, Smith PW, Sawyer RG, Hanks JB, Adams RB, Hedrick TL. Bilateral adrenal hemorrhage: The unrecognized cause of hemodynamic collapse associated with heparin-induced thrombocytopenia *. *Crit. Care Med.* 2011;39(4):833-8.
48. Warkentin TE. The diagnosis and management of heparin-induced thrombocytopenia. In: John JB, editor. *The Vein Book*. Burlington: Academic Press; 2007. p. 395-403.
49. Ojeda E, Perez MdC, Mataix R, Arbelo A, Jimenez S, Campo C, Balda I. Skin Necrosis with a Low Molecular Weight Heparin. *Br. J. Haematol.* 1992;82(3):620.
50. Warkentin TE. Heparin-induced skin lesions. *Br. J. Haematol.* 1996;92(2):494-7.
51. Amiral J, Bridey F, Dreyfus M, Vissoc AM, Fressinaud E, Wolf M, Meyer D. Platelet factor 4 complexed to heparin is the target for antibodies generated in heparin induced thrombocytopenia. *Thromb. Haemost.* 1992;68(1):95-6.
52. Visentin G, Ford S, Scott J, Aster RH. Antibodies from patients with heparin-induced thrombocytopenia/thrombosis are specific for platelet factor 4 complexed with heparin or bound to endothelial cells. *J. Clin. Invest.* 1994;93:81-8.
53. Rucinski B, Niewiarowski S, James P, Walz D, Budzynski A. Antiheparin proteins secreted by human platelets. purification, characterization, and radioimmunoassay. *Blood.* 1979;53(1):47-62.
54. Deuel TF, Keim PS, Farmer M, Heinrikson RL. Amino acid sequence of human platelet factor 4. *Proc. Natl. Acad. Sci. U. S. A.* 1977;74(6):2256-8.
55. Mayo KH, Chen MJ. Human platelet factor 4 monomer-dimer-tetramer equilibria investigated by proton NMR spectroscopy. *Biochemistry (Mosc.)*. 1989;28(24):9469-78.
56. Davoren A, Aster R. Heparin-induced thrombocytopenia and thrombosis. *Am. J. Hematol.* 2006;81(1):36-44.
57. Warkentin TE, Aird WC, Rand JH. Platelet-Endothelial Interactions: Sepsis, HIT, and Antiphospholipid Syndrome. *Hematology*. 2003;2003(1):497-519.
58. Warkentin TE, Dager WE. Heparin-Induced Thrombocytopenia. In: Hari GG, Robert JL, Charles AH, editors. *Chemistry and Biology of Heparin and Heparan Sulfate*. Amsterdam: Elsevier Science; 2005. p. 673-97.
59. Suh J-S, Aster RH, Visentin GP. Antibodies From Patients With Heparin-Induced Thrombocytopenia/Thrombosis Recognize Different Epitopes on Heparin: Platelet Factor 4. *Blood.* 1998;91(3):916-22.

60. Ziporen L, Li ZQ, Park KS, Sabnekar P, Liu WY, Arepally G, Shoenfeld Y, Kieber-Emmons T, Cines DB, Poncz M. Defining an Antigenic Epitope on Platelet Factor 4 Associated With Heparin-Induced Thrombocytopenia. *Blood*. 1998;92(9):3250-9.
61. Arepally GM, Kamei S, Park KS, Kamei K, Li ZQ, Liu W, Siegel DL, Kisiel W, Cines DB, Poncz M. Characterization of a murine monoclonal antibody that mimics heparin-induced thrombocytopenia antibodies. *Blood*. 2000;95(5):1533-40.
62. Li ZQ, Liu W, Park KS, Sachais BS, Arepally GM, Cines DB, Poncz M. Defining a second epitope for heparin-induced thrombocytopenia/thrombosis antibodies using KKO, a murine HIT-like monoclonal antibody. *Blood*. 2002;99(4):1230-6.
63. Maccarana M, Lindahl U. Mode of interaction between platelet factor 4 and heparin. *Glycobiology*. 1993;3(3):271-7.
64. Rauova L, Poncz M, McKenzie SE, Reilly MP, Arepally G, Weisel JW, Nagaswami C, Cines DB, Sachais BS. Ultralarge complexes of PF4 and heparin are central to the pathogenesis of heparin-induced thrombocytopenia. *Blood*. 2005;105(1):131-8.
65. Visentin GP, Moghaddam M, Beery SE, McFarland JG, Aster RH. Heparin is not required for detection of antibodies associated with heparin-induced thrombocytopenia/thrombosis. *J. Lab. Clin. Med.* 2001;138(1):22-31.
66. Visentin GP. Heparin-Induced Thrombocytopenia: Molecular Pathogenesis. *Thromb. Haemost.* 1999;82(2):448-56.
67. Rauova L, Zhai L, Kowalska MA, Arepally GM, Cines DB, Poncz M. Role of platelet surface PF4 antigenic complexes in heparin-induced thrombocytopenia pathogenesis: diagnostic and therapeutic implications. *Blood*. 2006;107(6):2346-53.
68. Newman PM, Chong BH. Further characterization of antibody and antigen in heparin-induced thrombocytopenia. *Br. J. Haematol.* 1999;107(2):303-9.
69. Denomme GA, Warkentin TE, Horsewood P, Sheppard JAI, Warner MN, Kelton JG. Activation of platelets by sera containing igg1 heparin-dependent antibodies: an explanation for the predominance of the Fc[gamma]r11a "low responder" (his131) gene in patients with heparin-induced thrombocytopenia. *J. Lab. Clin. Med.* 1997;130(3):278-84.
70. Kelton J, Sheridan D, Santos A, Smith J, Steeves K, Smith C, Brown C, Murphy W. Heparin-induced thrombocytopenia: laboratory studies. *Blood*. 1988;72(3):925-30.
71. Chong BH, Fawaz I, Chesterman CN, Berndt MC. Heparin-induced thrombocytopenia: mechanism of interaction of the heparin-dependent antibody with platelets. *Br. J. Haematol.* 1989;73(2):235-40.
72. Kelton J, Smith J, Warkentin T, Hayward C, Denomme G, Horsewood P. Immunoglobulin G from patients with heparin-induced thrombocytopenia binds to a complex of heparin and platelet factor 4. *Blood*. 1994;83(11):3232-9.
73. Horne MK, Alkins BR. Platelet binding of IgG from patients with heparin-induced thrombocytopenia. *J. Lab. Clin. Med.* 1996;127(5):435-42.
74. Newman PM, Chong BH. Heparin-induced thrombocytopenia: new evidence for the dynamic binding of purified anti-PF4-heparin antibodies to platelets and the resultant platelet activation. *Blood*. 2000;96(1):182-7.
75. Warkentin T, Hayward C, Boshkov L, Santos A, Sheppard J, Bode A, Kelton J. Sera from patients with heparin-induced thrombocytopenia generate platelet-derived microparticles with procoagulant activity: an explanation for the thrombotic complications of heparin-induced thrombocytopenia. *Blood*. 1994;84(11):3691-9.

76. Tardy-Poncet B, Piot M, Chapelle C, France G, Campos L, Garraud O, Decousus H, Mismetti P, Tardy B. Thrombin generation and heparin-induced thrombocytopenia. *J. Thromb. Haemost.* 2009;7(9):1474-81.
77. Chong BH. Heparin-induced thrombocytopenia. In: Michelson MDAD, Barry SC, editors. *Platelets (Second Edition)*. Burlington: Academic Press; 2007. p. 861-86.
78. Blank M, Shoenfeld Y, Tavor S, Praprotnik S, Boffa MC, Weksler B, Walenga MJ, Amiral J, Eldor A. Anti-platelet factor 4/heparin antibodies from patients with heparin-induced thrombocytopenia provoke direct activation of microvascular endothelial cells. *Int. Immunol.* 2002;14(2):121-9.
79. Pouplard C, Iochmann S, Renard B, Herault O, Colombat P, Amiral J, Gruel Y. Induction of monocyte tissue factor expression by antibodies to heparin-platelet factor 4 complexes developed in heparin-induced thrombocytopenia. *Blood.* 2001;97(10):3300-2.
80. Arepally GM, Mayer IM. Antibodies from patients with heparin-induced thrombocytopenia stimulate monocytic cells to express tissue factor and secrete interleukin-8. *Blood.* 2001;98(4):1252-4.
81. Scholl PR. Immunoglobulin Fc receptors in clinical immunology: Introduction. *Clin. Immunol. Newsletter.* 1996;16(9):121-4.
82. Karas S, Rosse W, Kurlander R. Characterization of the IgG-Fc receptor on human platelets. *Blood.* 1982;60(6):1277-82.
83. Carlsson LE, Santoso S, Baurichter G, Kroll H, Papenberg S, Eichler P, Westerdaal NAC, Kiefel V, van de Winkel JGJ, Greinacher A. Heparin-Induced Thrombocytopenia: New Insights Into the Impact of the Fc γ RIIa-R-H131 Polymorphism. *Blood.* 1998;92(5):1526-31.
84. Clark M, Clarkson S, Ory P, Stollman N, Goldstein I. Molecular basis for a polymorphism involving Fc receptor II on human monocytes. *J. Immunol.* 1989;143(5):1731-4.
85. Warmerdam PA, van de Winkel JG, Gosselin EJ, Capel PJ. Molecular basis for a polymorphism of human Fc gamma receptor II (CD32). *J. Exp. Med.* 1990;172(1):19-25.
86. Clark MR, Stuart SG, Kimberly RP, Ory PA, Goldstein IM. A single amino acid distinguishes the high-responder from the low-responder form of Fc receptor II on human monocytes. *Eur. J. Immunol.* 1991;21(8):1911-6.
87. Warmerdam P, van de Winkel J, Vlug A, Westerdaal N, Capel P. A single amino acid in the second Ig-like domain of the human Fc gamma receptor II is critical for human IgG2 binding. *J. Immunol.* 1991;147(4):1338-43.
88. Burgess JK, Lindeman R, Chesterman CN, Chong BH. Single amino acid mutation of FC γ receptor is associated with the development of heparin-induced thrombocytopenia. *Br. J. Haematol.* 1995;91(3):761-6.
89. Arepally G, McKenzie SE, Jiang X-M, Poncz M, Cines DB. Fc γ RIIA H/R131 Polymorphism, Subclass-Specific IgG Anti-Heparin/Platelet Factor 4 Antibodies and Clinical Course in Patients With Heparin-Induced Thrombocytopenia and Thrombosis. *Blood.* 1997;89(2):370-5.
90. Bachelot-Loza C, Saffroy R, Lasne D, Chatellier G, Aiach M, Rendu F. Importance of the Fc γ RIIa-Arg/His-131 Polymorphism in Heparin-induced Thrombocytopenia Diagnosis. *Thromb. Haemost.* 1998;79:523-8.
91. Chacko GW, Brandt JT, Coggeshall KM, Anderson CL. Phosphoinositide 3-Kinase and p72 Noncovalently Associate with the Low Affinity Fc Receptor on Human Platelets through an Immunoreceptor Tyrosine-based Activation Motif. *J. Biol. Chem.* 1996;271(18):10775-81.

92. Lambert MP, Rauova L, Bailey M, Sola-Visner MC, Kowalska MA, Poncz M. Platelet factor 4 is a negative autocrine in vivo regulator of megakaryopoiesis: clinical and therapeutic implications. *Blood*. 2007;110(4):1153-60.
93. Collier BS, Shattil SJ. The GPIIb/IIIa (integrin alphaIIb beta3) odyssey: a technology-driven saga of a receptor with twists, turns, and even a bend. *Blood*. 2008;112(8):3011-25.
94. Smyth SS, McEver RP, Weyrich AS, Morrell CN, Hoffman MR, Arepally GM, French PA, Dauerman HL, Becker RC, For The Platelet Colloquium P. Platelet functions beyond hemostasis. *J. Thromb. Haemost.* 2009;7(11):1759-66.
95. Boilard E, Nigrovic PA, Larabee K, Watts GF, Coblyn JS, Weinblatt ME, Massarotti EM, Remold-O'Donnell E, Farndale RW, Ware J, Lee DM. Platelets amplify inflammation in arthritis via collagen-dependent microparticle production. *Science*. 2010;327(5965):580-3.
96. Leslie M. Cell biology. Beyond clotting: the powers of platelets. *Science*. 2010;328(5978):562-4.
97. Ezumi Y, Shindoh K, Tsuji M, Takayama H. Physical and functional association of the Src family kinases Fyn and Lyn with the collagen receptor glycoprotein VI-Fc receptor gamma chain complex on human platelets. *J. Exp. Med.* 1998;188(2):267-76.
98. Quek LS, Pasquet JM, Hers I, Cornall R, Knight G, Barnes M, Hibbs ML, Dunn AR, Lowell CA, Watson SP. Fyn and Lyn phosphorylate the Fc receptor gamma chain downstream of glycoprotein VI in murine platelets, and Lyn regulates a novel feedback pathway. *Blood*. 2000;96(13):4246-53.
99. Kasirer-Friede A, Cozzi MR, Mazzucato M, De Marco L, Ruggeri ZM, Shattil SJ. Signaling through GP Ib-IX-V activates alpha IIb beta 3 independently of other receptors. *Blood*. 2004;103(9):3403-11.
100. Watson SP, Auger JM, McCarty OJ, Pearce AC. GPVI and integrin alphaIIb beta3 signaling in platelets. *J. Thromb. Haemost.* 2005;3(8):1752-62.
101. Yin H, Stojanovic A, Hay N, Du X. The role of Akt in the signaling pathway of the glycoprotein Ib-IX-induced platelet activation. *Blood*. 2008;111(2):658-65.
102. Gilio K, Munnix IC, Mangin P, Cosemans JM, Feijge MA, van der Meijden PE, Olieslagers S, Chrzanowska-Wodnicka MB, Lillian R, Schoenwaelder S, Koyasu S, Sage SO, Jackson SP, Heemskerk JW. Non-redundant roles of phosphoinositide 3-kinase isoforms alpha and beta in glycoprotein VI-induced platelet signaling and thrombus formation. *J. Biol. Chem.* 2009;284(49):33750-62.
103. Xiong JP, Stehle T, Goodman SL, Arnaout MA. New insights into the structural basis of integrin activation. *Blood*. 2003;102(4):1155-9.
104. Li Z, Delaney MK, O'Brien KA, Du X. Signaling during platelet adhesion and activation. *Arterioscler. Thromb. Vasc. Biol.* 2010;30(12):2341-9.
105. Adam F, Guillin MC, Jandrot-Perrus M. Glycoprotein Ib-mediated platelet activation. A signalling pathway triggered by thrombin. *Eur. J. Biochem.* 2003;270(14):2959-70.
106. Dean WL, Lee MJ, Cummins TD, Schultz DJ, Powell DW. Proteomic and functional characterisation of platelet microparticle size classes. *Thromb. Haemost.* 2009;102(4):711-8.
107. Reilly MP, Taylor SM, Hartman NK, Arepally GM, Sachais BS, Cines DB, Poncz M, McKenzie SE. Heparin-induced thrombocytopenia/thrombosis in a transgenic mouse model requires human platelet factor 4 and platelet activation through FcγRIIA. *Blood*. 2001;98(8):2442-7.

108. Reilly MP, Taylor SM, Franklin C, Sachais BS, Cines DB, Williams KJ, McKenzie SE. Prothrombotic factors enhance heparin-induced thrombocytopenia and thrombosis in vivo in a mouse model. *J. Thromb. Haemost.* 2006;4(12):2687-94.
109. Martel N, Lee J, Wells PS. Risk for heparin-induced thrombocytopenia with unfractionated and low-molecular-weight heparin thromboprophylaxis: a meta-analysis. *Blood.* 2005;106(8):2710-5.
110. Greinacher A, Eichler P, Lietz T, Warkentin TE. Replacement of unfractionated heparin by low-molecular-weight heparin for postorthopedic surgery antithrombotic prophylaxis lowers the overall risk of symptomatic thrombosis because of a lower frequency of heparin-induced thrombocytopenia. *Blood.* 2005;106(8):2921-2.
111. Warkentin TE, Sheppard J-AI, Horsewood P, Simpson PJ, Moore JC, Kelton JG. Impact of the patient population on the risk for heparin-induced thrombocytopenia. *Blood.* 2000;96(5):1703-8.
112. Matsuo T, Tomaru T, Kario K, Hirokawa T. Incidence of heparin-PF4 complex antibody formation and heparin-induced thrombocytopenia in acute coronary syndrome. *Thromb. Res.* 2005;115(6):475-81.
113. Mattioli AV, Bonetti L, Zennaro M, Ambrosio G, Mattioli G. Heparin/PF4 antibodies formation after heparin treatment: Temporal aspects and long-term follow-up. *Am. Heart J.* 2009;157(3):589-95.
114. Junqueira DR, Perini E, Penholati RR, Carvalho MG. Unfractionated heparin versus low molecular weight heparin for avoiding heparin-induced thrombocytopenia in postoperative patients. *Cochrane Database Syst. Rev.* 2012;9:CD007557.
115. Warkentin TE, Sheppard J-AI, Sigouin CS, Kohlmann T, Eichler P, Greinacher A. Gender imbalance and risk factor interactions in heparin-induced thrombocytopenia. *Blood.* 2006;108(9):2937-41.
116. Lubenow N, Hinz P, Thomaschewski S, Lietz T, Vogler M, Ladwig A, Junger M, Nauck M, Schellong S, Wander K, Engel G, Ekkernkamp A, Greinacher A. The severity of trauma determines the immune response to PF4/heparin and the frequency of heparin-induced thrombocytopenia. *Blood.* 2010;115(9):1797-803.
117. Greinacher A, Alban S, Omer-Adam MA, Weitschies W, Warkentin TE. Heparin-induced thrombocytopenia: A stoichiometry-based model to explain the differing immunogenicities of unfractionated heparin, low-molecular-weight heparin, and fondaparinux in different clinical settings. *Thromb. Res.* 2008;122(2):211-20.
118. Lhermusier T, Van Rottem J, Garcia C, Xuereb JM, Ragab A, Martin V, Gratacap MP, SiÉ P, Payrastre B. The Syk-kinase inhibitor R406 impairs platelet activation and monocyte tissue factor expression triggered by heparin-PF4 complex directed antibodies. *J. Thromb. Haemost.* 2011;9(10):2067-76.
119. Ahmad S, Haas S, Hoppensteadt DA, Lietz H, Reid U, Bender N, Messmore HL, Misselwitz F, Bacher P, Gaikwad BS, Jeske WP, Walenga JM, Fareed J. Differential effects of clivarin and heparin in patients undergoing hip and knee surgery for the generation of anti-heparin-platelet factor 4 antibodies. *Thromb. Res.* 2002;108(1):49-55.
120. Lindhoff-Last E, Gerdson F, Ackermann H, Bauersachs R. Determination of heparin-platelet factor 4-IgG antibodies improves diagnosis of heparin-induced thrombocytopenia. *Br. J. Haematol.* 2001;113(4):886-90.
121. Lindhoff-Last E, Nakov R, Misselwitz F, Breddin H-K, Bauersachs R. Incidence and clinical relevance of heparin-induced antibodies in patients with deep vein thrombosis treated with unfractionated or low-molecular-weight heparin. *Br. J. Haematol.* 2002;118(4):1137-42.

122. Fausett MB, Vogtlander M, Lee RM, Esplin MS, Branch DW, Rodgers GM, Silver RM. Heparin-induced thrombocytopenia is rare in pregnancy. *Am. J. Obstet. Gynecol.* 2001;185(1):148-52.
123. Prandoni P, Siragusa S, Girolami B, Fabris F, Group ftBI. The incidence of heparin-induced thrombocytopenia in medical patients treated with low-molecular-weight heparin: a prospective cohort study. *Blood.* 2005;106(9):3049-54.
124. Krauel K, Pötschke C, Weber C, Kessler W, Fürll B, Ittermann T, Maier S, Hammerschmidt S, Bröker BM, Greinacher A. Platelet factor 4 binds to bacteria, inducing antibodies cross-reacting with the major antigen in heparin-induced thrombocytopenia. *Blood.* 2011;117(4):1370-8.
125. Greinacher A, Holtfreter B, Krauel K, Gätke D, Weber C, Ittermann T, Hammerschmidt S, Kocher T. Association of natural anti-platelet factor 4/heparin antibodies with periodontal disease. *Blood.* 2011;118(5):1395-401.
126. Olah Z, Kerenyi A, Kappelmayer J, Schlammadinger A, Razso K, Boda Z. Rapid-onset heparin-induced thrombocytopenia without previous heparin exposure. *Platelets.* 2012;23(6):495-8.
127. Warkentin TE, Kelton JG. Temporal aspects of heparin-induced thrombocytopenia. *N. Engl. J. Med.* 2001;344(17):1286-92.
128. Warkentin TE. Drug-induced immune-mediated thrombocytopenia--from purpura to thrombosis. *N. Engl. J. Med.* 2007;356(9):891-3.
129. Warkentin TE. Heparin-induced thrombocytopenia: pathogenesis and management. *Br. J. Haematol.* 2003;121(4):535-55.
130. Sheridan D, Carter C, Kelton J. A diagnostic test for heparin-induced thrombocytopenia. *Blood.* 1986;67(1):27-30.
131. Greinacher A, Michels I, Kiefel V, Mueller-Eckhardt C. A rapid and sensitive test for diagnosing heparin-associated thrombocytopenia. *Thromb. Haemost.* 1991;66(6):734-6.
132. Warkentin TE, Sheppard J-AI, Moore JC, Moore KM, Sigouin CS, Kelton JG. Laboratory testing for the antibodies that cause heparin-induced thrombocytopenia: How much class do we need? *J. Lab. Clin. Med.* 2005;146(6):341-6.
133. Gratacap M-P, Héroult J-P, Viala C, Ragab A, Savi P, Herbert J-M, Chap H, Plantavid M, Payrastre B. FcγRIIA requires a Gi-dependent pathway for an efficient stimulation of phosphoinositide 3-kinase, calcium mobilization, and platelet aggregation. *Blood.* 2000;96(10):3439-46.
134. Juhl D, Eichler P, Lubenow N, Strobel U, Wessel A, Greinacher A. Incidence and clinical significance of anti-PF4/heparin antibodies of the IgG, IgM, and IgA class in 755 consecutive patient samples referred for diagnostic testing for heparin-induced thrombocytopenia. *Eur. J. Haematol.* 2006;76(5):420-6.
135. Law DA, Nannizzi-Alaimo L, Ministri K, Hughes PE, Forsyth J, Turner M, Shattil SJ, Ginsberg MH, Tybulewicz VLJ, Phillips DR. Genetic and Pharmacological Analyses of Syk Function in α IIb β 3 Signaling in Platelets. *Blood.* 1999;93(8):2645-52.
136. Warkentin TE, Sheppard JI, Moore JC, Kelton JG. The use of well-characterized sera for the assessment of new diagnostic enzyme-immunoassays for the diagnosis of heparin-induced thrombocytopenia. *J. Thromb. Haemost.* 2010;8(1):216-8.
137. Denys B, Stove V, Philippé J, Devreese K. A clinical-laboratory approach contributing to a rapid and reliable diagnosis of heparin-induced thrombocytopenia. *Thromb. Res.* 2008;123(1):137-45.
138. Bakchoul T, Giptner A, Najaoui A, Bein G, Santoso S, Sachs UJH. Prospective evaluation of PF4/heparin immunoassays for the diagnosis of heparin-induced thrombocytopenia. *J. Thromb. Haemost.* 2009;7(8):1260-5.

139. Cuker A, Arepally G, Crowther MA, Rice L, Datko F, Hook K, Propert KJ, Kuter DJ, Ortel TL, Konkle BA, Cines DB. The HIT Expert Probability (HEP) Score: a novel pre-test probability model for heparin-induced thrombocytopenia based on broad expert opinion. *J. Thromb. Haemost.* 2010;8(12):2642-50.
140. Warkentin TE, Kelton JG. Interaction of heparin with platelets, including heparin-induced thrombocytopenia. Bounameaux H, editor. New York: Marcel Dekker Inc; 1994. 75-127 p.
141. Warkentin TE, Hayward CP, Smith CA, Kelly PM, Kelton JG. Determinants of donor platelet variability when testing for heparin-induced thrombocytopenia. *J. Lab. Clin. Med.* 1992;120(3):371-9.
142. Lubenow N, Hinz P, Thomaschewski S, Lietz T, Vogler M, Ladwig A, Jünger M, Nauck M, Schellong S, Wander K, Engel G, Ekkernkamp A, Greinacher A. The severity of trauma determines the immune response to PF4/heparin and the frequency of heparin-induced thrombocytopenia. *Blood.* 2010;115(9):1797-803.
143. Elalamy I, Tardy-Poncet B, Mulot A, de Maistre E, Pouplard C, Nguyen P, Cleret B, Gruel Y, Lecompte T, Tardy B, group GHs. Risk factors for unfavorable clinical outcome in patients with documented heparin-induced thrombocytopenia. *Thromb. Res.* 2009;124(5):554-9.
144. Chong B, Gallus A, Cade J, Magnani H, Manoharan A, Oldmeadow M, Arthur C, Rickard K, Gallo J, Lloyd J, Seshadri P, Chesterman C. Prospective Randomised Open-label Comparison of Danaparoid with Dextran 70 in the Treatment of Heparin-induced Thrombocytopenia with Thrombosis. *Thromb. Haemost.* 2001;86:1170-5.
145. Vun CM, Evans S, Chong BH. Cross-reactivity study of low molecular weight heparins and heparinoid in heparin-induced thrombocytopenia. *Thromb. Res.* 1996;81(5):525-32.
146. Kuo K, Kovacs M. Successful treatment of heparin induced thrombocytopenia (HIT) with fondaparinux. *Thromb. Haemost.* 2005;93(5):999-1000.
147. Liu H, Fleming NW, Moore PG. Anticoagulation for patients with heparin-induced thrombocytopenia using recombinant hirudin during cardiopulmonary bypass. *J. Clin. Anesth.* 2002;14(6):452-5.
148. Saravanan P, Rege K, Falter F. Use of Continuous Venovenous Hemofiltration for Reversal of Anticoagulation With Lepirudin Post-Cardiopulmonary Bypass in a Patient With Heparin-Induced Thrombocytopenia After Heart Transplantation. *J. Cardiothorac. Vasc. Anesth.* 2007;21(2):269-72.
149. Koster A, Dyke CM, Aldea G, Smedira NG, McCarthy Ii HL, Aronson S, Hetzer R, Avery E, Spiess B, Lincoff AM. Bivalirudin During Cardiopulmonary Bypass in Patients With Previous or Acute Heparin-Induced Thrombocytopenia and Heparin Antibodies: Results of the CHOOSE-ON Trial. *The Annals of Thoracic Surgery.* 2007;83(2):572-7.
150. Cuker A, Cines DB. How I treat heparin-induced thrombocytopenia. *Blood.* 2012;119(10):2209-18.
151. Levy J, Hursting M. Heparin-induced Thrombocytopenia, a Prothrombotic Disease. *Hematol. Oncol. Clin. North Am.* 2007;21:65-88.
152. Spinler SA, Dager W. Overview of heparin-induced thrombocytopenia. *Am. J. Health. Syst. Pharm.* 2003;60(20) Supplement(5):S5-S11.
153. Lewis BE, Wallis DE, Berkowitz SD, Matthai WH, Fareed J, Walenga JM, Bartholomew J, Sham R, Lerner RG, Zeigler ZR, Rustagi PK, Jang IK, Rifkin SD, Moran J, Hursting MJ, Kelton JG. Argatroban anticoagulant therapy in patients with heparin-induced thrombocytopenia. *Circulation.* 2001;103(14):1838-43.

154. Battistelli S, Genovese A, Gori T. Heparin-induced thrombocytopenia in surgical patients. *Am. J. Surg.* 2010;199(1):43-51.
155. Bittl JA, Strony J, Brinker JA, Ahmed WH, Meckel CR, Chaitman BR, Maraganore J, Deutsch E, Adelman B. Treatment with Bivalirudin (Hirulog) as Compared with Heparin during Coronary Angioplasty for Unstable or Postinfarction Angina. *N. Engl. J. Med.* 1995;333(12):764-9.
156. Koster A, Dyke CM, Aldea G, Smedira NG, McCarthy Li HL, Aronson S, Hetzer R, Avery E, Spiess B, Lincoff AM. Bivalirudin During Cardiopulmonary Bypass in Patients With Previous or Acute Heparin-Induced Thrombocytopenia and Heparin Antibodies: Results of the CHOOSE-ON Trial. *Ann. Thorac. Surg.* 2007;83(2):572-7.
157. Dyke CM, Aldea G, Koster A, Smedira N, Avery E, Aronson S, Spiess BD, Lincoff AM. Off-Pump Coronary Artery Bypass With Bivalirudin for Patients With Heparin-Induced Thrombocytopenia or Antiplatelet Factor Four/Heparin Antibodies. *Ann. Thorac. Surg.* 2007;84(3):836-9.
158. Franchini M, Mannucci PM. A new era for anticoagulants. *Eur. J. Intern. Med.* 2009;20(6):562-8.
159. Mavrakanas T, Bounameaux H. The potential role of new oral anticoagulants in the prevention and treatment of thromboembolism. *Pharmacol. Ther.* 2011;130(1):46-58.
160. Krauel K, Hackbarth C, Füll B, Greinacher A. Heparin-induced thrombocytopenia: in vitro studies on the interaction of dabigatran, rivaroxaban, and low-sulfated heparin, with platelet factor 4 and anti-PF4/heparin antibodies. *Blood.* 2012;119(5):1248-55.
161. Arepally GM, Ortel TL. Heparin-Induced Thrombocytopenia. *N. Engl. J. Med.* 2006;355(8):809-17.
162. Warkentin TE, Greinacher A, Koster A, Lincoff AM. Treatment and prevention of heparin-induced thrombocytopenia: American College of Chest Physicians Evidence-Based Clinical Practice Guidelines (8th Edition). *Chest.* 2008;133(6 Suppl):340S-80S.
163. Fryer A, Huang Y-C, Rao G, Jacoby D, Mancilla E, Whorton R, Piantadosi CA, Kennedy T, Hoidal J. Selective O-Desulfation Produces Nonanticoagulant Heparin that Retains Pharmacological Activity in the Lung. *J. Pharmacol. Exp. Ther.* 1997;282(1):208-19.
164. Thourani VH, Brar SS, Kennedy TP, Thornton LR, Watts JA, Ronson RS, Zhao Z-Q, Sturrock AL, Hoidal JR, Vinten-Johansen J. Nonanticoagulant heparin inhibits NF- κ B activation and attenuates myocardial reperfusion injury. *Am. J. Physiol. Heart Circ. Physiol.* 2000;278(6):H2084-H93.
165. Rao NV, Argyle B, Xu X, Reynolds PR, Walenga JM, Prechel M, Prestwich GD, MacArthur RB, Walters BB, Hoidal JR, Kennedy TP. Low anticoagulant heparin targets multiple sites of inflammation, suppresses heparin-induced thrombocytopenia, and inhibits interaction of RAGE with its ligands. *Am. J. Physiol. Cell Physiol.* 2010;299(1):C97-C110.
166. Poole A, Gibbins JM, Turner M, van Vugt MJ, van de Winkel JGJ, Saito T, Tybulewicz VLJ, Watson SP. The Fc receptor γ -chain and the tyrosine kinase Syk are essential for activation of mouse platelets by collagen. *EMBO J.* 1997;16(9):2333-41.
167. Reilly MP, Sinha U, André P, Taylor SM, Pak Y, DeGuzman FR, Nanda N, Pandey A, Stolla M, Bergmeier W, McKenzie SE. PRT-060318, a novel Syk inhibitor, prevents heparin-induced thrombocytopenia and thrombosis in a transgenic mouse model. *Blood.* 2011;117(7):2241-6.
168. Yanagi S, Inatome R, Takano T, Yamamura H. Syk expression and novel function in a wide variety of tissues. *Biochem. Biophys. Res. Commun.* 2001;288(3):495-8.

169. Bajpai M, Chopra P, Dastidar SG, Ray A. Spleen tyrosine kinase: a novel target for therapeutic intervention of rheumatoid arthritis. *Expert Opin. Investig. Drugs*. 2008;17(5):641-59.
170. Podolanczuk A, Lazarus AH, Crow AR, Grossbard E, Bussel JB. Of mice and men: an open-label pilot study for treatment of immune thrombocytopenic purpura by an inhibitor of Syk. *Blood*. 2009;113(14):3154-60.
171. Bahjat FR, Pine PR, Reitsma A, Cassafer G, Baluom M, Grillo S, Chang B, Zhao FF, Payan DG, Grossbard EB, Daikh DI. An orally bioavailable spleen tyrosine kinase inhibitor delays disease progression and prolongs survival in murine lupus. *Arthritis Rheum*. 2008;58(5):1433-44.
172. Braselmann S, Taylor V, Zhao H, Wang S, Sylvain C, Baluom M, Qu K, Herlaar E, Lau A, Young C, Wong BR, Lovell S, Sun T, Park G, Argade A, Jurcevic S, Pine P, Singh R, Grossbard EB, Payan DG, Masuda ES. R406, an Orally Available Spleen Tyrosine Kinase Inhibitor Blocks Fc Receptor Signaling and Reduces Immune Complex-Mediated Inflammation. *J. Pharmacol. Exp. Ther*. 2006;319(3):998-1008.
173. Looney R, Abraham G, Anderson C. Human monocytes and U937 cells bear two distinct Fc receptors for IgG. *J. Immunol*. 1986;136(5):1641-7.
174. Thai LM, Ashman LK, Harbour SN, Hogarth PM, Jackson DE. Physical proximity and functional interplay of PECAM-1 with the Fc receptor FcγRIIa on the platelet plasma membrane. *Blood*. 2003;102(10):3637-45.
175. Polgar J, Eichler P, Greinacher A, Clemetson KJ. Adenosine Diphosphate (ADP) and ADP Receptor Play a Major Role in Platelet Activation/Aggregation Induced by Sera From Heparin-Induced Thrombocytopenia Patients. *Blood*. 1998;91(2):549-54.
176. Ramsland PA, Farrugia W, Bradford TM, Sardjono CT, Esparon S, Trist HM, Powell MS, Tan PS, Cendron AC, Wines BD, Scott AM, Hogarth PM. Structural Basis for FcγRIIa Recognition of Human IgG and Formation of Inflammatory Signaling Complexes. *J. Immunol*. 2011;187(6):3208-17.
177. Kohler G, Milstein C. Continuous cultures of fused cells secreting antibody of predefined specificity. *Nature*. 1975;256:495-7.
178. Miller RA, Maloney DG, Warnke R, Levy R. Treatment of B-Cell Lymphoma with Monoclonal Anti-Idiotype Antibody. *N. Engl. J. Med*. 1982;306(9):517-22.
179. Jaffers GJ, Fuller TC, Cosimi AB, Russell PS, Winn HJ, Colvin RB. Anti-Idiotypic and Non-Anti-Idiotypic Antibodies to OKT3 Arising Despite Intense Immunosuppression. *Transplantation*. 1986;41(5):572-8.
180. Meeker T, Lowder J, Maloney D, Miller R, Thielemans K, Warnke R, Levy R. A clinical trial of anti-idiotype therapy for B cell malignancy. *Blood*. 1985;65(6):1349-63.
181. Khazaeli MB, Conry RM, LoBuglio AF. Human Immune Response to Monoclonal Antibodies. *J. Immunother. Emphasis Tumor Immunol*. 1994;15(1):42-52.
182. Neuberger MS, Williams GT, Mitchell EB, Jouhal SS, Flanagan JG, Rabbitts TH. A hapten-specific chimaeric IgE antibody with human physiological effector function. *Nature*. 1985;314(6008):268-70.
183. Morrison SL, Johnson MJ, Herzenberg LA, Oi VT. Chimeric human antibody molecules: mouse antigen-binding domains with human constant region domains. *Proc. Natl. Acad. Sci. U. S. A*. 1984;81(21):6851-5.
184. Boulianne GL, Hozumi N, Shulman MJ. Production of functional chimaeric mouse/human antibody. *Nature*. 1984;312(5995):643-6.
185. Jones PT, Dear PH, Foote J, Neuberger MS, Winter G. Replacing the complementarity-determining regions in a human antibody with those from a mouse. *Nature*. 1986;321(6069):522-5.

186. Lupo L, Panzera P, Tandoi F, Carbotta G, Giannelli G, Santantonio T, Rendina M, Gentile A, Memeo V. Basiliximab Versus Steroids in Double Therapy Immunosuppression in Liver Transplantation: A Prospective Randomized Clinical Trial. *Transplantation*. 2008;86(7):925-31.
187. Chan AC, Carter PJ. Therapeutic antibodies for autoimmunity and inflammation. *Nat. Rev. Immunol.* 2010;10(5):301-16.
188. Blattman JN, Greenberg PD. Cancer Immunotherapy: A Treatment for the Masses. *Science*. 2004;305(5681):200-5.
189. Meissner HCM, Welliver RCM, Chartrand SAM, Law BJM, Weisman LEM, Dorkin HLM, Rodriguez WJM. Immunoprophylaxis with palivizumab, a humanized respiratory syncytial virus monoclonal antibody, for prevention of respiratory syncytial virus infection in high risk infants: a consensus opinion. *Pediatr. Infect. Dis. J.* 1999;18(3):223-31.
190. Reichert JM. Antibody-based therapeutics to watch in 2011. *mAbs*. 2011;3(1):76-99.
191. Zhang C. Hybridoma Technology for the Generation of Monoclonal Antibodies. In: Proetzel G, Ebersbach H, editors. *Antibody Methods and Protocols. Methods in Molecular Biology*. 901: Humana Press; 2012. p. 117-35.
192. Chowdhury PS, Wu H. Tailor-made antibody therapeutics. *Methods*. 2005;36(1):11-24.
193. Holliger P, Hudson PJ. Engineered antibody fragments and the rise of single domains. *Nat. Biotechnol.* 2005;23(9):1126-36.
194. Ward ES, Gussow D, Griffiths AD, Jones PT, Winter G. Binding activities of a repertoire of single immunoglobulin variable domains secreted from *Escherichia coli*. *Nature*. 1989;341(6242):544-6.
195. Bird RE, Hardman KD, Jacobson JW, Johnson S, Kaufman BM, Lee S-M, Lee T, Sharon HP, Riordan GS, Whitlow M. Single-Chain Antigen-Binding Proteins. *Science*. 1988;242(4877):423-6.
196. Pucca MB, Bertolini TB, Barbosa JE, Galina SVR, Porto GS. Therapeutic monoclonal antibodies: scFv patents as a marker of a new class of potential biopharmaceuticals. *Braz. J. Pharm. Sci.* 2011;47:31-8.
197. Sambrook J, Fritsch EF, Maniatis T. *Molecular Cloning: A Laboratory Manual* 3rd ed. Cold Spring Harbor, NY: Cold Spring Harbor Laboratory; 2001.
198. Kiefer F, Arnold K, Kunzli M, Bordoli L, Schwede T. The SWISS-MODEL Repository and associated resources. *Nucleic Acids Res.* 2009;37(Database issue):D387-92.
199. Kelley LA, Sternberg MJ. Protein structure prediction on the Web: a case study using the Phyre server. *Nat. Protoc.* 2009;4(3):363-71.
200. Schrödinger L. *The PyMOL Molecular Graphics System, Version 1.5.0.4* Schrödinger, LLC. 2010.
201. Kügler M, Stein C, Schwenkert M, Saul D, Vockentanz L, Huber T, Wetzel SK, Scholz O, Plückthun A, Honegger A, Fey GH. Stabilization and humanization of a single-chain Fv antibody fragment specific for human lymphocyte antigen CD19 by designed point mutations and CDR-grafting onto a human framework. *Protein Eng. Des. Sel.* 2009;22(3):135-47.
202. Ewert S, Honegger A, Plückthun A. Stability improvement of antibodies for extracellular and intracellular applications: CDR grafting to stable frameworks and structure-based framework engineering. *Methods*. 2004;34(2):184-99.
203. Jung S, Plückthun A. Improving in vivo folding and stability of a single-chain Fv antibody fragment by loop grafting. *Protein Eng.* 1997;10(8):959-66.

204. Honegger A, Pluckthun A. Yet another numbering scheme for immunoglobulin variable domains: an automatic modeling and analysis tool. *J. Mol. Biol.* 2001;309(3):657-70.
205. Wan L, Zeng L, Chen L, Huang Q, Li S, Lu Y, Li Y, Cheng J, Lu X. Expression, purification, and refolding of a novel immunotoxin containing humanized single-chain fragment variable antibody against CTLA4 and the N-terminal fragment of human perforin. *Protein Expr. Purif.* 2006;48(2):307-13.
206. Chen L-H, Huang Q, Wan L, Zeng L-Y, Li S-F, Li Y-P, Lu X-F, Cheng J-Q. Expression, purification, and in vitro refolding of a humanized single-chain Fv antibody against human CTLA4 (CD152). *Protein Expr. Purif.* 2006;46(2):495-502.
207. Sinacola JR, Robinson AS. Rapid refolding and polishing of single-chain antibodies from *Escherichia coli* inclusion bodies. *Protein Expr. Purif.* 2002;26(2):301-8.
208. Umetsu M, Tsumoto K, Hara M, Ashish K, Goda S, Adschiri T, Kumagai I. How Additives Influence the Refolding of Immunoglobulin-folded Proteins in a Stepwise Dialysis System. *J. Biol. Chem.* 2003;278(11):8979-87.
209. Guo J-Q, Li Q-M, Zhou J-Y, Zhang G-P, Yang Y-Y, Xing G-X, Zhao D, You S-Y, Zhang C-Y. Efficient recovery of the functional IP10-scFv fusion protein from inclusion bodies with an on-column refolding system. *Protein Expr. Purif.* 2006;45(1):168-74.
210. Hwang PM, Choy W-Y, Lo EI, Chen L, Forman-Kay JD, Raetz CRH, Privé GG, Bishop RE, Kay LE. Solution structure and dynamics of the outer membrane enzyme PagP by NMR. *Proc. Natl. Acad. Sci. U. S. A.* 2002;99(21):13560-5.
211. Knowles TJ, Finka R, Smith C, Lin Y-P, Dafforn T, Overduin M. Membrane Proteins Solubilized Intact in Lipid Containing Nanoparticles Bounded by Styrene Maleic Acid Copolymer. *J. Am. Chem. Soc.* 2009;131(22):7484-5.
212. Newman PM, Swanson RL, Chong BH. Heparin-induced Thrombocytopenia: IgG Binding to PF4-Heparin Complexes in the Fluid Phase and Cross-reactivity with Low Molecular Weight Heparin and Heparinoid. *Thromb. Haemost.* 1998;80:292-7.
213. Willing A, Garbuzova-Davis S, Sanberg P, Saporta S. Routes of Stem Cell Administration in the Adult Rodent. In: Weiner L, editor. *Neural Stem Cells. Methods in Molecular Biology™*. 438: Humana Press; 2008. p. 383-401.
214. Hoff J. Methods of Blood Collection in the Mouse. *Lab Anim.* 2000;29(10):47-53.
215. Boylan B, Berndt MC, Kahn ML, Newman PJ. Activation-independent, antibody-mediated removal of GPVI from circulating human platelets: development of a novel NOD/SCID mouse model to evaluate the in vivo effectiveness of anti-human platelet agents. *Blood.* 2006;108(3):908-14.
216. Newman PJ, Aster R, Boylan B. Human platelets circulating in mice: applications for interrogating platelet function and survival, the efficacy of antiplatelet therapeutics, and the molecular basis of platelet immunological disorders. *J. Thromb. Haemost.* 2007;5:305-9.
217. Tsurushita N, Vásquez M. Humanization of Monoclonal Antibodies. In: Tasuku H, Frederick WA, Michael SN, editors. *Molecular Biology of B Cells*. Burlington: Academic Press; 2003. p. 533-45.
218. Marks JD. Chapter 32 - Monoclonal Antibodies from Display Libraries. In: Tasuku H, Frederick WA, Michael S, Neuberger A2 - Tasuku Honjo FWA, Michael SN, editors. *Molecular Biology of B Cells*. Burlington: Academic Press; 2003. p. 511-31.
219. Kuus-Reichel K, Grauer LS, Karavodin LM, Knott C, Krusemeier M, Kay NE. Will immunogenicity limit the use, efficacy, and future development of therapeutic monoclonal antibodies? *Clin. Diagn. Lab. Immunol.* 1994;1(4):365-72.

220. Huston JS, Levinson D, Mudgett-Hunter M, Tai MS, Novotný J, Margolies MN, Ridge RJ, Brucoleri RE, Haber E, Crea R. Protein engineering of antibody binding sites: recovery of specific activity in an anti-digoxin single-chain Fv analogue produced in *Escherichia coli*. *Proc. Natl. Acad. Sci. U. S. A.* 1988;85(16):5879-83.
221. Huston JS, McCartney J, Tai M-S, Mottola-hartshorn C, Jin D, Warren F, Keck P, Oppermann H. Medical Applications of Single-Chain Antibodies. *Int. Rev. Immunol.* 1993;10(2-3):195-217.
222. Chaudhary VK, Batra JK, Gallo MG, Willingham MC, FitzGerald DJ, Pastan I. A Rapid Method of Cloning Functional Variable-Region Antibody Genes in *Escherichia coli* as Single-Chain Immunotoxins. *Proc. Natl. Acad. Sci. U. S. A.* 1990;87(3):1066-70.
223. Kabat EA, Wu TT, Bilofsky H, Reid-Miller M, Perry H. Sequences of proteins of immunological interest. *Anal. Biochem.* 1984;138(1):265.
224. Larrick JW, Chiang YL, Sheng-Dong R, Senck G, Casali P. Generation of specific human monoclonal antibodies by in vitro expansion of human B cells: a novel recombinant DNA approach. In: Borrebaeck CAK, editor. *In vitro immunisation in hybridoma technology*. Amsterdam: Elsevier Science Publishers B.V.; 1988. p. 231-46.
225. Orlandi R, Güssow DH, Jones PT, Winter G. Cloning immunoglobulin variable domains for expression by the polymerase chain reaction. *Proc. Natl. Acad. Sci. U. S. A.* 1989;86(10):3833-7.
226. ørum H, Andersen PS, øster A, Johansen LK, Riise E, Bjørnvad M, Svendsen I, Engberg J. Efficient method for construction comprehensive murine Fab antibody libraries displayed on phage. *Nucleic Acids Res.* 1993;21(19):4491-8.
227. Dübel S, Breitling F, Fuchs P, Zewe M, Gotter S, Welschof M, Moldenhauer G, Little M. Isolation of IgG antibody Fv-DNA from various mouse and rat hybridoma cell lines using the polymerase chain reaction with a simple set of primers. *J. Immunol. Methods.* 1994;175(1):89-95.
228. Clackson T, Hoogenboom HR, Griffiths AD, Winter G. Making antibody fragments using phage display libraries. *Nature.* 1991;352(6336):624-8.
229. Marks JD, Hoogenboom HR, Bonnert TP, McCafferty J, Griffiths AD, Winter G. By-passing immunization: Human antibodies from V-gene libraries displayed on phage. *J. Mol. Biol.* 1991;222(3):581-97.
230. Horton RM, Hunt HD, Ho SN, Pullen JK, Pease LR. Engineering hybrid genes without the use of restriction enzymes: gene splicing by overlap extension. *Gene.* 1989;77(1):61-8.
231. Skerra A, Pluckthun A. Assembly of a functional immunoglobulin Fv fragment in *Escherichia coli*. *Science.* 1988;240(4855):1038-41.
232. Better M, Chang CP, Robinson RR, Horwitz AH. *Escherichia coli* Secretion of an Active Chimeric Antibody Fragment. *Science.* 1988;240(4855):1041-3.
233. Glockshuber R, Malia M, Pfitzinger I, Plueckthun A. A comparison of strategies to stabilize immunoglobulin Fv-fragments. *Biochemistry (Mosc.).* 1990;29(6):1362-7.
234. Jurado P, Ritz D, Beckwith J, de Lorenzo Vc, Fernández LA. Production of Functional Single-Chain Fv Antibodies in the Cytoplasm of *Escherichia coli*. *J. Mol. Biol.* 2002;320(1):1-10.
235. Kudou M, Ejima D, Sato H, Yumioka R, Arakawa T, Tsumoto K. Refolding single-chain antibody (scFv) using lauroyl-l-glutamate as a solubilization detergent and arginine as a refolding additive. *Protein Expr. Purif.* 2011;77(1):68-74.
236. Zuberbühler K, Palumbo A, Bacci C, Giovannoni L, Som mavilla R, Kaspar M, Trachsel E, Neri D. A general method for the selection of high-level scFv and IgG

- antibody expression by stably transfected mammalian cells. *Protein Eng. Des. Sel.* 2009;22(3):169-74.
237. Ho M, Nagata S, Pastan I. Isolation of Anti-CD22 Fv with High Affinity by Fv Display on Human Cells. *Proc. Natl. Acad. Sci. U. S. A.* 2006;103(25):9637-42.
238. Wang Z, Mathias A, Stavrou S, Neville DM. A new yeast display vector permitting free scFv amino termini can augment ligand binding affinities. *Protein Eng. Des. Sel.* 2005;18(7):337-43.
239. Galeffi P, Lombardi A, Pietraforte I, Novelli F, Di Donato M, Sperandei M, Tornambe A, Fraioli R, Martayan A, Natali P, Benevolo M, Mottolese M, Ylera F, Cantale C, Giacomini P. Functional expression of a single-chain antibody to ErbB-2 in plants and cell-free systems. *J. Transl. Med.* 2006;4(1):39-51.
240. Yuan Q, Hu W, Pestka JJ, He SY, Hart LP. Expression of a Functional Antizearalenone Single-Chain Fv Antibody in Transgenic Arabidopsis Plants. *Appl. Environ. Microbiol.* 2000;66(8):3499-505.
241. Choo ABH, Dunn RD, Broady KW, Raison RL. Soluble Expression of a Functional Recombinant Cytolytic Immunotoxin in Insect Cells. *Protein Expr. Purif.* 2002;24(3):338-47.
242. Joosten V, Lokman C, van den Hondel C, Punt P. The production of antibody fragments and antibody fusion proteins by yeasts and filamentous fungi. *Microbial Cell Factories.* 2003;2(1):1-15.
243. Glockshuber R, Schmidt T, Plueckthun A. The disulfide bonds in antibody variable domains: effects on stability, folding in vitro, and functional expression in *Escherichia coli*. *Biochemistry (Mosc.)*. 1992;31(5):1270-9.
244. Sockolosky JT, Szoka FC. Periplasmic production via the pET expression system of soluble, bioactive human growth hormone. *Protein Expr. Purif.* 2013;87(2):129-35.
245. Sun W, Xie J, Lin H, Mi S, Li Z, Hua F, Hu Z. A combined strategy improves the solubility of aggregation-prone single-chain variable fragment antibodies. *Protein Expr. Purif.* 2012;83(1):21-9.
246. Sletta H, Tøndervik A, Hakvåg S, Aune TEV, Nedal A, Aune R, Evensen G, Valla S, Ellingsen TE, Brautaset T. The Presence of N-Terminal Secretion Signal Sequences Leads to Strong Stimulation of the Total Expression Levels of Three Tested Medically Important Proteins during High-Cell-Density Cultivations of *Escherichia coli*. *Appl. Environ. Microbiol.* 2007;73(3):906-12.
247. Bessette PH, Åslund F, Beckwith J, Georgiou G. Efficient folding of proteins with multiple disulfide bonds in the *Escherichia coli* cytoplasm. *Proc. Natl. Acad. Sci. U. S. A.* 1999;96(24):13703-8.
248. King J, Haase-Pettingell C, Robinson AS, Speed M, Mitraki A. Thermolabile folding intermediates: inclusion body precursors and chaperonin substrates. *FASEB J.* 1996;10(1):57-66.
249. Vallejo L, Rinas U. Strategies for the recovery of active proteins through refolding of bacterial inclusion body proteins. *Microbial Cell Factories.* 2004;3(1):11-22.
250. Xie X, Weisser NE, McLean MD, Hall JC. Complexes with anti-epitope tag IgGs improve the therapeutic potential of epitope-tagged antibody fragments. *Mol. Immunol.* 2010;47(7-8):1529-34.
251. Wang Y, Dossey AM, Froude JW, 2nd, Lubitz S, Tzur D, Semenchenko V, Wishart DS. PSA fluoroimmunoassays using anti-PSA ScFv and quantum-dot conjugates. *Nanomedicine (Lond)*. 2008;3(4):475-83.
252. Fick A, Wyzgol A, Wajant H. Production, purification, and characterization of scFv TNF ligand fusion proteins. *Methods Mol. Biol.* 2012;907:597-609.

253. Batra SK, Jain M, Wittel UA, Chauhan SC, Colcher D. Pharmacokinetics and biodistribution of genetically engineered antibodies. *Curr. Opin. Biotechnol.* 2002;13(6):603-8.
254. Kim M-k, Jeong H-J, Kao C-HK, Yao Z, Paik DS, Pie JE, Kobayashi H, Waldmann TA, Carrasquillo JA, Paik CH. Improved renal clearance and tumor targeting of ^{99m}Tc-labeled anti-Tac monoclonal antibody Fab by chemical modifications. *Nucl. Med. Biol.* 2002;29(2):139-46.
255. George J. Platelets. *The Lancet.* 2000;355(9214):1531-9.
256. Muzard J, Bouabdelli M, Zahid M, Ollivier V, Lacapere JJ, Jandrot-Perrus M, Billiald P. Design and humanization of a murine scFv that blocks human platelet glycoprotein VI in vitro. *FEBS J.* 2009;276(15):4207-22.
257. Investigators TE. Use of a Monoclonal Antibody Directed against the Platelet Glycoprotein IIb/IIIa Receptor in High-Risk Coronary Angioplasty. *N. Engl. J. Med.* 1994;330(14):956-61.
258. Zhang W, Li YS, Nardi MA, Dang S, Yang J, Ji Y, Li Z, Karpatkin S, Wisniewski T. Dissolution of arterial platelet thrombi in vivo with a bifunctional platelet GPIIIa49-66 ligand which specifically targets the platelet thrombus. *Blood.* 2010;116(13):2336-44.
259. Dang S, Hong T, Ding BS, Zhang W. A humanized single-chain variable fragment antibody against beta3 integrin in *Escherichia coli*. *Hybridoma (Larchmt).* 2011;30(6):543-8.
260. Zahid M, Loyau S, Bouabdelli M, Aubrey N, Jandrot-Perrus M, Billiald P. Design and reshaping of an scFv directed against human platelet glycoprotein VI with diagnostic potential. *Anal. Biochem.* 2011;417(2):274-82.
261. Aster RH, Curtis BR, McFarland JG, Bougie DW. Drug-induced immune thrombocytopenia: pathogenesis, diagnosis, and management. *J. Thromb. Haemost.* 2009;7(6):911-8.
262. Greinacher A, Völpel H, Janssens U, Hach-Wunderle V, Kemkes-Matthes B, Eichler P, Mueller-Velten HG, Pötzsch B, Group ftHI. Recombinant Hirudin (Lepirudin) Provides Safe and Effective Anticoagulation in Patients With Heparin-Induced Thrombocytopenia: A Prospective Study. *Circulation.* 1999;99(1):73-80.
263. Greinacher A, Janssens U, Berg G, Böck M, Kwasny H, Kemkes-Matthes B, Eichler P, Völpel H, Pötzsch B, Luz M, investigators ftH-ATS. Lepirudin (Recombinant Hirudin) for Parenteral Anticoagulation in Patients With Heparin-Induced Thrombocytopenia. *Circulation.* 1999;100(6):587-93.
264. Eichler J, Lubenow N, Greinacher A. Results of the third prospective study of treatment with lepirudin in patients with heparin-induced thrombocytopenia (HIT). *Blood.* 2002;100 (suppl 1):704a.
265. Lewis BE, Hursting MJ. Argatroban therapy in heparin-induced thrombocytopenia. In: Warkentin TE, Greinacher A, editors. *Heparin-induced thrombocytopenia*. 3rd ed. New York: Basel: Marcel Dekker; 2004. p. 437-74.
266. Zhou H, Fisher RJ, Papas TS. Optimization of primer sequences for mouse scFv repertoire display library construction. *Nucleic Acids Res.* 1994;22(5):888-9.
267. Ohshima M, Tadakuma T, Hayashi H, Inoue K, Itoh K. Generation of a recombinant single-chain variable fragment (scFv) targeting 5-methyl-2' - deoxycytidine. *J. Biochem. (Tokyo).* 2010;147(1):135-41.
268. Zylstra P, Franklin A, Hassan KA, Powell KL, Steele EJ, Blanden RV. Molecular evolution of V(H)9 germline genes isolated from DBA, BALB, 129 and C57BL mouse strains and sublines. *Immunogenetics.* 2003;55(3):182-8.

269. Schable KF, Thiebe R, Bensch A, Brensing-Kuppers J, Heim V, Kirschbaum T, Lamm R, Ohnrich M, Pourrajabi S, Roschenthaler F, Schwendinger J, Wichelhaus D, Zocher I, Zachau HG. Characteristics of the immunoglobulin V κ genes, pseudogenes, relics and orphans in the mouse genome. *Eur. J. Immunol.* 1999;29(7):2082-6.
270. Huston JS, Mudgett-Hunter M, Tai M-S, McCartney J, Warren F, Haber E, Oppermann H. [3] Protein engineering of single-chain Fv analogs and fusion proteins. In: John JL, editor. *Methods in Enzymology*. Volume 203: Academic Press; 1991. p. 46-88.
271. Hu X, O'Dwyer R, Wall JG. Cloning, expression and characterisation of a single-chain Fv antibody fragment against domoic acid in *Escherichia coli*. *J. Biotechnol.* 2005;120(1):38-45.
272. Ban N, Escobar C, Garcia R, Hasel K, Day J, Greenwood A, McPherson A. Crystal structure of an idiotype-anti-idiotype Fab complex. *Proc. Natl. Acad. Sci. U. S. A.* 1994;91(5):1604-8.
273. Ruzheinikov SN, Muranova TA, Sedelnikova SE, Partridge LJ, Blackburn GM, Murray IA, Kakinuma H, Takahashi-Ando N, Shimazaki K, Sun J, Nishi Y, Rice DW. High-resolution crystal structure of the Fab-fragments of a family of mouse catalytic antibodies with esterase activity. *J. Mol. Biol.* 2003;332(2):423-35.
274. Palakodeti A, Sandstrom A, Sundaresan L, Harly C, Nedellec S, Olive D, Scotet E, Bonneville M, Adams EJ. The Molecular Basis for Modulation of Human V γ 9V δ 2 T Cell Responses by CD277/Butyrophilin-3 (BTN3A)-specific Antibodies. *J. Biol. Chem.* 2012;287(39):32780-90.
275. Canobbio I, Stefanini L, Guidetti GF, Balduini C, Torti M. A new role for Fc γ RIIA in the potentiation of human platelet activation induced by weak stimulation. *Cell. Signal.* 2006;18(6):861-70.
276. Gao C, Boylan B, Fang J, Wilcox DA, Newman DK, Newman PJ. Heparin promotes platelet responsiveness by potentiating α IIb β 3-mediated outside-in signaling. *Blood.* 2011;117(18):4946-52.
277. Yokota T, Milenic DE, Whitlow M, Schlom J. Rapid Tumor Penetration of a Single-Chain Fv and Comparison with Other Immunoglobulin Forms. *Cancer Res.* 1992;52(12):3402-8.
278. Shawler DL, Bartholomew RM, Smith LM, Dilman RO. Human immunoresponse to multiple injections of murine monoclonal IgG. *J. Immunol.* 1985;135:1530-5.
279. Kortt AA, Malby RL, Caldwell JB, Gruen LC, Ivancic N, Lawrence MC, Howlett GJ, Webster RG, Hudson PJ, Colman PM. Recombinant anti-sialidase single-chain variable fragment antibody. Characterization, formation of dimer and higher-molecular-mass multimers and the solution of the crystal structure of the single-chain variable fragment/sialidase complex. *Eur. J. Biochem.* 1994;221(1):151-7.
280. Whitlow M, Filpula D, Rollence ML, Feng S-L, Wood JF. Multivalent Fvs: characterization of single-chain Fv oligomers and preparation of a bispecific Fv. *Protein Eng.* 1994;7(8):1017-26.
281. Atwell JL, Breheney KA, Lawrence LJ, McCoy AJ, Kortt AA, Hudson PJ. scFv multimers of the anti-neuraminidase antibody NC10: length of the linker between VH and VL domains dictates precisely the transition between diabodies and triabodies. *Protein Eng.* 1999;12(7):597-604.
282. Holliger P, Prospero T, Winter G. "Diabodies": small bivalent and bispecific antibody fragments. *Proc. Natl. Acad. Sci. U. S. A.* 1993;90(14):6444-8.

283. Bardwell JCA, McGovern K, Beckwith J. Identification of a protein required for disulfide bond formation in vivo. *Cell*. 1991;67(3):581-9.
284. Buchner J, Brinkmann U, Pastan I. Renaturation of a single-chain immunotoxin facilitated by chaperones and protein disulfide isomerase. *Biotechnology*. (N. Y.). 1992;10(6):682-5.
285. Lowe D, Dudgeon K, Rouet R, Schofield P, Jermutus L, Christ D. Aggregation, stability, and formulation of human antibody therapeutics. *Adv Protein Chem Struct Biol*. 2011;84:41-61.
286. Pantoliano MW, Bird RE, Johnson S, Asel ED, Dodd SW, Wood JF, Hardman KD. Conformational stability, folding, and ligand-binding affinity of single-chain Fv immunoglobulin fragments expressed in *Escherichia coli*. *Biochemistry (Mosc)*. 1991;30(42):10117-25.
287. Gilliland G, Luo J, Vafa O, Almagro J. Leveraging SBDD in Protein Therapeutic Development: Antibody Engineering. In: Tari LW, editor. *Structure-Based Drug Discovery. Methods in Molecular Biology*. 841: Humana Press; 2012. p. 321-49.
288. Chothia C, Lesk AM. Canonical structures for the hypervariable regions of immunoglobulins. *J. Mol. Biol*. 1987;196(4):901-17.
289. Kabat EA, Wu TT, Perry HM, Gottesman KS, Foeller C. Sequences of proteins of immunological interest. In: Services DoHaH, editor.: U.S. Government Printing Office; 1991.
290. Padlan EA. Anatomy of the antibody molecule. *Mol. Immunol*. 1994;31(3):169-217.
291. Kashmiri SVS, De Pascalis R, Gonzales NR, Schlom J. SDR grafting—a new approach to antibody humanization. *Methods*. 2005;36(1):25-34.
292. Riechmann L, Clark M, Waldmann H, Winter G. Reshaping human antibodies for therapy. *Nature*. 1988;332(6162):323-7.
293. Tempest PR, Bremner P, Lambert M, Taylor G, Furze JM, Carr FJ, Harris WJ. Reshaping a Human Monoclonal Antibody to Inhibit Human Respiratory Syncytial Virus Infection in Vivo. *Nat. Biotechnol*. 1991;9(3):266-71.
294. Queen C, Schneider WP, Selick HE, Payne PW, Landolfi NF, Duncan JF, Avdalovic NM, Levitt M, Junghans RP, Waldmann TA. A humanized antibody that binds to the interleukin 2 receptor. *Proc. Natl. Acad. Sci. U. S. A*. 1989;86(24):10029-33.
295. Reichert JM. Monoclonal antibodies in the clinic. *Nat. Biotechnol*. 2001;19(9):819-22.
296. Pelat T, Bedouelle H, Rees AR, Crennell SJ, Lefranc M-P, Thullier P. Germline Humanization of a Non-human Primate Antibody that Neutralizes the Anthrax Toxin, by in Vitro and in Silico Engineering. *J. Mol. Biol*. 2008;384(5):1400-7.
297. Wang H, Dai J, Li B, Fan K, Peng L, Zhang D, Cao Z, Qian W, Wang H, Zhao J, Guo Y. Expression, purification, and characterization of an immunotoxin containing a humanized anti-CD25 single-chain fragment variable antibody fused to a modified truncated *Pseudomonas* exotoxin A. *Protein Expr. Purif*. 2008;58(1):140-7.
298. Andersen DC, Reilly DE. Production technologies for monoclonal antibodies and their fragments. *Curr. Opin. Biotechnol*. 2004;15(5):456-62.
299. Burgess RR. Chapter 17 Refolding Solubilized Inclusion Body Proteins. In: Richard RB, Murray PD, editors. *Methods in Enzymology. Volume 463*: Academic Press; 2009. p. 259-82.
300. Li M, Su ZG, Janson JC. In vitro protein refolding by chromatographic procedures. *Protein Expr. Purif*. 2004;33(1):1-10.

301. Tsumoto K, Ejima D, Kumagai I, Arakawa T. Practical considerations in refolding proteins from inclusion bodies. *Protein Expr. Purif.* 2003;28(1):1-8.
302. Mayer M, Buchner J. Refolding of inclusion body proteins. *Methods Mol. Med.* 2004;94:239-54.
303. Katoh S, Katoh Y. Continuous refolding of lysozyme with fed-batch addition of denatured protein solution. *Process Biochemistry.* 2000;35(10):1119-24.
304. Vallejo LF, Rinas U. Optimized procedure for renaturation of recombinant human bone morphogenetic protein-2 at high protein concentration. *Biotechnol. Bioeng.* 2004;85(6):601-9.
305. Middelberg APJ. Preparative protein refolding. *Trends Biotechnol.* 2002;20(10):437-43.
306. Dong XY, Chen LJ, Sun Y. Refolding and purification of histidine-tagged protein by artificial chaperone-assisted metal affinity chromatography. *J. Chromatogr. A.* 2009;1216(27):5207-13.
307. Zhu XQ, Li SX, He HJ, Yuan QS. On-column refolding of an insoluble His6-tagged recombinant EC-SOD overexpressed in *Escherichia coli*. *Acta Biochim Biophys Sin (Shanghai).* 2005;37(4):265-9.
308. Jamshad M, Lin Y-P, Knowles TJ, Parslow RA, Harris C, Wheatley M, Poyner DR, Bill RM, Thomas ORT, Overduin M, Dafforn T. Surfactant-free purification of membrane proteins with intact native membrane environment. *Biochem. Soc. Trans.* 2011;39:813-8.
309. Maeda H, Bharate GY, Daruwalla J. Polymeric drugs for efficient tumor-targeted drug delivery based on EPR-effect. *Eur. J. Pharm. Biopharm.* 2009;71(3):409-19.
310. Tonge SR, Tighe BJ. Responsive hydrophobically associating polymers: a review of structure and properties. *Advanced Drug Delivery Reviews.* 2001;53(1):109-22.
311. Schmitt A, Guichard J, Masse JM, Debili N, Cramer EM. Of mice and men: comparison of the ultrastructure of megakaryocytes and platelets. *Exp. Hematol.* 2001;29(11):1295-302.
312. Giudicelli V, Duroux P, Ginestoux C, Folch G, Jabado-Michaloud J, Chaume D, Lefranc M-P. IMGT/LIGM-DB, the IMGT® comprehensive database of immunoglobulin and T cell receptor nucleotide sequences. *Nucleic Acids Res.* 2006;34(suppl 1):D781-D4.
313. Welch M, Govindarajan S, Ness JE, Villalobos A, Gurney A, Minshull J, Gustafsson C. Design parameters to control synthetic gene expression in *Escherichia coli*. *PLoS ONE.* 2009;4(9):e7002.
314. Niederfellner G, Lammens A, Mundigl O, Georges GJ, Schaefer W, Schwaiger M, Franke A, Wiechmann K, Jenewein S, Sloopstra JW, Timmerman P, Brannstrom A, Lindstrom F, Mossner E, Umana P, Hopfner KP, Klein C. Epitope characterization and crystal structure of GA101 provide insights into the molecular basis for type I/II distinction of CD20 antibodies. *Blood.* 2011;118(2):358-67.
315. Katschke KJ, Jr., Wu P, Ganesan R, Kelley RF, Mathieu MA, Hass PE, Murray J, Kirchhofer D, Wiesmann C, van Lookeren Campagne M. Inhibiting alternative pathway complement activation by targeting the factor D exosite. *J. Biol. Chem.* 2012;287(16):12886-92.
316. Krause JC, Ekiert DC, Tumpey TM, Smith PB, Wilson IA, Crowe JE, Jr. An insertion mutation that distorts antibody binding site architecture enhances function of a human antibody. *MBio.* 2011;2(1):e00345-10.

317. Batas B, Schiraldi C, Chaudhuri JB. Inclusion body purification and protein refolding using microfiltration and size exclusion chromatography. *J. Biotechnol.* 1999;68(2–3):149-58.
318. Devaux C, Moreau E, Goyffon M, Rochat H, Billiald P. Construction and functional evaluation of a single-chain antibody fragment that neutralizes toxin AahI from the venom of the scorpion *Androctonus australis hector*. *Eur. J. Biochem.* 2001;268(3):694-702.
319. Dolezal O, Pearce LA, Lawrence LJ, McCoy AJ, Hudson PJ, Kortt AA. ScFv multimers of the anti-neuraminidase antibody NC10: shortening of the linker in single-chain Fv fragment assembled in VL to VH orientation drives the formation of dimers, trimers, tetramers and higher molecular mass multimers. *Protein Eng.* 2000;13(8):565-74.
320. Arndt KM, Müller KM, Plückthun A. Factors Influencing the Dimer to Monomer Transition of an Antibody Single-Chain Fv Fragment†. *Biochemistry (Mosc.)*. 1998;37(37):12918-26.
321. Tsumoto K, Shinoki K, Kondo H, Uchikawa M, Juji T, Kumagai I. Highly efficient recovery of functional single-chain Fv fragments from inclusion bodies overexpressed in *Escherichia coli* by controlled introduction of oxidizing reagent—application to a human single-chain Fv fragment. *J. Immunol. Methods.* 1998;219(1–2):119-29.
322. Verdino P, Aldag C, Hilvert D, Wilson IA. Closely related antibody receptors exploit fundamentally different strategies for steroid recognition. *Proc. Natl. Acad. Sci. U. S. A.* 2008;105(33):11725-30.
323. Hwang WY, Foote J. Immunogenicity of engineered antibodies. *Methods.* 2005;36(1):3-10.
324. Baneyx F. Recombinant protein expression in *Escherichia coli*. *Curr. Opin. Biotechnol.* 1999;10(5):411-21.
325. Cheng Y-SE, Kwoh DY, Kwoh TJ, Soltvedt BC, Zipser D. Stabilization of a degradable protein by its overexpression in *Escherichia coli*. *Gene.* 1981;14(1–2):121-30.
326. Makhatadze GI, Privalov PL. Protein interactions with urea and guanidinium chloride: A calorimetric study. *J. Mol. Biol.* 1992;226(2):491-505.
327. Tikhonov RV, Pechenov SE, Belacheu IA, Yakimov SA, Klyushnichenko VE, Tunes H, Thiemann JE, Vilela L, Wulfson AN. Recombinant human insulin IX. Investigation of factors, influencing the folding of fusion protein-S-sulfonates, biotechnological precursors of human insulin. *Protein Expr. Purif.* 2002;26(2):187-93.
328. Tran-Moseman A, Schauer N, De Bernardez Clark E. Renaturation of *Escherichia coli*-Derived Recombinant Human Macrophage Colony-Stimulating Factor. *Protein Expr. Purif.* 1999;16(1):181-9.
329. Crowe J, Dobeli H, Gentz R, Hochuli E, Stieber D, Henco K. 6xHis-Ni-NTA Chromatography as a Superior Technique in Recombinant Protein Expression/Purification. In: Harwood A, editor. *Protocols for Gene Analysis. Methods in Molecular Biology.* 31: Humana Press; 1994. p. 371-87.
330. Wetlaufer DB, Branca PA, Chen G-X. The oxidative folding of proteins by disulfide plus thiol does not correlate with redox potential. *Protein Eng.* 1987;1(2):141-6.
331. Silva F, Queiroz JA, Domingues FC. Evaluating metabolic stress and plasmid stability in plasmid DNA production by *Escherichia coli*. *Biotechnology Advances.* 2012;30(3):691-708.

332. Tulumello DV, Deber CM. Efficiency of detergents at maintaining membrane protein structures in their biologically relevant forms. *Biochim. Biophys. Acta - Biomembranes*. 2012;1818(5):1351-8.
333. Rollin J, Pouplard C, Gratacap M-P, Leroux D, May M-A, Aupart M, Gouilleux-Gruart V, Payrastra B, Gruel Y. Polymorphisms of protein tyrosine phosphatase CD148 influence FcγRIIA-dependent platelet activation and the risk of heparin-induced thrombocytopenia. *Blood*. 2012;120(6):1309-16.
334. Yanaga F, Poole A, Asselin J, Blake R, Schieven GL, Clark EA, Law CL, Watson SP. Syk interacts with tyrosine-phosphorylated proteins in human platelets activated by collagen and cross-linking of the Fc gamma-IIA receptor. *Biochem. J*. 1995;311 (Pt 2):471-8.
335. Tavladoraki P, Girotti A, Donini M, Arias FJ, Mancini C, Morea V, Chiaraluce R, Consalvi V, Benvenuto E. A single-chain antibody fragment is functionally expressed in the cytoplasm of both *Escherichia coli* and transgenic plants. *Eur. J. Biochem*. 1999;262(2):617-24.
336. Lombardi A, Gianese G, Arcangeli C, Galeffi P, Sperandei M. Bacterial Cytoplasm Production of an EGFP-Labeled Single-Chain Fv Antibody Specific for the HER2 Human Receptor. *J. Biomol. Struct. Dyn*. 2011;29(3):425-39.
337. Liang SX, Pinkevych M, Khachigian LM, Parish CR, Davenport MP, Chong BH. Drug-induced thrombocytopenia: development of a novel NOD/SCID mouse model to evaluate clearance of circulating platelets by drug-dependent antibodies and the efficacy of IVIG. *Blood*. 2010;116(11):1958-60.
338. Hudson PJ, Souriau C. Engineered antibodies. *Nat. Med*. 2003;9(1):129-34.
339. Milstein C, Cuello AC. Hybrid hybridomas and their use in immunohistochemistry. *Nature*. 1983;305(5934):537-40.
340. Staerz UD, Bevan MJ. Hybrid hybridoma producing a bispecific monoclonal antibody that can focus effector T-cell activity. *Proc. Natl. Acad. Sci. U. S. A*. 1986;83(5):1453-7.
341. Suresh MR, Cuello AC, Milstein C. Bispecific monoclonal antibodies from hybrid hybridomas. *Methods Enzymol*. 1986;121:210-28.
342. Lindhofer H, Mocikat R, Steipe B, Thierfelder S. Preferential species-restricted heavy/light chain pairing in rat/mouse quadromas. Implications for a single-step purification of bispecific antibodies. *J. Immunol*. 1995;155(1):219-25.
343. Mezzanzanica D, Canevari S, Menard S, Pupa SM, Tagliabue E, Lanzavecchia A, Colnaghi MI. Human ovarian carcinoma lysis by cytotoxic T cells targeted by bispecific monoclonal antibodies: analysis of the antibody components. *Int. J. Cancer*. 1988;41(4):609-15.
344. Muller KM, Arndt KM, Strittmatter W, Pluckthun A. The first constant domain (C(H)1 and C(L)) of an antibody used as heterodimerization domain for bispecific miniantibodies. *FEBS Lett*. 1998;422(2):259-64.
345. de Kruif J, Logtenberg T. Leucine zipper dimerized bivalent and bispecific scFv antibodies from a semi-synthetic antibody phage display library. *J. Biol. Chem*. 1996;271(13):7630-4.
346. Kufer P, Lutterbüse R, Baeuerle PA. A revival of bispecific antibodies. *Trends Biotechnol*. 2004;22(5):238-44.
347. Holliger P, Brissinck J, Williams RL, Thielemans K, Winter G. Specific killing of lymphoma cells by cytotoxic T-cells mediated by a bispecific diabody. *Protein Eng*. 1996;9(3):299-305.
348. Korn T, Nettelbeck DM, Volkel T, Muller R, Kontermann RE. Recombinant bispecific antibodies for the targeting of adenoviruses to CEA-expressing tumour cells:

- a comparative analysis of bacterially expressed single-chain diabody and tandem scFv. *J. Gene Med.* 2004;6(6):642-51.
349. Choi BD, Cai M, Bigner DD, Mehta AI, Kuan C-T, Sampson JH. Bispecific antibodies engage T cells for antitumor immunotherapy. *Expert Opin. Biol. Ther.* 2011;11(7):843-53.
350. Mallender WD, Voss EW, Jr. Construction, expression, and activity of a bivalent bispecific single-chain antibody. *J. Biol. Chem.* 1994;269(1):199-206.
351. Gruber M, Schodin BA, Wilson ER, Kranz DM. Efficient tumor cell lysis mediated by a bispecific single chain antibody expressed in *Escherichia coli*. *J. Immunol.* 1994;152(11):5368-74.
352. Mack M, Riethmuller G, Kufer P. A small bispecific antibody construct expressed as a functional single-chain molecule with high tumor cell cytotoxicity. *Proc. Natl. Acad. Sci. U. S. A.* 1995;92(15):7021-5.
353. Kroll MH, Hellums JD, McIntire LV, Schafer AI, Moake JL. Platelets and shear stress. *Blood.* 1996;88(5):1525-41.
354. Dang S, Hong T, Wisniewski T, Zhang W. Dissolution of pre-existing platelet thrombus by synergistic administration of low concentrations of bifunctional antibodies against beta3 integrin. *PLoS ONE.* 2011;6(10):e27012.
355. Neblock DS, Chang CH, Mascelli MA, Fleek M, Stumpo L, Cullen MM, Daddona PE. Conjugation and evaluation of 7E3 x P4B6, a chemically cross-linked bispecific F(ab')₂ antibody which inhibits platelet aggregation and localizes tissue plasminogen activator to the platelet surface. *Bioconjug. Chem.* 1992;3(2):126-31.
356. James ND, Atherton PJ, Jones J, Howie AJ, Tchekmedyian S, Curnow RT. A phase II study of the bispecific antibody MDX-H210 (anti-HER2 x CD64) with GM-CSF in HER2+ advanced prostate cancer. *Br. J. Cancer.* 2001;85(2):152-6.
357. Repp R, van Ojik HH, Valerius T, Groenewegen G, Wieland G, Oetzel C, Stockmeyer B, Becker W, Eisenhut M, Steininger H, Deo YM, Blijham GH, Kalden JR, van de Winkel JG, Gramatzki M. Phase I clinical trial of the bispecific antibody MDX-H210 (anti-FcγRI x anti-HER-2/neu) in combination with Filgrastim (G-CSF) for treatment of advanced breast cancer. *Br. J. Cancer.* 2003;89(12):2234-43.
358. Jager M, Schoberth A, Ruf P, Hess J, Hennig M, Schmalfeldt B, Wimberger P, Strohle M, Theissen B, Heiss MM, Lindhofer H. Immunomonitoring results of a phase II/III study of malignant ascites patients treated with the trifunctional antibody catumaxomab (anti-EpCAM x anti-CD3). *Cancer Res.* 2012;72(1):24-32.
359. Ott MG, Marme F, Moldenhauer G, Lindhofer H, Hennig M, Spannagl R, Essing MM, Linke R, Seimetz D. Humoral response to catumaxomab correlates with clinical outcome: results of the pivotal phase II/III study in patients with malignant ascites. *Int. J. Cancer.* 2012;130(9):2195-203.
360. Papanikolaou G, Fotopoulou C, Braicu I, Chekerov R, Schmidt SC, Pietzner K, Sehouli J. First surgical experience of intraperitoneal treatment with the trifunctional antibody catumaxomab (anti-EpCam x anti-CD3) for epithelial ovarian cancer. *Anticancer Res.* 2011;31(8):2603-8.
361. Diermeier-Daucher S, Ortmann O, Buchholz S, Brockhoff G. Trifunctional antibody ertumaxomab: Non-immunological effects on Her2 receptor activity and downstream signaling. *mAbs.* 2012;4(5):614-22.
362. Nagorsen D, Kufer P, Baeuerle PA, Bargou R. Blinatumomab: a historical perspective. *Pharmacol. Ther.* 2012;136(3):334-42.
363. Otz T, Grosse-Hovest L, Hofmann M, Rammensee HG, Jung G. A bispecific single-chain antibody that mediates target cell-restricted, supra-agonistic CD28 stimulation and killing of lymphoma cells. *Leukemia.* 2009;23(1):71-7.

364. Lopez JA. The platelet glycoprotein Ib-IX complex. *Blood Coagul. Fibrinolysis*. 1994;5(1):97-120.
365. Berndt MC, Du X, Booth WJ. Ristocetin-dependent reconstitution of binding of von Willebrand factor to purified human platelet membrane glycoprotein Ib-IX complex. *Biochemistry (Mosc.)*. 1988;27(2):633-40.
366. Moore A, Ross GD, Nachman RL. Interaction of platelet membrane receptors with von Willebrand factor, ristocetin, and the Fc region of immunoglobulin G. *J. Clin. Invest.* 1978;62(5):1053-60.
367. Sullam PM, Hyun WC, Szöllösi J, Dong J-f, Foss WM, López JA. Physical Proximity and Functional Interplay of the Glycoprotein Ib-IX-V Complex and the Fc Receptor FcγRIIA on the Platelet Plasma Membrane. *J. Biol. Chem.* 1998;273(9):5331-6.
368. Andrews RK, Berndt MC, López JA. Chapter 7 - The glycoprotein Ib-IX-V complex. In: Michelson MDAD, Barry SC, editors. *Platelets (Second Edition)*. Burlington: Academic Press; 2007. p. 145-63.
369. Torti M, Bertoni A, Canobbio I, Sinigaglia F, Lapetina EG, Balduini C. Rap1B and Rap2B Translocation to the Cytoskeleton by von Willebrand Factor Involves FcγII Receptor-mediated Protein Tyrosine Phosphorylation. *J. Biol. Chem.* 1999;274(19):13690-7.
370. Gratacap M-P, Payrastre B, Viala C, Mauco G, Plantavid M, Chap H. Phosphatidylinositol 3,4,5-Trisphosphate-dependent Stimulation of Phospholipase C-γ2 Is an Early Key Event in FcγRIIA-mediated Activation of Human Platelets. *J. Biol. Chem.* 1998;273(38):24314-21.
371. Kelton JG, Arnold DM, Bates SM. Nonheparin Anticoagulants for Heparin-Induced Thrombocytopenia. *N. Engl. J. Med.* 2013;368(8):737-44.
372. Bodin S, Viala C, Ragab A, Payrastre B. A critical role of lipid rafts in the organization of a key FcγRIIa-mediated signaling pathway in human platelets. *Thromb. Haemost.* 2003;89(2):318-30.
373. Fitzgerald JR, Foster TJ, Cox D. The interaction of bacterial pathogens with platelets. *Nat. Rev. Microbiol.* 2006;4(6):445-57.
374. Amiral J, Meyer D. 12 Heparin-induced thrombocytopenia: diagnostic tests and biological mechanisms. *Baillieres Clin. Haematol.* 1998;11(2):447-60.
375. Zheng F, Qiu Y, Chen Y, Chen P, Zhu Y, Xie W, Zhu H, Zhu J. Cloning, purification and bioactivity assay of human CD28 single-chain antibody in *Escherichia coli*. *Cytotechnology*. 2009;60(1-3):85-94.
376. Yang X, Hu W, Li F, Xia H, Zhang Z. Gene cloning, bacterial expression, in vitro refolding, and characterization of a single-chain Fv antibody against PreS1(21-47) fragment of HBsAg. *Protein Expr. Purif.* 2005;41(2):341-8.
377. Sonoda H, Kumada Y, Katsuda T, Yamaji H. Functional expression of single-chain Fv antibody in the cytoplasm of *Escherichia coli* by thioredoxin fusion and co-expression of molecular chaperones. *Protein Expr. Purif.* 2010;70(2):248-53.
378. Sonoda H, Kumada Y, Katsuda T, Yamaji H. Effects of cytoplasmic and periplasmic chaperones on secretory production of single-chain Fv antibody in *Escherichia coli*. *J. Biosci. Bioeng.* 2011;111(4):465-70.
379. Ow DS, Lim DY, Nissom PM, Camattari A, Wong VV. Co-expression of Skp and FkpA chaperones improves cell viability and alters the global expression of stress response genes during scFvD1.3 production. *Microbiology Cell Factories*. 2010;9:22-35.
380. Desplancq D, Rinaldi AS, Stoessel A, Sibling AP, Busso D, Oulad-Abdelghani M, Van Regenmortel MH, Weiss E. Single-chain Fv fragment antibodies selected from an

- intrabody library as effective mono- or bivalent reagents for in vitro protein detection. *J. Immunol. Methods*. 2011;369(1-2):42-50.
381. Jurado P, de Lorenzo V, Fernández LA. Thioredoxin Fusions Increase Folding of Single Chain Fv Antibodies in the Cytoplasm of *Escherichia coli*: Evidence that Chaperone Activity is the Prime Effect of Thioredoxin. *J. Mol. Biol.* 2006;357(1):49-61.
382. Xiong H, Li S, Yang Z, Burgess RR, Dynan WS. *E. coli* expression of a soluble, active single-chain antibody variable fragment containing a nuclear localization signal. *Protein Expr. Purif.* 2009;66(2):172-80.
383. Qing G, Ma L-C, Khorchid A, Swapna GVT, Mal TK, Takayama MM, Xia B, Phadtare S, Ke H, Acton T, Montelione GT, Ikura M, Inouye M. Cold-shock induced high-yield protein production in *Escherichia coli*. *Nat Biotech.* 2004;22(7):877-82.
384. Hayashi K, Kojima C. pCold-GST vector: A novel cold-shock vector containing GST tag for soluble protein production. *Protein Expr. Purif.* 2008;62(1):120-7.
385. Hayashi K, Kojima C. Efficient protein production method for NMR using soluble protein tags with cold shock expression vector. *J. Biomol. NMR.* 2010;48(3):147-55.
386. Rouet R, Lowe D, Dudgeon K, Roome B, Schofield P, Langley D, Andrews J, Whitfield P, Jermutus L, Christ D. Expression of high-affinity human antibody fragments in bacteria. *Nat. Protoc.* 2012;7(2):364-73.
387. Stenberg E, Persson B, Roos H, Urbaniczky C. Quantitative determination of surface concentration of protein with surface plasmon resonance using radiolabeled proteins. *J. Colloid Interface Sci.* 1991;143(2):513-26.
388. Zwicker J, Lacroix R, Dignat-George F, Furie B, Furie B. Measurement of Platelet Microparticles. In: Gibbins JM, Mahaut-Smith MP, editors. *Platelets and Megakaryocytes. Methods in Molecular Biology.* 788: Springer New York; 2012. p. 127-39.
389. Roest M, Reininger A, Zwaginga JJ, King MR, Heemskerk JWM, the Biorheology Subcommittee of the SSCotI. Flow chamber-based assays to measure thrombus formation in vitro: requirements for standardization. *J. Thromb. Haemost.* 2011;9(11):2322-4.
390. Roskos LK, Davis CG, Schwab GM. The clinical pharmacology of therapeutic monoclonal antibodies. *Drug Dev. Res.* 2004;61(3):108-20.
391. Khalili H, Godwin A, Choi J-w, Lever R, Brocchini S. Comparative Binding of Disulfide-Bridged PEG-Fabs. *Bioconjug. Chem.* 2012;23(11):2262-77.
392. Webster R, Didier E, Harris P, Siegel N, Stadler J, Tilbury L, Smith D. PEGylated Proteins: Evaluation of Their Safety in the Absence of Definitive Metabolism Studies. *Drug Metab. Dispos.* 2007;35(1):9-16.
393. Bougie DW, Nayak D, Boylan B, Newman PJ, Aster RH. Drug-dependent clearance of human platelets in the NOD/scid mouse by antibodies from patients with drug-induced immune thrombocytopenia. *Blood.* 2010;116(16):3033-8.